UNIVERSITY OF SOUTHAMPTON

FACULTY OF NATURAL AND ENVIRONMENTAL SCIENCE

School of Chemistry

Long-lived states in multi-spin systems

by

Gabriele Stevanato

Thesis for the degree of Doctor of Philosophy

November 2015

UNIVERSITY OF SOUTHAMPTON

Abstract

FACULTY OF NATURAL AND ENVIRONMENTAL SCIENCE
School of Chemistry
Doctor of Philosophy

Long-lived states in multi-spin systems

by
Gabriele Stevanato

Long-lived states are nuclear spin configurations that, in suitable circumstances, decay very slowly towards thermal equilibrium. The first paper on the subject reported a long-lived order in 2,3-dibromothiophene between a pair of inequivalent proton nuclei of about 100 s at about 20 mT. The lifetime exceeded the relaxation time of longitudinal magnetization T_1 by more than one order of magnitude. Currently many systems can survive T_1 even at magnetic fields of several Tesla. Long lifetimes may benefit different methodologies used to investigate for example nuclear spin diffusion, chemical reactivity and metabolic processes. In addition hyperpolarization methods may profit from long-lived states in order to enhance both sensitivity and temporal resolution.

Although this research field is relatively young, the first publication being 11 years old, about 150 investigations so far have been published on peer-reviewed scientific journals on this subject.

In this work the main focus is to extend the analysis to multiple spin systems. The structure of the thesis is composed of a theoretical and an experimental part.

We propose a model based on nuclear spin permutations that uses the formalism of discrete group theory. This approach allows the classification of nuclear wave functions and internal Hamiltonian operators, according to nuclear spin permutation symmetry, in order to predict the number of long-lived orders and their analytical expression. The mathematical structure can also be applied to investigate fundamental bounds on spin conversion in the presence of symmetry. The theoretical model is grounded on a set of approximations used to define the symmetry operations and the corresponding permutation symmetry groups.

The experimental section includes examples of long-lived orders occurring under different magnetic, geometric and dynamic conditions. This large variety of regimes shows on one hand the ubiquitous character of long-lived species. On the other hand a common trait is identified in the formal characterisation that uses permutation and rotational symmetry concepts. For this reason a permutation symmetry characterisation is presented alongside the experimental description.

The role of local geometry in a rigid spin system is highlighted by comparing two isomers with a different local arrangement of spin nuclei, and showing how a long-lived order is predicted and detected only in one case.

Non rigid molecules can also display long-lived character. This is demonstrated by considering the methyl group $^{13}CH_3$ in γ-picoline. Interestingly, as proton nuclei are magnetically equivalent, the long-lived order accessibility cannot employ coherent mechanisms.

Finally a derivative of naphthalene is shown to possess an exceptionally long lifetime in solution and at room temperature. The accessibility of a very long lifetime opens up the possibility to store (hyper)polarization into singlet order and retrieve it later in time. A set of preliminary dissolution dynamic nuclear polarization experiments are also presented as a first attempt in this sense.

Contents

List of Figures

List of Tables

Declaration of Authorship

This thesis is the result of work done wholly while I was in registered candidature for a Ph.D. degree at this University. The material presented herein is based on work mostly done by myself. Where the work was carried out jointly with others, a substantial part is my own original work and co-workers and their roles have been, clearly, indicated. The material contained herein has not been submitted by the author for a degree at any other institution.
Date: January 19, 2016

Signed:

Acknowledgments

Many people over these last three years have made this experience extraordinary.
Malcolm has been truly a mentor to me. I am really grateful for the initial possibility he granted me to enrol in this PhD program. He has been always able to get the best from his co-workers through sincere praise and continuous encouragement, and he never refuses to rigorously and calmly answer even the most trivial scientific and non scientific questions.
Peppe and Maria made me feel at home in a familiar and joyful atmosphere since the very beginning. I remember, when I first arrived in UK, Peppe invited me for dinner in order to give me a "smooth transition to the english cuisine". Jiří has been a good friend and gave me, even recently, lot of good advices and support. Without Benno a large part of the experimental work wouldn't have been possible, and he also is a passionate chef. Graeme, Richard and Zenawi started the PhD with me and they have always been friendly and helpful. I am indebted to Soumya that guided me with the experimental work, and with his smiling attitude has made nice the hours in the lab/office. Salvo continues to be a very good friend and with his scientific counsel has been helping me over all these years. I am grateful to him and his girlfriend Agnieszka for their companionship. I hope I can get from Pär some of his ability and patience in running complex simulations. I've been learning a lot from Jean-Nicolas who is absolutely incomparable in terms of organization and scientific productivity. I wish all the best to Stuart, Cara, Michael, Ali and James for their studies and careers. Thanks David for introducing me into optimal control methodology. Thanks Ole, you have always helped me even if you had something else to do. Thanks Javier for your help with instrumentation, you have been really essential in this last year for everybody's projects. Karel has often impressed me by the very neat way of approaching scientific problems, and made the days in Prague for the recent EUROMAR very nice. Stefan has recently joined the group and I hope he can share with me his expertise in PHIP. Philip (Kuchel from Sydney) has been really an inspiring figure for me: curious, positive, smiling, hard working, passionate. I cannot find other words but it was truly a pleasure to have him around.
The iMR-CDT funded my phD program and was invaluable in scheduling several workshops and conference seminars. They were all very interesting and very well organized.

A big thanks to Chris and Yasmin.
Niente di quello che ho fatto sarebbe stato possibile senza l'amore e l'appoggio della mia famiglia: di Francesca che si e' fatta carico di tantissime cose, di Anna, dei miei suoceri Maria Rosa e Mario, di Gabriella e Roberto. Mia mamma Gina non mi ha mai fatto mancare il suo amore anche quando le scelte sono state difficili o poco comprensibili. Il suo esempio e' veramente prezioso. Grazie Giulio e grazie Marta che mi avete fatto sentire un po' meno solo con le vostre telefonate. E grazie ai miei cugini Barbara e Manuel e ai tanti amici: Rudi, Andrea (Tobe), Emanuele (Lucky) e Alessandro sempre pronti ad organizzare una pizza o un incontro quando torno in Italia. Grazie anche ai miei amici dell'universita' Dott. Giordani (cuea) e Dott. Prof. Davide (mona) che mi ha dato buoni consigli quando stavo per fare scelte importanti.
This work is dedicated to my beloved father Gianni who encouraged me with his daily example to always have thirst of knowledge facing difficulties as opportunities always fearless and with a positive attitude, and to you Anna who are the love of my life.

Gabriele
05th November 2015
Southampton (UK)

List of publications

The material of this thesis has been published in the following papers:

1. ***Long-lived nuclear spin states in methyl groups and quantum-rotor-induced polarization.***
   Meier B., Dumez J-N., **Stevanato G.**, Hill-Cousins J.T., Roy S.S., Håkansson, P., Mamone S., Brown R.C.D., Pileio G., Levitt M. H.
   J. Am. Chem. Soc., vol **135**, 50, pp 18746-18749, 2013.

2. ***A Nuclear Singlet Lifetime of More than One Hour in Room-Temperature Solution.***
   Stevanato G., Hill-Cousins J.T., Håkansson, P., Roy S.S., Brown L.J., Brown R.C.D., Pileio G., Levitt M. H.
   Angew. Chemie Int. Ed., vol **54**, 12, pp 3740-3743, 2015.

3. ***Theory of long-lived nuclear spin states in methyl groups and quantum-rotor induced polarisation.***
   Dumez, J-N., Håkansson, P., Mamone S., Meier B., **Stevanato G.**, Hill-Cousins J.T., Roy S.S., Brown R.C.D., Pileio G., Levitt M. H.
   J. Chem. Phys., vol **142**, 4, pp 044506, 2015.

4. ***Synthesis of an Isotopically Labeled Naphthalene Derivative That Supports a Long-Lived Nuclear Singlet State.***
   Hill-Cousins J.T., Pop I-A., Pileio G., **Stevanato G.**, Roy S.S., Levitt M. H., Brown L.J., Brown R.C.D.
   Org. Lett., vol **17**, 9, pp 2150-2153, 2015.

5. ***Enhancement of quantum rotor NMR signals by frequency-selective pulses.***
   Roy, S.S., Dumez, J-N., **Stevanato G.**, Meier B., Hill-Cousins J.T., Brown R.C.D., Pileio G., Levitt M. H.
   J. Magn. Reson., vol **250 C**, pp 25-28, 2014.

6. ***Long-lived nuclear spin states far from magnetic equivalence.***
   Stevanato G., Roy, S.S., Hill-Cousins J.T., Kuprov I., Brown L.J., Brown R.C.D.,

Pileio G., Levitt M. H.
Phys. Chem. Chem. Phys., vol **17**, 8, pp 5913-5922, 2015.

Chapter 1

Thesis Structure

The present work is the result of a 3-year project in Prof. Levitt's research group in Southampton (UK). It comprises a theoretical and an experimental part.

The theoretical part derives a formalization of long-lived states (LLS) in terms of nuclear spin permutation symmetry. This formalism is suitable in particular with multi-spin systems. A few advantages originate:

- This formalism derives a convenient representation of LLS as spin population imbalances of nuclear spin states spanning across different irreducible representations.
- A classification of the symmetry properties of the system's complete Hamiltonian permits to easily find out the number of conserved quantities (under a certain set of introduced approximations).
- A generalization of the Sørensen bound [14] in presence of exchange symmetry of the nuclear spin Hamiltonian, initially analysed by Nielsen and Sørensen [15, 16] and recently investigated by Levitt [17], is included as it allows to set extra boundary conditions.

The experimental part demonstrates the ubiquitous nature of LLS. They are identified and detected either in nearly chemically, magnetic and far from magnetic equivalent systems. The discovery of a more than one hour LLS in a hydrophobic naphthalene [1] derivative molecule is currently fostering the theoretical investigation on field dependent relaxation mechanisms and on practical ways to store and retrieve polarization over an extended time interval. A water soluble version of the molecule has been also investigated and is briefly presented. The naphthalene derivatives experiments are still work in progress. Finally a brief section is dedicated to preliminary hyperpolarization experiments on the hydrophobic naphthalene derivative performed at Ardenkjaer-Larsen's research group in DTU-Copenhagen as a first attempt to store hyperpolarized signal for long time. Experiments are divided as follows:

[1] When discussing the existence of "disconnected eigenstates" in Ref. 18, naphthalene has been cited as a possible interesting system.

- Experiments on derivatives of fumarate and maleate indicated in this work as *1-(ethyl-d5) 4-(propyl-d7)(E)-but-2-enedioate-2,3-*$^{13}C_2$ and *1-(ethyl-d5) 4-(propyl-d7)(Z)-but-2-enedioate-*$^{13}C_2$,
- Experiments on methyl rotor in γ-picoline,
- Experiments on naphthalene derivatives.

The thesis aims to generalize the theoretical description on LLS to systems encompassing more than two spins using a permutation symmetry approach to the problem. This requires to ground the concept of nuclear spin permutation symmetry on the context of NMR and most importantly a set of *ad hoc* approximations taking into account the specificity of the problem under analysis.

The work is organized as follows: The introductory part *NMR, symmetry and Quantum Mechanics* reviews the basic concepts used in this work. It is formed by two chapters:

2. **Introduction:** The chapter sets the context of the present work.
   - Starting from what Nuclear Magnetic Resonance is about, the concepts of magnetism and spin relaxation are briefly introduced to pave the way into long-lived nuclear spin orders.
   - As symmetry will be frequently invoked in the following chapters a review of the concept is considered, and some examples provided.
3. **Mathematical tools:** The chapter reviews the mathematical toolbox that is used throughout the thesis. Theorems are enunciated and used without derivation.
   - A review of finite group theory opens the chapter. Some examples are given that will be later used in the theoretical analysis.
   - Rotations and angular momenta are presented to introduce the Wigner-Eckart theorem.

The *Permutation symmetry* part formalizes long-lived states analysis in terms of nuclear spin permutations. It is formed by a single chapter:

4. **Theory:** The chapter is the core of the theoretical analysis.
   - It describes the concept of nuclear spin permutation and applies it in the classification of coherent and incoherent components of nuclear spin Hamiltonian.
   - A description of LLS in terms of spin population imbalances is used.
   - Emphasis is placed on the set of approximations necessary to perform the theoretical analysis.
   - The accessibility problem via coherent mechanisms is considered.

- The Sørensen theorem on maximum spin conversion [14] is reviewed, and the generalization, investigated by Nielsen and Sørensen [15, 16] and recently further analysed by Levitt [17], of unitary evolution in presence of symmetry is included for completeness.

Finally the part *Experiments* presents experiments on long-lived states in multi-spin systems. It includes a single chapter:

5. **Experiments:** The chapter deals with experiments on long-lived orders.

   - The role of geometrical arrangement of nuclei is analysed when comparing *1-(ethyl-d5) 4-(propyl-d7)(E)-but-2-enedioate-2,3-*$^{13}C_2$ ($^{13}C_2$-AFD) and *1-(ethyl-d5) 4-(propyl-d7)(Z)-but-2-enedioate-*$^{13}C_2$ ($^{13}C_2$-AMD). LLS in $^{13}C_2$-AFD are defined as *geometrically imposed*. It probably represents the first experimental demonstration of long-lived order far from magnetic equivalence. We conclude that near magnetic equivalence is not a necessary condition to have a LLS.
   - The long-lived state in γ-picoline is discussed as an example of *dynamically imposed* LLS.
   - A hydrophobic derivative of naphthalene showing a lifetime of more than one hour in solution and at room temperature is given.
   - The same investigation but with different results has been performed on a hydrophilic naphthalene derivative.
   - Some preliminary hyperpolarization experiments are shown as well.

The part *Final remarks* recaps the present work in a single chapter. Specifically:

6. **Conclusions:** The chapter summarizes results and problems encountered, proposing some future outlook on LLS research.

In the **Appendix** the derivation of the relaxation super-operator in presence of internal rotation in CH_3 groups is presented.

At the end of every chapter a brief summary is given to recapitulate the main points/results just presented.

Part I

NMR, Symmetry and Quantum Mechanics

Chapter 2

Introduction

2.1 NMR

Matter is made of molecules, made of atoms, made of nuclei.

The classification goes further as on the subnuclear level other particles, representing objects of study of high energy particle physics [19], can be identified. Chemistry, on the other hand, is related to molecules. In this area, scientific investigation is often concerned with structural identification, dynamics determination and chemical reactivity. Atomic nuclei, thanks to their magnetism, have proven to be vital in conveying all the above information. Nuclear magnetic moments associated with magnetic nuclei are sensitive to their local surroundings and yet interact only weakly with them. Most elements have at least one naturally occurring magnetic isotope. As a result, nuclei in the vast majority of systems can be interrogated about their local environments without much disturbing the system itself [20, 21].

This is, in essence, the scope of NMR (Nuclear Magnetic Resonance).

2.2 Bulk Magnetism

The interaction of matter with a magnetic field is expressed in terms of magnetic moment $\boldsymbol{\mu}$. The energy of this interaction is $E = -\boldsymbol{\mu} \cdot \mathbf{B}$. This indeed depends on the relative orientation of vectors $\boldsymbol{\mu}$ and $\mathbf{B}$ and the energy is lower when both point in the same direction in space. An object having a permanent magnetic moment that is free to move tends to align to the external magnetic field in order to minimize the magnetic energy. However most objects possess a magnetic moment only in presence of an external magnetic field and display an induced magnetism. In this case the induced magnetic moment is:

$$\boldsymbol{\mu}_{induced} = \mu_0^{-1} V \chi \mathbf{B} \tag{2.1}$$

where $\mu_0 = 4\pi \times 10^{-7}\mathrm{Hm}^{-1}$ is the magnetic constant, V is the volume of the object, $\mathbf{B}$ is the magnetic field and χ is the magnetic susceptibility, which expresses how readily an object displays a magnetic moment in the presence of a magnetic field. It is a scalar quantity that may be positive or negative. When positive the object, paramagnetic, tends to pull the magnetic field into the material. If negative, diamagnetic, it tends to push the magnetic field out of the material. The strong magnetism of paramagnetic and ferromagnetic materials is due to the presence of unpaired electrons.

2.3 Microscopic Magnetism

In the microscopic model of matter, magnetism arises mainly from circulation of electric current which contribute to a negative value of susceptibility, i.e. tends to stand opposite to the external magnetic field, but also from electronic and nuclear magnetic moments which contribute a positive value, i.e. tend to align to external magnetic field. Electrons and nuclei both possess an intrinsic magnetic moment, which is not due to electric current. The spin angular momentum and the magnetic moment are proportional to each other according to the relation:

$$\boldsymbol{\mu} = \gamma \boldsymbol{S} \tag{2.2}$$

where $\boldsymbol{\mu}$ and $\boldsymbol{S}$ are quantum mechanical operators, and γ is the gyromagnetic ratio measured in rad s^{-1} T^{-1}. Again this scalar quantity may have both signs. If positive, magnetic moment and spin point in the same direction.

2.4 Spin Precession

The spin angular momentum in presence of a magnetic field moves around it. We can imagine the motion of a magnetic moment like an arrow spanning the surface of a cone with a central axis having the same direction of the magnetic field, while keeping a constant angle between the magnetic moment and the field itself. This motion is called precession. The angle of precession depends on the initial spin polarization [21]. Every nucleus has a characteristic precession frequency at a particular magnetic field called the Larmor frequency:

$$\omega = -\gamma B \tag{2.3}$$

For a proton $\gamma = 267.5 \times 10^6$ rad s^{-1} T^{-1}. The sign indicates the sense of spin precession. Most nuclei have a positive gyromagnetic ratio, in which case Larmor frequency is negative. Some nuclei such as ^{29}Si and ^{15}N, which has also been studied in our group [22], have negative gyromagnetic ratio and a positive Larmor frequency. So in general in the absence of an external magnetic field the nuclear magnetic moments will

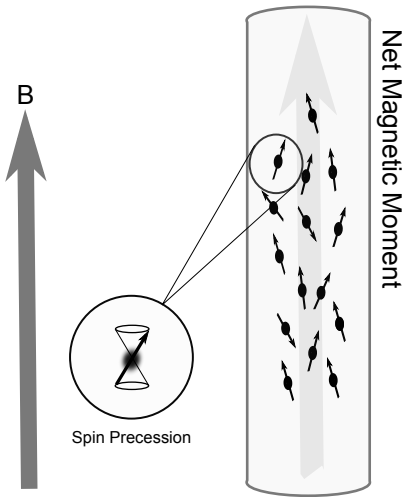

Figure 2.1: The anisotropic spin nuclear orientation distribution in presence of a static magnetic field creates a macroscopic net magnetic moment. An arrow spanning the surface of a cone represents the spin precession motion.

be uniformly distributed and we would have a net macroscopic magnetic moment close to zero. This situation changes drastically if we introduce an external perturbation: a magnetic field. We do not have a uniform distribution of spin polarization any longer, but a more ordered configuration. This happens because magnetic moments preferentially precess around the direction defined from the external magnetic field, independent of the fact that they are in molecules undergoing strong rotations and collisions. It is worth pointing out that it is not the precession itself to give rise to bulk magnetization, but the broken symmetry introduced by the external magnetic field. This usually strong perturbation (several Tesla) indeed removes the degeneracy between nuclear spins aligned parallel/antiparallel to the static magnetic field [1, 20, 21, 23].

2.5 Relaxation and long-lived orders

At any given moment the spin precesses about a magnetic field which is the sum of the static external magnetic field, and a microscopic field which is not only spatially dependent, but also time dependent. In practice this tiny field can in principle have any spatial direction and magnitude. The result is a magnetic moment fluctuating while precessing. These microscopic random fields are always present, and are responsible for the relaxation phenomena. The ordered configuration of spins aligned to the external magnetic field gradually evolves toward a disordered configuration in which the grade of polarizations expands to uniformity. However this is not entirely correct. The environment has in fact a finite temperature, and it is slightly more probable that spin is driven to an orientation with low magnetic energy than towards an orientation with high magnetic energy. In practice the system will get to a configuration called thermal equilibrium, which is stable but not static. In terms of energy level spin population, relaxation is the dynamic process leading the system to a configuration in which the populations are

given by the Boltzmann distribution for that specific temperature [20, 21, 23]. The sum of the microscopic magnetic moments over the sample volume causes a macroscopic quantity named bulk magnetization which may be expressed as a vector:

$$\mathbf{M}(t) = \{M_x(t), M_y(t), M_z(t)\} \tag{2.4}$$

Let us consider for a moment the ^{1}H nuclei in a water sample. The ^{1}H longitudinal magnetization $M_z(t)$ is proportional to the difference in magnetic energy between proton polarized parallel and antiparallel to the static magnetic field divided by the available thermal energy. The difference in magnetic energy is $\hbar\gamma B^0 \simeq 3.3 \times 10^{-25}$ J where $\hbar$ is the reduced Planck constant, γ is the proton gyromagnetic ratio and $B^0 = 11.75$ T is the static magnetic field in the z direction (assuming a 500 MHz magnet). The thermal available energy at equilibrium is equal to $kT \simeq 4.1 \times 10^{-21}$ J, where k is the Boltzmann constant and T the temperature. This quantity is approximately four orders of magnitude larger. The dynamic process leading to the build-up of the longitudinal magnetization can be studied by the following experiment: suppose we allow the water sample to equilibrate at zero magnetic field for enough time (a few minutes is in this case sufficient) and then the sample is rapidly brought into a strong magnetic field at time t_{on} (see Fig. 2.2-a). The macroscopic nuclear magnetization is initially zero and gradually grows to the thermal equilibrium value at that magnetic field. The build-up curve is usually approximately exponential:

$$M_z(t) = M_{z,eq}(1 - e^{-(t-t_{on})/T_1}) \tag{2.5}$$

If the magnetic field is suddenly switched off at a later time t_{off} such that $t_{off} - t_{on} \gg T_1$,

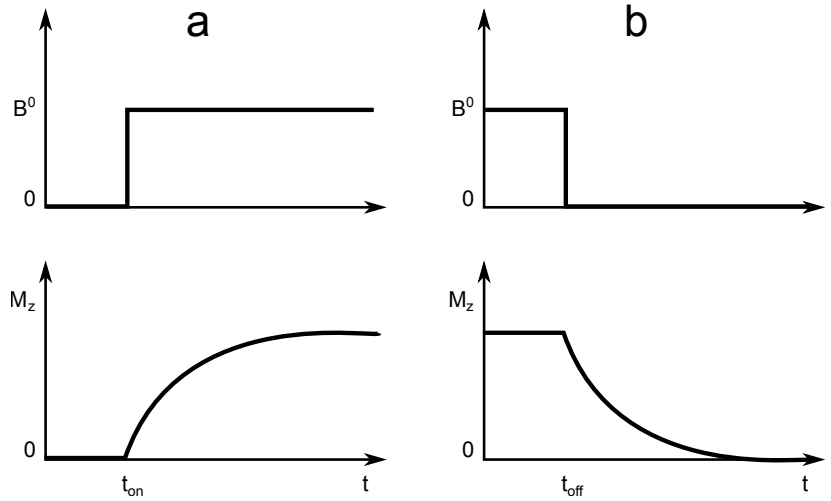

Figure 2.2: a) The build-up of longitudinal magnetization in presence of a strong magnetic field B^0. b) The decay of longitudinal magnetization after the magnetic field B^0 has been turned off.

the nuclear spin magnetization relaxes back to zero again (see Fig. 2.2-b) according to:

$$M_z(t) = M_{z,eq} e^{-(t-t_{off})/T_1} \tag{2.6}$$

The T_1 relaxation process involves a redistribution of spin population in order to get to the equilibrium configuration. This process implies an exchange of energy. A truly isolated nuclear spin system would show negligible rates of T_1 relaxation. However, a variety of relaxation interactions allows nuclear spins to exchange energy with their surroundings, the lattice, permitting the spin populations to equilibrate. This is why T_1 is also identified as spin-lattice relaxation time. This terminology, appropriated in solid-state crystal NMR where a lattice can be identified, has been inherited also in gas and liquid NMR where a proper lattice is not present. In the latter context the meaning is relaxation of the magnetization component M_z parallel to the external magnetic field. The external static magnetic field is assumed to be polarized along the z axis.

In an ordinary NMR experiment however instead of measuring spin magnetization along the field, the magnetization perpendicular to the field is measured. Let us suppose again to equilibrate the water sample in a strong magnetic field. The macroscopic nuclear magnetization reaches an equilibrium value along the magnetic field direction $M_{z,eq}$. At this stage there is no net magnetization on a xy plane perpendicular to the direction of the static magnetic field, because on average, the distribution of transverse magnetization is homogeneous. However upon application of a strong pulse [20, 21, 23] the magnetization vector can be rotated so that it will eventually lie in the xy plane. For example a strong 90 degree pulse with 0 phase (indicated as 90_0 in Fig. 2.3) will rotate the magnetization vector from the z direction to the $-y$ direction [20, 21]. Immediately

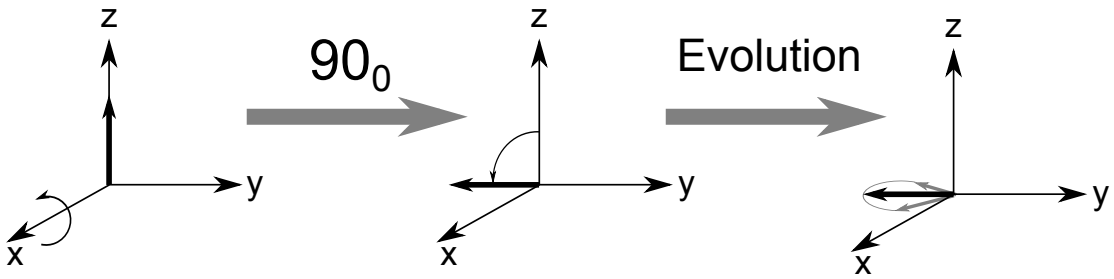

Figure 2.3: Upon application of a 90_0 radiofrequency pulse, the magnetization vector is rotated by 90 degrees from the z to the $-y$ direction. The magnetization vector then precesses about the z axis and a gradual loss of synchronicity between the precessing nuclear spins causes the transverse magnetization to return to zero with a T_2 decay time constant.

after the pulse the state of the system corresponds to a net polarization along the $-y$ axis. Since every single spin precesses, the bulk magnetization also precesses. While precessing in the xy plane the transverse magnetization also decays in time for the gradual loss

of synchronicity between the precessing nuclear magnets according to the equations:

$$\begin{aligned} M_y(t) &= -M_{z,eq}\cos(\omega^0 t)e^{-t/T_2} \\ M_x(t) &= M_{z,eq}\sin(\omega^0 t)e^{-t/T_2} \end{aligned} \tag{2.7}$$

where ω^0 is the Larmor frequency at B^0 magnetic field, and T_2 is the decay time constant of the component of magnetization perpendicular to the external magnetic field. In this case, on a microscopic level, different parts within the sample can sense slightly

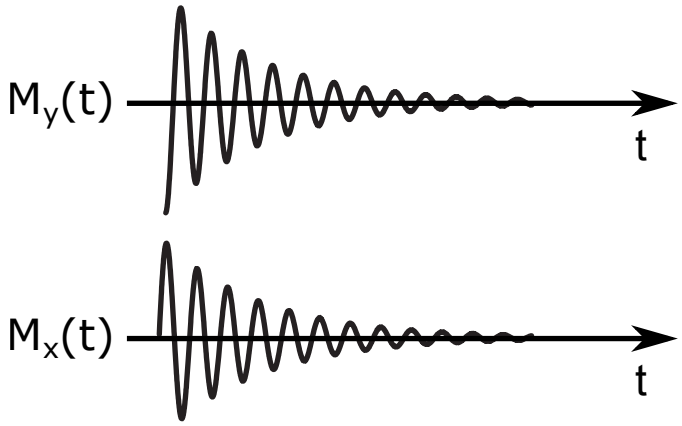

Figure 2.4: The oscillatory decays of the components $M_x(t)$ and $M_y(t)$ according to equations 2.7

different magnetic fields. This in turn will determine a random variation in the instantaneous precession of nuclear magnetic spins. As a result the initial phase coherence and synchronicity of the spins are lost. This process is named spin-spin relaxation. Also this term is a bit misleading, as it seems to suggest that is necessary an interaction between spins for the de-coherence process to happen. The necessary condition is instead an inhomogeneity over the sample of the external magnetic field sensed by spins. This is always the case in a real sample regardless of spin interactions. T_1 is usually longer than T_2, and for quite a long time it was thought that T_1 set an upper limit to detectable magnetization.

What if this limitation could be overcome extending the time range of detectable magnetization? In other words would it be possible to freeze the evolution/relaxation of a spin system in order to make it long-lived? Nature provides, as usual, an elegant and extraordinary example with the small hydrogen molecule. As reported in Ref. [24], in 1929, long before NMR was discovered, Paul Harteck and Karl-Friedrich Bonhoeffer, demonstrated the existence of two hydrogen nuclear-spin isomers by cooling hydrogen and determining the thermal conductivities of para- and ortho-hydrogen [25]. In para-hydrogen the two proton spins are antisymmetric while in the triplet ortho-hydrogen they are symmetric with respect to spin exchange. Para-hydrogen is the lower energy isomer and is highly populated at low temperature: at 80 °K the Boltzmann equilibrium distribution is 51.61% ortho- and 48.39% para-; at 20 °K ortho- is 0.18% and para- is

99.82% [26]. The interconversion between states is fostered by a paramagnetic catalyst. Once formed, the catalyst can be removed and para-hydrogen can be returned to room temperature where the equilibrium ratio of ortho/para will slowly re-establish itself. Due to its symmetry properties para-hydrogen is a long-lived nuclear spin configuration. In molecules other than hydrogen, nuclear spin configurations less sensitive than longitudinal/transverse magnetization to relaxation exist and were first experimentally demonstrated by Levitt and co-workers in Ref. [27, 28] on pairs of inequivalent nuclei. A further crucial step was the demonstration that long-lived orders (LLS) are possible even between chemically equivalent spin pairs [3, 18]. The subject, after more than 10 years, is still generating a considerable and vivid interest given the possibility to naturally combine LLS with currently available polarization techniques such as dissolution dynamic nuclear polarization (dDNP [29, 30]) or parahydrogen induced polarization (PHIP [24, 31, 32]) so that to get a spy capable on relaying information on structure, dynamics and chemical reactivity for a time never achieved before. Again, as for para-hydrogen, the symmetry of the nuclear wave function is at the very root of the extended lifetime in LLS.
As the word symmetry will be largely used from now onward, it might be beneficial to review what symmetry means starting from an intuitive and common geometrical perspective and giving some examples on how it has been hugely employed in physics and chemistry while addressing, in particular, quantum mechanical problems.

2.6 Introduction to symmetry

An object or a shape are said to be symmetric if there is a transformation, such as a reflection or a rotation, upon which the object is indistinguishable from its initial aspect. For example a geometrical square conserves its appearance after a rotation of $\frac{\pi}{2}$, π, or $\frac{3\pi}{2}$ around an axis passing through its geometric centre and orthogonal to the plane of the square. Such rotations are called *symmetry operations*, and the square is said to be *invariant* upon them. According to this definition, an arbitrary rotation is not a symmetry operation for a square. The situation might be completely different for a different object. Any rotation as previously defined would be a symmetry operation for a circle. Mathematics is the language of choice in the description of natural sciences, and it is of no surprise that the concept of symmetry can be extended beyond its original domain. The objects of classical physics are equations describing in terms of suitable variables the macroscopic behaviour of certain entities. Such equations are the *laws* of Physics. The relationship between symmetry and physical laws began with Newton, whose equations of motion are the same in frames of reference related by galileian transformations [33]. Lorentz and Poincaré were looking for a class of transformations upon which Maxwell equations were invariant, when they discovered the Lorentz transformations. The incompatibility between galileian and Lorentz transformations led

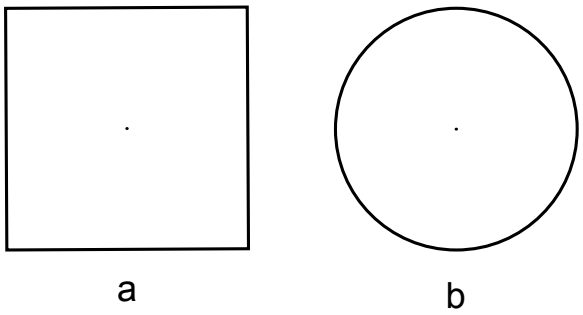

Figure 2.5: A square (a) and a circle (b). These objects are invariant to particular rotations about axes that are perpendicular to their plane and pass through their geometric centres (indicated by dots).

Einstein to the formulation of the theory of relativity. When Physics analyses the matter on a microscopic scale the standard approach is not represented by classical mechanics, but is usually accomplished by quantum mechanics. Quite remarkably as shown by the Stern and Gerlach experiment [34] a new variable is necessary to characterize a microscopic system: the spin angular momentum. The concept of spin is a difficult one. As W. Pauli said to R. Kronig (a PhD student at Columbia University in 1925), who first proposed to consider the electron rotating in space, the idea of spin "it is indeed very clever but of course has nothing to do with reality" [35]. Symmetry operations of physical laws involve space-time coordinates and are sometimes called *geometrical symmetries*, but may also involve internal coordinates such as the spin of a particle, and are called *internal symmetries*.
Identifying appropriate symmetry transformations is a central theme of modern physics. A deep mathematical relationship between symmetry and conservation laws is the one known as Noether's Theorem [36, 37]:

- **Noether's Theorem**: The covariance of equations of motion with respect to a continuous transformation with n parameters implies the existence of n quantities, or *constants of motion*, i.e., conservation laws.

For example in classical mechanics the covariance of Newton's equations with respect to a transformation of the form $\mathbf{r}' = \mathbf{r} + \mathbf{a}$ for any three dimensional vector $\mathbf{a}$ leads to the conservation of linear momentum. Similarly the covariance with respect to any transformation of the form $\mathbf{r}' = \mathbf{R} \cdot \mathbf{r}$ where $\mathbf{R}$ is a 3×3 rotation matrix leads to the conservation of angular momentum. Also the conservation of energy can be formalized as covariance of the Newton's equations with respect to a transformation of the time coordinate of the form $t' = t + \tau$. There is sometimes a tendency to use the terms conservation and invariance as synonymous. This is understandable on a qualitative level, however they should not be confused: "invariant" means that a quantity's numerical value is not altered by a coordinate transformation, whereas "conserved" means that a quantity, *within* a given coordinate system does not change through a process. For example, an electron has a specific rest charge q_0. If the electron is accelerated by using an appropriate electric field the charge remains the same: the charge is an invariant. The electron's spin is

also an invariant. Electron's mass and energy, on the other hand, can be measured to be different in different reference frames. The relativistic corrections for mass and energy depend on the Lorentz factor:

$$\begin{aligned} \gamma_{\text{Lorentz}} &= \frac{1}{\sqrt{1-\left(\frac{v}{c}\right)^2}} \\ m &= m_0 \times \gamma_{\text{Lorentz}} \\ E &= E_0 \times \gamma_{\text{Lorentz}} \\ q &= q_0 \\ \sigma &= \sigma_0 \end{aligned} \tag{2.8}$$

where c is the speed of light postulated to be invariant by the theory of Relativity, v, m, E, q, σ indicate velocity, mass, energy, charge and spin. The subscript 0 refers to the frame where the electron is at rest. Relativistic corrections are not really relevant to our purposes under many circumstances. Even the velocity of an electron in a hydrogen atomic orbital can be estimated to be orders of magnitude smaller than the speed of light. The speed of the electron can be very roughly estimated equalizing the kinetic and potential energies, and the confined motion of the particle accounted for the uncertainty principle [23, 38, 39]:

$$\frac{1}{2}mv^2 = \frac{q^2}{4\pi\epsilon_0 r} \qquad mv \sim \frac{\hbar}{2r} \qquad \Rightarrow \qquad \frac{v}{c} \sim 10^{-2} \tag{2.9}$$

2.7 Symmetry in one dimension

A one-dimensional example is sufficient to appreciate the importance of the symmetry analysis in a quantum-mechanical problem. Suppose we consider the time-independent Schröedinger equation for a particle of mass m in a potential $V(x)$.

$$\left[-\frac{\hbar^2}{2m}\frac{\mathrm{d}^2}{\mathrm{d}x^2} + V(x)\right]\phi(x) = E\phi(x) \tag{2.10}$$

where $\hbar = \frac{h}{2\pi}$, h being the Planck's constant, ϕ the particle's wave function, E the energy eigenvalue. The Hamiltonian operator for this system is:

$$\mathcal{H}(x) = -\frac{\hbar^2}{2m}\frac{\mathrm{d}^2}{\mathrm{d}x^2} + V(x) \tag{2.11}$$

The energy eigenvalues in a one-dimensional problem are non degenerate [38], so to any eigenfunction there is a unique corresponding energy eigenvalue. Suppose that the potential $V(x)$ is an even function of the coordinate x. Mathematically this means that

upon transformation of the coordinate system $x \to -x$,

$$V(x) = V(-x) \tag{2.12}$$

Examples of such potentials are the one-dimensional symmetric square well and the one-dimensional harmonic oscillator [23]. It must be realized that also the kinetic term

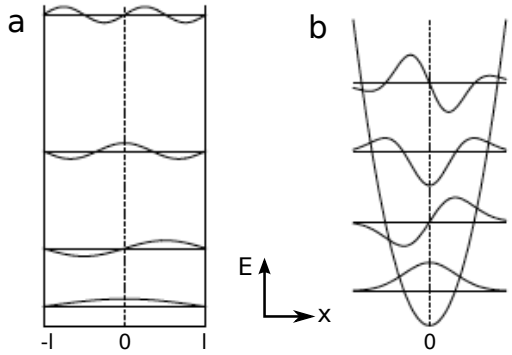

Figure 2.6: (a) A square-well potential (adapted from Ref. [1]). The potential is $V(x) = 0$ for $|x| < l$ and $V(x) \to \infty$ for $|x| \geq l$. (b) An harmonic oscillator potential $V(x) = \frac{1}{2}kx^2$, where k is a constant. The $x = 0$ axes are indicated by a dashed line. The first four wave functions $\phi(x)$ for both potentials are also presented. Note the different symmetry with respect to inversion.

$-\frac{\hbar^2}{2m}\frac{\mathrm{d}^2}{\mathrm{d}x^2}$ is symmetric upon inversion, and thus the inversion operation is a symmetry operation for the Hamiltonian $\mathcal{H}$ of the system:

$$\mathcal{H}(x) = \mathcal{H}(-x) \tag{2.13}$$

The question we are addressing can be formulated in the following way:
Does the symmetry property of the Hamiltonian imply any symmetry constraint on the wave functions solution of the problem in eq. 2.10?
The property in eq. 2.13 can be used to investigate the change of coordinates in the original time-independent Schröedinger equation:

$$\mathcal{H}(-x)\phi(-x) = \mathcal{H}(x)\phi(-x) = E\phi(-x) \tag{2.14}$$

Since E is non degenerate there is a unique wave function corresponding to this eigenvalue, and this can be accomplished only if:

$$\phi(-x) = A\phi(x), \tag{2.15}$$

where A is a constant. By transforming $x \to -x$ in the last equation:

$$\phi(x) = A\phi(-x), \tag{2.16}$$

and consequently

$$\phi(x) = A^2\phi(x), \tag{2.17}$$

This requires $A^2 = 1$. So either $A = 1$ or $A = -1$. This means that eigenfunctions of the system can be either *symmetric*:

$$\phi(x) = \phi(-x) \tag{2.18}$$

or *antisymmetric*

$$\phi(x) = -\phi(-x) \tag{2.19}$$

upon inversion. Therefore this example shows how starting from the symmetry property of the Hamiltonian it is possible to find a symmetry constraint for the particle's wave functions. The relevance of this simple result should be stressed. Several times during the following discussion starting from the symmetry properties of the coherent Hamiltonian, the nuclear wave functions will be classified accordingly. This in turn will offer a convenient way to build a basis suitable to represent and analyse all interactions that may be of interest for the spectroscopist.

2.8 Symmetry in atoms and molecules

A different aspect of symmetry stemming from the quantum mechanical nature of matter arises from the arrangement of atoms in molecules. The symmetry properties of atoms is relevant for the electronic, vibrational and rotational (*rovibronic* [40]) description of the system, and on describing how the system interacts with electromagnetic radiation [40]. For small molecules like CO, H_2O, CH_4 the rotational energy levels spacing divided by hc (where $h \sim 6.626 \times 10^{-34}$Js is the Planck's constant and $c \sim 300 \times 10^6$ m/s is the speed of light) are between 1 to 50 cm^{-1} and the vibrational energy level spacings divided by hc are about 1000 to 4000 cm^{-1}. For closed shell molecules the electronic energy level spacings are about 20 000 to 100 000 cm^{-1} [40]. We will rather use Hz unit, the correspondence being 1 $cm^{-1} \sim 30 \times 10^9$ Hz [23].
Nuclear Magnetic Resonance (NMR) relates to the study of nuclear spin, and involves the dynamic description of the spin once it is displaced from equilibrium by a radio frequency radiation. To put NMR in context let us consider a collection of identical protons in a 9.4 T magnetic field at a temperature of 300 °K. The quantization of the spin angular momentum along the axis defined by the direction of external magnetic field determines two possible energy levels [1, 20, 21, 23, 41]. The equilibrium ratio of populations between the two energy levels is dictated by the Boltzmann distribution:

$$\frac{n_\downarrow}{n_\uparrow} = e^{-\frac{\Delta E}{kT}}, \tag{2.20}$$

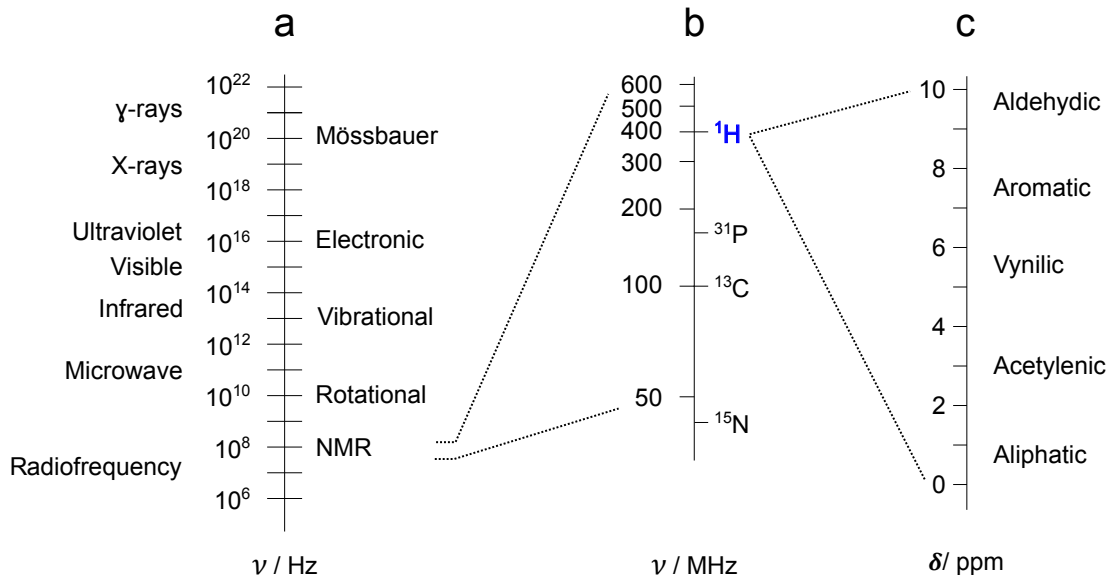

Figure 2.7: a): Electromagnetic spectrum [1]. b): Expanded region shows the NMR resonance frequencies at 9.4 T of some nuclei. c): Typical proton chemical shifts in ppm for some organic functional groups.

where $\Delta E = 2.65\times10^{-25}$J, $kT = 4.14\times10^{-21}$J, and $n_\uparrow$ and $n_\downarrow$ are the spin populations for spin oriented parallel or antiparallel to the external magnetic field. Therefore $\frac{\Delta E}{kT} \sim 10^{-5}$. Such small values of $\frac{\Delta E}{kT}$ allow to use the Taylor expansion for the exponential at the first order $e^{-x} \sim 1 - x + O(x^2)$ to obtain a normalized population difference:

$$\frac{n_\downarrow - n_\uparrow}{n_\downarrow + n_\uparrow} = \frac{\Delta E}{2kT} \tag{2.21}$$

The population difference between $n_\downarrow$ and $n_\uparrow$ in equation 2.21 is of about one part every 30 000. This suggests that there will be a very little tendency for spins to orient in the lower energy level. This difference is even smaller for protons in a lower magnetic field or for nuclei with a lower gyromagnetic ratio. Electronic spectroscopy on the other hand deals with much larger energy gaps of the order of 10^{15} Hz as per Fig. 2.7. At room temperature the number of molecules in their ground state is largely exceeding any other excited state.

In a standard NMR experiment radio frequency pulses are used to displace the spins from thermal equilibrium. When the radio frequency pulses terminate, the system tends to spontaneously return back to thermal equilibrium through a process named relaxation that has been quickly introduced. During relaxation useful information is encoded into the system, and one of the goals of NMR spectroscopy is how to decode this information.

The versatility of NMR allows for example to elucidate the molecular structure of complex systems by COSY experiments, to use the spatial dependence of proton nuclear resonance to create a non invasive body image in clinical MRI (Magnetic Resonance Imaging) and to gather information about molecular geometry, three dimensional struc-

ture and functionality in biomolecules.
The developments in the field of MRI in particular are relatively fast and recent. For example, the first MR images of a human brain were obtained in 1978 by two groups of researchers at EMI Laboratories leaded by Ian Robert Young and Hugh Clow [42]. In 1986, Charles L. Dumoulin and Howard R. Hart at General Electric developed MR angiography [43] and Denis Le Bihan [44], obtained the first images and later patented diffusion MRI. In 1990, Seiji Ogawa at AT&T Bell labs recognized that oxygen-depleted blood with dHb was attracted to a magnetic field, and discovered the technique that underlies Functional Magnetic Resonance Imaging (fMRI) [45]. The first study of the human brain at 3.0 T was published in 1994, and in 1998 at 8 T (information taken from `https://en.wikipedia.org/wiki/Magnetic_resonance_imaging_of_the_brain`). In 2003 Paul C. Lauterbur and Sir Peter Mansfield were jointly awarded the Nobel Prize in in Physiology or Medicine *"for their discoveries concerning magnetic resonance imaging"* `http://www.nobelprize.org/nobel_prizes/medicine/laureates/2003/`. Magnetic resonance in general represents therefore

Figure 2.9: Magnetic Resonance Imaging of human brain (picture taken from `https://en.wikipedia.org/wiki/Magnetic_resonance_imaging_of_the_brain`)

the root of technologies and applications crucial for human health. Despite the richness of such a technique, the nuclear spin relaxation still sets a severe limitation for the spectroscopist to observe the structure and dynamics of matter over an extended period of time. It proves to be particularly important to address the study of relaxation processes in order to individuate molecular systems displaying favourable relaxation properties. Favourable in this context is a relative terminology. There are applications such as CEST (chemical exchange saturation transfer) where strong relaxation is looked for. Indeed the enhanced relaxation induced by paramagnetic substances is extremely important in designing proper MRI contrast agents [46, 47]. As briefly mentioned before,

the investigation of nuclear spin states less sensitive to the major relaxation mechanisms has opened up a completely new and extremely important research field: the area of nuclear long-lived spin states [2, 3, 5, 10, 18, 27, 28, 48–56].
Since the last 11 years this research topic has led to numerous peer reviewed scientific publications (about 150) spanning, among the others, possible ways to predict and access long-lived spin order in regimes of near chemical or near magnetic equivalence [3, 6], strong magnetic inequivalence [55], theoretical formalization of singlet order [57–59] and long-lived order in methyl groups [53, 60], in para-ethanol [56], as well as examples of long-lived states in glycine protons in Ala-Gly [61], in exploring weak ligand-protein interactions [62, 63] and more recently examples of how long-lived orders can be hyperpolarized either at high magnetic field [64] or low magnetic field ($\sim \mu$T) [65] and used in conjunction with other techniques such as SABRE [48, 50]. In our research group an example has been provided of a system displaying a lifetime of more than one hour in solution and at room temperature [10]. This system is presented in the experimental chapter of this thesis.

2.9 Summary

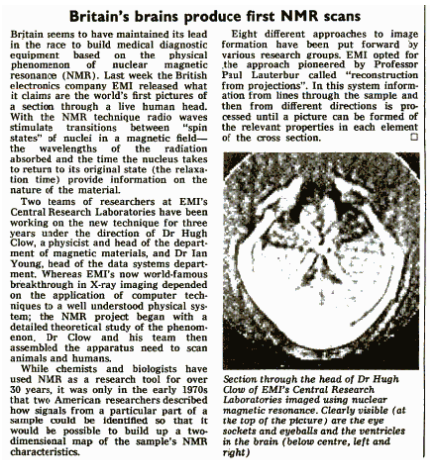

Britain's brains produce first NMR scans

Britain seems to have maintained its lead in the race to build medical diagnostic equipment based on the physical phenomenon of nuclear magnetic resonance (NMR). Last week the British electronics company EMI released what it claims are the world's first pictures of a section through a live human head. With the NMR technique radio waves stimulate transitions between "spin states" of nuclei in a magnetic field—the wavelengths of the radiation absorbed and the time the nucleus takes to return to its original state (the relaxation time) provide information on the nature of the material.

Two teams of researchers at EMI's Central Research Laboratories have been working on the new technique for three years under the direction of Dr Hugh Clow, a physicist and head of the department of magnetic materials, and Dr Ian Young, head of the data systems department. Whereas EMI's now world-famous breakthrough in X-ray imaging depended on the application of computer techniques to a well understood physical system; the NMR project began with a detailed theoretical study of the phenomenon. Dr Clow and his team then assembled the apparatus need to scan animals and humans.

While chemists and biologists have used NMR as a research tool for over 30 years, it was only in the early 1970s that two American researchers described how signals from a particular part of a sample could be identified so that it would be possible to build up a two-dimensional map of the sample's NMR characteristics.

Eight different approaches to image formation have been put forward by various research groups. EMI opted for the approach pioneered by Professor Paul Lauterbur called "reconstruction from projections". In this system information from lines through the sample and then from different directions is processed until a picture can be formed of the relevant properties in each element of the cross section. □

Section through the head of Dr Hugh Clow of EMI's Central Research Laboratories imaged using nuclear magnetic resonance. Clearly visible (at the top of the picture) are the eye sockets and eyeballs and the ventricles in the brain (below centre, left and right)

Figure 2.8: The original article appeared in the magazine *NewScientist* on November 11th 1978, accounting for the first image of the human brain, from Ian Robert Young and Hugh Clow.

In the present chapter starting from an introductory basic description of Nuclear Magnetic Resonance it has been shown how a fundamental and intrinsic property of many elements, the nuclear spin, can be fruitfully used in many circumstances to gather information about structure and molecular environment. The time-lapse for longitudinal magnetization to return to thermal equilibrium after a suitable radio-frequency excitation is not a fundamental bound. Nuclear spin states exist that can overcome this limitation: nuclear long-lived states. They are the objects of the present work, and of a considerable attention over the last 11 years. As insensitivity to relaxation mechanisms can be formalized as a symmetry property of nuclear spin wave functions and spin Hamiltonian operators, an elementary introduction to the concept of symmetry is provided through some examples.
The concept of symmetry will be re-formulated in the following chapters to analyse nuclear long-lived orders in different molecules and under different geometrical and dy-

namic regimes. The role of symmetry is a general one: it is spread across different branches of science and the Noether's theorem enlightens the deep connection between symmetry and conservation laws.

Chapter 3

Mathematical tools

3.1 Motivation

In the Introduction it has been shown the importance of symmetry using a one dimensional example. Symmetry is indeed a fundamental human concern virtually spread throughout all cultures. The Greek word *symmetros* and the Latin *symmetria* were meant originally to convey the notion of regularity, well proportion and harmonious. Several important prizes have recognized the importance of symmetry in fundamental areas from particle to nuclear physics, and group theory has also been applied to explore how symmetry and invariance of economic models can provide insights into their properties [36, 66].

To our purposes an exhaustive treatment of molecular spectroscopy in terms of symmetry has been given for example by Bunker and Jensen [40, 67]. In this chapter the basic mathematical language that is later used in the analysis of long-lived orders is introduced. Symmetry groups with a finite (and usually small) number of elements are reviewed but continuous Lie groups and Lie algebras are not considered. In order to formalize what is meant by symmetry, the notion of group is presented and some examples that may be useful in the analysis of systems like methyl rotors are given.

3.2 Groups: definition and examples

A group $\mathcal{G}$ is a set of elements $\{a, b, c \dots\}$ with a binary composition law, called *multiplication* that has the following properties [68]:

- **Closure**: The multiplication of any two elements of $\mathcal{G}$ is also an element of $\mathcal{G}$.

$$\forall a, b \in \mathcal{G} \quad a \cdot b = c \Rightarrow c \in \mathcal{G}. \tag{3.1}$$

- **Associativity**: The composition law is associative.

$$\forall a, b, c \in \mathcal{G} \quad (a \cdot b) \cdot c = a \cdot (b \cdot c) \tag{3.2}$$

- **Identity**: There exists a unique element called identity denoted by e such that:

$$\forall a \in \mathcal{G} \quad e \cdot a = a \cdot e \tag{3.3}$$

- **Inverse**: Every element in the group has a unique inverse belonging to the same group.

$$\forall a \in \mathcal{G} \quad \exists \quad a^{-1} \in \mathcal{G} : \quad a^{-1} \cdot a = a \cdot a^{-1} = e \tag{3.4}$$

The composition law that is called multiplication is an abstract rule to combine two elements of a group in order to determine a third element of the same group. The difference with ordinary multiplication becomes even more apparent from the fact that it does not need to be commutative. So the product $a{\cdot}b$ can be different from $b{\cdot}a$. If a group has a commutative composition law it is called *commutative* or *abelian*. The number of elements of a group is called the *order* of the group. Subsets of a group may still be endowed with a group structure. If that is the case the subset is defined as a *subgroup*. In the description of a physical system the elements of the group may correspond to coordinate transformations or permutations, with the composition law given by matrix multiplication. In this way the associativity property is guaranteed. Intuitively if two operations are symmetry operations for the system, so their product should be. The identity leaves the system unchanged and the inverse of each transformation reverses it.

Point group theory has long been used by chemists to classify molecules at equilibrium: lists of symmetry operations are defined and molecules grouped accordingly. For example H_2O has C_{2v} symmetry as it is symmetric with respect to a 2-fold rotation axis and a reflection about two different vertical planes [40, 68, 69]. A nice gallery of molecules with the corresponding symmetry groups and symmetry operations can be found for example at `http://symmetry.otterbein.edu/gallery/`.

It is worth reviewing two examples on rotations in space and permutations of objects that find a direct application on LLS analysis in the following chapters:

- **Rotations in 2D-space**: Let's consider the set of 2×2 matrices with real entries:

$$R = \begin{pmatrix} a & -b \\ b & a \end{pmatrix} \tag{3.5}$$

with $a, b \in \mathbb{R}$ and $\det R = 1$. a and b cannot be simultaneously zero. The matrix R is a general representation of a rotation in a 2-dimensional space around the same axis. This set forms the group SO(2). In order to verify it, all above defined group's properties should be met. According to the closure requirement,

the composition of two matrices should return another matrix of the same form. This can be verified using ordinary matrix multiplication as the composition law.

$$\begin{pmatrix} a & -b \\ b & a \end{pmatrix} \cdot \begin{pmatrix} c & -d \\ d & c \end{pmatrix} = \begin{pmatrix} ac - bd & -(bc + ad) \\ (bc + ad) & ac - bd \end{pmatrix}, \tag{3.6}$$

again $c, d \in \mathbb{R}$, and not simultaneously zero. The inverse of eq. 3.5 is:

$$R^{-1} = \frac{1}{a^2 + b^2} \begin{pmatrix} a & b \\ -b & a \end{pmatrix} = \begin{pmatrix} a & b \\ -b & a \end{pmatrix} = \begin{pmatrix} a & -b' \\ b' & a \end{pmatrix} \tag{3.7}$$

where it was used the fact that $\det R = 1 \Rightarrow a^2 + b^2 = 1$, and made the substitution $b = -b'$. The associativity is guaranteed by matrix multiplication. The two-dimensional identity matrix is the identity element of SO(2). In this example

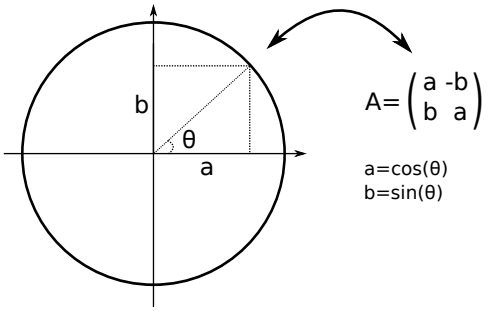

Figure 3.1: The one-to-one correspondence between an element of a 2-dimensional rotation matrix and a point of coordinates a and b in the complex plane. This correspondence is an *isomorphism* between SO(2) and the unit circle.

$a^2 + b^2 = 1$ is the equation of a circle with unitary radius. This suggests that a one-to-one correspondence can be established between the matrix in eq. 3.5 and the complex number $a + ib$ on the unit circle. This one-to-one correspondence is technically called an *isomorphism*, defined in section 3.4, between SO(2) and the unit circle. An angle θ can be defined so that $a = \cos(\theta)$ and $b = \sin(\theta)$ (see Fig. 3.1). It can be verified that the group is commutative or abelian. Equation 3.5 can then be rewritten in the usual form:

$$R = \begin{pmatrix} \cos(\theta) & -\sin(\theta) \\ \sin(\theta) & \cos(\theta) \end{pmatrix} \tag{3.8}$$

Rotations about the origin in a 3-dimensional space also form the group SO(3). In this case a general rotation in space can be decomposed as the product of three rotations around the canonical axes x, y, z by defining the set of Euler angles $\Omega = \{\alpha, \beta, \gamma\}$ in the following way:

$$R(\Omega) = R_z(\alpha) \cdot R_y(\beta) \cdot R_z(\gamma) \tag{3.9}$$

where,

$$R_z(\theta) = \begin{pmatrix} \cos(\theta) & -\sin(\theta) & 0 \\ \sin(\theta) & \cos(\theta) & 0 \\ 0 & 0 & 1 \end{pmatrix} \tag{3.10}$$

$$R_x(\theta) = \begin{pmatrix} 1 & 0 & 0 \\ 0 & \cos(\theta) & -\sin(\theta) \\ 0 & \sin(\theta) & \cos(\theta) \end{pmatrix} \tag{3.11}$$

$$R_y(\theta) = \begin{pmatrix} \cos(\theta) & 0 & -\sin(\theta) \\ 0 & 1 & 0 \\ \sin(\theta) & 0 & \cos(\theta) \end{pmatrix} \tag{3.12}$$

An important result, used in the theory of angular momenta [38], is that although finite rotations around the same axis are commutative, that is not the case for rotations involving different axes. For example if θ is finite:

$$R_z(\theta) \cdot R_x(\theta) \neq R_x(\theta) \cdot R_z(\theta), \tag{3.13}$$

Only if the rotation angle ϵ is infinitesimal, rotations about different axes commute. By defining the commutator $R_i(\epsilon) \cdot R_j(\epsilon) - R_j(\epsilon) \cdot R_i(\epsilon) = [R_i(\epsilon), R_j(\epsilon)]$ we have:

$$[R_i(\epsilon), R_j(\epsilon)] = 0 \quad \Longleftrightarrow \quad \epsilon \to 0 \quad \forall i, j \in \{x, y, z\} \quad i \neq j \tag{3.14}$$

The group of infinitesimal rotations is therefore *commutative*, whereas in general finite rotations are non commutative.

- $\mathbf{S_3}$: Suppose we have an ordered list of 3 objects. The initial order of the objects defines a configuration for the list. We can think of a permutation of two objects in the list as an operation exchanging their position in the list: a new list's configuration is attained in this way. In general a permutation can be a reordering involving all of the 3 elements. The permutation (213) replaces $2 \to 1$, $1 \to 3$, and $3 \to 2$. A list $\underline{123}$ can be for example acted upon in the following way:

$$\begin{aligned} (12)\underline{123} &= \underline{213} \\ (123)\underline{123} &= \underline{231} \\ (132)(23)\underline{123} = (132)\underline{132} &= \underline{321} \end{aligned} \tag{3.15}$$

Equation 3.15 needs further consideration. The composition of the permutations $(132) \cdot (23)$ that we have just indicated (132)(23) for simplicity, is equivalent to exchange object 1 with 3. Therefore is equivalent to the permutation (13). So

without explicitly referring to the list of objects $\underline{123}$ we say that:

$$(132)(23) = (13)$$

The permutation replacing $1 \rightarrow 1$, $2 \rightarrow 2$, and $3 \rightarrow 3$ is equivalent to not acting on the system and we indicate it as (). Can be also verified for example that:

$$\begin{aligned} [(13)(123)]\,(132) &= (13) \\ (13)\,[(123)(132)] &= (13)() = (13) \quad \text{so that} \quad (132) = (123)^{-1} \end{aligned} \tag{3.16}$$

Although the previous equations are not a mathematical proof, we have shown some examples on how the product or composition of permutations is a permutation (closure property), how the composition does not depend on how the operations are associated in pairs (associative property), how the inverse and identity permutations exist. It can be indeed proved that the permutations of three elements is a group: S_3. The order of S_3 is 6 and the elements can be explicitly written as:

$$S_3 = \{(), (12), (13), (23), (123), (132)\} \tag{3.17}$$

Moreover S_3 is a *non-abelian* group given that the composition rule is not commutative:

$$\begin{aligned} (132)(23) &= (13) \\ (23)(132) &= (12) \end{aligned} \tag{3.18}$$

A geometric realization of S_3 can be established by considering the symmetry transformations of an equilateral triangle. There is a one-to-one correspondence between the elements of S_3 and the operations on the vertices of a triangle (see Fig. 3.2). A subset of S_3 that it is still endowed with a group structure is formed by elements:

$$C_3 = \{(), (123), (132)\} \tag{3.19}$$

C_3 is therefore not just a subset but also a subgroup of S_3.

Permutation groups are largely used in the following treatment, and C_3 is considered in the analysis of CH_3 groups. The general importance of the permutation group S_n resides in the Cayley's Theorem establishing a one-to-one correspondence between *every* finite group $\mathcal{G}$ of order $|\mathcal{G}|$ and a subgroup of S_n for some n [70, 71]. The permutation group S_3 is an example of a *finite* group of order 6. SO(3) is an example of an *infinite* group as the angular parameter can be continuously varied in its domain. Elements of finite groups have the interesting property that if they are multiplied by themselves enough times, they eventually recover the identity element. The order k of a permutation (ij) is the minimum number k so that $(ij)^k = ()$. For example the order of the permutation

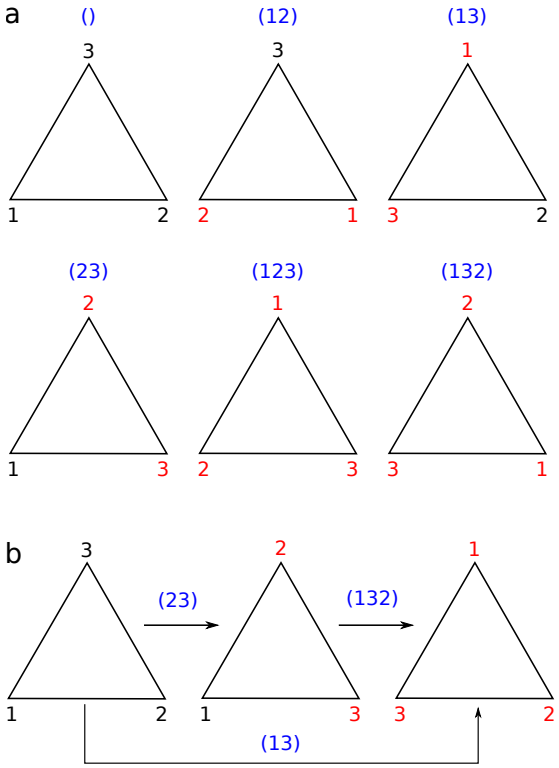

Figure 3.2: (a) The permutations of the S_3 group in blue and the result of their application on the vertices of a triangle. The correspondence is an *isomorphism* between S_3 and the triangle. (b) Graphical representation of the composition of permutations (132)(23) = (13). In red are represented the vertices acted upon by the permutation.

(132) is 3, given that $(132)^3 = (132)(132)(132) = ()$ and the order of (12) is 2 because $(12)^2 = (12)(12) = ()$. The order of an element must not be confused with the order of the group corresponding to the number of its members.

3.3 Representations of Groups

In the application of group theory to the analysis of physical or chemical problems, the group elements usually correspond to symmetry operations carried out on spatial coordinates in $\mathbb{R}, \mathbb{R}^2, \mathbb{R}^3$ (see examples in eq. 2.10, and SO(2) and SO(3)) or, as we will see later, on spin coordinates. When these operations are represented as linear transformations with respect to a coordinate system, then they may be represented as matrices (see SO(2) and SO(3) examples). These matrices form what is called a *representation* of the symmetry group with each element corresponding to a particular matrix. In quantum mechanical applications the symmetry operations are performed on the Hamiltonian(s), whose invariance properties define the symmetry group. In NMR problems nuclear wave functions can then be classified according to the Hamiltonian symmetry operations and a suitable *symmetrized basis* to represent the interactions can be created.

3.4 Homomorphisms and Isomorphisms

Suppose we have two finite groups $\mathcal{G} = \{P_1, P_2, \dots\}$ and $\mathcal{G}' = \{P'_1, P'_2, \dots\}$. The two groups need not to have the same order. Suppose there is a mapping $\sigma : \mathcal{G} \to \mathcal{G}'$ which preserves the composition or product rule. This means that:

$$P'_1 = \sigma(P_1), P'_2 = \sigma(P_2) \quad \Rightarrow \quad \sigma(P_1 P_2) = \sigma(P_1)\sigma(P_2) = P'_1 P'_2 \tag{3.20}$$

If the order of the two groups is the same then this mapping is said to be an *isomorphism* and the groups are *isomorphic* to one another. This is sometimes denoted as $\mathcal{G} \approx \mathcal{G}'$. If the two groups contain a different number of elements then the mapping is a *homomorphism* and the two groups are *homomorphic*. Therefore an isomorphism is a one-to-one

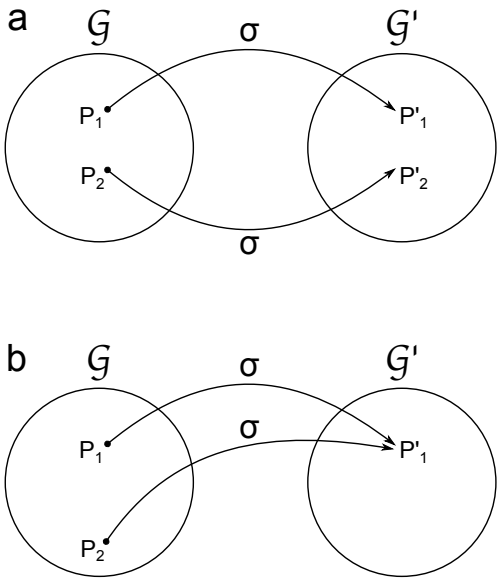

Figure 3.3: (a) Isomorphism between $\mathcal{G}$ and $\mathcal{G}'$. (b) Homomorphism between $\mathcal{G}$ and $\mathcal{G}'$.

correspondence between two groups, and a homomorphism is a multi-to-one correspondence. Isomorphisms and homomorphisms are not limited to finite groups and not even to groups with discrete elements (see example of eq. 3.5).

3.5 Reducible and Irreducible representations

A matrix representation of dimension n of an abstract group $\mathcal{G}$ is a homomorphism or isomorphism between the elements of $\mathcal{G}$ and the group of non singular $n \times n$ matrices. The determinant of each matrix needs to be different from zero for the inverse matrix to exist. The composition operation is the ordinary matrix multiplication. In mathematics an isomorphic representation is called *faithful* representation, whereas a homomorphic representation is called *unfaithful*. The difference will be clearer with an example.

- **Faithful representation**: Let us consider again the group S_3: In Fig. 3.2 the different permutations have been represented on their action on the vertices of a triangle. Let us represent the triangle in a two-dimensional space as in Fig. 3.4. The different permutations exchanging the spatial coordinates can be given the

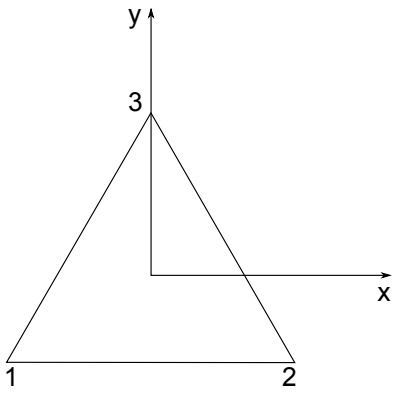

Figure 3.4: The coordinate system used to generate a two-dimensional representation of the symmetry group of a triangle. The origin of the reference frame is the geometrical centre of the triangle.

matrix representation:

$$() = \begin{pmatrix} 1 & 0 \\ 0 & 1 \end{pmatrix} \quad (12) = \begin{pmatrix} -1 & 0 \\ 0 & 1 \end{pmatrix} \quad (13) = \frac{1}{2}\begin{pmatrix} 1 & -\sqrt{3} \\ -\sqrt{3} & -1 \end{pmatrix}$$
$$(23) = \frac{1}{2}\begin{pmatrix} 1 & \sqrt{3} \\ \sqrt{3} & -1 \end{pmatrix} \quad (123) = \frac{1}{2}\begin{pmatrix} -1 & -\sqrt{3} \\ \sqrt{3} & -1 \end{pmatrix} \quad (132) = \frac{1}{2}\begin{pmatrix} -1 & \sqrt{3} \\ -\sqrt{3} & -1 \end{pmatrix} \tag{3.21}$$

By denoting the coordinates of the vertex i as the column vector $V_i = (x_i, y_i)^{\mathbb{T}}$ is clear that:

$$\begin{pmatrix} -1 & 0 \\ 0 & 1 \end{pmatrix} \cdot \begin{pmatrix} x_2 \\ y_2 \end{pmatrix} = \begin{pmatrix} -x_2 \\ y_2 \end{pmatrix} = \begin{pmatrix} x_1 \\ y_1 \end{pmatrix} \qquad \Longleftrightarrow \qquad (12) \cdot V_2 = V_1 \tag{3.22}$$

so that (12) in equation 3.21 is the matrix representation of the permutation (12). The above matrices are a faithful representation of S_3 as there is a one-to-one correspondence between the matrix group and the symmetry operations in S_3. Furthermore it can be verified that the matrix representations of the permutations $(12), (13), (23)$ correspond to geometrical reflections upon planes bisecting one of the triangle's sides and their determinant is -1, while matrices representing $(123), (132)$ correspond to geometrical rotations about the z-axis and their determinant is $+1$.

- **Unfaithful representation**: A different mapping between the elements of S_3 and the set $\{-1, +1\}$ can be considered:

$$\{(12), (13), (23)\} \to \{-1\} \qquad \{(), (123), (132)\} \to \{+1\} \tag{3.23}$$

  According to previous definition this mapping represents a homomorphism between the S_3 permutations and the determinant of their matrix representation. Finally the mapping of all elements to unity is also a trivial representation of any group, though clearly an unfaithful one.

Given a matrix representation D:

$$\{P_1, P_2 \dots\} \quad \xrightarrow{D} \quad \{D(P_1), D(P_2), \dots\} \quad = \quad \{D_1, D_2, \dots\} \tag{3.24}$$

of an abstract group with elements $\mathcal{G} = \{P_1, P_2, \dots\}$, a new representation can be obtained by performing a transformation known as *similarity*:

$$\{B \cdot D_1 \cdot B^{-1}, B \cdot D_2 \cdot B^{-1}, \dots\} \tag{3.25}$$

Such transformation can be thought as a change of basis in the space used for matrix representations. In this notation B is the matrix of the change of basis. Following the definitions of isomorphism and homomorphism it is already known that the representations need not to have the dimension equal to the order of the group. Let us suppose we have representations of dimensions m and n. A representation, in block-diagonal form, of dimension $m + n$ can be realized in the following way:

$$\{\begin{pmatrix} D_1 & 0 \\ 0 & D'_1 \end{pmatrix}, \begin{pmatrix} D_2 & 0 \\ 0 & D'_2 \end{pmatrix}, \} \tag{3.26}$$

where $\{D_1, D_2, \dots\}$ is a n dimensional representation and $\{D'_1, D'_2, \dots\}$ is a m dimensional representation of $\mathcal{G}$. The symbol 0 is used indistinctly to indicate a $n \times m$ or a $m \times n$ matrix as required by its supermatrix position. Each of the $m + n$-dimensional matrices in the new representation is called a *direct sum* of the n- and m-dimensional component matrices. It is indicated by the symbol $\oplus$:

$$\{D_1 \oplus D'_1, D_2 \oplus D'_2, \dots\} \tag{3.27}$$

Representations such as those in eq. 3.27 are termed *reducible* because they are the direct sum of two (or more) representations. More exactly if the *same* similarity transformation brings all of the matrices of a representation into the same block form, then this representation is said to be reducible. Otherwise it is *irreducible*. Irreducible representations cannot be expressed in terms of representations of lower dimensionality. By definition a one-dimensional representation is always irreducible. The representation dis-

cussed in example • **Faithful representation** is irreducible. There is no similarity transformation block-diagonalizing *all* of the matrices. The easiest way to see this is from the point of view of the commutability of two matrices. *If two matrices can be brought into diagonal form by the same similarity transformation, then they commute*. It can be verified that this is not the case for the matrices in example • **Faithful representation**. Irreducible representations can be thought of as the basic components from which all representations can be constructed. Representations of groups in quantum mechanics are an important subject. As will be discussed later, the eigenfunctions of a Hamiltonian will transform under the symmetry operations of that Hamiltonian according to a particular representation of that group. Identifying whether a representation is reducible or irreducible is not always an easy task. A more systematic approach to this question lays on some theorems of representation theory that will only be enunciated. The great orthogonality theorem leads to a simple set of criteria for determining irreducibility.

3.6 The great orthogonality theorem

Let $\{D_1, D_2, \cdots, D_{|\mathcal{G}|}\}$ and $\{D'_1, D'_2, \cdots, D'_{|\mathcal{G}|}\}$ be two inequivalent irreducible representation of $\mathcal{G} = \{P_1, P_2, \cdots, P_{|\mathcal{G}|}\}$ having dimensionality d and d'. The matrices D_α and D'_α in the two representations correspond to the element P_α in $\mathcal{G}$. Then

$$\sum_\alpha (D_\alpha)^*_{ij}(D'_\alpha)_{i'j'} = 0 \tag{3.28}$$

for all matrix elements. For the elements of a single unitary irreducible representation,

$$\sum_\alpha (D_\alpha)^*_{ij}(D_\alpha)_{i'j'} = \frac{|\mathcal{G}|}{d}\delta_{i,i'}\delta_{j,j'} \tag{3.29}$$

where d is the dimension of the representation. If we have k irreducible representations for a finite group each of dimensionality d_k, one of the consequences of the great orthogonality theorem is the following:

$$\sum_k d_k^2 \leq |\mathcal{G}| \tag{3.30}$$

where $|\mathcal{G}|$ is the order of the group $\mathcal{G}$. We can apply these results to the group S_3.

- **S_3**: For the group S_3, we have that $|\mathcal{G}| = 6$ and we have identified two one-dimensional irreducible representations when discussing unfaithful representations and one two-dimensional irreducible representation when defining faithful representations. Using equation 3.29, we have:

$$\sum_k d_k^2 = 1^2 + 1^2 + 2^2 = 6$$

The great orthogonality theorem assures that there are no additional irreducible representations to be considered.

The great orthogonality theorem can be interpreted as a statement about the orthogonality between the matrix elements corresponding to different irreducible representations of a group. However it is often the case that the full matrix representation is not required, but only the *traces* within classes of group elements. They are called *characters*. If the group $\mathcal{G} = \{P_1, P_2, \cdots, P_{|\mathcal{G}|}\}$, we say that P_1 and P_2 are *conjugated* if exists $P_j \in \mathcal{G}$ such that:

$$P_j^{-1} P_1 P_j = P_2 \tag{3.31}$$

A class C is formed by all elements conjugated to one another. In terms of representation theory, elements belonging to the same class C have also the same character χ [68], due to the invariance of the trace of a matrix to similarity transformations. If there are n_α elements in the class from the great orthogonality theorem can be derived that:

$$\sum_{\alpha=1}^{C} n_\alpha \chi_\alpha^k \chi_\alpha^{k'*} = |\mathcal{G}| \delta_{k,k'} \tag{3.32}$$

where k and k' denote different irreducible representations. From the great orthogonality theorem can also be derived a further useful relation:

$$\sum_k \chi_\alpha^k \chi_\beta^{k*} = \frac{|\mathcal{G}|}{n_\alpha} \delta_{\alpha,\beta} \tag{3.33}$$

It is possible to demonstrate [68, 71] that for a finite group *the number of irreducible representations is equal to the number of classes of that group.* The principal use of characters for our purposes, is in the decomposition of reducible representations into irreducible ones. The procedure can be considered analogous to projecting a vector into a complete set of orthogonal basis vectors. The decomposition theorem is fundamental in this accomplishment.

3.7 Decomposition theorem

The character χ_α for the αth class of any representation can be uniquely written in terms of the corresponding characters of the irreducible representations of the group as

$$\chi_\alpha = \sum_k a_k \chi_\alpha^k,$$

where

$$a_k = \frac{1}{|\mathcal{G}|} \sum_\alpha n_\alpha \chi_\alpha^{k*} \chi_\alpha.$$

Tables of characters are central in many chemical and physical applications. As a final example the character table for S_3 and its subgroup C_3 are derived from the previous theorems as an exercise.

- **S_3 character table**: The first step in the construction of the character table is to consider that $|S_3| = 6$ and that there are three classes. There are then three irreducible representations whose dimensionality d_i must satisfy the following equation:

$$d_1^2 + d_2^2 + d_3^2 = 6 \tag{3.34}$$

The unique solution of this equation is $d_1 = 1$, $d_2 = 1$, $d_3 = 2$. There are two one-dimensional irreducible representations and one two-dimensional irreducible representation. In the character table of any group one entry is straightforward: the total-symmetric or identical representation is always a one-dimensional irreducible representation. In addition the characters corresponding to the identity element are equal to the dimensionality of the representation, since they are the trace of the identity matrix with that dimensionality. Therefore the character table for S_3 is:

S_3	()	(12), (13), (23)	(123), (132)
Γ_1	1	1	1
Γ_2	1	α	β
Γ_3	2	γ	δ

where Γ_i denotes the i-th irreducible representation and coefficients α, β, γ and δ should be determined. The great orthogonality theorem in eq. 3.28, is an orthogonality relation for the rows of a character table, and yields for example the following equations:

$$1 + 3\alpha + 2\beta = 0,$$
$$1 + 3\alpha^2 + 2\beta^2 = 6,$$

In addition considering that in this example transpositions (ij) can be interpreted as geometrical reflections and that permutations (ijk) are geometrical rotations, since the one dimensional representations must obey the multiplication table, a further constraint is given by:

$$\alpha^2 = 1 \quad \text{and} \quad \beta^2 = \beta$$

These conditions should be met simultaneously. Therefore $\alpha = -1$ and $\beta = 1$. From equation 3.33:

$$1 + \alpha + 2\gamma = 0,$$
$$1 + \beta + 2\delta = 0,$$

substituting the values for α and β already obtained we finally have:

$$\gamma = 0 \quad \text{and} \quad \delta = -1$$

The complete character table for S_3 is therefore,

S_3	()	(12), (13), (23)	(123), (132)
Γ_1	1	1	1
Γ_2	1	-1	1
Γ_3	2	0	-1

- **C_3 character table**: C_3 is a subgroup of S_3. It is a subset of S_3 formed by the elements $C_3 = \{(), (123), (132)\}$ satisfying the properties of a group. All elements belongs to different classes. For example:

$$(132)(123)(132)^{-1} = (132)(123)(123) = (123), \tag{3.35}$$

and each element is conjugated with itself. There are then three irreducible representations whose dimensionality d_i must satisfy the following equation:

$$d_1^2 + d_2^2 + d_3^2 = 3 \tag{3.36}$$

This implies $d_1 = d_2 = d_3 = 1$. The character table of C_3 is expressed as:

C_3	()	(123)	(132)
Γ_1	1	1	1
Γ_2	1	α	β
Γ_3	1	γ	δ

As a result of the great orthogonality theorem and eq. 3.33, the following results must hold:

$$\begin{aligned} 1 + \alpha + \beta &= 0, \\ 1 + \alpha\alpha^* + \beta\beta^* &= 3 \\ \alpha^2 &= \beta, \end{aligned} \tag{3.37}$$

where it is explicitly accounted for the possibility for α and β to be complex. The orthogonality relation over the columns of the character table leads to $\gamma = \beta$ and $\alpha = \delta$ and the solution is $\alpha = e^{i\frac{2\pi}{3}}$. The character table for C_3 is:

C_3	()	(123)	(132)
Γ_1	1	1	1
Γ_2	1	$e^{i\frac{2\pi}{3}}$	$e^{i\frac{4\pi}{3}}$
Γ_3	1	$e^{i\frac{4\pi}{3}}$	$e^{i\frac{2\pi}{3}}$

The character table of C_3 will be useful when analysing the symmetry properties in molecules containing CH_3 groups.

3.8 Rotations and angular momenta

We already have seen how rotations in space can be represented by matrices. Because rotations affect physical systems, the state ket representing it, in Dirac notation, is expected to look different in different frames of reference.

$$|\alpha\rangle_{\mathrm{R}} = \mathcal{D}(\mathrm{R})\,|\alpha\rangle \tag{3.38}$$

where $\mathcal{D}(\mathrm{R})$ is a rotation matrix. The dimensionality of the state ket is dependent on the spin system considered. Take, as an example, a NMR tube filled with water placed in a strong magnetic field. It can be formalized as an ensemble of spin 1/2 particles (the ^{1}H nuclei) if we disregard the amount of $^1\mathrm{H}_2^{17}\mathrm{O}$ water molecules including a ^{17}O nucleus that has spin 5/2 (^{17}O natural abundance is about 0.03%). In this case proton nuclei can either align parallel or antiparallel with the external magnetic field, or populate a state that is a superposition of those states. In either circumstance the appropriate representation of the state ket can be obtained by a two-entry vector, and as a result the rotation matrix $\mathcal{D}(\mathrm{R})$ is 2×2. The case of heavy water (D_2O) is slightly different. Deuterons nuclei are appropriately described by a three-entry rather than a two-entry vector. Therefore the rotation matrix $\mathcal{D}(\mathrm{R})$ is 3×3.

In order to build the operator $\mathcal{D}(\mathrm{R})$ in its general form, one could proceed in analogy with classical mechanics [38]. In both translations and time evolution the infinitesimal generator operator has the form:

$$U_\epsilon = 1 - iG\epsilon, \tag{3.39}$$

where G is an hermitian operator. For an infinitesimal translation by a displacement dx and an infinitesimal time evolution with time displacement dt:

$$\begin{aligned} G &\to \frac{p_x}{\hbar}, \qquad \epsilon \to dx \\ G &\to \frac{\mathcal{H}}{\hbar}, \qquad \epsilon \to dt \end{aligned} \tag{3.40}$$

In classical mechanics the angular momentum is the generator of rotations in the same way in which momentum and Hamiltonian engender translation and time evolution respectively. Following Sakurai's approach [38] we define the operator J_k as the generator of an infinitesimal rotation about an angle $d\phi$:

$$G \to \frac{J_k}{\hbar}, \qquad \epsilon \to d\phi \tag{3.41}$$

With the operator J_k Hermitian, the unitary infinitesimal rotation operator can be represented:

$$\mathcal{D}(\mathrm{R})(\mathbf{n}, d\phi) = 1 - i\,\frac{\mathbf{J}\cdot\mathbf{n}}{\hbar}d\phi \tag{3.42}$$

A finite rotation about the z-axis by a finite angle ϕ can be attained by:

$$\begin{aligned}\mathcal{D}(\mathrm{R_z})(\phi) &= \lim_{N\to\infty}\left[1 - i\,\frac{\mathbf{J}\cdot\mathbf{n}}{\hbar}\frac{\phi}{N}\right]^N \\ &= \exp(\,\frac{-i\,J_z\phi}{\hbar}) \\ &= 1 - \,\frac{i\,J_z\phi}{\hbar} - \,\frac{J_z^2\phi^2}{2\hbar^2} + \cdots\end{aligned} \tag{3.43}$$

Rotations represented in equation 3.43 allow to explicitly find out the commutation rules for angular momenta [38]:

$$\begin{aligned}\left[J_x, J_y\right] &= i\hbar J_z \\ \left[J_y, J_z\right] &= i\hbar J_x \\ \left[J_z, J_x\right] &= i\hbar J_y\end{aligned} \tag{3.44}$$

From eq. 3.44 can be derived the existence of a new operator $\mathbf{J}^2$ commuting with every J_k and with the non hermitian operators $J_\pm \equiv J_x \pm J_y$:

$$\begin{aligned}\mathbf{J}^2 &\equiv J_xJ_x + J_yJ_y + J_zJ_z \\ \left[\mathbf{J}^2, J_k\right] &= 0 \qquad \forall k \in \{x, y, z\} \\ \left[\mathbf{J}^2, J_\pm\right] &= 0\end{aligned} \tag{3.45}$$

As a result $\mathbf{J}^2, J_z, J_\pm$ share the same eigenvectors and for any given j an orthonormal basis $|j, m_j\rangle$ can be defined such that:

$$\begin{aligned}\mathbf{J}^2\,|j, m_j\rangle &= j(j+1)\,|j, m_j\rangle \\ J_z\,|j, m_j\rangle &= m_j\,|j, m_j\rangle \\ J_\pm\,|j, m_j\rangle &= \left[j(j+1) - m_j(m_j+1)\right]^{\frac{1}{2}}|j, m_j\rangle\end{aligned} \tag{3.46}$$

The quantization of angular momentum in equation 3.46 is a consequence of the angular momentum commutation relationships, which, in turn, follow from the properties of rotations together with the definition of J_k as the generator of rotation.

We are now in a position of studying the matrix elements of the rotation operator $\mathcal{D}(\mathrm{R})$:

$$\mathcal{D}^j_{m'm}(\mathrm{R}) = \langle j, m'_j|\exp(-i\frac{\mathbf{J}\cdot\mathbf{n}}{\hbar}\phi)\,|j, m_j\rangle \tag{3.47}$$

These matrix elements $\mathcal{D}^{j}_{m'm}(\mathrm{R})$ are called Wigner functions. The commutation relationship between $\mathbf{J}^2$ and J_k causes $\mathcal{D}(\mathrm{R})$ to be an eigenket of $\mathbf{J}^2$:

$$\begin{aligned} \mathbf{J}^2\mathcal{D}(\mathrm{R})\,|j,m_j\rangle &= \mathcal{D}(\mathrm{R})\mathbf{J}^2\,|j,m_j\rangle \\ &= j(j+1)\hbar^2\mathcal{D}(\mathrm{R})\,|j,m_j\rangle \end{aligned} \tag{3.48}$$

Rotations cannot change the j value. Rotation matrices of a definite j form a group, and as already stated the most general form of rotation can be attained by means of Euler angles [38]. Let's now consider two angular momenta $\mathbf{J_1}$ and $\mathbf{J_2}$ of particles 1 and 2 respectively. As the two angular momenta evolve in different subspaces:

$$[J_{1k}, J_{2l}] = 0 \qquad \forall\{k,l\} \in \{x,y,z\} \tag{3.49}$$

At the same time the commutation relations in eq. 3.44 are abide by each particle in its relative subspace. The total angular momentum of the entire system can be defined as follows:

$$\mathbf{J} \equiv \mathbf{J_1} \otimes \mathbb{I}_2 + \mathbb{I}_1 \otimes \mathbf{J_2} \qquad \text{usually indicated as} \qquad \mathbf{J} = \mathbf{J_1} + \mathbf{J_2} \tag{3.50}$$

For given values of the angular momenta, j_1 and j_2, the total angular momentum j can assume only certain values according to the triangular inequality [21]:

$$|j_1 - j_2| \leq j \leq (j_1 + j_2) \tag{3.51}$$

As the matrix representation of j_1 and j_2 is $2j_1 + 1$ and $2j_2 + 1$ dimensional, the $2j + 1$ dimensional matrix representation of j can be decomposed in blocks with dimension $|j_1 - j_2|, |j_1 - j_2| + 1, \ldots (j_1 + j_2)$ in the orthonormal complete basis $|j, m_j; j_1 j_2\rangle$. The projection of the uncoupled basis onto the coupled one engenders the Clebsch-Gordan coefficients:

$$C^{jm_j}_{j_1 m_1, j_2 m_2} = \left\langle jm_j, j_1 j_2 | j_1 m_1; j_2 m_2 \right\rangle \tag{3.52}$$

For a given set of j_1 and j_2, $C^{jm_j}_{j_1 m_1, j_2 m_2}$ represent the entries of the unitary transformation linking the coupled basis and the uncoupled one:

$$\begin{aligned} |jm_j; j_1, j_2\rangle &= \sum_{m_1 m_2} C^{jm_j}_{j_1 m_1, j_2 m_2}\,|j_1 m_1; j_2 m_2\rangle\,, \\ |j_1 m_1; j_2 m_2\rangle &= \sum_{jm_j} C^{jm_j}_{j_1 m_1, j_2 m_2}\,|jm_j; j_1 j_2\rangle \end{aligned} \tag{3.53}$$

3.9 Spherical tensor operators

If we consider two column vectors **U** and **V** one can take the Cartesian coordinates of each vector and generate the outer ($\otimes$) product:

$$T_{ij} \equiv U_i V_j \tag{3.54}$$

We have a total of nine components and T_{ij} is defined as a rank-2 Cartesian tensor. For example if $\mathbf{a} = (1, 2, 3)$ and $\mathbf{b} = (4, 5, 6)$, then:

$$\mathbf{a} \otimes \mathbf{b} = \begin{pmatrix} 1 \\ 2 \\ 3 \end{pmatrix} \cdot (4, 5, 6) = \begin{pmatrix} 4 & 5 & 6 \\ 8 & 10 & 12 \\ 12 & 15 & 18 \end{pmatrix}$$

A Cartesian tensor like T_{ij} is reducible. It is indeed possible to decompose it into the sum of different objects that transform differently under rotations. Specifically for the outer product $\mathbf{T} = \mathbf{U} \otimes \mathbf{V}$ we have:

$$U_i V_j = \frac{\mathbf{U} \cdot \mathbf{V}}{3} \delta_{ij} + \frac{\left(U_i V_j - U_j V_i\right)}{2} + \left(\frac{U_i V_j + U_j V_i}{2} - \frac{\mathbf{U} \cdot \mathbf{V}}{3} \delta_{ij} \right) \tag{3.55}$$

The term $\mathbf{U} \cdot \mathbf{V}$ is a scalar product invariant under rotations. The second term $U_i V_j - U_j V_i$ is an antisymmetric tensor that can be written as vector product $\epsilon_{ijk} \, (\mathbf{U} \times \mathbf{V})_k$. Indeed:

$$\begin{aligned} (\mathbf{U} \times \mathbf{V})_k &= \det \begin{pmatrix} e_x & e_y & e_z \\ U_x & U_y & U_z \\ V_x & V_y & V_z \end{pmatrix} \\ &= e_x \left(U_y V_z - V_y U_z \right) - e_y \left(U_x V_z - V_x U_z \right) + e_z \left(U_x V_y - V_x U_y \right) \end{aligned}$$

The second term encompasses therefore three independent components. The last term is a 3×3 symmetric traceless tensor with 5 ($= 6 - 1$) independent components. Overall the number of independent components of **T** is:

$$3 \times 3 = 1 + 3 + 5 \tag{3.56}$$

It can be noticed that the numbers on the right-hand side of the above equation match the multiplicities of objects with angular momentum $l = 0$, $l = 1$, and $l = 2$ respectively. This suggests a possible decomposition of **T** in terms of spherical harmonics with $l = 0$, 1 and 2. Indeed equation 3.55 represents an example of decomposition of a Cartesian tensor into irreducible spherical tensors.

In general we define a spherical tensor operator T^k_q of rank k as a set of $2k + 1$

operators transforming under rotation as an angular momentum $|k, q\rangle$:

$$\mathcal{D}^{\dagger}(\mathrm{R})T^{k}_{q}\mathcal{D}(\mathrm{R}) = \sum_{q'=-k}^{k} \mathcal{D}^{k}_{qq'}(\mathrm{R})T^{k}_{q'} \tag{3.57}$$

Spherical tensors and spherical tensor operators will be largely applied in the following discussions and analysis as a convenient way to represent Hamiltonian operators whose symmetry properties under permutation of nuclear spin labels we are interested in. The starting representation of a Hamiltonian operator will usually be of the form [38, 72, 73]:

$$\mathcal{H}^{\Lambda} = \sum_{l}\sum_{m=-l}^{l}(-1)^{m}A^{\Lambda}_{lm}(t)T^{\Lambda}_{l,-m} \tag{3.58}$$

where Λ denotes the specific spin interaction considered, A^{Λ}_{lm} is a spherical tensor of rank l and component m and $T^{\Lambda}_{l,-m}$ is a spherical tensor operator of rank l and component $-m$. If Λ for example is the intra-molecular dipolar interaction mechanism:

$$A^{\Lambda}_{lm} = A^{\mathrm{DD}}_{20} = -(\sqrt{6}\mu_0/4\pi)\gamma_i\gamma_j\hbar r^{-3}_{ij} \tag{3.59}$$

and the spherical tensor operators (we drop the superscript $\Lambda = \mathrm{DD}$ for simplicity) are:

$$\begin{aligned} T_{2,\pm2} &= \frac{1}{2}I^{\pm}_1 \cdot I^{\pm}_2 \\ T_{2,\pm1} &= \frac{1}{2}(I^{\pm}_1 \cdot I_{2z} - I_{1z} \cdot I^{\pm}_2) \\ T_{2,0} &= -\frac{1}{2\sqrt{6}}(I^{-}_1 \cdot I^{+}_2 + I^{+}_1 \cdot I^{-}_2) + \sqrt{\frac{2}{3}}I_{1z}I_{2z} \end{aligned} \tag{3.60}$$

3.10 The Wigner-Eckart Theorem

As we have seen above nuclear spin Hamiltonians are often expressed in terms of irreducible spherical tensor operators (ISTOs) [38, 72, 73]. The matrix elements of ISTOs are governed by the Wigner-Eckart theorem [38, 73]:

$$\langle j, m_j | T_{l,q} | j' m'_j \rangle = \langle j | T_l | j' \rangle C^{jm_j}_{lqj'm'_j} \tag{3.61}$$

where the reduced matrix element $\langle j | T_l | j' \rangle$ is independent of m_j, q and m'_j and $C^{jm_j}_{lqj'm'_j}$ is a Clebsch-Gordan coefficient. This leads to the rotational selection rule:

$$\langle j | T_l | j' \rangle = 0 \quad \text{if} \quad l \notin \{|j - j'|, |j - j'| + 1 \ldots |j + j'|\} \quad \text{or} \quad m_j \neq q + m'_j \tag{3.62}$$

This selection rule is generated by the rotational symmetries of the nuclear spin states and the spin Hamiltonian components.

According to the Wigner-Eckart theorem operating with a spherical tensor operator of rank l on an angular momentum eigenstate is like adding a state with angular momentum l to the angular momentum eigenstate. The matrix elements one finds for the spherical tensor operator are proportional to a Clebsch-Gordan coefficient, which arises when considering adding two angular momenta.

Let us consider the example of two spins 1/2 added together. One example is the case of two homo-nuclei in an A_2 system. *How do the angular momentum eigenstates transform upon application of a Hamiltonian operator of a given rank?* The answer to this question consists in a two-step application of the Wigner-Eckart theorem:

1. Determine the angular momentum eigenstates for the entire system.

2. Apply the Wigner-Eckart theorem to the angular momentum eigenstates.

We denote the spin of the particles as $\mathbf{I_1} = 1/2$, $\mathbf{I_2} = 1/2$ and we wish to find out the spin angular momentum of the system $\mathbf{I}$. According to equation 3.51 we have:

$$\mathbf{I} = \mathbf{I_1} + \mathbf{I_2} = \begin{cases} \frac{1}{2} - \frac{1}{2} = 0 & \uparrow\downarrow \\ \\ \frac{1}{2} + \frac{1}{2} = 1 & \uparrow\uparrow \end{cases} \tag{3.63}$$

Therefore the system is appropriately described by a total angular momentum 0 and 1. The spin-zero manifold is named *singlet* as there is only the value $m_I = 0$. The spin-one manifold includes the three possible values $m_I = -1, 0, 1$, and is consequently denoted as *triplet*. The nuclear spin wave functions can be classified accordingly as:

$$\begin{aligned} |S_0\rangle &= \frac{1}{\sqrt{2}}\left(|\alpha\beta - \beta\alpha\rangle\right) \\ |T_{-1}\rangle &= |\beta\beta\rangle \\ |T_0\rangle &= \frac{1}{\sqrt{2}}\left(|\alpha\beta + \beta\alpha\rangle\right) \\ |T_1\rangle &= |\alpha\alpha\rangle \end{aligned} \tag{3.64}$$

The Wigner-Eckart theorem can now be applied to establish whether transitions between singlet and triplet wave functions can be promoted by a Hamiltonian operator of a given rank. Let us consider a rank-2 operator, as for example the internal dipolar Hamiltonian in eq. 3.58, coupling together singlet and triplet:

$$\langle S_0| T^{\mathrm{DD}}_{2,m} |T_{1m'}\rangle = \langle 0| T^{\mathrm{DD}}_2 |1\rangle C^{00}_{2m1m'} \tag{3.65}$$

Now, the application of the rank-2 operator $T^{\mathrm{DD}}_{2,m}$ onto the triplet state $|T_{1m'}\rangle$ has to be thought as the addition of a angular momentum **2** with an angular momentum **1**. There-

fore:

$$\mathbf{1}+\mathbf{2}=\begin{cases}|\mathbf{1}-\mathbf{2}|=\mathbf{1}\\ |\mathbf{1}-\mathbf{2}|+\mathbf{1}=\mathbf{2}\\ \mathbf{1}+\mathbf{2}=\mathbf{3}\end{cases} \tag{3.66}$$

As $\mathbf{0}\notin\mathbf{2}+\mathbf{1}$ no transitions between singlet and triplet occur. However given that $\mathbf{1}\in\mathbf{2}+\mathbf{1}$ a rank-1 nuclear interaction as CSA can induce singlet-triplet transitions.

3.11 Summary

The beginning of this chapter presents the formal definition of group as a collection of objects related one another by the four properties: closure, associativity, identity and inverse. Groups may be formed by a finite or infinite number of elements. Rotations in 2D or 3D are examples of infinite groups as depending on an angular parameter that can be varied continuously. On the other hand the permutation of three objects S_3 and its subgroup C_3 are examples of finite groups that will be useful when discussing the symmetry properties of methyl groups.

In practical applications rather than manipulating members of the group itself, it is convenient to work with their representations. In particular a N-dimensional matrix representation of a group is a mapping between every member of the group and the space formed by $N\times N$ square matrices. If all members of the group have a different matrix representation then the mapping (representation) is said faithful. Otherwise it is unfaithful.

The orthogonality theorems are introduced without any derivation. They are instrumental in deriving the character tables of any permutation symmetry group, which allows in turn the classification of nuclear wave functions and spin operators as will be hopefully clear in the next chapters. The character tables of S_3 and C_3 are derived as an example.

The rotation operator acting on spin coordinates is presented following the approach of Sakurai [38]. Addition of angular momenta and definition of spherical tensor operators are briefly reviewed to introduce the Wigner-Eckart theorem that can be fruitfully applied in many quantum mechanical problems.

The toolbox presented in this chapter does not pretend to be neither exhaustive or complete, but it has been tailored to introduce problems that will be further examined in the Theory chapter and as a complement in the experimental analysis of the Experiments chapter.

Part II

Permutation symmetry

Chapter 4

Theory

4.1 Motivation

When introducing the mathematical toolbox that will be used to analyse the molecular systems discussed in this thesis, we were often concerned with transformations leaving the geometrical appearance of an object unchanged after being acted upon by a symmetry operation. In molecular spectroscopy a typical case is the geometrical appearance of a molecule in its equilibrium configuration [40, 67]. However it is in general rather unclear how the symmetry properties of a molecule at equilibrium have anything to do with the physical description of the same system while undergoing rotations in space, vibrations and even changes in the electronic state. Molecular spectroscopy describes these phenomena in terms of suitable Hamiltonian operators. Symmetry has been used ever since the early nineteen-thirties [74] to investigate the electronic structure of polyatomic molecules and to classify the molecular symmetry properties of non-rigid systems such as ethane and hydrazine which can pass from one configuration to another [75]. In our case, as NMR is concerned with the nuclear spins, a useful symmetry theory is expected to investigate the symmetry properties of nuclear spin Hamiltonians in order to gather information on nuclear spin states, and in particular on long-lived states. The theory developed can be important in describing different NMR experiments [2–5, 10, 27, 51, 55], and makes it possible not only to identify long-lived nuclear spin species [59], but offers the criteria to establish whether they are experimentally accessible and what is the maximum obtainable conversion under a unitary transformation (excluding relaxation) [14–17]. It is important to underline that permutation analysis has been employed before: R.G. Jones used symmetry analysis and permutation symmetry theory in describing a variety of experimental scenarios of interacting and non-interacting groups of spins [76]. In the following we will apply permutation symmetry theory in the context of nuclear long-lived states analysis. This chapter is organised as follows:

- Symmetry and NMR

- Nuclear spin permutation symmetries
- Symmetrized basis and vanishing integral rule
- Spin System definition
- Conserved quantities in the spin system
- Symmetry of the coherent Hamiltonian
- Symmetry of the fluctuating Hamiltonians
- Symmetry of the complete Hamiltonian
- Approximations
- LLS accessibility via coherent mechanisms
- Maximum conversion to LLS
- LLS: from near eigenstates to population imbalances
- Summary

The study and analysis of long-lived nuclear spin orders involves either permutation and rotational symmetries. They have both been introduced when presenting the mathematical toolbox (see section 3.2 and section 3.8). In general they are complementary as they both need to be considered when examining long-lived orders.

4.2 Symmetry and NMR

The problem of identifying the eigenkets of a time-independent nuclear spin Hamiltonian can be dramatically simplified by accounting for the symmetry properties of the system [76–78]. This has been early recognized by many authors as for example Woodman [79] in the sixties and Pyper [80, 81] in the early seventies. Even before that in the nineteen-thirties Mulliken applied group theory as a tool for classifying the states of polyatomic molecules [74].

The basis kets for Hilbert space representations can indeed be chosen such that they transform as the irreducible representations of a group including a certain number of symmetry operations. These operations can be expressed as matrices that commute with the matrix representation of the Hamiltonian. As pointed out by Pyper [80, 81] the advantage of this procedure is double: on the one hand there are no non-zero matrix elements of the Hamiltonian between basis kets transforming according to different irreducible representations, and on the other hand the radiofrequency field induces no transitions between eigenkets of different symmetry. As we will see in the following these are crucial properties in the long-lived states analysis. The application of the

symmetry analysis has been extended by Longuet-Higgins [75] beyond the range represented by rigid molecular systems to non-rigid molecules that have more than one equilibrium configuration.
In general terms, the relevant symmetry group largely depends on the problem being addressed and for this reason it is somehow arbitrary. In molecular spectroscopy, the most general procedure to derive the *the molecular symmetry group* [40, 67] is the one described by Bunken and Jensen: it requires the definition of the CNPI (Complete Nuclear Permutation Inversion group) that includes all the possible permutations of identical nuclei with and without the inversion operation (it is the operation consisting in the inversion of all nuclear and electronic coordinates leaving the spin of the particles unchanged). Some of the symmetry operations in the CNPI group may be physically unfeasible or, stated in a different way, the feasibility of a symmetry operation depends on a certain set of assumptions. The molecular symmetry group is exactly the CNPI group purified from the unfeasible operations. In addition, the observed structure and effective symmetry of a molecule also depends on the technique used to study it. The time scale of ultraviolet spectroscopy is very short and short-lived species including several conformers and rotamers each with its own symmetry properties can be studied [76]. The symmetry of a system, object of NMR analysis, can be considerably different from the symmetry of the molecule as a whole for multiple reasons, as for example:

- A limited number of nuclei has a non-zero nuclear magnetic moment
- Rapid internal motions can impose particular symmetries

In the following, as opposite to the molecular symmetry group description, we will only be concerned with nuclear spins and the symmetry operations will never regard electronic coordinates and spins. In addition during the discussion it is also often necessary to introduce a certain set of approximations in order to treat the problem from the symmetry point of view (see section 4.18). The role and the extent of these approximations' validity is at the very core of this LLS description.

4.3 Permutation symmetries

Permutation operators for nuclear spins are denoted by symbols of the form $(ijk\ldots n)$ indicating the cyclic permutation of nuclear spin labels $i \rightarrow j$, $j \rightarrow k\ldots$, $n \rightarrow i$. Permutation operators may be applied to kets and to operators, for example:

$$(123)\,|\alpha\beta\beta\rangle = |\beta\alpha\beta\rangle \qquad \text{and} \qquad (123)I_{1z}I_{2x}I_{3y}(123)^{-1} = I_{1y}I_{2z}I_{3x} \tag{4.1}$$

The group formed by the nuclear spin permutations that are symmetry operations for an operator is the *permutation symmetry group* of that operator. We have seen in chapter 3 that a group representation is an isomorphism between the n elements of a group and the group of $m \times m$ matrices with real/complex entries. For nuclear spin permutations,

once defined an orthonormal and complete basis for the Hilbert space, every symmetry operation can be given a matrix representation. Saying that the ideal permutation P_i is a symmetry operation for the operator O, is equivalent to say that the matrix $\mathbb{P}_i$ representing P_i commutes with the matrix $\mathbb{O}$ representing O:

$$\mathbb{P}_i \cdot \mathbb{O} \cdot \mathbb{P}_i^{-1} = \mathbb{O} \qquad \Longleftrightarrow \qquad [\mathbb{P}_i, \mathbb{O}] = 0, \tag{4.2}$$

From now onward the same symbol for an operator and its matrix representation will be used. Permutations operators forming a symmetry group for the operator O, *all* commute with O. If we consider for example, in a three-spin system, the operator:

$$T_{00}^{123} = \mathbf{I}_1 \cdot \mathbf{I}_2 + \mathbf{I}_1 \cdot \mathbf{I}_3 + \mathbf{I}_2 \cdot \mathbf{I}_3$$

it is easy to verify that all elements P_i of $S_3 = \{(), (12), (13), (23), (123), (132)\}$ leave the operator invariant. This can be formally expressed in two equivalent ways:

$$P_i T_{00}^{123} P_i^{-1} = T_{00}^{123} \qquad \text{and} \qquad [P_i, T_{00}^{123}] = 0 \qquad \forall P_i \in S_3, \tag{4.3}$$

in other words S_3 is the permutation group of T_{00}^{123}.

4.4 Symmetrized Basis and vanishing integral rule

Consider an operator $\mathcal{H}$ which commutes with all elements of the group $\mathcal{G}$=$\{P_1 \ldots, P_{|\mathcal{G}|}\}$. We denote the irreducible representations as Υ^i, with $i \in \{1, 2 \ldots, n\}$ and $n \leq |\mathcal{G}|$. The eigenstates of $\mathcal{H}$:

$$\mathcal{H} |r\rangle = \lambda_r |r\rangle \tag{4.4}$$

can be classified according to the irreducible representations of $\mathcal{H}$. By using the projection operator formalism [40, 67, 68, 71] a symmetrized basis set in Hilbert space can be constructed. One of the typical issues in different types of spectroscopy arises when trying for example to establish which energy levels can be coupled by an external perturbation $\mathcal{H}^1$. It can be demonstrated[40, 67, 68, 71] that only if the total-symmetric representation Υ^{symm} is included in the representation Υ^1 of $\mathcal{H}^1$, then the integral

$$\mathcal{H}^1_{sr} = \langle s| \mathcal{H}^1 |r\rangle \tag{4.5}$$

is different from zero. The total-symmetric representation is an homomorphism between all the elements of the group and the element 1. It is an unfaithful one-dimensional representation for any group. In order to have a $\mathcal{H}^1$-induced coupling between two eigenstates $|r\rangle$ and $|s\rangle$ transforming as the irreducible representations Υ^r and Υ^s respec-

tively, the following relation should be satisfied:

$$\langle s|\,\mathcal{H}^1\,|r\rangle \neq 0 \qquad \Longleftrightarrow \qquad \Upsilon^{symm} \subseteq \Upsilon^{s*} \otimes \Upsilon^1 \otimes \Upsilon^r \tag{4.6}$$

For $\mathcal{H}^1_{sr}$ to be different from zero, its representation must be of the form:

$$\Upsilon^1 = a_s \Upsilon^{symm} \oplus \ldots \qquad \text{with} \qquad a_s \neq 0 \tag{4.7}$$

4.5 Spin system definition

An NMR sample can be defined as a collection of independent and identical spin systems: an *ensemble* [21]. The definition of spin system is important and involves some idealisations discussed explicitly in section 4.18. For example a sample containing H_2 molecules can be represented as an ensemble comprising about 10^{22} spins that, to a good approximation, do not influence each other. The statistical description using the density matrix approach [41] involves matrices whose dimension is of the order of $(2I+1)^N$ where I denotes the spin, and N the number of spins. More generally we will encounter spin systems composed of N coupled spins, denoted by $\{I_1, I_2 \ldots, I_N\}$ of different isotopic types $I, S \ldots, W$. The total number of spins can therefore be decomposed as:

$$N = N_I + N_S + \cdots + N_W \tag{4.8}$$

A general quantum state of the spin system can be regarded as a vector in the $\mathbb{N}_H$-dimensional Hilbert space whose dimension is:

$$\mathbb{N}_H = \prod_{i=1}^{N} (2I_i + 1) \tag{4.9}$$

For coupled spins-1/2, $\mathbb{N}_H = 2^N$. Similarly a spin operator can be regarded as a vector in the $\mathbb{N}_L$-dimensional Liouville space [41]. The dimensions of the two spaces are related: $\mathbb{N}_L = \mathbb{N}_H^2$. The rigorous formalization of even relatively small spin systems can require the use of considerably large matrices and computational effort. A convenient approach is to tailor the spin system according to the problem to be analysed. A chemical and physical insight on the network of interactions occurring for a certain phase of matter and time scales, is usually the ground for this initial idealisation to be made. As a result macroscopic observables are predicted and analysed in a Hilbert or Liouville space obtained not from $\sim 10^{20}$ spins but usually, in this work and in literature, from less than 10 spins. For example $^{13}C_2$-diphenyl acetylene in ref. [4] is treated as a six-spin system, AFD and AMD in ref. [55] are formalized as four-spin systems, paraethanol in Ref. [56] and $^{13}C_2$-**I** in ref. [10] are considered under many purposes as two-spin systems (although in Ref. [56] a third spin is essential for detection purposes). Important

mechanisms driving formation and diffusion of enhanced nuclear spin polarization in large-spin ($\sim 10^{20}$) environments such as the DNP solid effect, direct and indirect cross effects and thermal mixing are also formalized resorting to relatively low-dimensional spin systems [41, 82–84].

4.6 Time dependent Hamiltonian

The ensemble of spin nuclei evolves subjected to time-dependent interactions collectively expressed by a spin Hamiltonian operator $\mathcal{H}(t)$ accounting for internal interactions between the spin system and the molecular environment on one side, and external interactions with NMR apparatus on the other side. We therefore decompose $\mathcal{H}(t)$ into

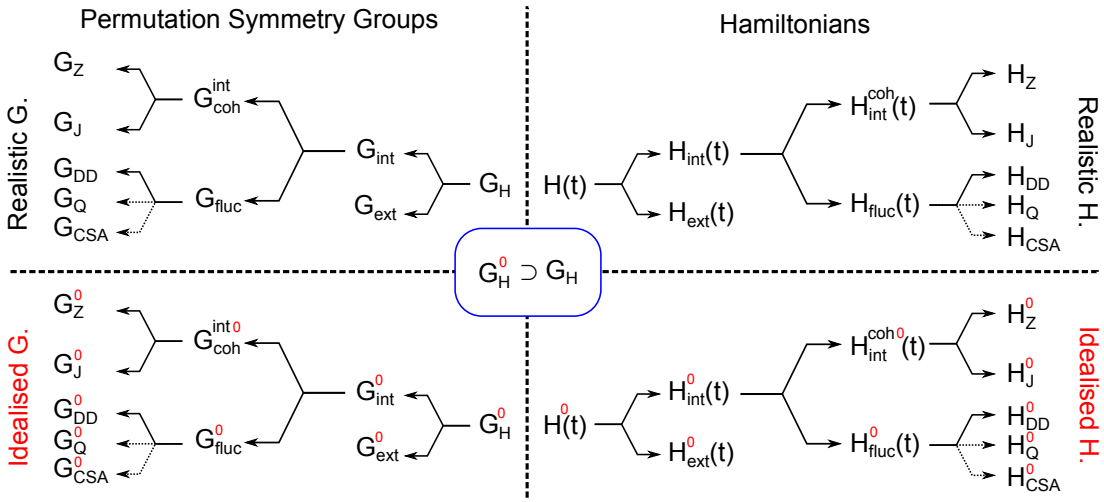

Figure 4.1: On top right half of the picture the time-dependent Hamiltonian is decomposed into an internal $\mathcal{H}_{\text{int}}$ and external $\mathcal{H}_{\text{ext}}$ parts. The internal part is subsequently divided into its coherent $\mathcal{H}_{\text{int}}^{\text{coh}}$ and fluctuating $\mathcal{H}_{\text{fluc}}$ components. As we focus on a solution state type of description $\mathcal{H}_{\text{int}}^{\text{coh}}$ is formed by a Zeeman contribution $\mathcal{H}_Z$, and a J coupling term $\mathcal{H}_J$. Many fluctuating terms can be identified as, for example, the internal dipolar, quadrupolar and chemical shift interactions. We consider, unless stated otherwise, the dipolar Hamiltonian $\mathcal{H}_{\text{DD}}$ as the main and sole relaxation mechanism. On bottom right, following idealisations described in section 4.18, an analogue idealised structure denoted with a red superscript is shown and will be used in LLS investigation. On the top left hand side of the picture the realistic permutation symmetry groups for every corresponding Hamiltonian. On the bottom left the corresponding idealised counterpart. The idealised symmetry group for the complete Hamiltonian (see section 4.7), used in LLS analysis, has a higher symmetry than the realistic complete Hamiltonian.

two time-dependent terms:

$$\mathcal{H}(t) = \mathcal{H}_{\text{int}}(t) + \mathcal{H}_{\text{ext}}(t) \tag{4.10}$$

The internal term acquires a time-dependence either through local internal motions and the stochastic tumbling of the molecules (and in some cases bulk motion of the sam-

ple as a whole as is the case in MAS-NMR [21, 85]), while the time-dependence of the external term derives from the sequence of external magnetic fields that is applied by the apparatus [57]. The internal Hamiltonian contains direct terms for the interactions among nuclear spins and with the electronic environment (the dipole-dipole and quadrupole couplings) as well as indirect terms in which the electrons mediate interactions of the nuclear spins with each other (J couplings), with the external magnetic field (chemical shifts) and with the molecular angular momentum (spin-rotation) [21, 41, 86]. A further classification distinguishes between *coherent* interactions interesting in the same way all members of the ensemble, and stochastic *fluctuating* terms that are in general different for different members of the ensemble and which fluctuate in time. Although the fluctuating part of the spin Hamiltonian has zero average when taken over the ensemble, it still induces transverse magnetic field components that are in general responsible for the sample's thermalization towards Boltzmann equilibrium. Mathematically:

$$\mathcal{H}_{\text{int}}(t) = \mathcal{H}^{\text{coh}}_{\text{int}}(t) + \mathcal{H}_{\text{fluc}}(t) \tag{4.11}$$

where for a solution state NMR sample,

$$\langle \mathcal{H}_{\text{fluc}} \rangle \;=\; 0 \tag{4.12}$$

The $\langle \dots \rangle$ denotes an ensemble average. The theory of long-lived states requires a close examination of the symmetries of both the internal and the external Hamiltonian, including the stochastic terms that are responsible for nuclear spin relaxation. The sole consideration and analysis of coherent terms can sometimes lead to deceptive conclusions [55].

4.7 Conserved quantities in the spin system

The coherent and fluctuating terms in eq. 4.10 are responsible for the spin system evolution in time. The main purpose of long-lived states analysis is the identification and characterization of conserved quantities in the spin system, i.e. entities that do not evolve (practically they evolve slowly) in time [57, 59]. In this section we introduce the general framework that can be used to identify the number and structure of the conserved quantities in any spin system in terms of permutation symmetry.
The state of a system at any given time can be obtained by the density matrix operator $\rho(t)$. The Liouville-von Neumann equation gives the time evolution of $\rho(t)$ under the time-dependent Hamiltonian in equation 4.10:

$$\frac{\partial}{\partial t}\rho(t) = -i[\mathcal{H}(t), \rho(t)] \tag{4.13}$$

A nuclear spin state is a conserved quantity for the spin system if the corresponding operator $\rho_{LLS}(t)$ commutes with $\mathcal{H}(t)$:

$$\frac{\partial}{\partial t}\rho_{LLS}(t) = -i[\mathcal{H}(t), \rho_{LLS}(t)] = 0 \tag{4.14}$$

The Hamiltonian is usually decomposed as the sum of several terms that are related to different spin interactions and includes according to Fig. 4.1, coherent and stochastic contributions. The structure of the Hamiltonian is in general as follows:

$$\mathcal{H}(t) = \mathcal{H}_1(t) + \mathcal{H}_2(t) + \cdots + \mathcal{H}_p(t) \tag{4.15}$$

Each term $\mathcal{H}_i(t)$ representing a different spin interaction can be assigned an associated permutation symmetry group $\mathcal{G}_i$. If a permutation symmetry operation P_j is a symmetry operation for each $\mathcal{H}_i(t)$, then it is also a symmetry operation for $\mathcal{H}(t)$.

$$[\mathcal{H}_i(t), P_j] = 0 \quad \forall i \in \{1, 2 \ldots, p\} \qquad \Longrightarrow \qquad [\mathcal{H}(t), P_j] = 0 \tag{4.16}$$

The permutation symmetry group of $\mathcal{H}(t)$ is therefore formed by the permutation symmetry operations shared by every $\mathcal{H}_i(t)$:

$$\mathcal{G} = \mathcal{G}_1 \cap \mathcal{G}_2 \cap \cdots \cap \mathcal{G}_p \tag{4.17}$$

Note that $\mathcal{G}$ can never be empty given that the identity operator () is always a symmetry operation for any $\mathcal{H}_i(t)$. Suppose that $\mathcal{G} = \{P_1 \ldots P_j \ldots P_{|\mathcal{G}|}\}$. The number of conjugacy classes in $\mathcal{G}$ defines the number of irreducible representations.
Let us now consider a population operator representing a conserved quantity for the spin system under analysis. Such an operator is unaffected by any thermalization process leading the spin system to Boltzmann equilibrium and, as a result, its spin population is ideally constant at any time. However this accomplishment requires that the corresponding nuclear spin state is "uncoupled" or "disconnected" [2, 5, 18] from any other nuclear spin state under the action of any term included in $\mathcal{H}(t)$. The vanishing integral rule in section 4.4 can offer a symmetry argument in order to establish whether a nuclear spin state is totally disconnected from any other spin state. However if the state was to be utterly disconnected, its lifetime would be infinite. This is certainly never the experimental case. The analytic study of LLS uses a set of approximations that are further discussed in section 4.18. For example some approximations are immediately introduced in the definition of spin system and only a few relevant thermalization interactions are usually considered. In reality, the limited validity of these approximations leads to a finite lifetime for the LLS. The strategy that will be followed in the LLS analysis consists:

1. in the identification of the (approximated) symmetry group of $\mathcal{H}^{\text{coh}}$ ($G_{\text{coh}}^{\text{int}0}$ in

	()	(12)
Υ^g	1	1
Υ^u	1	-1

Table 4.1: The two-spin system character table for the permutation symmetry group including the identity operation () and the transposition (12). The irreducible representations are indicated as Υ^g (the total-symmetric representation) and Υ^u.

Fig. 4.1) and the consequent classification of the nuclear wave functions forming a basis for the Hilbert space.

2. The further investigation of the (approximated) symmetry group for $\mathcal{H}_{\text{fluc}}$ (G^0_{fluc} in Fig. 4.1) will allow to establish which relevant integrals are vanishing.

Once again it is worth stressing that the identification of the symmetry group for a given Hamiltonian relies on a set of approximations leading to the formalization of approximated or idealised symmetry properties (indicated with the superscript ^{0} in Fig. 4.1). The role of these approximations, that is the essence and a major limitation of the current analysis, will be reviewed in section 4.18. In the following two basic examples show how the vanishing integral rule can be applied in the LLS analysis.

4.8 States spanning the same irreducible representation

In a homo-nuclear two-spin system, if two nuclear spin states transform according to the same irreducible representation they can in general be coupled together either by $\mathcal{H}_{\text{ext}}(t)$, that acts symmetrically on spins, and/or by $\mathcal{H}_{\text{int}}(t)$. When this occurs the nuclear spin population of these states tends to equilibrate towards a Boltzmann distribution in a time scale characteristic of the nuclear energy levels considered. Using a symmetry adapted basis set nuclear wave functions can be classified into singlet and triplets that are antisymmetric and symmetric with respect to the spin permutation exchanging the labels of the two spins (see Table 4.1). As an example the operator $I_{1x} + I_{2x}$ can be classified according to the irreducible representations in Table 4.1 and its capability to promote transitions within a manifold of defined symmetry investigated:

$$\begin{aligned}
|S\rangle &\sim \Upsilon^u \\
|T_i\rangle &\sim \Upsilon^g \qquad \forall i \in \{-1, 0, 1\} \\
I_{1x} + I_{2x} &\sim \Upsilon^g \\
\langle T_i | I_{1x} + I_{2x} | T_j \rangle &\text{ can be } \neq 0 \quad \text{and} \quad \Upsilon^g \subseteq \Upsilon^g \otimes \Upsilon^g \otimes \Upsilon^g \\
\langle S | I_{1x} + I_{2x} | S \rangle &\text{ can be } \neq 0 \quad \text{and} \quad \Upsilon^g \subseteq \Upsilon^{u*} \otimes \Upsilon^g \otimes \Upsilon^u
\end{aligned} \tag{4.18}$$

where the symbol $\sim$ reads "transform as" or "spans the", Υ^g and Υ^u denote the symmetric (or *gerade*) and antisymmetric (or *ungerade*) irreducible representations with respect to the label exchange of the two spins. The operator $I_{1x} + I_{2x}$ represents the

a) $\frac{1}{\sqrt{2}}\times$

	$\|S\rangle$	$\|T^1\rangle$	$\|T^0\rangle$	$\|T^{-1}\rangle$
$\|S\rangle$	0	0	0	0
$\|T^1\rangle$	0	0	1	0
$\|T^0\rangle$	0	1	0	1
$\|T^{-1}\rangle$	0	0	1	0

b)

	$\|S\rangle$	$\|T^1\rangle$	$\|T^0\rangle$	$\|T^{-1}\rangle$
$\|S\rangle$	0	0	1	0
$\|T^1\rangle$	0	0	0	0
$\|T^0\rangle$	1	0	0	0
$\|T^{-1}\rangle$	0	0	0	0

Figure 4.2: Matrix representations of operators: in a) $I_{1x} + I_{2x}$ and in b) $I_{1z} - I_{2z}$ for a two-spin system in singlet triplet basis.

operatorial form of a transverse magnetic field that is typically used in NMR, MRI or ESR to excite the sample's transverse magnetization. As shown in Fig. 4.2-a the non zero matrix elements, in the representation of $I_{1x} + I_{2x}$, are in the triplet manifold that is formed by nuclear wave functions transforming as Υ^g. Therefore according to equation 4.18 transverse electromagnetic radiation can induce transitions within the triplet subspace. Indeed population operators in the symmetric manifold equilibrate exponentially to their equilibrium Boltzmann distribution with a T_1 time constant. In a similar fashion an antisymmetric operator such as $I_{1z} - I_{2z}$ would not inter-convert nuclear spin states within the same manifold.

$$\begin{aligned} I_{1z} - I_{2z} &\sim \Upsilon^u \\ \langle T_i | I_{1z} - I_{2z} | T_j \rangle &= 0 \qquad \text{and} \qquad \Upsilon^g \not\subseteq \Upsilon^u = \Upsilon^g \otimes \Upsilon^u \otimes \Upsilon^g \\ \langle S | I_{1z} - I_{2z} | S \rangle &= 0 \qquad \text{and} \qquad \Upsilon^g \not\subseteq \Upsilon^u = \Upsilon^u \otimes \Upsilon^u \otimes \Upsilon^u \end{aligned} \tag{4.19}$$

In Fig. 4.18-b non-zero matrix elements representing $I_{1z} - I_{2z}$ do not inter-convert symmetric states.

4.9 States spanning different irreducible representations

Symmetry does not prohibit states belonging to different irreducible representations to be coupled together by suitable operators. If we consider again the previous two-spin system, we have that:

$$\begin{aligned} |S\rangle &\sim \Upsilon^u \\ |T_i\rangle &\sim \Upsilon^g \qquad \forall i \in \{-1, 0, 1\} \\ I_{1z} - I_{2z} &\sim \Upsilon^u \\ \langle S | I_{1z} - I_{2z} | T_i \rangle &\neq 0 \qquad \text{and} \qquad \Upsilon^g \subseteq \Upsilon^{u*} \otimes \Upsilon^u \otimes \Upsilon^g \end{aligned} \tag{4.20}$$

According to equation 4.20 two nuclear spin states transforming as two different irreducible representations can be coupled together by an antisymmetric operator such as $I_{1z} - I_{2z}$. We can think this operator as representing a symmetry breaking mechanism formalizing a chemical shift difference between the two spins [27, 28, 59]. The operator $I_{1z} - I_{2z}$ will result important when discussing later in section 4.21 the accessibility problem on the LLS analysis. In two-spin systems this is the only coherent operator acting asymmetrically upon the two spins. In multi-spin environments the coupling network among members of the spin system may allow for other asymmetric coherent operators to be considered: for solution-state NMR samples, $J_{1i} I_{1z} \cdot I_{iz} - J_{2i} I_{2z} \cdot I_{iz}$. However when considering, in the two-spin example, whether a symmetric operator such as $I_{1x} + I_{2x}$ can induce transitions between nuclear spin states spanning different manifolds the outcome is different.

$$\langle S | I_{1x} + I_{2x} | T \rangle = 0 \qquad \text{and} \qquad \Upsilon^g \not\subset \Upsilon^u = \Upsilon^{u*} \otimes \Upsilon^g \otimes \Upsilon^g \tag{4.21}$$

Note that from the symmetry standpoint, equation 4.21 is valid not just for $I_{1x} + I_{2x}$ but for any total-symmetric operator transforming as Υ^g. For example, eq. 4.21 is valid for the intra-pair dipolar Hamiltonian that is symmetric with respect to the permutation of the two spin labels. It is usually one of the most important relaxation mechanisms for a pair of spins 1/2. This symmetry property is at the central core of LLS analysis.

4.10 Symmetry of the coherent Hamiltonian

The model that we are investigating is a typical solution state NMR experiment where the sample is in an isotropic liquid phase. The coherent part of the spin Hamiltonian

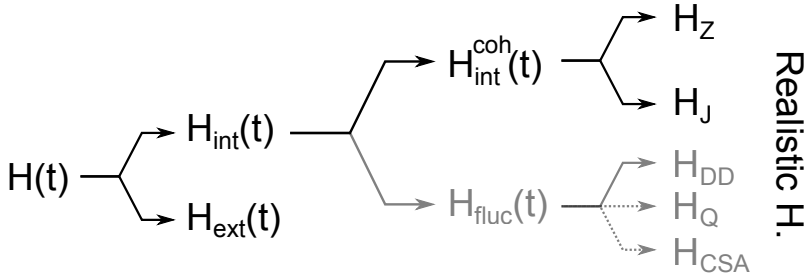

Figure 4.3: The realistic Hamiltonian $\mathcal{H}(t)$ is formed by an internal part common to all molecules in the ensemble. Its coherent partition includes the terms $\mathcal{H}_Z$ and $\mathcal{H}_J$. The interaction between molecules and NMR apparatus is indicated by the term $\mathcal{H}_{\text{ext}}(t)$. In black color the parts that are considered in this section.

influences all ensemble members in an identical fashion. Following Fig. 4.3 derived from Fig. 4.1, we divide $\mathcal{H}(t)$ into two main categories: interactions generated between each molecule and the external NMR apparatus, $\mathcal{H}_{\text{ext}}(t)$, and those occurring within the spin system $\mathcal{H}_{\text{int}}(t)$. The physical assumption behind this approximation is that the electromagnetic fields generated by the apparatus vary in space on a distance scale much

longer than the molecular dimensions.
This assumption can be verified considering the magnetic field created along the x direction in a typical NMR experiment upon the application of a strong idealized pulse polarized along x. We model the excitation coil as a Helmholtz coil of radius $R = 2.5$ cm. The magnetic field created by a single coil with a n wire loops and its variation along x have the expression:

$$B^{RF}(x) = \frac{\mu_0 n I R^2}{2(R^2 + x^2)^{3/2}} \tag{4.22}$$

$$\Delta B^{RF}(x) = \frac{dB^{RF}(x)}{dx}\Delta x \tag{4.23}$$

Considering a strong ideal $\pi/2$ pulse of 10 μs, the nutation frequency is 25 kHz and the magnetic field $B^{RF} \sim 1$ mT for ^{1}H (considering an idealized geometry where the axis of the coil is perpendicular to z the direction of the static magnetic field) [21]. This gives a current in the coils of about 30 A if $n = 1$ and using equation 4.22, $\Delta B^{RF}(x) \sim 10^{-10}$ T on a region of $\Delta(x) \simeq 50$ Å. In addition the variation of the longitudinal magnetic field in a molecule can be in the range of several ppm. The gradient of the transverse magnetic field, in the limit of these idealized assumptions, over molecular dimension can be neglected.

In our classification, the coherent part of the internal Hamiltonian is formed by $\mathcal{H}_Z$ and $\mathcal{H}_J$:

$$\mathcal{H}_{\text{int}}^{\text{coh}} = \mathcal{H}_Z + \mathcal{H}_J \tag{4.24}$$

A molecular system is composed by different nuclei precessing around the external static magnetic field according to different Larmor frequencies. We assume that nuclear spin permutations interest only nuclei of the same isotopic type. This will be denoted in section 4.18 as the high field approximation. The case of an external zero or ultra low magnetic field should be treated separately. As an example if our system is composed by the species $I, S \ldots, W$, the external spin Hamiltonian formalizing the electromagnetic excitation field can be expressed as a nuclear spin operator proportional to $I_x = I_{I,x} + I_{S,x} + \cdots + I_{W,x}$ and *all* the possible permutations would be: $S_I \otimes S_S \otimes \cdots \otimes S_W$. The symmetry group of the external Hamiltonian is formed by the spin permutations that are symmetry operations for $\mathcal{H}_{\text{ext}}$, that is:

$$[P_i, \mathcal{H}_{\text{ext}}(t)] = 0 \quad \forall (t, P_i \in \mathcal{G}_{\text{ext}}) \qquad \text{where} \qquad \mathcal{G}_{\text{ext}} \subseteq \{S_I \otimes S_S \otimes \cdots \otimes S_W\} \tag{4.25}$$

The interaction between the nuclei and the static magnetic field, formalized by the Zeeman Hamiltonian, could also well be considered as part of $\mathcal{H}_{\text{ext}}(t)$. However we follow the common practice used in literature by including the Zeeman Hamiltonian into $\mathcal{H}_{\text{int}}^{\text{coh}}$.

At any instant in time:

$$\begin{aligned} \mathcal{H}_{\text{int}}^{\text{coh}} &= \mathcal{H}_Z + \mathcal{H}_J \quad , \\ \mathcal{H}_Z &= \sum_j \Omega_j^0 I_{jz} \quad , \\ \mathcal{H}_J &= \sum_{j<k} 2\pi J_{jk} \mathbf{I}_j \cdot \mathbf{I}_k \end{aligned} \tag{4.26}$$

where Ω_j^0 are resonance offset frequencies and J_{jk} is the scalar J coupling term. In full analogy to what we have previously done we can identify the permutation symmetry groups for $\mathcal{H}_Z$ and $\mathcal{H}_J$ as:

$$[P_i, \mathcal{H}_Z] = 0 \qquad \forall P_i \in \mathcal{G}_Z \qquad \text{and} \qquad [Q_i, \mathcal{H}_J] = 0 \qquad \forall Q_i \in \mathcal{G}_J \tag{4.27}$$

where P_i and Q_i are nuclear spin permutations and $\mathcal{G}_Z$ and $\mathcal{G}_J$ the corresponding permutation symmetry groups. According to the general framework introduced in section 4.7 the permutation symmetry group $\mathcal{G}_{\text{coh}}^{\text{int}}$ is the smallest subgroup shared by $\mathcal{G}_Z$ and $\mathcal{G}_J$:

$$\mathcal{G}_{\text{coh}}^{\text{int}} = \mathcal{G}_Z \cap \mathcal{G}_J \tag{4.28}$$

Equation 4.26 assumes that the system under analysis possesses a well defined and time-independent J coupling network. This is often the case, but we need to mention that molecules exist where the J-couplings to certain spins are not experimentally observed. A *fast chemical exchange* causes chemical bonds to rapidly form and reform, while a nucleus jumps between different molecules. It is the case of OH protons in ethanol (CH_3CH_2OH) [21]. Another possibility is the fast longitudinal relaxation induced by the presence of *quadrupolar* nuclei. These nuclei have spin >1/2 and couple strongly with electric field gradients in the molecule. As the molecule rotates these electric field gradients rotate as well, producing locally large fluctuating magnetic fields that enhance the nuclear spin relaxation. In practice the J coupling between a spin I with a fast relaxing nucleus Q is neglected if:

$$|2\pi J_{IQ} T_1^Q| \ll 1 \tag{4.29}$$

This in turn influences also the spin system definition (see section 4.5).

Incidentally, as a brief digression, we mention that the fast relaxation property of quadrupolar nuclei (and other paramagnetic species) has been extensively exploited in proton relaxation studies (NMRD profiles) [87]. In particular when a spin 1/2 specie is dipolar-coupled to a quadrupolar nucleus, by tuning the external magnetic field so that the spin 1/2 nuclear Larmor frequency matches the quadrupolar transitions at that field, the nuclear spin 1/2 relaxation gets considerably enhanced [88]. This allows to distinguish spin 1/2 nuclei in proximity of quadrupolar nuclei from bulk spin 1/2 species.

This contrast for instance is useful in the MRI detection of osteoarthritis in knee and hip joints [89].

4.11 Chemical and Magnetic equivalence

One of the outstanding features of NMR is the ability of distinguishing different sets of protons within the same organic molecule [1]. For example the two sets of methyl acetate protons H_a and H_b in Fig. 4.4-a resonate at two slightly different frequencies (2.05 and 3.67 ppm relatively to TMS), whereas acetone nuclei in Fig. 4.4-b resonate at the same frequency (2.16 ppm). In the case of methyl acetate nuclei H_a and H_b

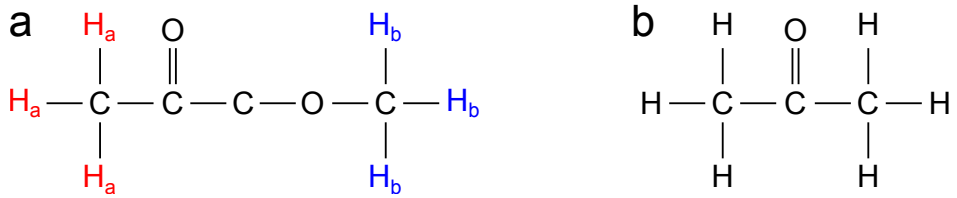

Figure 4.4: a) The two inequivalent sets of proton nuclei in methyl acetate are indicated in red and blue. b) the proton nuclei in acetone are equivalent.

(see Fig. 4.4) sense a slightly different local magnetic field. This is not determined by a gradient of the external static magnetic field over the molecular dimensions, but on the different local electronic environment. On the contrary all proton nuclei in acetone (Fig. 4.4-b) experience the same local magnetic field, when averaged over rapid molecular motions. The formal definition of chemical equivalence for a pair of spins requires two conditions to be both satisfied [21]:

1. The spins are of the same isotopic species,

2. There exists a molecular symmetry operation exchanging the two spins.

The interaction between each spin and the magnetic field in the absence of any excitation scheme is formalized by $\mathcal{H}_Z$. Permutation symmetry allows the reformulation of chemical equivalence: two nuclei are chemically equivalent when the corresponding labels can be exchanged without affecting $\mathcal{H}_Z$. In formula:

$$I_j \quad \text{and} \quad I_k \quad \text{are} \quad \text{chemically} \quad \text{equivalent} \qquad \Longleftrightarrow \qquad (\dots j \dots k \dots) \in \mathcal{G}_Z \tag{4.30}$$

In the example of methyl acetate in Fig. 4.4-a, any spin operation exchanging a proton H_a with a proton H_b *is not* a symmetry operation for the corresponding $\mathcal{H}_Z$ and $\mathcal{H}_{\text{int}}^{\text{coh}}$: that is why H_a and H_b are not chemically equivalent.
A different category widely used in chemistry to establish equivalence between nuclei is *magnetic equivalence*. Two nuclei are said to be magnetic equivalent when:

1. The spins have the same chemical shift and either

2. The spins have identical J couplings to *all other* spins in the molecule, or

3. There are no other spins in the molecule.

As an example the proton nuclei in benzene are chemically but also magnetic equivalent. From previous definition magnetic equivalence implies chemical equivalence but not vice versa. Formally we can say that:

$$I_j \quad \text{and} \quad I_k \quad \text{are} \quad \text{magnetic} \quad \text{equivalent} \qquad \Longleftrightarrow \qquad (\ldots j \ldots k \ldots) \in \mathcal{G}_J \subset \mathcal{G}_Z \tag{4.31}$$

As a result magnetic equivalence is a more restrictive condition.

4.12 An example of chemical and magnetic equivalence

An idealized example might help clarify this distinction. Let us assume to have a molecular four-spin system formed by two isotopic species I and S. We assume I_1 and I_2 to have the same chemical shift, and the same for S_3 and S_4. In addition the system can be magnetic equivalent as in Fig. 4.5-a, or only chemically equivalent as in Fig. 4.5-b. The hetero-nuclear J-couplings in Fig. 4.5-a are identical, whereas in Fig. 4.5-b are different. The aim is to build up the permutation symmetry group for the coherent Hamiltonian

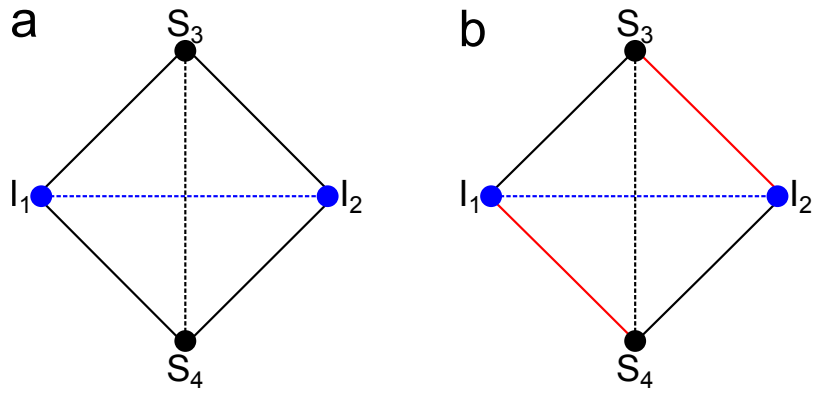

Figure 4.5: Idealized four-spin system in a) magnetic equivalent and b) chemically equivalent. The J coupling network is indicated by solid and dashed lines. Lines of the same colour and format indicate identical J couplings.

and comparing the different equivalence regimes. For the magnetic equivalent system

the symmetry group for the $\mathcal{H}_{\text{int}}^{\text{coh}}$ is the following:

$$\begin{aligned} \mathcal{G}_Z &= \{(), (12), (34), (12)(34)\} \\ \mathcal{G}_J &= \{(), (12), (34), (12)(34)\} \\ \mathcal{G}_Z \cap \mathcal{G}_J = \mathcal{G}_{\text{coh}}^{\text{int}} &= \{(), (12), (34), (12)(34)\} \end{aligned} \tag{4.32}$$

Exchanging a homo nuclear pair is indeed not only a symmetry operation for the Zeeman Hamiltonian, but also for the J coupling term, due to the fact that hetero nuclear J couplings are the same. However when at least one of the spin I experiences a different J coupling with the S-spin manifold, the second condition for magnetic equivalence fails. This is the case exemplified in Fig. 4.5-b. The symmetry group for $\mathcal{H}_{\text{int}}^{\text{coh}}$ is in the latter case:

$$\begin{aligned} \mathcal{G}_Z &= \{(), (12), (34), (12)(34)\} \\ \mathcal{G}_J &= \{(), (12)(34)\} \\ \mathcal{G}_Z \cap \mathcal{G}_J = \mathcal{G}_{\text{coh}}^{\text{int}} &= \{(), (12)(34)\} \end{aligned} \tag{4.33}$$

As we can see in eq. 4.33, the symmetry group $\mathcal{G}_J$ is a subgroup of $\mathcal{G}_Z$ but *does not* include the transpositions (2-element permutations) (12) or (34). Indeed I_1 and I_2 as well as S_3 and S_4 are magnetically inequivalent.

4.13 Symmetry of the fluctuating Hamiltonian

We now pass on to consider, following Fig. 4.6 derived from Fig. 4.1, the stochastic part of the spin Hamiltonian that fluctuates in time. The analysis of relaxation pro-

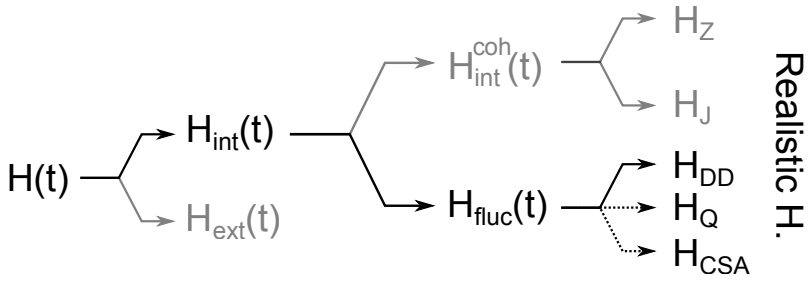

Figure 4.6: The realistic Hamiltonian $\mathcal{H}(t)$ is formed by an internal part common to all molecules in the ensemble, that is further composed by a coherent internal Hamiltonian analysed in section 4.10 and a stochastic partition. The latter includes terms such as $\mathcal{H}_{\text{DD}}$, $\mathcal{H}_{\text{Q}}$ and $\mathcal{H}_{\text{CSA}}$. In black colour the parts that are considered in this section.

cesses leading the spin system towards equilibrium is not only a theoretical subject extensively studied since the dawning of NMR [73, 90–92] but also a practically important subject when investigating on DNP (Dynamic Nuclear Polarization), spin diffusion processes [82–84] and possible ways to prolong nuclear spin lifetime in NMR and MRI

applications. From this standpoint long-lived orders are doubly important: it is theoretically required to understand why they are long-lived, and they may offer a practical route to store and retrieve polarization for a much longer time than dictated by T_1 and T_2, the characteristic time constants of longitudinal and transverse magnetization respectively [9, 64]. It was immediately recognized that the antisymmetric structure of singlet nuclear wave function is the key ingredient making the *singlet order* long-lived [27, 28]. Here we analyse this permutation symmetry requirement even in systems encompassing more than two spins showing how, under suitable approximations, long-lived spin order can concern multi-spin environments as well [55].

4.14 Correlation Function

As we have seen in section 4.5 and as will be further developed in section 4.18, the definition of spin system at equilibrium involves some forms of idealisation. However a dynamic description requires to further take into account the fact that the relative local geometry in the spin system is not time-independent. Indeed the coordinates of nuclei vary in time due to nuclear vibrations, and the molecular frame used to represent them is constantly undergoing translations and rotations in space as the molecules tumbles with respect to the laboratory frame [21, 41, 73, 86]. Indeed the available thermal energy at 20 °C, a typical experimental condition, is of the order of $\sim 10^{-21}$ J corresponding to about ~ 300 cm^{-1}. As a result several rotational levels in the molecule are occupied (see section 2.8).

The quantity called *correlation function* expresses how the stochastic fluctuating Hamiltonian at time t is correlated with itself at a later time $t + \tau$:

$$G_{fluc}(\tau) = \langle \mathcal{H}_{\text{fluc}}(t)\mathcal{H}_{\text{fluc}}(t+\tau)\rangle = \int_{-\infty}^{+\infty} \| \mathcal{H}_{\text{fluc}}(t)\mathcal{H}_{\text{fluc}}(t+\tau) \| \, d\tau, \tag{4.34}$$

where $G_{fluc}(\tau)$ is the correlation function for the fluctuating Hamiltonian under analysis and should not be confused with the permutation symmetry group $\mathcal{G}_{\text{fluc}}$. The symbol $\| \cdots \|$ denotes the Frobenius norm, and $\langle \cdots \rangle$ indicates an ensemble average. For $\tau = 0$

$$G_{fluc}(0) = \langle \mathcal{H}_{\text{fluc}}(t)^2 \rangle = \sigma^2 \tag{4.35}$$

That is the correlation function at time zero is equal to the variance σ^2 of $\mathcal{H}_{\text{fluc}}$ [73], given that $\langle \mathcal{H}_{\text{fluc}} \rangle = 0$. For $\tau \to \infty$ the values of $\mathcal{H}_{\text{fluc}}(t)$ and $\mathcal{H}_{\text{fluc}}(t+\tau)$ are completely uncorrelated. As we expect the correlation function to be a continuous and decaying function of time, a reasonable choice [73] is to consider:

$$G_{fluc}(\tau) = G(0)e^{-|\tau|/\tau_c} \tag{4.36}$$

It can indeed be demonstrated that an exponential decay correlation function can be

obtained for the spherical harmonics of the angles specifying molecular orientation in a liquid [73]. The correlation function can be interpreted either as a measure of the timescale of the random oscillations or as an average time for a molecular axis to change its direction by one radian [1, 73]. For a molecule in solution several regimes corresponding to different components of $\mathcal{H}_{\text{fluc}}$ can be identified. In particular rapid vibrations occur with a correlation time τ_{vib} of the order of tens of femtoseconds ($\sim 30 \times 10^{-15}$), whereas molecular rotations have correlation times τ_c typically from picoseconds ($\sim 10^{-12}$ seconds) to nanoseconds ($\sim 10^{-9}$ seconds). When the molecule displays local internal flexibility or possesses a rotating group, the correlation function shows an intermediate regime. We define this dynamics as internal motion, and the coupling of nuclear spins to this internal motion as *Spin Internal Motion* interaction. The corresponding correlation time τ_{SIM} is usually between $\sim 100 \times 10^{-15}$ to $\sim 10 \times 10^{-12}$ seconds:

$$\tau_{vib} < \tau_{SIM} < \tau_c \tag{4.37}$$

The existence of internal molecular motion implies that the molecule does not have a well defined symmetry at any point in time. However it is still possible to apply the permutation symmetry analysis once we consider the stochastic Hamiltonian averaged over a certain time interval.

4.15 Hamiltonian Averaging over vibrations

In equation 4.37 vibrational modes are assumed to have approximately three orders of magnitude shorter correlation time than rotational motions. Therefore to a good extent vibrational and rotational regimes can be considered completely separated. A further assumption is that the fast nuclear vibrations are assumed not to significantly contribute to nuclear spin relaxation. The latter is grounded on the following: if we consider a vibrational mode of 1000 cm^{-1}, this correspond to an angular velocity of $2\pi \times 3 \times 10^{13}$ rad sec^{-1}. For proton nuclei to have such a Larmor frequency a magnetic field of 70×10^4 T would be required, more than four orders of magnitude the current available magnets.

The probability of finding a component of the stochastic motion at a particular frequency is given by the *spectral density*, whose functional form in the case of an exponential correlation function is:

$$J(\omega) = \frac{2\tau_C}{1 + \omega^2 {\tau_C}^2} \tag{4.38}$$

$J(\omega)$ has its maximum value for $\tau_C = 1/\omega_0$. For higher frequencies the spectral density becomes flatter. As long as fast nuclear vibrations are discarded $\mathcal{H}_{\text{fluc}}$ can be replaced

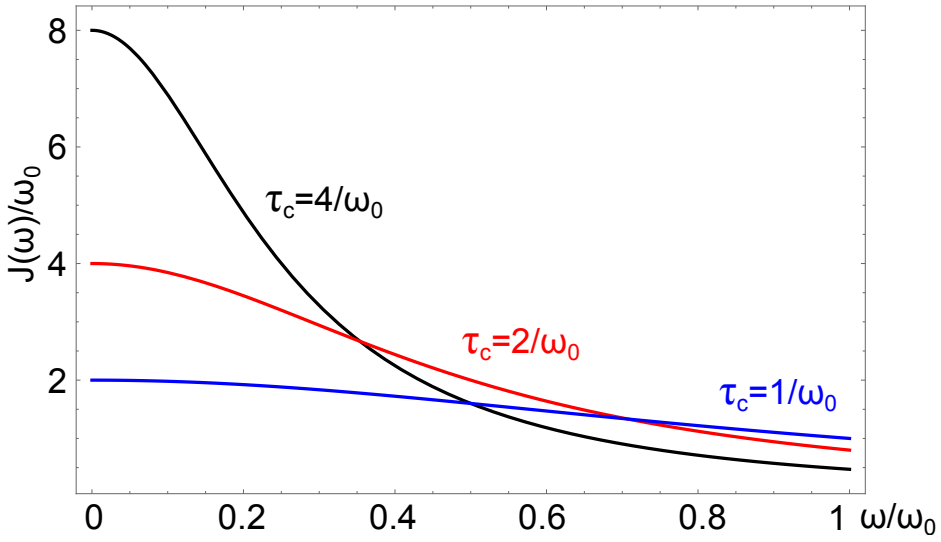

Figure 4.7: The spectral density function $J(\omega)$ in equation 4.38 drawn for three different values of τ_C.

by a *vibrationally averaged Hamiltonian* defined as follows:

$$\mathcal{H}_{\text{fluc}}^{<\text{vib}>}(t) = \int_{-\infty}^{+\infty} \mathcal{H}_{\text{int}}(t+t')g_{vib}(t')dt' \tag{4.39}$$

The smoothing function $g_{vib}(t')$ has a unit integral and decays from a maximum at $t' = 0$ to a very small value for $|t'| > \tau_{vib}$. The result after vibrational averaging is still a time-dependent stochastic Hamiltonian. The stochastic character of $\mathcal{H}_{\text{fluc}}^{<\text{vib}>}(t)$ is retained by the overall molecular rotation. In practice and to a good approximation $\mathcal{H}_{\text{fluc}}^{<\text{vib}>}(t)$ is the fluctuating Hamiltonian calculated assuming the internal geometric configuration of the molecule at equilibrium. When vibrational averaging is taken into account, the symmetry group of the internal spin Hamiltonian is identical to that possessed by the equilibrium molecular structure:

$$\mathcal{G}_{\text{fluc}} = \mathcal{G}_{\text{coh}}^{\text{int}} = \mathcal{G}_{\text{int}} \tag{4.40}$$

In the special example in Fig. 4.5 where we represented two centrosymmetric systems, the permutation symmetry group for the fluctuating spin Hamiltonian is:

$$\begin{aligned} \text{Magnetic equivalent system} \quad & \mathcal{G}_{\text{fluc}} = \mathcal{G}_{\text{coh}}^{\text{int}} = \{(), (12), (34), (12)(34)\} \\ \text{Chemically equivalent system} \quad & \mathcal{G}_{\text{fluc}} = \mathcal{G}_{\text{coh}}^{\text{int}} = \{(), (12)(34)\} \end{aligned} \tag{4.41}$$

The above example shows how magnetically equivalent systems have larger permutation symmetry groups than chemically equivalent ones. This is due to the fact that homo nuclear transpositions such as (12) and (34) are not symmetry operations for a chemical equivalent system. In addition in multi-spin systems the centrosymmetric arrangement of the spin nuclei turns out to be important to minimize the relaxation contributions

either of the internal dipolar and quadrupolar Hamiltonians [5, 55, 93, 94] as well as nuclear CSA [95].

4.16 Hamiltonian Averaging over internal motions

Systems subjected to internal flexibility may display an intermediate motional regime characterized by a correlation time τ_{SIM} as in equation 4.37. This correlation time is longer than τ_{vib} and shorter than τ_c. Averaging the fluctuating Hamiltonian over spin internal motions might still be a good approximation. Similarly to equation 4.39 we can define:

$$\mathcal{H}_{\text{fluc}}^{<\text{IM}>}(t) = \int_{-\infty}^{+\infty} \mathcal{H}_{\text{fluc}}(t+t')g_{IM}(t')dt' \tag{4.42}$$

where the smoothing function $g_{IM}(t')$ has a unit integral and decays from a maximum at $t' = 0$ to a very small value for $|t'| > \tau_{IM}$. The general validity of equation 4.42 is questionable as spin internal motions can be in many circumstances much slower than nuclear vibrations. However the usually higher degree of symmetry of $\mathcal{H}_{\text{fluc}}^{<\text{IM}>}$ can lead to important physical insights that would otherwise remain concealed.
An important example is offered by a system containing a rotating methyl group with the protons labelled $\{I_1, I_2, I_3\}$. Methyl groups have been a subject extensively investigated in the last decades [60, 96–99] and we will discuss about it in the experimental session. For simplicity we neglect, in our example, the presence of other spins in the molecule. Let us assume that the internal rotational motion occurs with a correlation time τ_{SIM} in a regime according to equation 4.37. In the equilibrium configuration the protons can be thought as arranged in a triangular fashion. The internal dipolar Hamiltonian, even after vibrational averaging, lacks permutation symmetry. Indeed it lacks any geometrical inversion centre. However by averaging on a much longer timescale (i.e. in the limit $\tau_{SIM} \rightarrow 0$) as per equation 4.42 the group of the fluctuating Hamiltonian acquires a much higher symmetry. For the methyl system under analysis:

$$\begin{aligned} \mathcal{G}_{\text{fluc}}^{<\text{vib}>} &= \{()\} \\ \mathcal{G}_{\text{fluc}}^{<\text{IM}>} &= \{(), (123), (132)\} \\ \mathcal{G}_{\text{fluc}}^{<\text{vib}>} &\subset \mathcal{G}_{\text{fluc}}^{<\text{IM}>} \end{aligned} \tag{4.43}$$

As we will see later, the higher symmetry of $\mathcal{G}_{\text{fluc}}^{<\text{IM}>}$ leads to the predictions of long-lived orders that would not be attainable by using $\mathcal{G}_{\text{fluc}}^{<\text{vib}>}$. We need to stress that the use of $\mathcal{G}_{\text{fluc}}^{<\text{IM}>}$ is permissible when there is a net separation between τ_{SIM} and τ_c, i.e. between the spin internal motion of the methyl group and the overall rotation of the molecule in solution. Such long-lived spin orders were suggested by the quantum-rotor-induced polarisation experiments of Icker and Berger [100–102]. These experiments prompted an elegant and detailed theoretical description of the quantum-rotor-induced

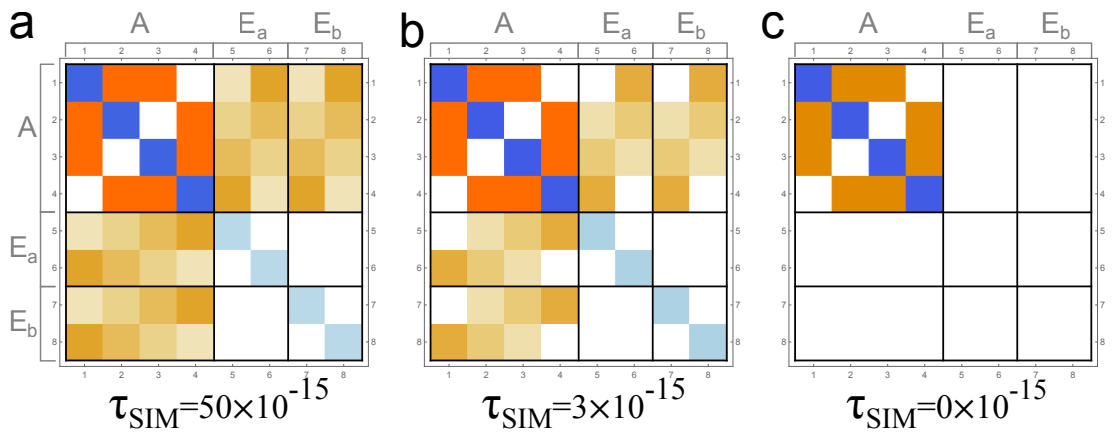

Figure 4.8: The matrices represent the intramolecular dipolar Hamiltonian superoperator in the 8×8 population subspace in a) for $\tau_{SIM} = 50 \times 10^{-15}$s, in b) for $\tau_{SIM} = 3 \times 10^{-15}$s and in c) for $\tau_{SIM} = 0 \times 10^{-15}$s for a three-spin-1/2 system modelling the proton nuclei in a methyl group . The geometrical arrangement of protons is an equilateral triangle with nuclei spaced by 1.5 Å. Other parameters used are $\tau_c = 5 \times 10^{-12}$s, $J_{12} = J_{13} = J_{23} = 20$ Hz, $\omega_H = 500$ MHz, and an identical chemical shift for all protons. The magnitude of the matrix elements is represented by a colour: the white corresponds to zero value.

polarisation phenomenon by Dumez et al. [60]

4.17 Symmetry of the idealised complete Hamiltonian

Following the schematic of Fig. 4.1 and the framework introduced in section 4.7 the symmetry of the internal Hamiltonian is a direct consequence of the symmetry of $\mathcal{G}_{\text{coh}}^{\text{int}}$ and $\mathcal{G}_{\text{fluc}}$. In addition, considering that $\mathcal{H}_{\text{ext}}$ can be represented by a spin operator $\propto I_x + S_x + \cdots + W_x$ that is total-symmetric with respect to any homo-nuclear permutation we have $\mathcal{G}_{\text{int}} = \mathcal{G}_{\text{coh}}^{\text{int}} \cap \mathcal{G}_{\text{fluc}}$ and $\mathcal{G}_{\text{H}} = \mathcal{G}_{\text{int}} \cap \mathcal{G}_{\text{ext}}$. We define $\mathcal{G}_{\text{H}}$ as the symmetry group of the complete Hamiltonian. However this does not represent the ultimate group used in the LLS analysis. As will be examined in section 4.18 the number of idealisations involved in the examination of $\mathcal{H}_{\text{int}}(t)$ components leads to the definition of an *idealised symmetry group of the complete Hamiltonian* $\mathcal{G}_{\text{H}}^0$ that might usually have a higher symmetry:

$$\begin{aligned} \mathcal{G}_{\text{int}}^0 &= \mathcal{G}_{\text{int}}^{\text{coh},0} \cap \mathcal{G}_{\text{fluc}}^0 \\ \mathcal{G}_{\text{H}}^0 &= \mathcal{G}_{\text{int}}^0 \cap \mathcal{G}_{\text{ext}}^0 \end{aligned} \tag{4.44}$$

where the superscript "0" is intended to indicate a set of idealisations (see also Fig. 4.1). According to our approach population operators that do not evolve in time must be, by definition, invariant under any permutation that is a symmetry operation for the idealised complete Hamiltonian. The number of conjugacy classes of $\mathcal{G}_{\text{H}}^0$ defines the number of irreducible representations. The coherent and fluctuating Hamiltonians cannot

induce transitions between states spanning across different irreducible representations of the idealised complete Hamiltonian group. Hence the spin evolution must preserve a population difference between states transforming according to different irreducible representations of $\mathcal{G}_{\mathrm{H}}^{0}$.
This allows to express a long lived order as an average spin population imbalance between states spanning across different irreducible representations:

$$LLS = \frac{1}{N_k}\sum_k |k\rangle\langle k| - \frac{1}{N_l}\sum_l |l\rangle\langle l|, \tag{4.45}$$

where $|k\rangle \sim \Upsilon^k$ and $|l\rangle \sim \Upsilon^l$ are nuclear spin states in a symmetry adapted basis transforming according to different irreducible representations. N_k and N_l are the number of states that can be classified according to Υ^k and Υ^l respectively. In a two-spin system for example $\Upsilon^k = \Upsilon^g$, $\Upsilon^l = \Upsilon^u$, $N_k = 3$ (triplet states) and $N_l = 1$ (singlet state).
The important conclusion is that *the number of irreducible representations of $\mathcal{G}_{\mathrm{H}}^{0}$ defines the number of conserved quantities of the spin system.* As $\mathcal{G}_{\mathrm{H}}^{0}$ conserves the group structure, it needs at least to include the identity operator. There is always at least one irreducible representation and as a result a trivial conserved quantity: the overall spin population. Depending on the system under analysis a set of approximations affect the definition of the symmetry properties of the different components of the Hamiltonian in eq. 4.10 and as a result the composition of $\mathcal{G}_{\mathrm{H}}^{0}$. This in turn may influence the prediction of LLS. A careful choice of the introduced approximations is essential in any LLS analysis.

4.18 Approximations

The definition of the symmetry property of any Hamiltonian encountered so far is grounded on a set of approximations with limited validity. The presence of these approximations invest long-lived states with finite lifetime. We have already seen in section 4.13 that the stochastic terms are considered only after a vibrational averaging or after averaging over internal modes. Furthermore the analysis so far has involved only nuclear spin states, overlooking completely the electronic coordinates. We indeed assume, according to the Born-Oppenheimer approximation that the motion of atomic nuclei and electrons in a molecule can be separated. A complete treatment of the subject would require the definition of the concept of *Molecular Symmetry Group*. Bunker and Jensen have studied this topic extensively [40, 67]. In addition nuclear spin states insensitive to major relaxation mechanisms are NMR silent and therefore it is often necessary to *deliberately* break the symmetry in order to *access* and *detect* the nuclear spin order [2–7, 22, 27, 28, 64, 103–106]. Without access would not be possible to use them to deposit and later retrieve readable magnetization. It is therefore essential, as anticipated in section 4.17 to make a further distinction between *idealised spin Hamiltonians*

$\mathcal{H}^0$ and *realistic spin Hamiltonians* $\mathcal{H}$. As a result of the introduced approximations, the symmetry group of the idealized spin Hamiltonian will be in general larger than the symmetry group of the realistic Hamiltonian:

$$\mathcal{G}_{\mathrm{H}} \subseteq \mathcal{G}^0_{\mathrm{H}} \tag{4.46}$$

A permutation symmetry theory based on $\mathcal{G}^0_{\mathrm{H}}$ predicts infinitely long-lived spin states. We know that this is completely unrealistic. However the main theoretical motivation about using $\mathcal{H}^0$ and consequently $\mathcal{G}^0_{\mathrm{H}}$ is that it offers the possibility to predict the existence of long-lived states while guiding at the same time the design of experimental procedures for exploiting them. Furthermore an analytical expression for a long-lived state is usually accomplished without even diagonalizing a Liouvillian superoperator [55]. Indeed the investigation is usually performed in the Hilbert space of dimension $\mathbb{N}_H$ rather than in the Liouville space of dimension $\mathbb{N}_L = \mathbb{N}_H^2$ (see section 4.5). In the formalization of a quantum mechanical analysis of LLS, approximations are ubiquitous and we therefore summarize the principal idealisations used:

1. *Idealization of the spin system.*
   The initial spin system does not comprise all the N spins forming the molecule that is analysed. As it has been pointed out at the end of section 4.5 in numerous relevant cases we assume that a reduced spin system can still provide sufficient information.

   (a) Typically remote nuclei with negligible J coupling and/or small dipolar interactions are not included in the initial spin system for simplicity.

   (b) Quadrupolar nuclei with a negligible quadrupolar coupling constant and low dipolar interaction are in many cases disregarded. This might not always be the case: The Warren group has showed how long-lived states are possible even in presence of quadrupolar nuclei [5]. The example in Ref [5] (deuterated dyacetilene) can indeed be solved by permutation symmetry by including ^{2}H nuclei in the initial spin system definition.

   (c) We do not consider in the permutation symmetry analysis interactions between spin on different molecules, although we know that these interactions modulated by the relative translation can induce significant relaxation at low magnetic field (we incidentally mention that in section 5.4.3 an estimation of the rate constant due to the intermolecular interaction between $^{13}C_2$-**I** and the solvent molecules is given from the experimental T_S magnetic field profiles acquired).

   (d) We do not consider molecular oxygen or other paramagnetic species present in solution, although is usually extremely effective in thermalising the spin system.

The spin system is therefore an *idealised spin system* smaller than the realistic one:

$$\Sigma^0 \subset \Sigma \tag{4.47}$$

where Σ^0 and Σ indicate the idealised and realistic spin systems respectively.

2. *Idealization of the external Hamiltonian.*
The external Hamiltonian involves the interaction of the spin system with external magnetic fields that can be in principle either static or oscillating. However we have previously included the spin interaction with the static field in $\mathcal{H}_Z$, therefore we only consider the contribution of oscillating magnetic fields on $\mathcal{H}_{\text{ext}}$. We assume that external fields interact with nuclear spins of the same isotopic type in the same way. This is an idealisation as the local electronic environment in a molecule can lead to tiny deviations of the perceived magnetic field. As long as the static magnetic field allows a clear discrimination of the nuclear Larmor frequencies of different isotopes $I, S \ldots W$, we have:

$$\mathcal{G}^0_{\text{ext}} = S_I \otimes S_S \otimes \cdots \otimes S_W \qquad \text{(High magnetic field)} \tag{4.48}$$

where the symmetric permutation group of S_I comprises $N_I!$ permutations of the I spins. The order of the group $\mathcal{G}^0_{\text{ext}}$ is therefore $N_I! \times N_S! \cdots \times N_W!$. Although nuclear magnetic resonance at extremely low or zero magnetic field has long been unpopular in the NMR community due to the low nuclear spin polarization and the poor sensitivity of inductive coils at low frequencies, recently the possibility to combine parahydrogen induced polarisation (PHIP) and long-lived states has boosted the theoretical and experimental efforts in this field [49, 50, 65, 107]. At zero magnetic field $\mathcal{G}^0_{\text{ext}}$ turns out to be even larger as we allow hetero nuclear permutations to happen:

$$\mathcal{G}^0_{\text{ext}} = S_N \qquad \text{(Zero magnetic field)} \tag{4.49}$$

3. *Idealisation of the coherent Hamiltonian*

   (a) *Idealisation of the Zeeman Hamiltonian.* The Zeeman Hamiltonian $\mathcal{H}_Z$ (see Fig. 4.1) is the part of $\mathcal{H}^{\text{coh}}_{\text{int}}$ establishing the relation between the spin system and the static magnetic field. We have discussed in section 4.10 the concept of chemical and magnetic equivalence in terms of permutation symmetry. Rigorously speaking if $\mathcal{H}_Z$ does not contain the permutation (ij) then spins I_i and I_j are inequivalent. However as we mentioned at the beginning of this section and in section 4.7 considering the operator $I_{1z} - I_{2z}$, we need a symmetry breaking mechanism to access LLS. In spin systems where homo nuclei are slightly chemically inequivalent and in the absence of resonant radio-frequency fields we *include* (ij) as a permutation symmetry operation

for $\mathcal{G}_{\mathrm{Z}}^{0}$. The range of validity of this approximation defines the *near chemical equivalence* regime:

$$|(\delta_i - \delta_j)\omega^0| \ll |\pi J_{ij}| \qquad \text{(Near chemical equivalence)} \tag{4.50}$$

Long-lived states have been nonetheless demonstrated for systems where homo-nuclei have a difference in chemical shift larger than the intra-pair J coupling. It is for example the case of $^{15}N_2O$ discussed in Ref. [22]. The chemical sift difference for the two nitrogen nuclei is $\Delta\delta = 82.3$ ppm. Given that for ^{15}N the gyromagnetic ratio is -4.316 MHz/T the chemical shift difference corresponds to $\sim$ 355 Hz/T. The intra-pair J coupling is 8.1 Hz. Therefore if the evolution magnetic field is lower than 22.8 mT, the approximation in equation 4.50 is still valid. In Ref. [22] a LLS of about 30 minutes was detected in a magnetic field of 2 mT.
Near chemical equivalence in equation 4.50 can be also imposed by application of sufficiently strong resonant radio-frequency spin locking fields. The appropriate condition in this case is:

$$\begin{aligned} |\omega_i^{eff} - \omega_j^{eff}| &\ll |\pi J_{ij}| \\ \omega_j^{eff} &= \sqrt{(\delta_j - \delta_{rf})^2\omega_0^2 + \omega_{nut}^2} \end{aligned} \tag{4.51}$$

A detailed theoretical description of long-lived states in presence of spin-locking has been given by Pileio [57].

(b) *Idealisation of the J coupling Hamiltonian.* The J coupling Hamiltonian $\mathcal{H}_J$ is the part of $\mathcal{H}_{\mathrm{int}}^{\mathrm{coh}}$ accounting for the coherent electron-mediated interactions in solution within the spin system. The permutation (ij) is a symmetry operation for $\mathcal{H}_J$ only if I_i and I_j are magnetic equivalent. However perfect magnetic equivalence in rigid systems hinders long-lived state accessibility. We say that spins I_i and I_j are *near magnetic equivalent* if the degree of asymmetric coupling with the spin I_k satisfies the following equation:

$$\pi|J_{ik} - J_{jk}| \ll \pi J_{ij} \qquad \text{(Near magnetic equivalence)} \tag{4.52}$$

When equation 4.52 is accomplished we include the permutation (ij) in the idealised permutation group $\mathcal{G}_{\mathrm{J}}^{0}$. Again the realistic asymmetry in the J coupling network renders the lifetime of LLS finite. However $\mathcal{G}_{\mathrm{J}}^{0} \supset \mathcal{G}_J$ reveals in many systems long-lived orders that would remain concealed otherwise. The near magnetic equivalent multi-spin systems investigated by the Warren group operate under the validity of equation 4.52 and can be investigated resorting to $\mathcal{G}_{\mathrm{J}}^{0}$. This is discussed further in section 4.21 in example **Ex 4**.

A *near magnetic equivalence domain* can be formalized by combining equa-

tions 4.50 and 4.52 as:

$$(\delta_i - \delta_j)^2\omega^{02} + \pi^2(J_{ik} - J_{jk})^2 \leq \pi^2 J_{ij}^2 \;\; \forall\, k \notin \{i, j\} \tag{4.53}$$

The global near magnetic equivalence condition in equation 5.1 is not necessary for the existence and detectability of LLS as it has been recently demonstrated [55] and further discussed in the experimental part of this work.
Summarizing the idealised symmetry group of the idealised coherent Hamiltonian $\mathcal{H}_{\text{int}}^{\text{coh,0}}$ can be expressed as:

$$\mathcal{G}_{\text{int}}^{\text{coh,0}} = \mathcal{G}_{\text{Z}}^{0} \cap \mathcal{G}_{\text{J}}^{0} \tag{4.54}$$

4. *Idealisation of the fluctuating Hamiltonian*
As we have seen in section 4.13 the fluctuating Hamiltonian usually encompasses several terms.

   (a) *Truncation*: For spin-1/2 systems usually only the dipolar term is retained. Therefore:

$$\begin{aligned} \mathcal{H}_{\text{fluc}} &= \mathcal{H}_{\text{DD}} + \mathcal{H}_{\text{CSA}} + \ldots \\ \mathcal{H}_{\text{fluc}}^{0} &= \mathcal{H}_{\text{DD}}^{0} \end{aligned} \tag{4.55}$$

   In presence of a local inversion geometry [55, 93–95] also the CSA interaction in rigid system is invariant with respect to transpositions across the inversion centre.

   (b) *Long-range and intermolecular interaction*: As we have seen in the definition of the idealised spin system Σ^0, long-range interactions within the same molecule or between different molecules are commonly neglected. They play a role limiting the lifetime of LLS. Their influence might be field-dependent, in particular the approximation might be better at higher magnetic fields (see in section 5.4.3 the estimation of the rate constant between $^{13}C_2$-**I** and the acetone solvent molecules).

   (c) *Vibrational averaging*: As discussed above averaging over rapid molecular vibrations restores the symmetry of the molecular point group. The limited validity of this approximation depends on the relative values of τ_{vib} and τ_c. In particular it is acceptable as long as $\tau_{vib} \ll \tau_c$.

   (d) *Averaging over internal modes*: The use of motionally averaged symmetry groups is a strong assumption that requires a good separation in timescales between internal modes and molecular tumbling. The case of methyl groups analysed in Ref. [53, 60, 108] can be analysed assuming a motionally averaged fluctuating Hamiltonian $\mathcal{H}_{\text{fluc}}^{\text{<IM>}}$ rather than $\mathcal{H}_{\text{fluc}}$. The corresponding

$\mathcal{G}_{\text{fluc}}^{\text{<IM>}}$ is often larger than $\mathcal{G}_{\text{fluc}}^{\text{<vib>}}$ and $\mathcal{G}_{\text{fluc}}$, so that LLS may emerge that are not clear when considering a smaller permutation symmetry group.

(e) *Local molecular symmetry*: Sometimes LLS are localized in regions of the molecule displaying a high local symmetry, even though the molecule as a whole has a reduced symmetry.

The idealised complete symmetry group in conclusion is:

$$\mathcal{G}_{\text{H}}^{0} = \mathcal{G}_{\text{DD}}^{0} \left(\cap\, \mathcal{G}_{\text{CSA}}^{0} \cap \dots\right) \tag{4.56}$$

Interactions other than the internal dipolar Hamiltonian are included in parentheses as they are not considered in this investigation of LLS number and analytical expressions. However when estimating a realistic lifetime for LLS all relevant relaxation mechanisms need to be included.

4.19 Maximum conversion to LLS.

The problem of accessing a nuclear spin order starting from an initial density operator under a unitary evolution has been long investigated and formalized mainly by Sørensen and co-workers [14–16, 109]. They investigated fundamental bounds on the coherent transformation of spin density operators components [14].

We reconsider here this topic as it completes the analysis on LLS. A detailed exposition accounting for its relevance in hyperpolarization experiments can be found in Ref. [17]. To introduce the formalism let us consider a generic N-spin-1/2 system. A typical high field NMR experiment in its basic form encompasses some standard steps:

- The system thermalizes at a magnetic field of few Tesla;
- A set of NMR pulses and intervals is applied;
- The signal is detected.

Assuming that the system undergoes a unitary transformation during the NMR experiment, a very immediate question is whether is possible to establish what is the maximum conversion attainable from an initial density operator A to a final target operator B. The density operator specifying the state of a spin system needs to be thought as a vector in the $2^{2\times N}$ dimensional Liouville space. Unitary (and non unitary) transformations in this space are essentially rotations converting one vector-operator into another. The basic NMR experiment can therefore be described in the following terms:

$$UAU^{\dagger} = bB + C \tag{4.57}$$

where U is the unitary evolution operator ($U^\dagger = U^{-1}$) and C is an operator orthogonal to B, i.e. $\mathrm{Tr}(B^\dagger C) = 0$. The value of b is bounded by the Sørensen theorem as follows:

$$b_{\min} \leq b \leq b_{\max} \tag{4.58}$$

where

$$\begin{aligned} b_{\min} = b_{\min}(A \rightarrow B) &= \|B\|^{-2} \Lambda_{A\uparrow} \cdot \Lambda_{B\downarrow} \\ b_{\max} = b_{\max}(A \rightarrow B) &= \|B\|^{-2} \Lambda_{A\uparrow} \cdot \Lambda_{B\uparrow} \\ \|B\|^2 &= \Lambda_{B\uparrow} \cdot \Lambda_{B\uparrow} \end{aligned} \tag{4.59}$$

The notation $\Lambda_{A\uparrow}$ and $\Lambda_{A\downarrow}$ indicates vectors containing the spectrum (set of eigenvalues $\{a_1, a_2, \ldots a_n\}$) of the generic operator A in ascending and descending order respectively:

$$\begin{aligned} \Lambda_{A\uparrow} &= \{a_1, a_2, \ldots a_n\} \qquad \text{with} \quad a_1 \leq a_2 \leq \cdots \leq a_n \\ \Lambda_{A\downarrow} &= \{a_n, a_{n-1}, \ldots a_1\} \qquad \text{with} \quad a_n \geq a_{n-1} \geq \cdots \geq a_1 \end{aligned} \tag{4.60}$$

Similarly for B. When the operators A and B share the same spectrum $b_{\max} = 1$, otherwise the conversion may be partial. The notation:

$$\begin{aligned} &b_{\min}(A \rightarrow B) \\ &b_{\max}(A \rightarrow B) \end{aligned} \tag{4.61}$$

indicates throughout the text the minimum and maximum achievable conversion starting from an initial state represented by the operator A to a final target state represented by the operator B under unitary evolution. Let us give an example relevant for LLS:

Ex 1 M2S in absence of symmetry: We consider a homo nuclear two-spin system and apply the above Sørensen theorem to investigate the transformation between longitudinal magnetization and singlet order. We presume that the evolution operator U is invariant only under the identity operator. This signifies that the conversion from magnetization to singlet (M2S) happens in absence of symmetry. A singlet triplet basis to represent the operators is assumed. The matrix representation of the normalized operators $I_z = I_{1z} + I_{2z}$ (longitudinal magnetization) and $\mathrm{SO} = \mathbf{I_1} \cdot \mathbf{I_2}$ (singlet order) is:

$$I_z = \frac{1}{\sqrt{2}} \begin{array}{c} \begin{matrix} |S\rangle & |T^1\rangle & |T^0\rangle & |T^{-1}\rangle \end{matrix} \\ \begin{pmatrix} 0 & 0 & 0 & 0 \\ 0 & 1 & 0 & 0 \\ 0 & 0 & 0 & 0 \\ 0 & 0 & 0 & -1 \end{pmatrix} \end{array} \qquad \mathrm{SO} = -\frac{1}{2\sqrt{3}} \begin{array}{c} \begin{matrix} |S\rangle & |T^1\rangle & |T^0\rangle & |T^{-1}\rangle \end{matrix} \\ \begin{pmatrix} 3 & 0 & 0 & 0 \\ 0 & -1 & 0 & 0 \\ 0 & 0 & -1 & 0 \\ 0 & 0 & 0 & -1 \end{pmatrix} \end{array} \tag{4.62}$$

The spectra of the two operators listed in ascending order is as follows:

$$\Lambda_{I_z\uparrow} = \frac{1}{\sqrt{2}} \times \begin{pmatrix} -1 \\ 0 \\ 0 \\ 1 \end{pmatrix} \qquad \Lambda_{\mathrm{SO}\uparrow} = \frac{1}{2\sqrt{3}} \times \begin{pmatrix} -1 \\ -1 \\ -1 \\ 3 \end{pmatrix} \tag{4.63}$$

Estimating a magnetization to singlet conversion is equivalent to indicate the maximum achievable projection of a final state onto singlet order after a unitary transformation designated by the superoperator $\hat{U}$ starting from initial magnetization:

$$b_{\max}(I_z \to \mathrm{SO}) = \left| \frac{\mathrm{Tr}(\mathrm{SO}^\dagger \cdot \hat{U} \cdot I_z)}{\mathrm{SO}^\dagger \cdot \mathrm{SO}} \right|_{\max} = \frac{\Lambda_{I_z\uparrow} \cdot \Lambda_{\mathrm{SO}\uparrow}}{\Lambda_{\mathrm{SO}\uparrow} \cdot \Lambda_{\mathrm{SO}\uparrow}} = \sqrt{\frac{2}{3}} \tag{4.64}$$

The reverse transformation from singlet order to magnetization gives the same result:

$$b_{\max}(\mathrm{SO} \to I_z) = \left| \frac{\mathrm{Tr}(I_z^\dagger \cdot \hat{U} \cdot \mathrm{SO})}{I_z^\dagger \cdot I_z} \right|_{\max} = \frac{\Lambda_{I_z\uparrow} \cdot \Lambda_{\mathrm{SO}\uparrow}}{\Lambda_{I_z\uparrow} \cdot \Lambda_{I_z\uparrow}} = \sqrt{\frac{2}{3}} \tag{4.65}$$

Overall the magnetization to singlet to magnetization sequence of events has a optimum rate given by the product:

$$b_{\max}(I_z \to \mathrm{SO} \to I_z) = b_{\max}(\mathrm{SO} \to I_z) b_{\max}(I_z \to \mathrm{SO}) = \frac{2}{3} \tag{4.66}$$

In the original investigation, as well as in the previous example, Sørensen did not consider any particular symmetry of the Hamiltonian responsible for the dynamic evolution of the spin system. In the language we are developing, this is equivalent to assuming that the permutation symmetry group of the complete Hamiltonian only includes the identity operator. When the complete Hamiltonian, or at least the idealised counterpart undergoing the set of approximations discussed in section 4.18, displays further symmetry properties a generalisation of the Sørensen bounds can be developed.

This important generalization has been investigated by Nielsen and Sørensen [15, 16], and recently elegantly applied by Levitt to discuss some common hyperpolarized NMR experiments and the transfer of parahydrogen-induced hyperpolarized singlet order to magnetization in systems displaying chemical and magnetic equivalence. [17].

4.20 Evolution under symmetric Hamiltonians

Let us suppose that the idealised internal coherent Hamiltonian can be described by a symmetry group $\mathcal{G}_{\mathrm{int}}^{\mathrm{coh},0} \supset \{()\}$. In practice $\mathcal{G}_{\mathrm{int}}^{\mathrm{coh},0}$ includes more than just the identity

operator. The number c of conjugacy classes of $\mathcal{G}_{\text{int}}^{\text{coh},0}$ defines the number of irreducible representations $\Upsilon^1, \ldots \Upsilon^c$. The unitary evolution operator $U(t, t_0)$ from the initial time point t_0 to the final time point t satisfies the Liouville Von-Neumann equation:

$$\frac{d}{dt}U(t, t_0) = -i\mathcal{H}(t)U(t, t_0) \tag{4.67}$$

with the initial condition $U(t_0, t_0) = 1$. The crucial point is that if $\mathcal{H}$ is symmetrical under the nuclear spin permutation group $\mathcal{G}_{\text{int}}^{\text{coh},0}$, then the unitary evolution operator factorises into separate evolution operators for each irreducible representation of $\mathcal{G}_{\text{int}}^{\text{coh},0}$:

$$U = U^{\Upsilon^1} U^{\Upsilon^2} \cdots U^{\Upsilon^c} \tag{4.68}$$

where

$$\frac{d}{dt}U^{\Upsilon^j}(t, t_0) = -i\mathcal{H}^{\Upsilon^j}(t)U^{\Upsilon^j}(t, t_0) \tag{4.69}$$

The evolution operator for an irreducible representation Υ^i commutes with operators transforming according to a different irreducible representation Υ^j:

$$U^{\Upsilon^i} Q^{\Upsilon^j} U^{\Upsilon^{i\dagger}} = Q^{\Upsilon^j}; \qquad \Upsilon^i \neq \Upsilon^j \tag{4.70}$$

Let us now consider the case of an initial and target operators A and B transforming according to the symmetry group $\mathcal{G}_{\text{int}}^{\text{coh},0}$ of the idealised internal coherent Hamiltonian We write both operators in terms of their irreducible components:

$$\begin{aligned} A &= \sum_{i=1}^{c} A^{\Upsilon^i} \\ B &= \sum_{i=1}^{c} B^{\Upsilon^i} \end{aligned} \tag{4.71}$$

The transformation of A into B involves the transformation of all the irreducible components. Essentially the Sørensen theorem can be reformulated for each irreducible component:

$$U^{\Upsilon^j} A^{\Upsilon^j} U^{\Upsilon^{j\dagger}} = b^{\Upsilon^j} B^{\Upsilon^j} + C^{\Upsilon^j} \tag{4.72}$$

with $\text{Tr}(B^{\Upsilon^j} C^{\Upsilon^j} = 0)$. The transformation coefficients are subjected to unitary bounds:

$$b^{\Upsilon^j_{\text{min}}} \leq b^{\Upsilon^j} \leq b^{\Upsilon^j_{\text{max}}} \tag{4.73}$$

and

$$\begin{aligned} b_{\min}^{\Upsilon^j} &= \|B^{\Upsilon^j}\|^{-2}\Lambda_{A\uparrow}^{\Upsilon^j}\cdot\Lambda_{B\downarrow}^{\Upsilon^j} \\ b_{\max}^{\Upsilon^j} &= \|B^{\Upsilon^j}\|^{-2}\Lambda_{A\uparrow}^{\Upsilon^j}\cdot\Lambda_{B\uparrow}^{\Upsilon^j} \end{aligned} \tag{4.74}$$

The maximum coefficient for a symmetry constrained transformation $b_{\max}^{\mathrm{SC}}$ from an initial operator A to a final operator B is given by:

$$\begin{aligned} b_{\max}^{\mathrm{SC}} &= \frac{\mathrm{Tr}(B^\dagger UAU^\dagger)}{\mathrm{Tr}(B^\dagger B)} \\ &= \|B\|^{-2}\sum_{j=1}^{c} b_{\max}^{\Upsilon^j}\|B^{\Upsilon^j}\|^2 \\ &= \|B\|^{-2}\sum_{j=1}^{c}\Lambda_{A\uparrow}^{\Upsilon^j}\cdot\Lambda_{B\uparrow}^{\Upsilon^j} \end{aligned} \tag{4.75}$$

Similarly

$$b_{\min}^{\mathrm{SC}} = \|B\|^{-2}\sum_{j=1}^{c}\Lambda_{A\uparrow}^{\Upsilon^j}\cdot\Lambda_{B\downarrow}^{\Upsilon^j} \tag{4.76}$$

In general the following equation applies:

$$b_{\min} \le b_{\min}^{\mathrm{SC}} \le b_{\max}^{\mathrm{SC}} \le b_{\max} \tag{4.77}$$

The above derivation as well as several examples accounting for the application of this generalized theorem in two- and multi-spin systems are reported in the paper from Levitt [17].

For completeness we consider again the case of a homo-nuclear two-spin system where the evolution operator U is symmetric with respect to exchange of the two spin labels.

Ex 2 M2S in presence of symmetry: In this example conversion from magnetization to singlet (M2S) happens in presence of symmetry, and the relevant equation to be applied to obtain the maximum conversion is equation 4.75. A singlet-triplet basis to represent the operators is again assumed. The matrix representation of normalized operators of $I_z = I_{1z} + I_{2z}$ (longitudinal magnetization) and SO = $\mathbf{I_1}\cdot\mathbf{I_2}$ (singlet order) remains the same as in equation 4.62. We designate the two irreducible representations g and u standing for Υ^g and Υ^u in Table 4.1 for brevity. The spectra of the two operators are now grouped by irreducible representations

in ascending order as follows:

$$\Lambda^{g}_{I_z\uparrow} = \frac{1}{\sqrt{2}} \begin{pmatrix} -1 \\ 0 \\ 1 \end{pmatrix}$$

$$\Lambda^{g}_{\mathrm{SO}\uparrow} = \frac{1}{2\sqrt{3}} \times \begin{pmatrix} -1 \\ -1 \\ -1 \end{pmatrix}$$

$$\Lambda^{u}_{I_z\uparrow} = \frac{1}{\sqrt{2}} \begin{pmatrix} 0 \end{pmatrix}$$

$$\Lambda^{u}_{\mathrm{SO}\uparrow} = \frac{1}{2\sqrt{3}} \times \begin{pmatrix} 3 \end{pmatrix} \tag{4.78}$$

We can estimate $b^{\mathrm{SC}}_{\mathrm{max}}$ by

$$b^{\mathrm{SC}}_{\mathrm{max}}(I_z \rightarrow \mathrm{SO}) = \left| \frac{\mathrm{Tr}(\mathrm{SO}^{\dagger} \cdot \hat{U} \cdot I_z)}{\mathrm{SO}^{\dagger} \cdot \mathrm{SO}} \right|_{\mathrm{max}} = \frac{\Lambda^{g}_{I_z\uparrow} \cdot \Lambda^{g}_{\mathrm{SO}\uparrow}}{\Lambda^{g}_{\mathrm{SO}\uparrow} \cdot \Lambda^{g}_{\mathrm{SO}\uparrow}} + \frac{\Lambda^{u}_{I_z\uparrow} \cdot \Lambda^{u}_{\mathrm{SO}\uparrow}}{\Lambda^{u}_{\mathrm{SO}\uparrow} \cdot \Lambda^{u}_{\mathrm{SO}\uparrow}} = 0 \tag{4.79}$$

Therefore for any unitary transformation is impossible to convert longitudinal magnetization into singlet order by coherent means when the evolution operator is total-symmetric. The same result was previously obtained by applying the vanishing integral rule.

To our purposes the computation of either $b^{\mathrm{SC}}_{\mathrm{max}}$ and b_{max} proves to be extremely important when discussing the nuclear spin permutation group $\mathcal{G}^{\mathrm{acc}}$ for the accessibility operators (see section 4.21). If starting from an equilibrium configuration represented by an initial density operator, the maximum obtainable conversion to a generic LLS represented either by $b^{\mathrm{SC}}_{\mathrm{max}}$ or b_{max} is zero, then in the limit of the introduced approximations, detection of LLS is doomed to failure.

4.21 LLS accessibility via coherent mechanisms

As we have just seen in section 4.18, $\mathcal{H}^{\mathrm{coh}}_{\mathrm{int}}$ is usually replaced by the idealised version $\mathcal{H}^{\mathrm{coh,0}}_{\mathrm{int}}$. The theoretical analysis is indeed performed assuming as a valid approximation an idealised $\mathcal{G}^{0}_{\mathrm{Z}}$ and $\mathcal{G}^{0}_{\mathrm{J}}$ and therefore a legitimate use of $\mathcal{G}^{\mathrm{coh,0}}_{\mathrm{int}}$ is supposed. However for the LLS to be accessible we usually need a symmetry breaking mechanism, otherwise LLS would be completely NMR silent, as demonstrated in **Ex 2** in the previous section. Whereas the identification of LLS relies on the analysis of idealised Hamilto-

nian operators, the accessibility problem requires us to consider the symmetry group of the realistic Hamiltonian. In order to drive spin population between different spin states we need at least a matrix element to couple them. In permutation symmetry language this implies that the symmetry group of the *access operator* $\mathcal{H}^{\text{acc}}$ needs to have a *lower* symmetry than the one of $\mathcal{H}^{\text{coh,0}}_{\text{int}}$.

$$\mathcal{G}^{\text{acc}} \subset \mathcal{G}^{\text{coh,0}}_{\text{int}} \tag{4.80}$$

The accessibility problem is better presented in conjunction with the maximum spin conversion stated beforehand via the following examples:

- A inequivalent two-spin system.
- A inequivalent four-spin system.

Ex 3 In systems modelled as two-spin, two nuclei can be rendered chemically inequivalent only if they are subjected to slightly different local magnetic fields. We assume the Hamiltonian in equation 4.26 under the regime defined by equation 4.50. We have:

$$\begin{aligned} \mathcal{G}^0_{\text{Z}} = \mathcal{G}^0_{\text{J}} &= \{(), (12)\} \\ \mathcal{G}^{\text{coh,0}}_{\text{int}} &= \{(), (12)\} \\ \mathcal{G}^0_{\text{DD}} &= \{(), (12)\} \\ \mathcal{G}^0_{\text{H}} = \mathcal{G}^{\text{coh,0}}_{\text{int}} \cap \mathcal{G}^0_{\text{DD}} &= \{(), (12)\} \\ \mathcal{G}^{\text{acc}} = \mathcal{G}_{\text{Z}} &= \{()\} \end{aligned} \tag{4.81}$$

Here $\mathcal{H}_Z = \Omega^0_1 I_{1z} - \Omega^0_2 I_{2z}$ (see Fig. 4.2) is not symmetric with respect to (12). Ω^0_i is the offset frequency of nucleus i. According to section 4.17 the number of long-lived orders is given by the conjugacy classes in $\mathcal{G}^0_{\text{H}}$. In this example we have two conjugacy classes and therefore two LLS. The first is represented by the overall spin population, the second one is the population imbalance between states symmetric or antisymmetric with respect the (12) transposition: *the singlet order*. It is expressed as:

$$LLS = \Delta_{g,u} = \frac{1}{3}\sum_{i=1}^{3} |T_i\rangle\langle T_i| - |S\rangle\langle S|, \tag{4.82}$$

where the expression $\Delta_{g,u}$ accounts for the fact that triplet states transform as Υ^g and singlet state as Υ^u. Given that $\mathcal{G}^{\text{acc}} \subset \mathcal{G}^{\text{coh,0}}_{\text{int}}$ a coherent mechanism can be devised to promote transitions between nuclear spin states spanning singlet and triplet manifolds. This is accomplished for example from M2SS2M [6, 9] and SLIC [11] pulse sequences. As previously shown thermal magnetization can be

converted into singlet order and reconverted into readable magnetization with an optimum conversion, predicted by the Sørensen theorem, of 2/3.

Ex 4 Multi-spin systems are somehow richer in terms of coherent accessibility. Multi-spin environments can indeed be classified as nearly chemically equivalent according to equation 4.50, or nearly magnetic equivalent according to equation 4.52. In the case of near chemical equivalence a treatment similar to the previous example can be done.

We now consider the case of a four-spin system. To fix the idea we refer to either protonated or deuterated diacetylene as per Ref. [5]. Homo-nuclei have identical

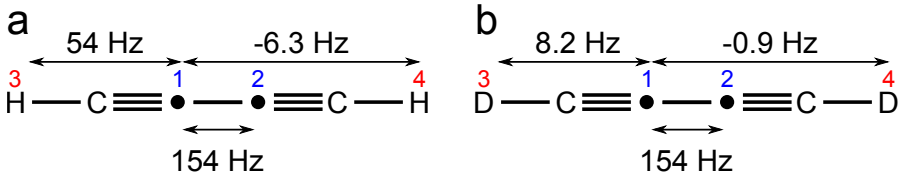

Figure 4.9: Protonated diacetylene in a) and deuterated diacetylene in b). J couplings as reported in Ref. [2]. Labels 1 and 2 denote ^{13}C nuclei, whereas labels 3 and 4 denote in a) ^{1}H nuclei and in b) ^{2}H nuclei. For both molecules $J_{13} = J_{24}$ and $J_{14} = J_{23}$.

chemical shift, and given that the carbon-carbon J-coupling is 154 Hz and that the difference in the hetero-nuclear J coupling is 60.3 Hz for protonated-diacetylene and 9.1 Hz for deuterated-diacetylene we are in the regime specified by equation 4.52 (see Fig. 4.9). We indicate ^{13}C nuclei with labels 1 and 2, and ^{1}H or ^{2}H nuclei with labels 3 and 4. For both linear molecules $J_{13} = J_{24}$ and $J_{14} = J_{23}$ and considering the Hamiltonians in equation 4.26 we have :

$$\begin{aligned}
\mathcal{G}_{\mathrm{Z}}^{0} = \mathcal{G}_{\mathrm{J}}^{0} &= \{(), (12), (34), (12)(34)\} \\
\mathcal{G}_{\mathrm{int}}^{\mathrm{coh},0} &= \{(), (12), (34), (12)(34)\} \\
\mathcal{G}_{DD} &= \{(), (12)(34)\} \\
\mathcal{G}_{\mathrm{DD}}^{0} &= \{(), (12), (34), (12)(34)\} \\
\mathcal{G}_{\mathrm{H}}^{0} = \mathcal{G}_{\mathrm{int}}^{\mathrm{coh},0} \cap \mathcal{G}_{\mathrm{DD}}^{0} &= \{(), (12), (34), (12)(34)\} \\
\mathcal{G}^{\mathrm{acc}} = \mathcal{G}_{J} &= \{(), (12)(34)\}
\end{aligned} \tag{4.83}$$

In this example $\mathcal{H}^{\mathrm{acc}} = \mathcal{H}_J$ is symmetric only with respect to the simultaneous permutation of ^{13}C and ^{1}H or ^{2}H. As a result according to $\mathcal{G}_{\mathrm{H}}^{0}$ we predict the existence of four long-lived orders. We focus now on protonated dyacetilene for simplicity, and label the four irreducible representations of $\mathcal{G}_{\mathrm{H}}^{0}$ as Υ^{gg}, Υ^{uu}, Υ^{gu}, Υ^{ug}. The symmetry adapted basis in the matrix representations in Fig. 4.10 is the singlet triplet product basis:

$$\mathbb{B}_{ST} = \{ST\}_{12} \otimes \{ST\}_{34} \tag{4.84}$$

and the $2^{2\times2} = 16$ wave functions can be classified according to:

$$\begin{aligned}
\Upsilon^{nspins} &= \Upsilon^{gg} \oplus \Upsilon^{uu} \oplus \Upsilon^{gu} \oplus \Upsilon^{ug} \\
\{|T_i\rangle\}_{12} \otimes \{|T_j\rangle\}_{34} &\sim \Upsilon^{gg} \qquad \forall i,j \in \{1,0,-1\} \\
\{|S\rangle\}_{12} \otimes \{|S\rangle\}_{34} &\sim \Upsilon^{uu} \\
\{|T_i\rangle\}_{12} \otimes \{|S\rangle\}_{34} &\sim \Upsilon^{gu} \qquad \forall i \in \{-1,0,1\} \\
\{|S\rangle\}_{12} \otimes \{|T_j\rangle\}_{34} &\sim \Upsilon^{ug} \qquad \forall j \in \{-1,0,1\}
\end{aligned} \tag{4.85}$$

The manifold gg in Fig. 4.10 includes for example the 9 spin states transforming as Υ^{gg}. Similarly for the other spin states. From the matrix representations in Fig. 4.10-a matrix elements $\propto (J_{13} - J_{14})$ connect the gg and uu subspaces. A

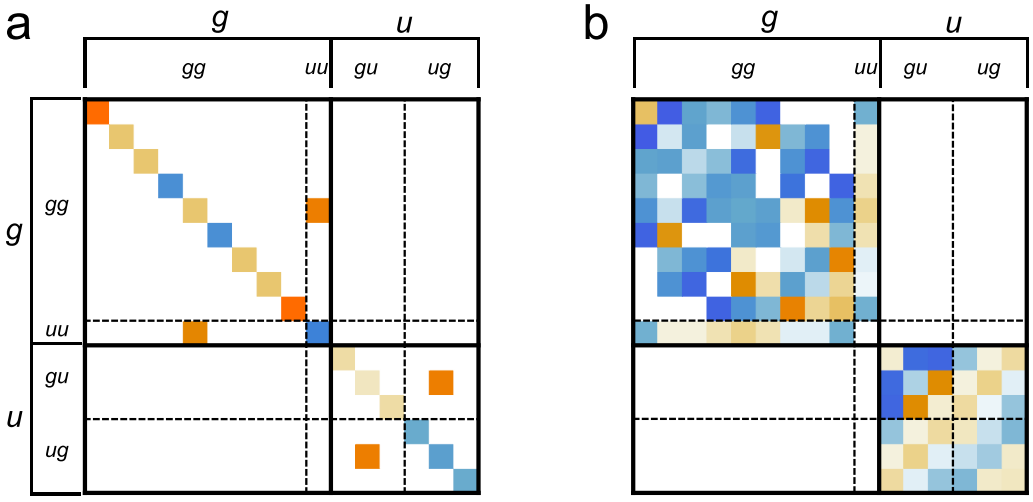

Figure 4.10: Matrix representations in a) of $\mathcal{H}_{\text{int}}^{\text{coh}}$ and in b) of $\mathcal{H}_{\text{DD}}$ for the protonated diacetylene system of Ref. [2].

pulse sequence as for instance M2S [6, 105] or SLIC [11] could then be used to access the population imbalance between these manifolds. In Fig. 4.10 are represented the realistic $\mathcal{H}_{\text{int}}^{\text{coh}}$ and $\mathcal{H}_{\text{DD}}$. In particular, as we have just seen, the realistic dipolar Hamiltonian is only symmetric with respect to (12)(34):

$$\mathcal{G}_{DD} = \{(), (12)(34)\} \subset \{(), (12), (34), (12)(34)\} = \mathcal{G}_{\text{DD}}^{0} \tag{4.86}$$

and therefore given that several matrix elements in $\mathcal{H}_{\text{DD}}$ representation connect the manifolds gg and uu, the population imbalance between gg and uu would not be expected to be long-lived. However, given the distance between ^{1}H and ^{13}C labelled positions, the off-diagonal elements in the $\mathcal{H}_{\text{DD}}$ representation are sufficiently small in the examples considered in Ref [5] to justify the adoption of $\mathcal{H}_{\text{DD}}^{0}$. As pointed out in the section 4.18 if this idealisation was not made the LLS would remain concealed. One of the four long-lived orders corresponding in Fig. 4.10 to the imbalance between g and u manifolds cannot be coherently

accessed due to the fact that the system is perfect chemical equivalent. The other two non trivial long-lived orders can be expressed as follows:

$$\begin{aligned} LLS\,1 = \Delta_{gg,uu} &= \frac{1}{9}\sum_{i=1}^{9} |gg\rangle_i \langle gg|_i - |uu\rangle \langle uu| \\ LLS\,2 = \Delta_{gu,ug} &= \frac{1}{3}\sum_{i=1}^{3} |gu\rangle_i \langle gu|_i - \frac{1}{3}\sum_{i=1}^{3} |ug\rangle_i \langle ug|_i \end{aligned} \tag{4.87}$$

The reason the $\Delta_{g,u}$ population imbalance (see Fig.4.10) cannot be coherently accessed by an operator with symmetry $\mathcal{H}^{\text{acc}}$ has to be sought in the presence of the symmetry operation (12)(34). Restriction of $\mathcal{G}^{\text{acc}}$, as shown in Fig. 4.11, allowing the access $\Delta_{g,u}$ population imbalance could be formally obtained by:

(a) Introduction of asymmetry in $\mathcal{H}_Z$ by means of introducing a chemical shift difference between like nuclei. Operators such as $\Omega_1^0 I_{1z} - \Omega_2^0 I_{2z}$ and $\Omega_3^0 I_{3z} - \Omega_4^0 I_{4z}$ could provide the symmetry breaking mechanism.

(b) Introduction of asymmetry in $\mathcal{H}_J$ by removing the condition $J_{13} = J_{24}$ and $J_{14} = J_{23}$. An operator such as $J_{13} I_{1z} I_{3z} - J_{24} I_{2z} I_{4z}$ and $J_{23} I_{2z} I_{3z} - J_{14} I_{1z} I_{4z}$.

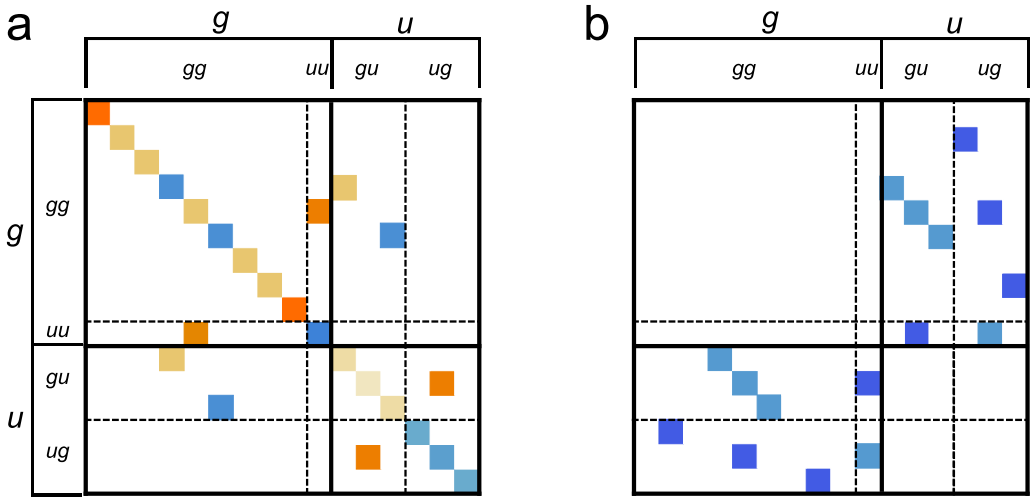

Figure 4.11: Matrix representations using the symmetry adapted basis in equation 4.84 in a four-spin system in a) of operator $\mathcal{H}_J$ with hetero-nuclear J couplings such that $J_{13} \neq J_{24} \neq J_{23} \neq J_{14}$, and in b) of the operator $\mathcal{H}_Z$ with $\Omega_1^0 \neq \Omega_2^0 \neq \Omega_3^0 \neq \Omega_4^0$.

4.22 LLS: from near eigenstates to population imbalances

In this section I will review how the concept of long-lived order has evolved during the years and try to show how the symmetry analysis conveys possibly the most general approach to this topic so far. We will comment upon a few cases.

- **Chemical equivalence** Let us suppose a molecule has two homo-nuclear isolated and chemical equivalent spin-1/2 nuclei. They share the same resonance frequency Ω^0 and the only coupling J_{12} is between themselves. The internal coherent and dipolar Hamiltonian operators can be expressed as follows:

$$\begin{aligned} \mathcal{H}_Z &= \Omega^0(I_{1z} + I_{2z}) \\ \mathcal{H}_J &= 2\pi J_{12}\mathbf{I_1}\cdot\mathbf{I_2} \\ \mathcal{H}_{\text{int}}^{\text{coh}} &= \mathcal{H}_Z + \mathcal{H}_J \\ \mathcal{H}_{\text{DD}} &= \sum_{m=-2}^{m=2}(-1)^m A_{2m}^{12} T_{2-m}^{12} \end{aligned} \tag{4.88}$$

with $A_{20}^{12} = \sqrt{6}b_{12}$ and $A_{2m\neq 0}^{12} = 0$. The matrix representation of $\mathcal{H}_{\text{int}}^{\text{coh}}$ in a singlet-triplet Hilbert space basis is:

$$\mathcal{H}_{\text{int}}^{\text{coh}} = \begin{array}{c} \begin{array}{cccc} |S\rangle & |T^1\rangle & |T^0\rangle & |T^{-1}\rangle \end{array} \\ \begin{pmatrix} \frac{-3J_{12}\pi}{2} & 0 & 0 & 0 \\ 0 & \frac{J_{12}\pi}{2}+\Omega^0 & 0 & 0 \\ 0 & 0 & \frac{J_{12}\pi}{2} & 0 \\ 0 & 0 & 0 & \frac{J_{12}\pi}{2}-\Omega^0 \end{pmatrix} \end{array} \tag{4.89}$$

whereas the dipolar Hamiltonian in the same basis can be expressed as:

$$\mathcal{H}_{\text{DD}} = \begin{array}{c} \begin{array}{cccc} |S\rangle & |T^1\rangle & |T^0\rangle & |T^{-1}\rangle \end{array} \\ \begin{pmatrix} 0 & 0 & 0 & 0 \\ 0 & \frac{1}{8}b_{12}(1+3\cos(2\beta)) & \frac{3b_{12}e^{-i\gamma}\cos(\beta)\sin(\beta)}{2\sqrt{2}} & \frac{3}{4}b_{12}e^{-i2\gamma}\sin^2(\beta) \\ 0 & \frac{3b_{12}e^{-i\gamma}\cos(\beta)\sin(\beta)}{2\sqrt{2}} & -\frac{1}{4}b_{12}(1+3\cos(2\beta)) & -\frac{3b_{12}e^{-i\gamma}\cos(\beta)\sin(\beta)}{2\sqrt{2}} \\ 0 & \frac{3}{4}b_{12}e^{-i2\gamma}\sin^2(\beta) & -\frac{3b_{12}e^{-i\gamma}\cos(\beta)\sin(\beta)}{2\sqrt{2}} & \frac{1}{8}b_{12}(1+3\cos(2\beta)) \end{pmatrix} \end{array} \tag{4.90}$$

for a generic orientation $\Omega = \{\alpha, \beta, \gamma\}$ (not to be confused with Ω^0) of the inter-nuclear axis with respect to the laboratory frame. The term $b_{12} = -\frac{\mu_0}{4\pi}\frac{\gamma^2\hbar}{r_{12}^3}$ is the dipole-dipole coupling constant. The singlet state $|S\rangle = \frac{1}{\sqrt{2}}(|\alpha_1\beta_2)\rangle - |\beta_1\alpha_2)\rangle$ is not only a pure eigenstate of the internal coherent Hamiltonian, but in addition it is not dipolar-coupled to any of the triplet states (see eq. 4.90). Moreover if the random magnetic fields at the sites of the two nuclei are perfectly correlated and have the same root mean square (rms) value, then the singlet state is also unaffected by the random fields [110, 111]:

$$T_S^{-1} = 2\gamma^2(B_1^2 + B_2^2 + 2CB_1B_2)(j_0 + 2j_1) \tag{4.91}$$

where γ is the gyromagnetic ratio, $B_i = \sqrt{\langle \mathbf{B_i} \cdot \mathbf{B_i} \rangle}$ is the rms of the random fields magnitudes at the nuclear sites, $C = \langle \mathbf{B_1} \cdot \mathbf{B_2} \rangle / B_1 B_2$ represents the extent that the random fields are correlated to one another and the $j_m = j_1(m\gamma B^0)$ are the rank-1 spectral densities of the random field fluctuations. These properties led to initially recognize, and the terminology still survives in the common parlance, the singlet state population $|S\rangle\langle S|$ as the long-lived order for a two-spin system.

A long-lived order, in this context, has to be intended as a conserved quantity that does not evolve under the evolution defined by the Liouvillian superoperator which includes coherent and fluctuating contributions leading to relaxation:

$$\begin{aligned} \frac{d}{dt}\rho_{\mathrm{LLS}}(t) &= \hat{\mathcal{L}}\rho_{\mathrm{LLS}}(t) = 0 \\ \hat{\mathcal{L}} &= -i\hat{\mathcal{H}} + \hat{\Gamma} \end{aligned} \tag{4.92}$$

where ρ_{LLS} is the LLS operator that does not evolve in time, $\hat{\mathcal{L}}$ is the Liouvillian superoperator formed by the commutation superoperator $\hat{\mathcal{H}}$ and the double commutation relaxation superoperator $\hat{\Gamma}$. The vector space formed by the eigenoperators of $\hat{\mathcal{L}}$ with zero eigenvalues is defined as the null space of $\hat{\mathcal{L}}$. The dimension of this space is always different from zero and may be greater or equal to one. Indeed it always contains the identity operator representing the conservation of the overall spin population for an isolated spin system. For the case of a homo-nuclear chemical equivalent spin system in presence of intramolecular dipole interaction and/or perfectly correlated random magnetic fields with identical rms at the sites of the two nuclei, it also includes the operator $\rho_{\mathrm{LLS}} \propto \mathbf{I_1} \cdot \mathbf{I_2}$. This operator is also called *singlet order*. The matrix representation of the normalized operator $\mathbf{I_1} \cdot \mathbf{I_2}$ is reported in example **Ex 1**, and defines a population imbalance between manifolds of different symmetry:

$$\begin{aligned} \Delta_{gu} = \rho_{\mathrm{LLS}} &= \frac{1}{3}\sum_i |g\rangle_i\langle g|_i - |u\rangle\langle u| \\ &= \frac{1}{3}\sum_{m=\{-1,0,1\}} |T^m\rangle\langle T^m| - |S\rangle\langle S| \end{aligned} \tag{4.93}$$

In equation 4.93 ρ_{LLS} has been expressed as the population imbalance between states that are symmetric (g) and antisymmetric (u) with respect to nuclear spin exchange, i.e. the permutation (12) (see character table 4.1). A complete theoretical analysis for long-lived nuclear spin states in solution can be found in Ref.[57, 59, 110].

- **Near chemical equivalence** In molecules with two inequivalent nuclei, singlet state is not an eigenstate of the coherent internal Hamiltonian as it is connected with rapid-relaxing triplet states. The Zeeman Hamiltonian has the form $\mathcal{H}_Z =$

$\Omega_1^0 I_{1z} + \Omega_2^0 I_{2z}$ and the following matrix representation:

$$\mathcal{H}_{\text{int}}^{\text{coh}} = \begin{array}{c} \begin{matrix} |S\rangle & |T^1\rangle & |T^0\rangle & |T^{-1}\rangle \end{matrix} \\ \begin{pmatrix} \frac{-3J_{12}\pi}{2} & 0 & \frac{\delta\Omega}{2} & 0 \\ 0 & \frac{J_{12}\pi}{2} + \frac{\Sigma\Omega}{2} & 0 & 0 \\ \frac{\delta\Omega}{2} & 0 & \frac{J_{12}\pi}{2} & 0 \\ 0 & 0 & 0 & \frac{J_{12}\pi}{2} - \frac{\Sigma\Omega}{2} \end{pmatrix} \end{array} \tag{4.94}$$

where $\delta\Omega = \Omega_1^0 - \Omega_2^0$ and $\Sigma\Omega = \Omega_1^0 + \Omega_2^0$. In this case the term $\delta\Omega$ breaks the symmetry of the system and connects states spanning across different manifolds. External intervention can be applied to modulate the relevance of this term. For example lifting the NMR sample in regions of low magnetic fields or the application of a spin locking pulse can effectively reduce the incidence of $\delta\Omega$ and, under these conditions, $|S\rangle$ is a *near eigenstate* for the coherent internal Hamiltonian [6, 57, 105]. In the limit $\delta\Omega \to 0$ the analysis is identical to the chemical equivalent case. M2S and SLIC pulse sequences have been developed to allow the coherent access of the singlet order in systems nearly equivalent [6, 11, 105]. In the near chemical equivalence regime the long-lived order can be defined as a perturbation of the population imbalance between manifolds of different symmetry as expressed in equation 4.93.

- **Near magnetic equivalence** When the spin system includes more than two spins the coherent accessibility to the singlet state between two homo-nuclei may be granted by the J coupling network even in presence of chemical equivalence. This is the case for investigations in Ref.[2–5]. For example in the AA'XX' spin system modelling the protonated $^{13}C_2$-diacetylene molecule (also discussed in **Ex 4** using a permutation symmetry approach), the two ^{13}C and the two ^1H nuclei are chemically equivalent but magnetic inequivalent. As discussed in Ref. [3], in the matrix representation of the internal coherent Hamiltonian using the singlet-triplet product basis $\mathbb{B}_{ST} = \{ST\}_{CC} \otimes \{ST\}_{HH}$ (essentially identical to the one used in equation 5.9), the 2×2 subspace can be identified:

$$\begin{array}{c} \begin{matrix} |T_{CC}^0 T_{HH}^0\rangle & |S_{CC} S_{HH}\rangle \end{matrix} \\ \begin{pmatrix} \frac{1}{2}(J_{CC} + J_{HH}) & -\frac{1}{2}(J_{CH} - J_{CH'}) \\ -\frac{1}{2}(J_{CH} - J_{CH'}) & -\frac{1}{2}(J_{CC} + J_{HH}) \end{pmatrix} \end{array} \tag{4.95}$$

where J_{CC} and J_{HH} are the homo-nuclear ^{13}C and ^1H J couplings respectively, whereas J_{CH} and $J_{CH'}$ are the two hetero-nuclear J couplings. The product of the two singlet states $|S_{CC} S_{HH}\rangle$ is connected to the product of the two triplet states $|T_{CC}^0 T_{HH}^0\rangle$ by a term that is proportional to the degree of asymmetry of the system: $-\frac{1}{2}(J_{CH} - J_{CH'})$.

Incidentally it should be noted that in the present case $|S_{CC} S_{HH}\rangle = |uu\rangle$ and that

$|T^0_{CC}T^0_{HH}\rangle$ is one of the $|gg\rangle_i$ following the notation used in **Ex 4**.
Therefore if $\frac{1}{2}(J_{CH} - J_{CH'}) \ll \frac{1}{2}(J_{CC} + J_{HH})$ the state $|S_{CC}S_{HH}\rangle$ is a *near eigenstate* or a *disconnected eigenstate* [3, 18] of the internal coherent Hamiltonian of the system under investigation. This is certainly the case for protonated $^{13}C_2$-diacetylene with $J_{CH} - J_{CH'} \simeq 60$ Hz and $J_{CC} + J_{HH} \geq 154$ Hz. However this is in general not enough to make a *disconnected eigenstate* as the $|S_{CC}S_{HH}\rangle$ also a long-lived order. Indeed the dipole-dipole Hamiltonian for the protonated $^{13}C_2$-diacetylene molecule can promote transitions between $|S_{CC}S_{HH}\rangle$ and $|T^0_{CC}T^0_{HH}\rangle$, but the matrix element $\langle T^0_{CC}T^0_{HH}|\,\mathcal{H}_{\rm DD}\,|S_{CC}S_{HH}\rangle$ is sufficiently small to preserve the population operator $|S_{CC}S_{HH}\rangle\langle S_{CC}S_{HH}|$. In a first approximation this matrix element (and other connecting $|S_{CC}S_{HH}\rangle$ with other states that are symmetric upon the simultaneous nuclear spin permutation of the two ^{13}C and the two ^{1}H as represented in Fig. 4.10-b) can be neglected. This same assumption allowed in **Ex 4** to consider the permutation (12) and (34) as valid permutation symmetry operations for the internal dipolar Hamiltonian in $\mathcal{G}^0_{\rm DD}$. According to our previous analysis we recognize the long-lived order as the population operator:

$$\begin{aligned}\Delta_{gg,uu} &= \frac{1}{9}\sum_{i=1}^{9}|gg\rangle_i\langle gg|_i - |uu\rangle\langle uu| \\ &= \frac{1}{9}\sum_{m,m\prime=\{-1,0,1\}}|T^m_{CC}T^{m\prime}_{HH}\rangle\langle T^m_{CC}T^{m\prime}_{HH}| - |S_{CC}S_{HH}\rangle\langle S_{CC}S_{HH}| \quad (4.96)\end{aligned}$$

- **Strong magnetic inequivalence** In Chapter 5 a long-lived order is discussed in a system (*1-(ethyl-d5) 4-(propyl-d7)(E)-but-2-enedioate-2,3-*$^{13}C_2$ named $^{13}C_2$-AFD) that can be formally treated as a strong magnetic inequivalent four-spin system composed by two ^{13}C and two ^{1}H nuclei (see Fig. 5.2-c and Table 5.1). The presence of asymmetric ester groups introduces a small chemical shift difference between ^{13}C and ^{1}H nuclei (see the values reported in Table 5.1). This slight chemical inequivalence is essential to experimentally access a long-lived order as will be further discussed later in Chapter 5 but can initially be disregarded in the computation of the eigenstates of the internal coherent Hamiltonian. Under this assumption the analysis is formally identical to the previous one, with the only remarkable difference that for $^{13}C_2$-AFD $J_{CH} - J_{CH'} \simeq 170$ Hz and $J_{CC} + J_{HH} \simeq 87$ Hz and therefore $|S_{CC}S_{HH}\rangle\langle S_{CC}S_{HH}|$ *is not a near or disconnected eigenstate*.
However, as will be demonstrated in Chapter 5, this is not a necessary requirement and a long-lived order can still be predicted and described as the population

imbalance:

$$\begin{aligned}\Delta_{gu} &= \frac{1}{10}\sum_{i=1}^{10}|g\rangle_i\langle g|_i - \frac{1}{6}\sum_{i=1}^{6}|u\rangle_i\langle u|_i \\ &= \frac{1}{10}\Big(\sum_{m,m\prime=\{-1,0,1\}}|T^m_{CC}T^{m\prime}_{HH}\rangle\langle T^m_{CC}T^{m\prime}_{HH}| + |S_{CC}S_{HH}\rangle\langle S_{CC}S_{HH}|\Big) \\ &- \frac{1}{6}\Big(\sum_{m=\{-1,0,1\}}|T^m_{CC}\langle S_{HH}|\rangle + |S_{CC}\langle T^m_{HH}|\rangle\Big) \end{aligned} \tag{4.97}$$

where g and u are nuclear spin states symmetric and antisymmetric with respect to the simultaneous permutation of ^{13}C and ^{1}H.

- **Magnetic equivalence with internal dynamics** We finally mention the case of a LLS in a magnetic equivalent system, considered in-depth in Chapter 5, that cannot be described by the nomenclature of *near or disconnected eigenstate*: the methyl group in γ-picoline. This system is formed by three magnetic equivalent ^{1}H and one ^{13}C nuclei and the nuclear wave-functions can be classified according to their symmetry properties (see Chapter 5). However the absence of any inversion geometry in the spin system causes the nuclear spin states to be coupled to one another by the mutual dipole-dipole interactions. There is no state protected against it. However the transition probabilities between states of different symmetry in equation 5.40 depend on the value of the proton rotational correlation time τ_{R}, and for a strongly unhindered rotations (as in the case of ^{13}C-γ-picoline) in the limit $\tau_{\mathrm{R}} \to 0$, the manifold spanned by states of symmetry A becomes separated by the E_{a} and E_{b} manifolds. Therefore the population imbalance between nuclear spin states of symmetry A and E is preserved under evolution and has been detected to be longer lived than either $T_1(^{1}\mathrm{H})$ and $T_1(^{13}\mathrm{C})$. We describe the long-lived order for this system as

$$\Delta_{A,E} = \frac{1}{8}\sum_{i=1}^{8}|i,A\rangle\langle i,A| - \frac{1}{4}\Big(\sum_{i=9}^{12}|i,E_a\rangle\langle i,E_a| + \sum_{i=13}^{16}|i,E_b\rangle\langle i,E_b|\Big) \tag{4.98}$$

As the previous examples and other presented in Chapter 5 show, the permutation symmetry analysis allows to describe LLS as population imbalances of nuclear spin states spanning across different irreducible representations and it possibly represents the most general description of LLS occurring under different geometrical and dynamical regimes.

4.23 Summary

In this chapter a formalization of the LLS analysis has been proposed using a discrete group theory approach. Permutation symmetry can be employed in multi-spin systems to classify coherent and incoherent interactions. The latter is the essential step leading to the definition of the number of conserved quantities in the spin system and their expression in terms of population imbalances.

An important role is played by the set of introduced approximations. Depending on their range of validity they can affect the permutation symmetry group of the complete Hamiltonian, and as a result the number of LLS and the prediction regarding their accessibility. Some advantages and disadvantages can be recognized:

- Advantages:
  - Classification of the nuclear wave functions, coherent and incoherent Hamiltonians according to their symmetry properties can help to identify LLS and design coherent ways to access them.
  - A matrix representation on a suitable symmetrized basis can provide "intuitive" insight on LLS.
  - The representation of LLS as spin population imbalances results straightforward using a symmetry-based approach.
- Disadvantages:
  - The set of introduced approximations has to be properly calibrated. It directly affects the elements in the symmetry group of the complete Hamiltonian. As a result, different levels of approximations may lead to distinct outcomes.

It is worth outlining that as any scientific theory should be backed from experimental evidence, this also applies in the present case. The experiment is crucial to verify *ex post* the correct set of approximations, and allows to modify it if necessary. For this reason in the following chapter the experimental results are discussed alongside with a formalization of the system under analysis in terms of permutation symmetry theory.

Part III

Experiments

Chapter 5

Experiments

5.1 Motivation

From a practical standpoint nuclear spin states with a relaxation time longer than T_1 are justly defined as long-lived orders. In addition long-lived coherences with lifetimes longer than T_2 have also been investigated [112, 113]. Although a large part of research concerns LLS between pairs of homo-nuclei, hetero-nuclei [49] and multi-spin environments [2–5, 18, 48, 50, 103] can also display long-lived character. Indeed a coherent symmetry breaking mechanism grounded on the asymmetry of intra-molecular J coupling network requires at least 3 spins.

In this chapter the interplay between chemical and magnetic equivalence is often evoked as it is essential when coherent accessibility of LLS is sought-after. We also show that ubiquitous nature of long-lived states includes spin systems far from magnetic equivalence when the proper geometrical requirement is met, and non-rigid molecular systems such as the methyl group. The case of 4-methyl pyridine (γ-picoline) is presented as an example of hyperpolarized long-lived order that can be populated at cryogenic temperatures in a liquid helium bath ($\sim$ 4 °K) without the intervention of radical species or microwave irradiation. Although the long-lived character that is described below for γ-picoline is typical of other methyl-systems, the possibility of efficiently hyperpolarize it just by resorting to liquid helium temperatures is rather peculiar. It depends, as will be discussed, on the rotational barrier separating states of different symmetry [53, 60, 97, 101, 102, 108, 114].

Several themes emerge altogether. There is a geometrical as well as a dynamical character associated to diverse forms of LLS. Near magnetic equivalence is neither necessary nor sufficient for a spin system to be long-lived. Internal dynamics associated with flexible parts of the molecule can induce transverse magnetic fields effective as relaxation mechanisms. This mechanism, currently under investigation, is reported as spin internal motion (SIM). A set of criteria can be identified when screening for long-lived molecules.

The chapter is organised as follows:

- Long-lived states in rigid molecules far from magnetic equivalence
- Long-lived states in non-rigid three spin systems
- One hour long-lived state in solution and room temperature
- Summary

5.2 LLS far from magnetic equivalence

In systems formed by more than two spins the existence of spin orders protected by thermalization processes depends strongly on the geometrical arrangement of nuclei, the magnitude of spin-spin couplings and chemical shift differences. All these terms are accounted for in the complete nuclear spin hamiltonian modelling the molecular system under analysis. Grant and Vinogradov [94] and Hogben and co-workers [115] studied either analytically and numerically the long-lived properties of molecular environments encompassing multiple spins. It was shown for example that for a dipolar coupled three-spin system only the linear geometrical arrangement of the spins returns a long-lived state [94]. As we will see later, the latter statement for a three-spin system is rigorously true in rigid systems but fails when internal degrees of freedom may impose further symmetry realizing what we define *dynamically-imposed long-lived states* [53, 60]. In addition LLSs can materialize in perfectly rigid dipolar-coupled larger clusters of spins when the topology includes an inversion centre [10, 55, 94, 115]. However it is worth noting that the absence of local centrosymmetry does not preclude the existence of long-lived spin orders when either the geometrical remoteness of the central spin pair from the other members of the spin system is provided [2–5, 51, 54, 116], or in the presence of fast intramolecular dynamics [53, 60].
In the following discussion, we provide an experimental demonstration of a *geometrically-imposed long-lived nuclear spin state* in an asymmetrically substituted derivative of $^{13}C_2$-fumarate (*trans*-[2,3-$^{13}C_2$]-but-2-enedioate). As discussed below, this system exhibits local centrosymmetry but is far from the regime of magnetic equivalence. The confirmed existence of a long-lived state in this system verifies the analyses in Ref. [94, 115], and shows that near-magnetic-equivalence is not a necessary condition for generating and observing long-lived nuclear spin states.

5.2.1 Introduction

As already discussed in previous chapter (see section 4.10) a pair of nuclei I_j and I_k is *near magnetic equivalent* if the following condition holds:

$$(\omega_j^0 - \omega_k^0)^2 + \pi^2 (J_{jl} - J_{kl})^2 \leq \pi^2 J_{jk}^2 \quad \forall\, l \notin \{j, k\} \tag{5.1}$$

Under conditions of near magnetic equivalence, the mixing of singlet and triplet states by the symmetry-breaking interactions is strongly suppressed by the intra-pair J coupling: a phenomenon called *J-stabilization* [104]. In this regime, efficient decay of singlet order between spins I_j and I_k is induced neither by correlated fluctuations of local magnetic fields at the sites of the two spins, nor by fluctuations of the mutual dipole-dipole coupling of I_j and I_k. The suppression of these important relaxation mechanisms often leads to a long-lived state with a relaxation time much longer than the conventional magnetization relaxation time, T_1 [104]. The condition in equation 5.1 is de-

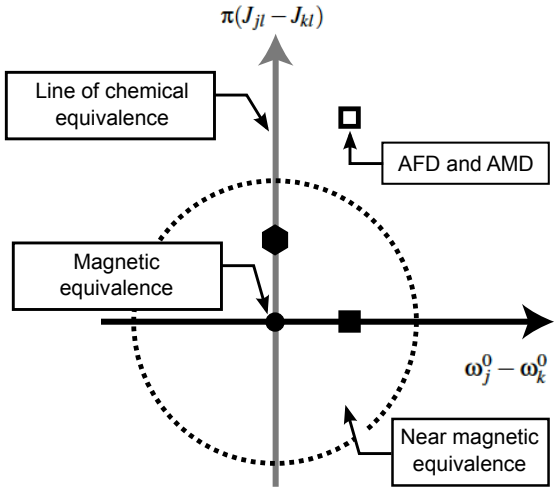

Figure 5.1: Pictorial representation of the concepts of chemical and magnetic equivalence for a pair of spins labelled j and k. The label l identifies homonuclear spin species coupled with the pair. The dashed circle has a radius $\left|\pi J_{jk}\right|$. The filled circle indicates the point of exact magnetic equivalence. Points on the vertical axis (gray) correspond to systems whose nuclei are chemically equivalent. The filled hexagon represents a spin system whose nuclei are chemically equivalent but slightly magnetically inequivalent [2–5]. The filled square indicates a spin system formed by two nuclei which are slightly chemically inequivalent [6, 7]. The open square, falling well outside the dashed circle, represents spin systems in the regime of strong magnetic inequivalence, as studied in this work. *Reproduced from Phys. Chem. Chem. Phys.* **17**, *5913(2015) with permission from the PCCP Owner Societies.*

picted graphically in Fig. 5.1. The horizontal axis indicates the difference in chemically shifted resonance frequencies of the two spins in the pair, while the vertical axis represents difference of out-of-pair J couplings to other spins in the same molecule. The dashed circle indicates the intra-pair J coupling. Spin pairs may be characterized as being *chemically equivalent* (corresponding to points on the vertical axis) or *magnetically equivalent* (point at the origin). Spin pairs with parameters within the dashed circle present *near magnetic equivalence*.

There have been extensive investigations of isolated spin-1/2 pairs with slightly different chemical shifts, represented by the filled square in Fig. 5.1. In some cases, the chemical shift difference is sufficiently small that the near-magnetic-equivalence condition in equation 5.1 is satisfied without intervention in high magnetic fields [6, 52].

In other cases is satisfied by transporting the sample into a region of low applied magnetic field [22, 105] or by applying resonant radiofrequency fields [57]. In the regime of near magnetic equivalence, long-lived order may be accessed by carefully timed pulse trains [6, 9] or by continuous radiofrequency fields of suitable amplitude [11, 117].
It is also possible to attain near-magnetic-equivalence by a deviation in the vertical direction, corresponding to small differences in J couplings to spins outside the pair, providing that equation 5.1 is still satisfied. This has been demonstrated for chemically equivalent systems (points along the vertical axis) [2–5].
In this chapter we show the existence of long-lived order in a four-spin-1/2 system which does not conform to condition in equation 5.1. This spin system displays *strong magnetic inequivalence* with parameters represented by an open square falling well outside the dashed circle in Fig. 5.1. By comparing two strongly magnetic inequivalent isomers, one exhibiting local centrosymmetry of a four-spin system, and one without centrosymmetry, we show that only the centrosymmetric system displays a long-lived state. In this special case, the long-lived state is geometrically imposed by the *local centrosymmetry* of the rigid molecular structure, as suggested in refs. [94, 115]. These cases highlight the important role of symmetry in both the coherent and fluctuating spin Hamiltonian, in determining the existence of LLS.

5.2.2 Experiments

The molecular structures of the examined samples are shown in Fig. 5.2. Both materials are di-esters of [2,3-$^{13}C_2$]-but-2-enedioate which contains a central spin system comprising two ^{13}C nuclei and two ^{1}H nuclei; the fumarate derivative (panes (a) and (c)) has a *trans* double bond, while the maleate derivative (panes (b) and (d)) has a *cis* double bond. In both cases, the two ester groups are different, causing the two ^{13}C sites (and their attached protons) to have slightly different chemical shifts. As discussed below, this slight chemical asymmetry is necessary for accessing the long-lived state. All ester groups are deuterated in order to reduce their relaxation contributions. In the following discussion, the [2,3-$^{13}C_2$]-fumarate derivative in Fig. 5.2-a [*1-(ethyl-d5) 4-(propyl-d7)(E)-but-2-enedioate-2,3-*$^{13}C_2$] is referred to as $^{13}C_2$-AFD (asymmetric fumarate diester); the [2,3-$^{13}C_2$]-maleate derivative in Fig. 5.2-b [*1-(ethyl-d5) 4-(propyl-d7)(Z)-but-2-enedioate-*$^{13}C_2$] is referred to as $^{13}C_2$-AMD (asymmetric maleate diester). $^{13}C_2$-AFD contains a 4-spin-1/2 system displaying a local centre of inversion, midway between the two ^{13}C nuclei (Fig. 5.2-c); the local 4-spin-1/2 system in $^{13}C_2$-AMD, on the other hand, displays a reflection plane but is not locally centrosymmetric (Fig. 5.2-d). The samples were synthesized as described in the supporting information of Ref. [55] and more extensively in Ref. [118].
In both cases 30 mg of the diester were dissolved in 0.5 ml of CD_3OD, added to a Wilmad low pressure/vacuum 5 mm NMR tube, degassed thoroughly using the freeze-pump-thaw technique (5 cycles), and hermetically sealed. All NMR experiments were

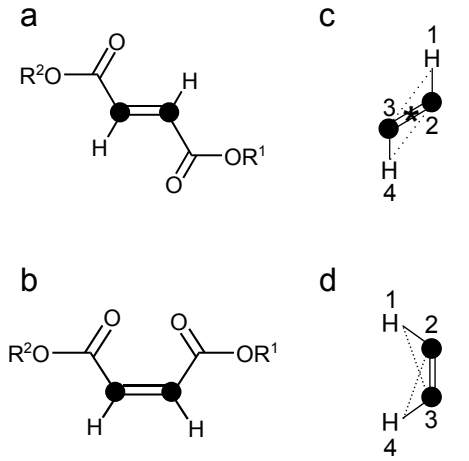

Figure 5.2: Molecular structure of (a) $^{13}C_2$-AFD and (b) of $^{13}C_2$-AMD. Filled circles denote ^{13}C nuclei. For both molecules $R^1 = CD_2CD_3$ and $R^2 = CD_2CD_2CD_3$. (c) The local spin system of $^{13}C_2$-AFD, with geometrical inversion centre marked by an asterisk. (d) The local spin system of $^{13}C_2$-AMD. *Reproduced from Phys. Chem. Chem. Phys.* **17**, *5913(2015) with permission from the PCCP Owner Societies.*

performed at a magnetic field of 11.75 T on a Bruker 500 MHz Avance III spectrometer using a Bruker 5mm triple-resonance liquid-state probe.
The ^{13}C and ^{1}H 1D-NMR spectra were fitted using *Spinach* simulation software [12, 13]. The obtained chemical shift and coupling parameters are given in Table 5.1. The spin systems in both $^{13}C_2$-AMD and $^{13}C_2$-AFD are far from magnetic equivalence. The coupling difference $|J_{12} - J_{13}|$ is more than twice $|J_{23}|$, well outside the near-magnetic-equivalence condition expressed in equation 5.1.
Experimental investigation of the long-lived states in the four-spin-1/2 systems of $^{13}C_2$-AFD and $^{13}C_2$-AMD was accomplished by the double-resonance pulse sequences shown in Fig. 5.5. These pulse sequences are based on the magnetization-to-singlet (M2S) and singlet-to-magnetization (S2M) pulse sequences used to study LLS in homonuclear 2-spin-1/2 systems [6, 105] and in near-equivalent heteronuclear systems [2–5]. A schematic outline of the density operator transformations involved in the M2S for a two-spin system is later reported in Chapter 5 in section 5.5.2.

In the current case, each of the M2S and S2M sequences may be performed on either the ^{13}C or the ^{1}H channel, giving rise to the four pulse sequence combinations reported in Fig. 5.5. All four sequence variants access the same collective state denoted Δ_{gu}, as

		$^{13}C_2$-AFD	$^{13}C_2$-AMD
Simulation	J_{23}	71.0 ± 0.6 Hz	71.6 ± 0.8 Hz
	$J_{13} = J_{24}$	−2.8 ± 0.03 Hz	−1.16 ± 0.02 Hz
	$J_{12} = J_{34}$	166.7 ± 0.2 Hz	166.5 ± 0.2 Hz
	J_{14}	15.7 ± 0.2 Hz	11.95 ± 0.4 Hz
	$\Delta\delta_{23}$	62 ± 5 ppb	92 ± 4 ppb
	$\Delta\delta_{14}$	7 ± 0.9 ppb	1.8 ± 0.2 ppb
Experiment	$\Delta(^{13}C)$	3.5 ms	3.7 ms
	$\Delta(^{1}H)$	16 ms	21 ms
	$n_1(^{13}C)$	14	14
	$n_2(^{13}C)$	7	7
	$n_1(^{1}H)$	6	18
	$n_2(^{1}H)$	3	9
	$\omega_{ev}^{nut}(^{1}H)/2\pi$	520 Hz	520 Hz
	$\omega_{ev}^{nut}(^{13}C)/2\pi$	700 Hz	700 Hz
	$T_1(^{13}C)$	6.0 ± 0.1 s	6.0 ± 0.1 s
	$T_1(^{1}H)$	6.0 ± 0.1 s	4.5 ± 0.1 s

Table 5.1: Spin system and pulse sequences parameters for $^{13}C_2$-AFD and $^{13}C_2$-AMD in CD_3OD. J couplings and chemical shift differences were obtained by fitting the 1D-NMR spectra with *Spinach*[12, 13]. The pulse sequence parameters $\Delta(^{13}C)$, $\Delta(^{1}H)$, $n_1(^{13}C)$, $n_1(^{1}H)$, $\omega_{ev}^{nut}(^{13}C)/2\pi$, $\omega_{ev}^{nut}(^{1}H)/2\pi$ were optimized experimentally for both molecules. Relaxation time constants T_1 were measured by standard inversion-recovery at a magnetic field of 11.75 T. *Reproduced from Phys. Chem. Chem. Phys.* **17***, 5913(2015) with permission from the PCCP Owner Societies.*

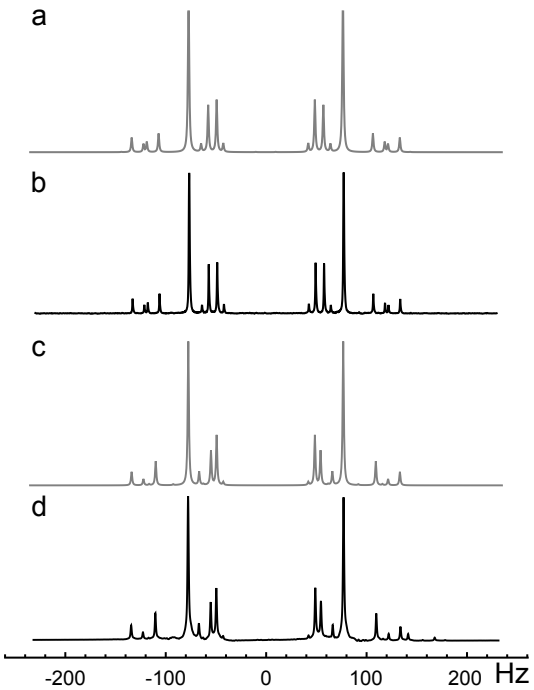

Figure 5.3: NMR 1D-spectra of $^{13}C_2$-AFD: (a) Simulated ^{13}C spectrum; (b) experimental ^{13}C spectrum. (c) simulated ^{1}H spectrum; (d) experimental ^{1}H spectrum. *Reproduced from Phys. Chem. Chem. Phys.* **17***, 5913(2015) with permission from the PCCP Owner Societies.*

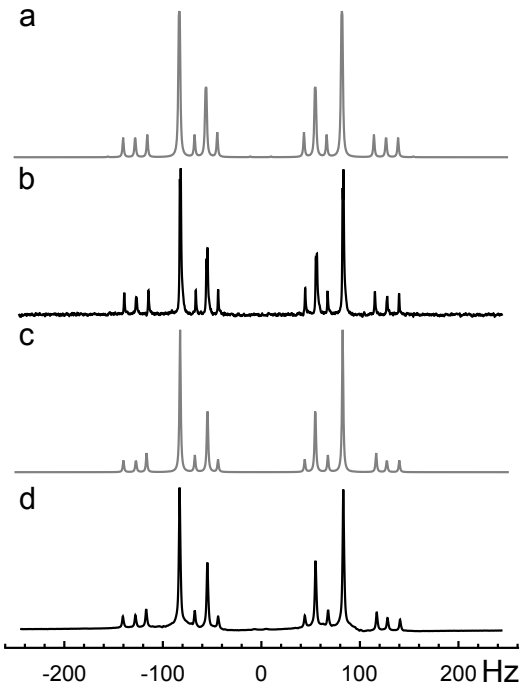

Figure 5.4: NMR 1D-spectra of $^{13}C_2$-AMD: (a) Simulated ^{13}C spectrum; (b) experimental ^{13}C spectrum. (c) simulated ^{1}H spectrum; (d) experimental ^{1}H spectrum. *Reproduced from Phys. Chem. Chem. Phys.* **17***, 5913(2015) with permission from the PCCP Owner Societies.*

reported by the simulation in Fig. 5.6 performed using *SpinDynamica*[119].

$$\begin{aligned}\Delta_{gu} &= -\frac{1}{\sqrt{3}}(\mathbf{I}_2\cdot\mathbf{I}_3+\mathbf{I}_1\cdot\mathbf{I}_4-4(\mathbf{I}_2\cdot\mathbf{I}_3)(\mathbf{I}_1\cdot\mathbf{I}_4))\\ &= \frac{1}{10}\sum_{i=1}^{10}|i,A_g\rangle\langle A_g,i|-\frac{1}{6}\sum_{i=1}^{6}|i,B_u\rangle\langle B_u,i|\end{aligned} \tag{5.2}$$

This operator, as per recipe identified in section 4.17, represents the population difference between spin states that are symmetric (g) and antisymmetric (u) with respect to simultaneous exchanges of the nuclear labels of ^{1}H and the ^{13}C nuclei. In the case of $^{13}C_2$-AFD this four-spin state is long-lived.
The logical steps leading to the experimental design were the following:

- The M2S sequence converts either ^{1}H or ^{13}C magnetization into Δ_{gu}.
- This state evolves during a variable evolution interval τ_{ev}, during which an unmodulated irradiation field ($\sim 800\,\mu$W) is applied on both RF channels (nutation frequencies reported in Table 5.1). This suppresses the small chemical shift difference induced by the different ester substituents [57].
- An S2M sequence, applied on either the ^{1}H or ^{13}C channel, converts the state Δ_{gu} into observable transverse magnetization, which is then detected.

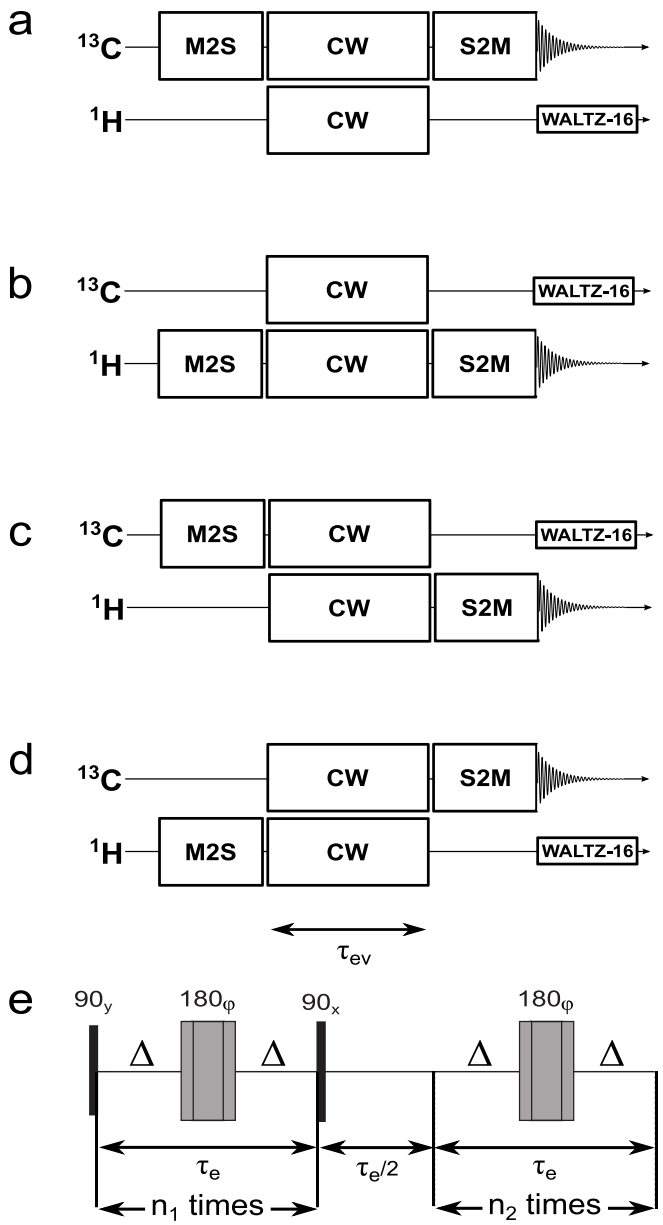

Figure 5.5: Pulse sequences used to access the Δ_{gu} state in $^{13}C_2$-AFD and $^{13}C_2$-AMD. Excitation and detection of Δ_{gu} is done using M2S and S2M pulse sequences, respectively. M2S and S2M are run on the same RF channel in (a) and (b) or on different channels in (c) and (d). The exact scheme of an M2S sequence is shown in (e). The S2M pulse sequence is obtained by running M2S in reverse time order. The echo duration is given by $\tau_e \sim 1/(2J_{14})$ when the sequence is applied to the ^{1}H channel, and $\tau_e \sim 1/(2J_{23})$ when using the ^{13}C channel. The number of loops is always $n_1 = 2n_2$. During the variable evolution time τ_{ev} a weak continuous wave irradiation of $800\mu W$ is applied on both RF channels ($\omega_{ev}^{nut}(^{13}C)/2\pi = 700$ Hz, $\omega_{ev}^{nut}(^1H)/2\pi = 520$ Hz) to impose chemical equivalence. A WALTZ-16 decoupling sequence [8] is applied to the ^{1}H channel during detection of the ^{13}C signal; WALTZ-16 is applied to the ^{13}C channel when the ^{1}H signal is detected. *Reproduced from Phys. Chem. Chem. Phys.* **17***, 5913(2015) with permission from the PCCP Owner Societies.*

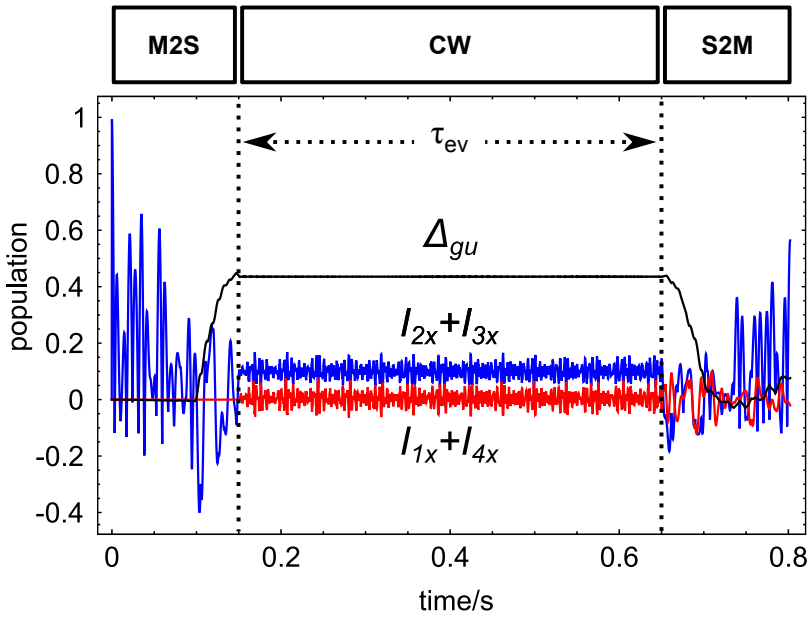

Figure 5.6: Simulated trajectories for the transfer of longitudinal magnetization into carbon transverse magnetization $I_{2x} + I_{3x}$ in blue, proton transverse magnetization $I_{1x} + I_{4x}$ in red and Δ_{gu} spin order in black under the pulse sequence in Fig.5.5a for $^{13}C_2$-AFD. The spin system is assumed to evolve under the influence of $\mathcal{H}^{coh}$ with parameters reported in Table 5.1 and $\tau_{ev} = 0.5$ s . No relaxation was included in the simulations. *Reproduced from Phys. Chem. Chem. Phys.* **17**, *5913(2015) with permission from the PCCP Owner Societies.*

- A WALTZ-16 decoupling sequence [8] is applied on the ^{1}H channel during ^{13}C observation, to collapse the spectrum into a single peak. Conversely, the ^{1}H NMR signal is detected in the presence of ^{13}C WALTZ-16 decoupling.

The signal amplitudes for the two compounds, using the four different pulse sequence variants, are plotted against τ_{ev} in Fig. 5.7. The decay time constants reported in Table 5.2 are consistent among the four different experiments. The experimental points were fitted using a single exponential decay curve when exciting and detecting the spin system on different RF channels. A double exponential decay curve was instead applied when excitation and detection occured on the same RF channel.

Pulse Sequence	$^{13}C_2$-AFD /s	$^{13}C_2$-AMD /s
M2S(^{13}C)-S2M(^{13}C)	61.0 ± 1.0	2.5 ± 0.2
M2S(^{1}H)-S2M(^{1}H)	63.2 ± 2.5	2.1 ± 0.1
M2S(^{13}C)-S2M(^{1}H)	59.9 ± 3.2	2.5 ± 0.2
M2S(^{1}H)-S2M(^{13}C)	61.6 ± 2.0	2.7 ± 0.2

Table 5.2: Experimental decay time constants for the spin operator term Δ_{gu} as determined by fitting the experimental results in Fig. 5.7. In the case of $^{13}C_2$-AFD, the operator Δ_{gu} is a LLS. *Reproduced from Phys. Chem. Chem. Phys.* **17**, *5913(2015) with permission from the PCCP Owner Societies.*

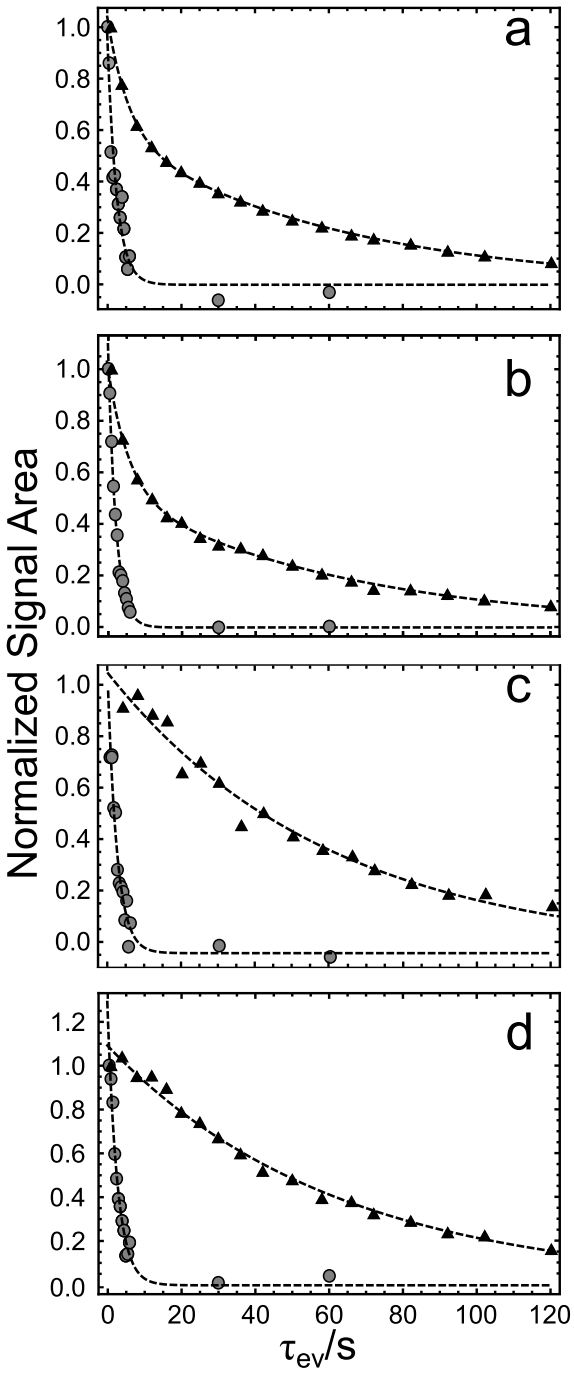

Figure 5.7: Experimental results are shown for pulse sequence in (a) Fig. 5.5a, (b) Fig. 5.5b, (c) Fig. 5.5c and (d) Fig. 5.5d. Black triangles refer to $^{13}C_2$-AFD, and gray circles to $^{13}C_2$-AMD. The dashed lines are best fits to bi-exponential decays in (a) and (b) and single exponential decays in (c) and (d). The time constants for $^{13}C_2$-AFD are: (a) 61.01 ± 0.1 s; (b) 63.2 ± 2.5 s; (c) 59.9 ± 3.2 s; (d) 61.6 ± 2.0 s. The time constants for $^{13}C_2$-AMD are: (a) 2.5 ± 0.2 s; (b) 2.1 ± 0.1 s; (c) 2.5 ± 0.2 s; (d) 2.7 ± 0.2 s. *Reproduced from Phys. Chem. Chem. Phys.* **17***, 5913(2015) with permission from the PCCP Owner Societies.*

In the case of $^{13}C_2$-AFD, the state Δ_{gu} is found to have a decay time constant of $\sim 10T_1$, marking the existence of a four-spin LLS protected against dipole-dipole relaxation and the other mechanisms contributing to the rapid decay of longitudinal magnetization. In the case of $^{13}C_2$-AMD, where a local centre of inversion is absent, the state Δ_{gu} decays faster than T_1 and hence cannot be designated as a long-lived state.
The experimental results confirm the link between local molecular geometry and the existence of LLS in multi-spin systems.

5.2.3 Analysis

We now apply the permutation symmetry analysis developed in the previous chapter to predict the number and analytical expression of LLS. The coherent Hamiltonian can be expressed as follows:

$$\mathcal{H}_{\text{int}} = \mathcal{H}_{\text{int}}^{\text{coh},0} + \mathcal{H}_{\text{int}}^{\text{coh},'} \tag{5.3}$$

where $\mathcal{H}_{\text{int}}^{\text{coh},0}$ respects the idealized symmetry of the molecular spin system and $\mathcal{H}_{\text{int}}^{\text{coh},'}$ is a small perturbation due to the asymmetric remote substituents. In isotropic liquids, each of these is a superposition of Zeeman and J-coupling terms, i.e. $\mathcal{H}_Z = \mathcal{H}_Z^0 + \mathcal{H}_Z^{'}$ and $\mathcal{H}_J = \mathcal{H}_J^0 + \mathcal{H}_J^{'}$, where in the current cases

$$\begin{aligned}
\mathcal{H}_Z^0 &= \frac{1}{2}\omega_H^0(\delta_1 + \delta_4)\,(I_{1z} + I_{4z}) \\
&\quad + \frac{1}{2}\omega_C^0(\delta_2 + \delta_3)\,(I_{2z} + I_{3z}) && (5.4)\\
\mathcal{H}_J^0 &= \pi(J_{12} + J_{34})\,(I_{1z}I_{2z} + I_{3z}I_{4z}) \\
&\quad + \pi(J_{13} + J_{24})\,(I_{1z}I_{3z} + I_{2z}I_{4z}) \\
&\quad + 2\pi(J_{14}\mathbf{I}_1 \cdot \mathbf{I}_4 + J_{23}\mathbf{I}_2 \cdot \mathbf{I}_3) && (5.5)\\
\mathcal{H}_Z^{'} &= \frac{1}{2}\omega_H^0(\delta_1 - \delta_4)\,(I_{1z} - I_{4z}) \\
&\quad + \frac{1}{2}\omega_C^0(\delta_2 - \delta_3)\,(I_{2z} - I_{3z}) && (5.6)\\
\mathcal{H}_J^{'} &= \pi(J_{12} - J_{34})\,(I_{1z}I_{2z} - I_{3z}I_{4z}) \\
&\quad + \pi(J_{13} - J_{24})\,(I_{1z}I_{3z} - I_{2z}I_{4z}) && (5.7)
\end{aligned}$$

Here ω_C^0 and ω_H^0 are the Larmor frequencies of ^{13}C and ^{1}H, and δ_i represents the chemical shift of nucleus I_i. The terms $\mathcal{H}_Z^0$ and $\mathcal{H}_J^0$ respect the *local* symmetry of the four-spin system, while the terms $\mathcal{H}_Z^{'}$ and $\mathcal{H}_J^{'}$ contain the small symmetry-breaking terms induced by the remote asymmetric ester groups. In the experiments described here, the asymmetric term $\mathcal{H}_{\text{int}}^{\text{coh},'}$ is exploited during the M2S and S2M sequences to access the state Δ_{gu}. During the evolution interval τ_{ev}, the effect of $\mathcal{H}_{\text{int}}^{\text{coh},'}$ is suppressed by the applied RF field used to impose chemical equivalence.
The *symmetry group of the coherent Hamiltonian*, denoted $\mathcal{G}^{\text{coh},0}$, is defined here as the group of spin permutation operations which commutes with $\mathcal{H}_{\text{int}}^{\text{coh},0}$.

$\mathbb{B}_{ST}$	$p^{(23)}$	$p^{(14)}$	$p^{(14)(23)}$	M
$\|T^{23}_{1}T^{14}_{1}\rangle$	g	g	g	2
$\|T^{23}_{0}T^{14}_{1}\rangle$	g	g	g	1
$\|T^{23}_{1}T^{14}_{0}\rangle$	g	g	g	1
$\|T^{23}_{1}T^{14}_{-1}\rangle$	g	g	g	0
$\|T^{23}_{0}T^{14}_{0}\rangle$	g	g	g	0
$\|T^{23}_{-1}T^{14}_{1}\rangle$	g	g	g	0
$\|T^{23}_{0}T^{14}_{-1}\rangle$	g	g	g	-1
$\|T^{23}_{-1}T^{14}_{0}\rangle$	g	g	g	-1
$\|T^{23}_{-1}T^{14}_{-1}\rangle$	g	g	g	-2
$\|S^{23}_{0}S^{14}_{0}\rangle$	u	u	g	0
$\|T^{23}_{1}S^{14}_{0}\rangle$	g	u	u	1
$\|T^{23}_{0}S^{14}_{0}\rangle$	g	u	u	0
$\|T^{23}_{-1}S^{14}_{0}\rangle$	g	u	u	-1
$\|S^{23}_{0}T^{14}_{1}\rangle$	u	g	u	1
$\|S^{23}_{0}T^{14}_{0}\rangle$	u	g	u	0
$\|S^{23}_{0}T^{14}_{-1}\rangle$	u	g	u	-1

Table 5.3: The first column lists the components of the basis set $\mathbb{B}_{ST}$ in equation 5.9 used for describing both $^{13}C_2$-AFD, $^{13}C_2$-AMD. Each ket is classified according to its parity under exchange of the two ^{13}C nuclei, exchange of the two ^{1}H nuclei, and simultaneous exchange of both homonuclear pairs. The last column indicates the total magnetic quantum number. *Reproduced from Phys. Chem. Chem. Phys.* **17***, 5913(2015) with permission from the PCCP Owner Societies.*

In the current case, the group $\mathcal{G}^{\text{coh},0}$ consists of just two operations, for both molecules:

$$\mathcal{G}^{\text{coh},0}(\text{AFD}) = \mathcal{G}^{\text{coh},0}(\text{AMD}) = \{(), (14)(23)\} \tag{5.8}$$

where () is the identity. The presence of the permutation (14) indicates that spins I_1 and I_4 are chemically equivalent (as far as the idealized Hamiltonian $\mathcal{H}^{\text{coh},0}_{\text{int}}$ is concerned). The fact that the permutation (14) does not appear in the group $\mathcal{G}^{\text{coh},0}$ as an isolated element, but as a product with a different permutation (23), as pointed out in the previous chapter indicates that spins I_1 and I_4 are magnetically inequivalent. The same is true for I_2 and I_3. The group $\mathcal{G}^{\text{coh},0}$ has two irreducible representations denoted A_g and B_u, with opposite parity under the operation (14)(23).

In the absence of any symmetry breaking interactions, the NMR spectral peaks are generated by transitions within the A_g or B_u manifolds. In reality a symmetry breaking mechanism, as we often stressed, is needed to observe a population imbalance between states transforming according to different irreducible representations. The 1D-spectra contain such information. As an example in Fig. 5.8 the ^{1}H 1D-spectrum of $^{13}C_2$-AFD with the corresponding simulation is reported again indicating the spectral lines relative to transitions within the A_g (in red), and B_u (in blue) manifolds. In addition, it can be seen that there are spectral lines indicated by grey full dots representing transitions

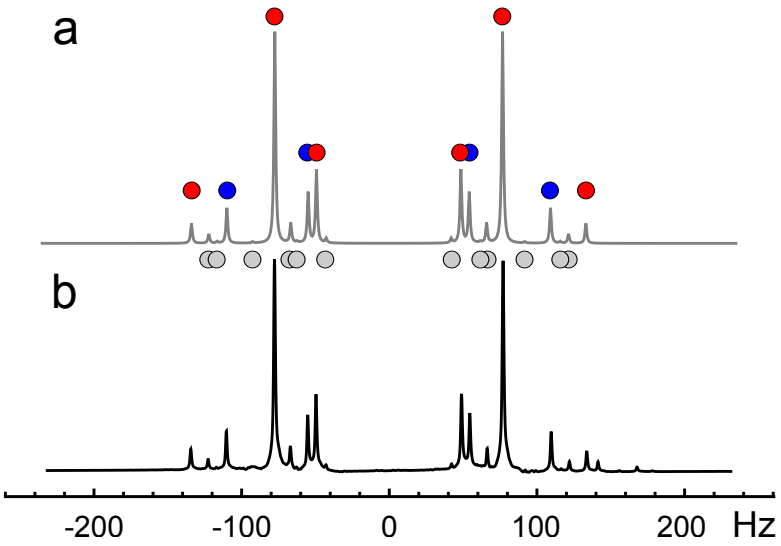

Figure 5.8: NMR 1D-spectra of $^{13}C_2$-AFD: (a) Simulated ^{1}H spectrum; (b) Experimental ^{1}H spectrum. Spectral lines corresponding to transitions within the A_g manifold are indicated by red full circles. Blue full circles denote spectral lines referring to B_u manifold transitions. Transitions between A_g and B_u nuclear spin states are indicated by grey full points.

connecting A_g and B_u manifolds. The intensity of the spectral lines marked by a grey filled circle is a clear visualization of the entity of the introduced approximations in the theoretical formalization we are accomplishing.

The suitable basis set, reflecting the symmetry property of the system, is in this case a direct product of the singlet-triplet bases formed by homo-nuclear spin pairs:

$$\mathbb{B}_{ST} = \{ST\}_{23} \otimes \{ST\}_{14} \tag{5.9}$$

A permutation (ij) acting upon a ket belonging to $\{ST\}_{ij}$ gives:

$$(ij)\,|\psi_{ij}\rangle = p^{(ij)}\,|\psi_{ij}\rangle \tag{5.10}$$

$|\psi_{ij}\rangle$ is said to be *symmetric* or *gerade* (g) when $p^{(ij)} = +1$; *antisymmetric* or *ungerade* (u) when $p^{(ij)} = -1$.

As different spin permutations may be multiplied, a four-spin state can be either symmetric (g) or antisymmetric (u) under the homonuclear spin permutation $(ij)(kl)$, that is $p^{(ij)(kl)} = +1$ (for g) or $p^{(ij)(kl)} = -1$ (for u).

States belonging to $\mathbb{B}_{ST}$ can be classified (see Table 5.3) according to the magnetic

quantum number M and their parities under the homonuclear spin permutations:

$$\begin{aligned}(I_{1z}+I_{2z}+I_{3z}+I_{4z})(|\psi_{14}\rangle\otimes|\psi_{23}\rangle) &= M(|\psi_{14}\rangle\otimes|\psi_{23}\rangle)\\ (14)(|\psi_{14}\rangle\otimes|\psi_{23}\rangle) &= p^{(14)}(|\psi_{14}\rangle\otimes|\psi_{23}\rangle)\\ (23)(|\psi_{14}\rangle\otimes|\psi_{23}\rangle) &= p^{(23)}(|\psi_{14}\rangle\otimes|\psi_{23}\rangle)\\ (14)(23)(|\psi_{14}\rangle\otimes|\psi_{23}\rangle) = p^{(14)}p^{(23)}(|\psi_{14}\rangle\otimes|\psi_{23}\rangle) &= \\ p^{(14)(23)}(|\psi_{14}\rangle\otimes|\psi_{23}\rangle)&\end{aligned} \tag{5.11}$$

The 16 states reported in Table 5.3 form an orthonormal basis set and are classified according to their symmetry with respect to the permutation (14)(23) into irreducible representations A_g and B_u:

$$\Gamma_{\text{spin}} = 10A_g \oplus 6B_u \tag{5.12}$$

Consider now the fluctuating spin interactions which cause relaxation. An example of such interactions is given by the dipole-dipole interaction between the nuclei, which may be written as follows:

$$\mathcal{H}_{\text{DD}}(t) = \sum_{\{i,j\}}\sum_{m=-2}^{+2} c^{\text{DD},ij} D^2_{0m}(\Omega^{ij}_{PL}(t))T^{ij}_{2m} \tag{5.13}$$

where $c^{\text{DD},ij} = -(\sqrt{6}\mu_0/4\pi)\gamma_i\gamma_j\hbar r_{ij}^{-3}$, D^2 is a second-rank Wigner rotation matrix, Ω^{ij}_{PL} represents the set of three Euler angles defining the orientation of the internuclear vector between I_j and I_k in the laboratory frame, and T^{ij}_2 is a second-rank irreducible spherical tensor.

As previously discussed at an arbitrary time point t, molecular vibrations distort the molecular geometry away from its equilibrium configuration, breaking the geometrical symmetry. Hence, in general, the instantaneous value of $\mathcal{H}_{\text{DD}}(t)$ (and other fluctuating terms) does not display any symmetry. However, since rapid vibrations are usually too fast to cause significant NMR relaxation (see equation 4.38), the relevant spin Hamiltonian for relaxation purposes may be locally averaged over molecular vibrations (typically on the sub-picosecond timescale), denoted here $\langle\mathcal{H}_{\text{DD}}(t)\rangle_{\text{vib}}$. This *vibrationally averaged spin Hamiltonian* reflects the geometrical symmetry of the equilibrium molecular structure, and displays the corresponding spin permutation symmetry.

In general, $\langle\mathcal{H}_{\text{DD}}(t)\rangle_{\text{vib}}$ may be calculated from equation 5.13 by using nuclear coordinates from the equilibrium molecular geometry, but with small adjustments to the interaction strengths caused by vibrational averaging [73].

As previously done for $\mathcal{H}_{\text{int}}$ we will consider in this section the nuclear spin permutations that are symmetry operations for $\langle\mathcal{H}_{\text{DD}}(t)\rangle_{\text{vib}}$ in both molecular systems. In the case of $^{13}C_2$-AFD, the permutation (14)(23) is a symmetry operation for the vibrationally-averaged dipole-dipole spin Hamiltonian because of the inversion geometry of the local

molecular structure. The double permutation always exchanges pairs of nuclei with parallel internuclear vectors, so that the spatial interaction tensors are identical for all molecular orientations. Similar considerations apply for other interaction terms such as the chemical shift anisotropy [95].
The group of the vibrationally-averaged fluctuating Hamiltonian is therefore given by

$$\mathcal{G}^0_{\text{fluc}}(\text{AFD}) = \{E, (14)(23)\} \tag{5.14}$$

where $\mathcal{G}^0_{\text{fluc}}$ contains the group of spin permutation operators that commute with $\langle\mathcal{H}_{\text{fluc}}\rangle_{\text{vib}}$. In the case of the *cis* isomer, the equilibrium geometry is not sufficient to impose symmetry on the vibrationally averaged spin Hamiltonian. We therefore get a trivial symmetry group in this case,

$$\mathcal{G}^0_{\text{fluc}}(\text{AMD}) = \{E\} \tag{5.15}$$

Figure 5.9 illustrates the symmetry properties of the vibrationally averaged intramolec-

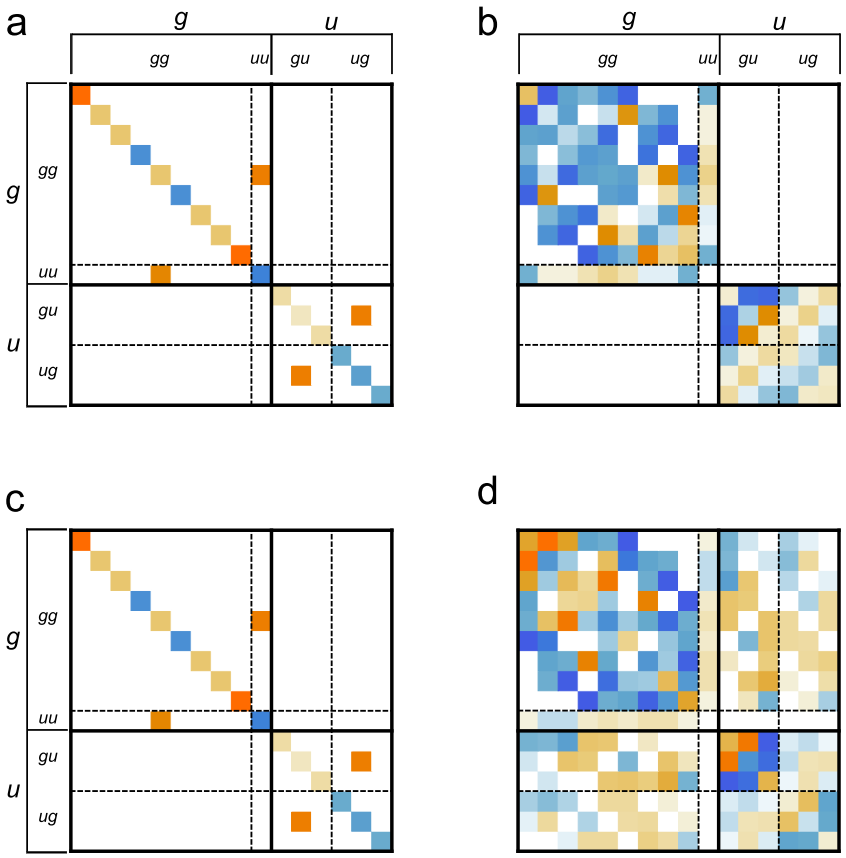

Figure 5.9: Matrix plot representations of $\mathcal{H}^{\text{coh},0}_{\text{int}}$ and $\langle\mathcal{H}_{\text{DD}}(t)\rangle_{\text{vib}}$ hamiltonians for $^{13}C_2$-AFD in panels (a), (b) and for $^{13}C_2$-AMD in panels (c) and (d) respectively. $\langle\mathcal{H}_{\text{DD}}(t)\rangle_{\text{vib}}$ hamiltonian is block diagonal for $^{13}C_2$-AFD (panel (b)). The basis is $\mathbb{B}_{ST}$, and the ordering follows the convention adopted in Table 5.3. *Reproduced from Phys. Chem. Chem. Phys.* **17**, *5913(2015) with permission from the PCCP Owner Societies.*

ular dipole-dipole interaction, in the two molecular systems. The figure shows matrix representations of $\langle \mathcal{H}_{\mathrm{DD}} \rangle_{\mathrm{vib}}$ in the basis $\mathbb{B}_{ST}$. In the case of $^{13}C_2$-AFD (Fig. 5.9-b), the matrix representation of $\langle \mathcal{H}_{\mathrm{DD}} \rangle_{\mathrm{vib}}$ is block-diagonal in this basis, since the vibrationally averaged dipole-dipole Hamiltonian has the same symmetry as $\mathcal{H}_{\mathrm{int}}^{\mathrm{coh},0}$ (equations 5.8 and 5.14). In the case of $^{13}C_2$-AMD (Fig. 5.9-d), on the other hand, off-diagonal elements connecting different irreducible representations appear, since $\langle \mathcal{H}_{\mathrm{DD}} \rangle_{\mathrm{vib}}$ has a lower symmetry than $\mathcal{H}_{\mathrm{int}}^{\mathrm{coh},0}$ (equation 5.15). It is important to stress the following points:

- The sole consideration of the symmetry properties of the coherent hamiltonian (Fig. 5.9-a and Fig. 5.9-c) to infer the existence of LLS could be deceptive.
- The symmetry group for $\mathcal{H}_{\mathrm{int}}^{\mathrm{coh},0}$ is identical for both $^{13}C_2$-AFD and $^{13}C_2$-AMD (Eq. 5.8) but a long-lived order is expected only in one case.
- In general, if the molecular structure is rigid, and the equilibrium geometry of the local spin system is centrosymmetric, the group $\mathcal{G}_{\mathrm{fluc}}^{0}$ has dimension 2. If the molecule is rigid but non-centrosymmetric, $\mathcal{G}_{\mathrm{fluc}}^{0}$ has dimension 1.

The symmetry properties of the coherent and fluctuating Hamiltonians can be combined to derive the correct symmetry properties for the complete Hamiltonian. The *idealised symmetry group for the complete Hamiltonian* can be obtained from $\mathcal{G}^{\mathrm{coh},0}$ and $\mathcal{G}_{\mathrm{fluc}}^{0}$ by:

$$\mathcal{G}_{\mathrm{H}}^{0} = \mathcal{G}^{\mathrm{coh},0} \cap \mathcal{G}_{\mathrm{fluc}}^{0} \tag{5.16}$$

For the two molecules discussed here, we have:

$$\mathcal{G}_{\mathrm{H}}^{0}(\mathrm{AFD}) = \{E, (14)(23)\} \tag{5.17}$$

$$\mathcal{G}_{\mathrm{H}}^{0}(\mathrm{AMD}) = \{E\} \tag{5.18}$$

The coherent and fluctuating Hamiltonians cannot induce transitions between states which belong to different irreducible representations of the group $\mathcal{G}_{\mathrm{H}}^{0}$. Hence the spin evolution must preserve a population difference between states belonging to different irreducible representations of $\mathcal{G}_{\mathrm{H}}^{0}$. Such a population difference is a constant of motion and does not evolve, providing that the realistic spin interactions conform exactly the idealized symmetry assumed in the theoretical model. In practice, deviations from ideal symmetry invariable cause slow relaxation, but the lifetime of such a state may nevertheless be long compared to the relaxation of most other states.
In the case of $^{13}C_2$-AFD, which has a two-dimensional idealized complete Hamiltonian symmetry group (equation 5.17), there is a LLS given by the difference in mean population of states with A_g and B_u symmetry:

$$\Delta_{gu} = \frac{1}{10} \sum_{i=1}^{10} |i, A_g\rangle \langle A_g, i| - \frac{1}{6} \sum_{i=1}^{6} |i, B_u\rangle \langle B_u, i| \tag{5.19}$$

This corresponds to the following combination of spherical tensor operators:

$$\Delta_{gu} = T_{00}^{23} + T_{00}^{14} - 4\sqrt{3}T_{00}^{23}T_{00}^{14} \tag{5.20}$$

where $T_{00}^{ij} = -3^{-1/2}\mathbf{I}_i \cdot \mathbf{I}_j$ is the rank-0 spherical tensor operator between nuclei i and j. Equation 5.20 highlights the invariance of the LLS under rotations of both spin ^{1}H and ^{13}C spin states, and can also be written as:

$$\Delta_{gu} = -\frac{1}{\sqrt{3}}(\mathbf{I}_2 \cdot \mathbf{I}_3 + \mathbf{I}_1 \cdot \mathbf{I}_4 - 4(\mathbf{I}_2 \cdot \mathbf{I}_3)(\mathbf{I}_1 \cdot \mathbf{I}_4)) \tag{5.21}$$

The operator Δ_{gu} is a LLS in the case of $^{13}C_2$-AFD, since the double spin permutation (14)(23) is an element of $\mathcal{G}_{\mathrm{H}}^0$(AFD) (see Eq. 5.17).
In the case of $^{13}C_2$-AMD, the idealized complete Hamiltonian symmetry group is one-dimensional even in a regime of perfect chemical equivalence (see equation 5.18) and there is no long-lived state, except for the trivial mean of all spin state populations that is always a conserved quantity for an isolated spin system.

5.2.4 Local geometry and transition probabilities

In this section we further consider the LLS dependence on the equilibrium molecular geometry. The standard methodology in LLS analysis [57, 59] consists in the diagonalization of the Liouvillian superoperator that can be set up to include all the relevant relaxation mechanisms. Using the Abragam-Redfield second-order perturbation theory [41, 120] and assuming an extreme narrowing limit with $|\omega^0\tau_C| \ll 1$, where the tumbling correlation time τ_C is much smaller than the inverse of the Larmor frequency ω^0, the Liouvillian and relaxation superoperators for rank-2 interactions can be expressed as:

$$\begin{aligned} \hat{\mathcal{L}} &= -i\hat{\mathcal{H}}_{\mathrm{int}}^{\mathrm{coh}} + \hat{\Gamma} \\ \hat{\Gamma} &= -\sum_{\lambda,\lambda'} c^{\lambda}c^{\lambda'} J_0^{\lambda,\lambda'} \sum_m (-1)^m \hat{T}_{2m}^{\lambda}\hat{T}_{2-m}^{\lambda'} \end{aligned} \tag{5.22}$$

The sum in equation 5.22 is over the spin interactions λ, but we restrict our considerations to the relaxation induced by the intra-molecular dipole-dipole interaction (equation 5.24) for simplicity. We indicate the dipolar coupling term between spins i and j as $c^{\mathrm{DD},ij} = -\sqrt{6}\mu_0\gamma_i\gamma_j\hbar/(4\pi r_{ij}^3)$. The hat symbol in equation 5.22 indicates a superoperator. Expressions for spherical tensor operators T_{2m}^{λ} with $m = -2, \ldots 2$ and their relative commutation superoperators can be found in Ref. [73] and readily implemented for calculations using for example *SpinDynamica* [119]. $J_0^{\lambda,\lambda'}$ is the spectral density at

zero frequency for the correlation between interactions λ and λ':

$$J_0^{\lambda,\lambda'} = \frac{1}{5}\sum_{m_1=-2}^{2} \tau_C D^2_{0m_1}(\Omega^{\lambda}_{PM}(ij)) D^{2*}_{0m_1}(\Omega^{\lambda'}_{PM}(i'j')), \tag{5.23}$$

where $\Omega^{\lambda}_{PM}(ij)$ is the set of Euler angles describing a trasformation from the principal axis system P of the interaction λ to the molecular fixed frame M for the dipolar coupled pair of spins ij [58].
The rigid geometries of the four nuclear spins in $^{13}C_2$-AMD and $^{13}C_2$-AFD may be obtained from each other by rotating one of the heteronuclear ^{13}CH single bonds around the axis passing through the $^{13}C_2$ double bond (see Fig. 5.10-a). The dynamics of the nuclear spin system is described by the Liouville-Von Neumann equation and can be represented by a set of eigenvalues-eigenoperators pairs $\{L_q, Q_q\}$ obeying the following equation:

$$\hat{\mathcal{L}}^{\mathrm{DD}} Q_q = L_q Q_q \tag{5.24}$$

$$L_q = -\lambda_q + i\omega_q \tag{5.25}$$

In general $\hat{\mathcal{L}}_{\mathrm{DD}}$ is not hermitian so the eigenvalues may be complex. Eigenoperators Q_q with complex eigenvalues correspond to coherences oscillating at frequency ω_q and decaying to equilibrium with a rate constant λ_q. Eigenoperators Q_q with real eigenvalues ($\omega_q = 0$) correspond to spin state populations decaying with a rate λ_q. The eigenvalue $\lambda_q = 0$ relates to the identity operator, corresponding to the conservation of the sum of all spin-state populations. Numerical simulation performed with *SpinDynamica* [119] in Fig. 5.10-b shows the dependence of the smallest non-zero rate constant λ_{min} on the torsional angle θ. It was assumed the J coupling parameters to be independent on the torsional angle and equal to those reported in Table 5.1 for $^{13}C_2$-AFD. This approximation appears to be reasonable given the small difference in parameters as obtained by fitting the 1D-NMR spectra and listed in Table 5.1. The relaxation superoperator takes into account all dipole-dipole couplings in the 4-spin system and assumes rigid molecular geometry and isotropic molecular tumbling with a correlation time $\tau_C = 15$ ps. As expected, a long-lived state with infinite relaxation time is predicted only when $\theta = 180°$, which is the geometric equilibrium configuration for $^{13}C_2$-AFD.
Equation 5.23 can also be used to calculate the transition probability between any pair of vectors in Liouville space in the extreme narrowing limit. It is possible in particular to calculate the transition probability between manifolds of different symmetry induced by intramolecular dipolar relaxation according to the formula:

$$W^{gu,\mathrm{DD}} = \sum_{\{ij\},\{i'j'\}} R^{\mathrm{DD}}_{ij,i'j'} = \sum_{g\sim A_g}\sum_{u\sim B_u} (g|\hat{\Gamma}^{\mathrm{DD}}|u) \tag{5.26}$$

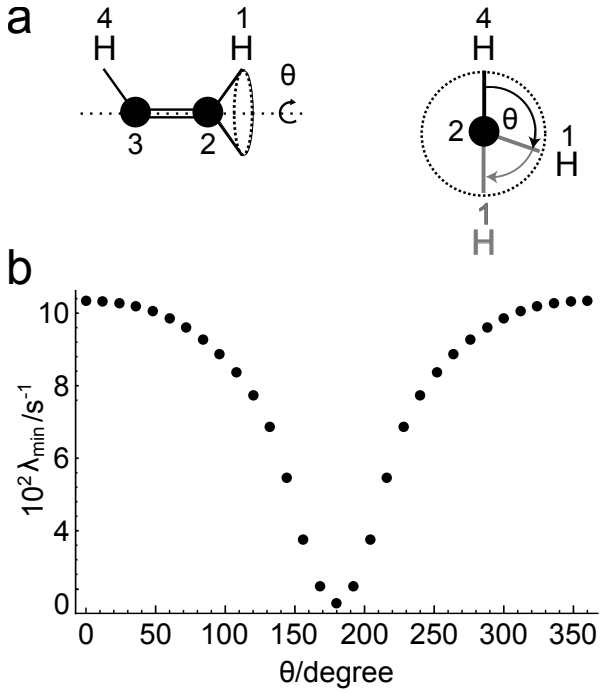

Figure 5.10: (a) The geometric configurations obtainable by rotation of the single ^{13}CH bond through the $^{13}C_2$ double bond axis. The front view and the through $^{13}C_2$ double bond view are given. $\theta = 0°$ and $\theta = 180°$ correspond to equilibrium spin systems configurations of $^{13}C_2$-AMD and $^{13}C_2$-AFD respectively. (b) The smallest non-zero decay rate constant λ_{min} plotted against torsional angle θ, obtained by numerical analysis of the Liouvillian superoperator. Only dipole-dipole relaxation is included, with a rotational correlation time of $\tau_C = 15$ ps. A zero value, signing the existence of a infinitely LLS, is present only when $\theta = 180°$: the geometric configuration of $^{13}C_2$-AFD. *Reproduced from Phys. Chem. Chem. Phys.* **17***, 5913(2015) with permission from the PCCP Owner Societies.*

where $|g)$ and $|u)$ are generic Liouville space vectors of symmetry A_g and B_u respectively. By explicitly indicating $\Omega^{\mathrm{DD}}_{PM}(ij) = \{\alpha, \beta, \gamma\}$ and $\Omega^{\mathrm{DD}}_{PM}(i'j') = \{\alpha', \beta', \gamma'\}$ the generic transition probability rate $R^{\mathrm{DD}}_{ij,i'j'}$ is:

$$R^{\mathrm{DD}}_{ij,i'j'} = -c^{DD,ij}c^{DD,i'j'}\frac{3}{40}\tau_C(1 + 3\cos(2\beta') + \cos(2\beta)(3 + 9\cos(2\beta')) + 12\cos(\gamma - \gamma')\sin(2\beta)\sin(2\beta') + 12\cos(2(\gamma - \gamma'))\sin^2(\beta)\sin^2(\beta')) \quad (5.27)$$

In the present case, using equation 5.27, we can express equation 5.26 as follows:

$$W^{gu,\mathrm{DD}} = \frac{5}{2}(R^{\mathrm{DD}}_{1212} - 2R^{\mathrm{DD}}_{1234} + R^{\mathrm{DD}}_{2424} - 2R^{\mathrm{DD}}_{2413} + R^{\mathrm{DD}}_{1313} + R^{\mathrm{DD}}_{3434}) \quad (5.28)$$

where $1, 4$ are ^{1}H nuclei and $2, 3$ are ^{13}C nuclei. Numerical calculations show that for a rigid nuclear centrosymmetric disposition, equation 5.28 is identically zero as expected for the idealised representation of $^{13}C_2$-AFD. However the same expression is different from zero for a $^{13}C_2$-AMD idealised geometric arrangement, suggesting that

transitions between manifolds of different symmetry occur. It can be shown that the same result is attainable when including also CSA interaction [95]. The role of the local nuclear arrangement in the spin system results indeed important when designing molecular probes expected to be long lived even at relatively high external magnetic fields [55, 59].

5.3 LLS in methyl groups

5.3.1 Introduction

The class of compounds that we have considered in the previous sections and many other presented in literature [2, 5, 18, 51, 54, 56, 61–63, 116, 121, 122] shows the possibility to have LLS in extremely different regimes. The model used for all of them includes a rigid equilibrium configuration of the nuclear coordinates. In such a rigid model the geometrical arrangement plays an important role and indeed we have defined the LLS in $^{13}C_2$-AFD as *geometrically imposed*. However a large variety of molecules exists that cannot be correctly modelled as rigid systems. Even these non-rigid systems may be long-lived in suitable circumstances. Indeed molecules containing rapidly rotating methyl groups may exhibit long-lived states in solution [53, 100]. Rapid internal rotation of methyl group imposes long-lived character to the system. We have defined the corresponding long-lived state as *dynamically imposed* [53].
Here we analyse the case of methyl group in γ-picoline where a very low methyl rotational barrier allows a hyperpolarized LLS to be populated by thermal equilibration at liquid helium temperature. Following dissolution, cross-relaxation of the hyperpolarized LLS, induced by hetero-nuclear dipolar couplings, generates strongly enhanced anti phase NMR signals. This mechanism explains the NMR signal enhancements observed for ^{13}C-γ-picoline [100].
As previously discussed, long-lived orders in multi-spin rigid systems immune to intramolecular dipole-dipole relaxation occur when the geometrical arrangement of nuclei possesses an inversion centre (see section 5.2.4). The three proton nuclei in a methyl group can be represented as the vertices of an equilateral triangle, and do not display an inversion geometry. Therefore a long-lived state is not anticipated in this case. However when the internal dynamic of the methyl group is accounted for, long-lived states can be experimentally detected as demonstrated in Ref. [53, 60, 100, 101, 108].
In particular as discussed below long-lived states exist when $\tau_R \ll \tau_C$. In Ref. [53] is shown that the solution-state polarization effects in ^{13}C-γ-picoline, described by Icker and Berger in Ref. [100], may be explained by a quantum-rotor-induced population imbalance between states belonging to different irreducible representations of the nuclear spin permutation group of the complete Hamiltonian, where the population imbalance occurs at temperatures below the rotor splitting. Upon dissolution this imbalance per-

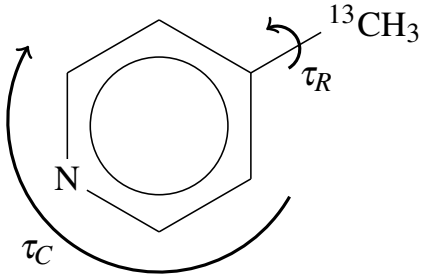

Figure 5.11: Structure of ^{13}C-γ-picoline. The relaxation behaviour of the LLS is controlled by the correlation times τ_R and τ_C which characterize the rotational diffusion of the methyl group and the entire molecule, respectively. *Reprinted with permission from J. Am. Chem. Soc. 2013,* **135***(50), 18746-18749. Copyright 2013 American Chemical Society.*

sists and equilibration occurs only slowly via cross-relaxation processes which give rise to enhanced NMR signals.

5.3.2 Experiment

The methyl region of the ^{13}C and ^{1}H NMR spectra for γ-picoline are shown in Fig. 5.12. All spectra were obtained without proton decoupling. Fig. 5.12-a shows the ^{13}C spectrum of a thermal equilibrium sample, displaying the well known 1:3:3:1 quartet pattern with a hetero-nuclear J coupling, J_{CH} = 127 Hz. The spectrum was obtained after dissolution and complete relaxation by adding 32 transients following a 90° pulse. The spectrum in Figure 5.12-b was obtained by equilibrating ^{13}C-γ-picoline for approximately 2 hours at a temperature of 4 °K, rapidly dissolving it in degassed chloroform using dissolution-DNP equipment[123], transferring it to a 9.4 T magnet, waiting another 10 s (see Fig. 5.13), applying a ^{13}C pulse with a flip angle of $\sim$ 10°, and taking the Fourier transform of the signal transient. As in the original Icker-Berger experiment [100], a greatly enhanced ^{13}C multiplet is observed, with irregular peak amplitudes of alternating sign. The magnitude of the enhancement varies from peak to peak and is in the range 240 - 700. The significantly larger enhancement compared to reference 100 is attributed to the use of a fast dissolution apparatus. Figure 5.12-(d-e) show the analogous data for the methyl protons. Again 32 transients following a 90° pulse were added for the thermal signal in Figure 5.12-d. The hyperpolarized ^{1}H spectrum in Fig. 5.12-e was obtained using a 5° flip angle 10 s after injection of the sample into the magnet. The measured enhancement for the two peaks is approximately ±30.

Fig. 5.14-a shows experimental data for the ^{13}C peak amplitudes as a function of time (crosses). The four datasets are obtained by applying ^{13}C pulses of approximately 10° flip angle, separated by 5 seconds. After a short build-up period, the spectral in-

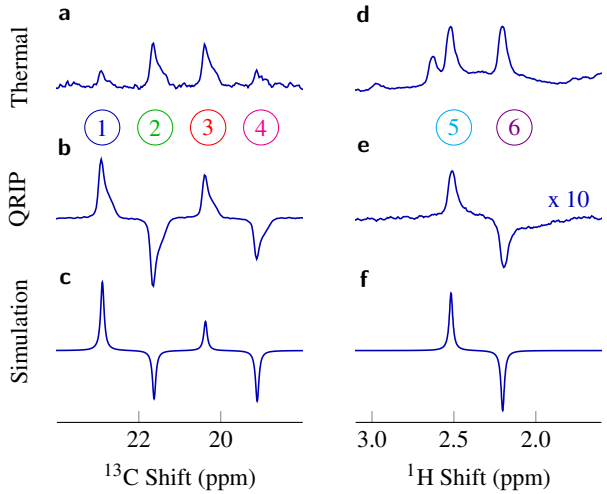

Figure 5.12: (a) Experimental ^{13}C spectrum after thermal equilibration in the magnetic field [90° flip angle, 32 transients added] (b) enhanced spectrum after dissolution [~ 10° flip angle] (c) numerical simulation (d) experimental ^{1}H spectrum after thermal equilibration in the magnetic field [90° flip angle, 32 transients added] (e) enhanced spectrum after dissolution [~ 5° flip angle] and (f) simulated spectrum. All spectra obtained on a solution of ^{13}C-γ-picoline in degassed $CHCl_3$ without proton decoupling in a magnetic field of 9.4 Tesla. Simulations included dipole-dipole relaxation, CSA relaxation (with $\sigma^C_{zz}-\sigma^C_{iso} = 24$ ppm and $\sigma^H_{zz}-\sigma^H_{iso} = 5$ ppm) and random-field relaxation [$(\gamma_C \bar{B}^C_{rand})^2\tau_{rand} = 44\times10^{-3}$ s^{-1} and $(\gamma_H \bar{B}^H_{rand})^2\tau_{rand} = 24\times10^{-3}$ s^{-1}]. The correlation times were $\tau_C = 5$ and $\tau_R = 0.6$ ps. An initial relaxation delay of 15 s with no CSA relaxation was included to account for the delay before sample injection. *Reprinted with permission from J. Am. Chem. Soc. 2013,* **135***(50), 18746-18749. Copyright 2013 American Chemical Society.*

tensities decay approximately exponentially with respect to time, with a time constant $T_{\text{LLS}} = 43 \pm 1$s. Fig. 5.14-b shows analogous data for the ^{1}H magnetization obtained in a second experiment using ~ 5° flip angle pulses every 5 seconds. The time constant of the decay is found to be 38 s, i.e. slightly smaller than as measured on the carbon magnetization. In Fig. 5.14-c, two decays are shown on a logarithmic scale. The T_1 behaviour of the ^{1}H and ^{13}C nuclei is indicated by dashed lines. Separate measurements of the spin-lattice relaxation time constants give $T_1(^1\text{H}) = 6.1\pm0.3$ s and $T_1(^{13}\text{C}) = 10\pm1$ s in degassed $CHCl_3$, i.e. the lifetime of the long-lived state exceeds that of the ^{1}H and ^{13}C magnetization by factors of 7 and 4, respectively. Fig. 5.12-(c,f) shows numerical simulations performed by Dr. Dumez, of the ^{13}C and ^{1}H spectra, based on the following mechanism:

- quantum rotor polarization of the $^{13}CH_3$ group at low temperature;
- conversion of the quantum rotor polarization into hyperpolarized long-lived order in solution;
- slow conversion of the hyperpolarized long-lived order into magnetization components through cross-correlated hetero-nuclear dipole-dipole relaxation.

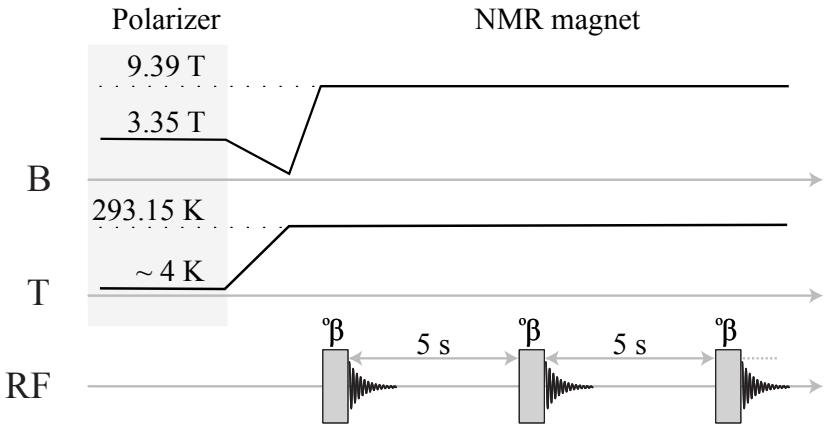

Figure 5.13: Pulse sequence used in γ-picoline experiments. Thermalization at 4 °K occurs for about 2 hours. The frozen solution is melted by injection of hot and degassed chloroform, and transferred at 9.4 T. The signal is acquired repetitively every 5 seconds. $^{\circ}\beta$ represents the flip angle used: 5 and 10 degrees for ^{1}H and ^{13}C experiments respectively.

5.3.3 Analysis

The molecular symmetry group of the CH_3 rotor is C_3(M), using the notation of Bunker and Jensen[40]. This group has three irreducible representations, denoted A, E_a and E_b (see Table 5.4). The Pauli principle, applied to this group, requires that the spatial A states are associated with the nuclear spin state of symmetry A, which has total nuclear spin $I = 3/2$. Similarly the spatial E_a and E_b states are associated with spin states of symmetry E_b and E_a respectively, which have total nuclear spin $I = 1/2$. Importantly in γ-picoline, the potential barrier for CH_3 rotation is so low that the CH_3 rotates almost freely. There is a rotational splitting $\Delta E = 520\ \mu$eV [114] corresponding to a temperature of $\Delta E/k_B = 6$ °K between the ground spatial A state (spin $I = 3/2$) and the first excited rotational state with symmetry E_a and E_b (spin $I = 1/2$). Equilibration of the sample at a temperature below ~ 6 °K creates a large population difference between A and E, and hence between the $I = 3/2$ and $I = 1/2$ spin manifolds[97]. Other molecules containing methyl groups such as lithium acetate and 2,6-dibromomesitylene have been observed to display identical effect [101]. In addition systems with a rotational splitting corresponding to a temperature lower than ~ 4 °K show a reduced enhancement (like toluene) or no effect at all [102]. Icker and co-workers pointed out that the dependence of the rotational splitting on intermolecular interactions in the solid state may be crucial to explain the absence of QRIP in some systems [102].

The interactions governing the time evolution of the spin ensemble in an isotropic liquid can be classified according to their permutation symmetry properties. In the present

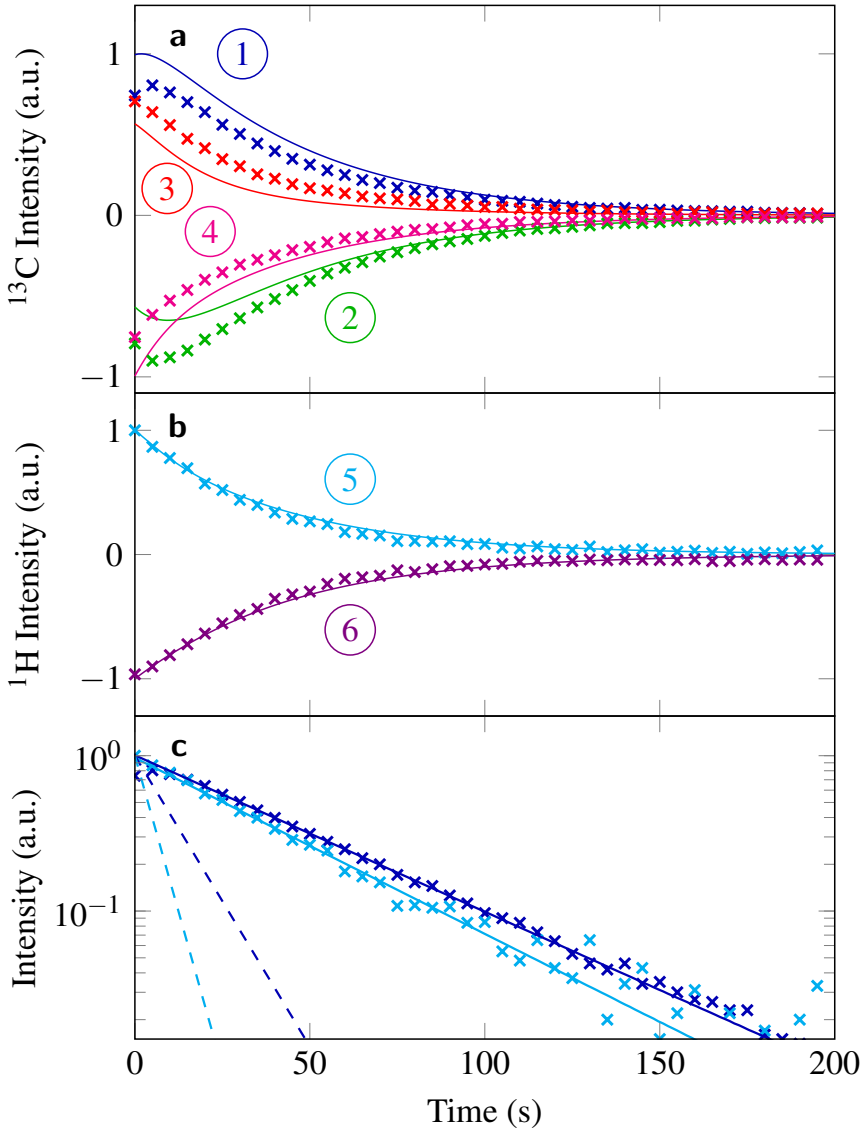

Figure 5.14: (a) Crosses: Amplitudes of the ^{13}C peaks as a function of time, in an experiment in which a series of 10° pulses, separated by 5s, is applied after dissolution and transfer to the high-field magnet. Solid lines: A set of numerical simulations, performed by Dr. Dumez, of the peak amplitudes, scaled vertically for best fit to experimental data. (b) The same data as in (a) for the ^{1}H peaks, obtained using 5° pulses. (c) Decay of two representative signals (1 and 5 in Figure 2) plotted on a logarithmic scale. The solid lines are obtained by fitting a mono-exponential decay to the data at times $\geq$ 20 s. The fit procedure yields constants of 43.1 ± 0.4 s and 38 ± 2 s for ^{13}C (blue) and ^{1}H (cyan), respectively. The experimental T_1 decays of the ^{13}C (blue) and ^{1}H (cyan) magnetization are shown by dashed straight lines, for comparison. The simulation parameters are as in Fig. 5.12.*Reprinted with permission from J. Am. Chem. Soc. 2013,* **135***(50), 18746-18749. Copyright 2013 American Chemical Society.*

case for a $^{13}CH_3$ system, the coherent Hamiltonian can be expressed as usual as:

$$\begin{aligned} \mathcal{H}^{\text{coh}} &= \mathcal{H}_Z + \mathcal{H}_J \\ \mathcal{H}_Z &= \sum_{i=1}^{3} \omega_{\text{H}} I_{iz} + \omega_{\text{C}} S_z \qquad (5.29) \\ \mathcal{H}_J &= 2\pi \sum_{i<j} J_{\text{HH}} I_i \cdot I_j + 2\pi \sum_{i=1} 3 J_{\text{CH}} I_{iz} \cdot S_z, \qquad (5.30) \end{aligned}$$

$\omega_{\text{H}} = -\gamma_{\text{H}} B_0 (1 + \delta_{\text{H}})$ and γ_{H} is the gyromagnetic ratio for ^{1}H, B_0 is the static magnetic field and δ_{H} is the ^{1}H chemical shift. Similarly for ^{13}C. The incoherent interactions can be generally expressed as follows:

$$\mathcal{H}^{\lambda}_{\text{fluc}}(t) = c^{\lambda} \sum_{l=0}^{2} \sum_{m=-l}^{l} (-1)^m A^{\lambda}_{lm} T^{\lambda}_{l-m}, \qquad (5.31)$$

where c^{λ} are the same constants reported above for DD and CSA interactions, and T^{λ}_{l-m} are spherical tensor operators of rank l and component $-m$. By indicating the three proton nuclei as $1, 2, 3$ the symmetry group of the coherent Hamiltonian is:

$$\mathcal{G}_{\text{coh}} = \{(), (123), (132)\} \qquad (5.32)$$

$\mathcal{G}_{\text{coh}}$ is isomorphic to C_3 with irreducible representations A, E_a and E_b as in Table 5.4.
If we consider the symmetry properties of equation 5.31 for the intra-molecular dipolar

	()	(123)	(132)
A	1	1	1
E_a	1	ϵ	ϵ^*
E_b	1	ϵ^*	ϵ

Table 5.4: Character table for $\mathcal{G}_{\text{coh}}$ in equation 5.32 relative to a methyl group system. $\epsilon = e^{i2\pi/3}$ and $*$ indicates the complex conjugated.

Hamiltonian averaged over internal vibrations, as the system does not have an inversion centre, no symmetries other than the identity operation can be identified. However such an approach does not account for internal rotations happening on a time-scale half-way between the tumbling and vibrational correlation times. As discussed more extensively in section 4.16 this intermediate motional regime imposes a higher symmetry to the system. As a result the correct symmetry group in presence of intra-molecular dipolar relaxation is:

$$\mathcal{G}_{DD} = \{(), (123), (132)\} \qquad (5.33)$$

and the group of the complete Hamiltonian under the current approximations that do not consider other minor relaxation mechanisms is:

$$\mathcal{G}_{\mathrm{H}} = \mathcal{G}_{\mathrm{coh}} \cap \mathcal{G}_{DD} = \{(), (123), (132)\} \tag{5.34}$$

The nuclear wave functions can be classified according to equation 5.32 obtaining (see also Fig. 5.15):

$$\Gamma_{nspins} = 8A \oplus 4E_a \oplus 4E_b, \tag{5.35}$$

and therefore a total number of three long-lived orders is predicted. Apart from the total conservation of spin population, the other two can be identified in the spin population imbalances between states spanning the irreducible representations A and E, and E_a and E_b.

$$\Delta_{A,E} = \frac{1}{8}\sum_{i=1}^{8} |i,A\rangle\langle i,A| - \frac{1}{4}(\sum_{i=9}^{12} |i,E_a\rangle\langle i,E_a| + \sum_{i=13}^{16} |i,E_b\rangle\langle i,E_b|) \tag{5.36}$$

$$\Delta_{E_a,E_b} = \frac{1}{4}(\sum_{i=9}^{12} |i,E_a\rangle\langle i,E_a| - \sum_{i=13}^{16} |i,E_b\rangle\langle i,E_b|) \tag{5.37}$$

The relaxation properties of $^{13}CH_3$ moiety in solution can also be investigated using the Abragam-Redfield second-order perturbation theory [120]. In the extreme narrowing limit, where the correlation times are much smaller than the inverse of the Larmor frequencies, the relaxation superoperator for rank-2 interactions may be written, in a static reference frame, as in equation 5.22. The spectral density at zero frequency for the correlation between interactions λ and λ':

$$J_0^{\lambda,\lambda'} = \frac{1}{5}\sum_{m_1=-2}^{2} \frac{\tau_R\tau_C}{\tau_R + m_1^2\tau_C} D^2_{0m_1}(\Omega^{\lambda}_{PR}) D^{2*}_{0m_1}(\Omega^{\lambda'}_{PR}), \tag{5.38}$$

where Ω^{λ}_{PR} is the set of Euler angles that describes a transformation from the principal axis system of the interaction P to a rotor frame R fixed with respect to the methyl group and with its z-axis aligned with the local 3-fold symmetry axis. A complete derivation of equation 5.38 can be found in Appendix.
In the limit of rapid methyl rotation ($\tau_R \ll \tau_C$), the relaxation superoperator acquires symmetry C_3 as qualitatively represented in Fig. 4.8, and can be formalized by the superoperator:

$$\hat{\Gamma} = \sum_p c_p \hat{F}^C_p \hat{G}^C_p, \tag{5.39}$$

where c_p are constants and $\hat{F}^C_p$ and $\hat{G}^C_p$ are commutation superoperators for fully symmetric operators F_p and G_p. This form leads to vanishing transition probabilities between Hilbert-space states of different spin permutation symmetries. As an example the

transition probability W_2^{AE} for symmetry-breaking double-quantum transitions caused by dipole-dipole relaxation, shown in Figure 5.15 in red, is found to be:

$$W_2^{AE} = \frac{3}{320}\tau_R \left(c^{\mathrm{DD,CH}}\right)^2 \sin^2\theta \times \frac{\tau_C(17\tau_C + 5\tau_R + 3\cos(2\theta)(5\tau_C + \tau_R))}{(\tau_C + \tau_R)(4\tau_C + \tau_R)}, \tag{5.40}$$

where θ is the angle between a CH bond and the 3-fold symmetry axis of the methyl group. The transition rate W_2^{AE} indeed becomes zero in the limit of infinitely fast methyl rotation.
The dynamic symmetry expressed in Equation (5.39) is imposed by the rapid methyl rotation and results in long-lived states that are protected against all relaxation mechanisms internal to the methyl group. One such state corresponds to the difference in the mean populations of the A and E manifolds. This Liouville-space state corresponds to the Hilbert-space operator:

$$\Delta_{A,E} = \mathbf{I_1} \cdot \mathbf{I_2} + \mathbf{I_1} \cdot \mathbf{I_3} + \mathbf{I_2} \cdot \mathbf{I_3}. \tag{5.41}$$

This operator is invariant to all nuclear spin rotations, and hence to applied magnetic fields. It is the three-spin analogue of singlet order for spin-1/2 pairs[59]. In practice, the finite correlation time τ_R leads to coupling of the long-lived state to population differences across the ^{1}H and ^{13}C transitions which may be converted into observable transverse magnetization components by resonant radio-frequency (RF) pulses.
Finite τ_R is thus simultaneously the cause of the finite lifetime of the A/E population imbalance and of its conversion into observable magnetization. It can be shown that equation 5.36 is equivalent to equation 5.41, and equation 5.37 can be expressed as:

$$\Delta_{E_a,E_b} = \mathbf{I_1} \cdot (\mathbf{I_2} \times \mathbf{I_3}). \tag{5.42}$$

From a geometrical standpoint equations 5.41 and 5.42 represent the two scalar quantities (surface area and volume) that can be obtained combining the vectors $\mathbf{I_1}, \mathbf{I_2}, \mathbf{I_3}$ in a three dimensional vector space. In the same way $\mathbf{I_1} \cdot \mathbf{I_2}$, the singlet order, is the scalar quantity in the two dimensional vector space formed by vectors $\mathbf{I_1}, \mathbf{I_2}$.

5.3.4 Polarization at 4 °K

Symmetry and statistical thermodynamics arguments can be fruitfully applied to convey an estimation of the polarization level at a given temperature.
Following an approach used by Allen [124] we model the methyl group in γ-picoline as a two-dimensional rigid rotor. A single inertia axis is assumed and the rotational

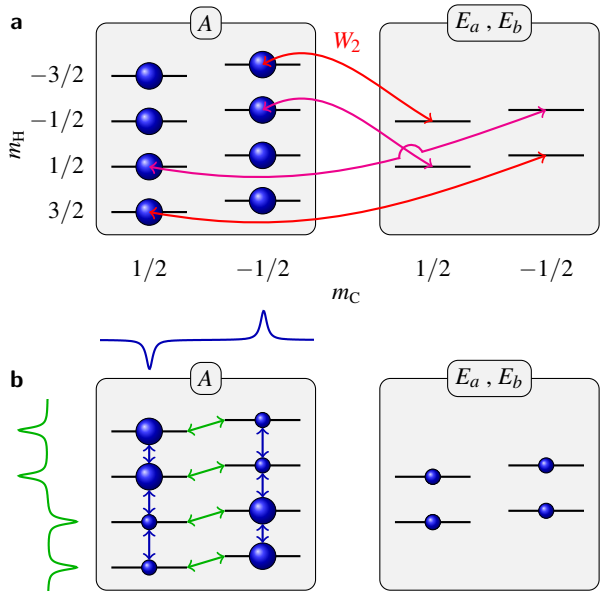

Figure 5.15: Energy level diagram for a $^{13}CH_3$ system. The populations immediately after dissolution from liquid helium temperature are shown as circles. For simplicity, the initial E manifolds are shown as completely depleted. Selected double-quantum ^{13}C-^{1}H cross-relaxation processes are indicated with red arrows. These processes lead to populations such as shown in (b). Population differences within the A and E manifolds are converted into observable ^{13}C-^{1}H (green) and ^{1}H (blue) magnetization when an RF pulse is applied, leading to the respective anti phase spectra shown on the left and top of (b). *Reprinted with permission from J. Am. Chem. Soc. 2013,* **135***(50), 18746-18749. Copyright 2013 American Chemical Society.*

energies can be expressed as follows:

$$E_m = \frac{\hbar^2}{2I} m^2 \tag{5.43}$$

where $\hbar$ is the Planck's constant divided by 2π, I is the inertia moment and m is the projection of the angular momentum along the inertia axis. We define a rotational temperature and re-express the energies:

$$\begin{aligned} B &= \frac{\hbar^2}{2IK_B} \\ E_m &= Bm^2 \end{aligned} \tag{5.44}$$

where $K_B \simeq 1.38 \times 10^{-23} JK^{-1}$. For γ-picoline, as previously seen, $B \simeq 6$ °K. Therefore the corresponding inertia moment can be estimated $I \simeq 6.71 \times 10^{-47} Kgm^2$. According to Pauli Exclusion Principle the total wave function has to be anti-symmetric with respect to the exchange of identical fermions (spin 1/2 particles). The wave function ψ of the system can be, in general, factorized into electronic (e), vibrational (v), rotational (r) and nuclear spin (n) contributions [39, 40, 67]:

$$\psi = \psi^e \psi^v \psi^r \psi^n \tag{5.45}$$

Depending on the temperature several states may be populated. However at low-temperature regimes (< 400 °K) only the ground electronic and vibrational states are to be considered given that the thermal available energy is insufficient to promote transitions to excited levels. We therefore focus on the product $\psi^r \psi^n$.
Each symmetry element of the group C_3 can be represented as the product of an even number transpositions. Therefore, to satisfy the Pauli's Exclusion Principle, the $\psi^r \psi^n$ wave function must be total-symmetric, i.e. transform as A symmetry species. The resulting admissible combinations of rotor-nuclear wave functions must be:

$$A^r \otimes A^n \qquad E_a^r \otimes E_b^n \qquad E_b^r \otimes E_a^n \tag{5.46}$$

The rotational wave functions for a planar rigid rotor can be expressed as:

$$\psi^r = \frac{1}{\sqrt{2}} \exp(im\phi) \tag{5.47}$$

with m rotational quantum number. In general the effect of C_3 symmetry operations on rotational wave functions will be to transform an eigenfunction into itself, into $\epsilon = e^{i2\pi/3}$ times itself and into ϵ^* times itself. The symmetry of the rotational eigenfunctions is

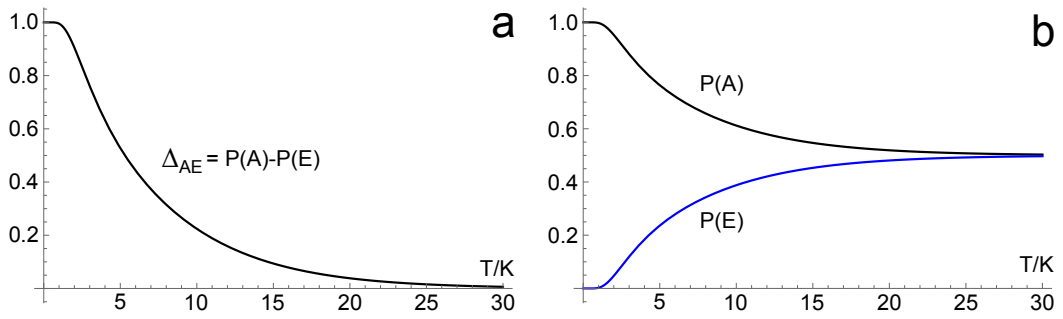

Figure 5.16: (a): $P(A)-P(E)$ (obtained from equation 5.51) as a function of temperature representing a $\Delta_{A,E}$ population imbalance calculated modelling the methyl group in γ-picoline as a rigid rotor with a single inertia axis. The polarization level at thermal equilibrium at 4 °K is approximately 60%. (b): $P(A)$ (in black) and $P(E)$ (in blue) populations for rotational states of symmetry A and E in a temperature range from 0 to 30 °K.

maintained when m varies in steps of 3. We can identify three subsets:

$$\begin{aligned} m &= m_A \cup m_{E_a} \cup m_{E_b} \\ m_A &= \{\cdots -3, 0, 3, 6 \ldots\} \qquad (5.48) \\ m_{E_a} &= \{\cdots -4, -1, 2, 5 \ldots\} \qquad (5.49) \\ m_{E_b} &= \{\cdots -5, -2, 1, 4 \ldots\} \qquad (5.50) \end{aligned}$$

For $m = m_A$ the rotational wave function has symmetry A. When $m = m_{E_b}$ the rotational wave function has symmetry E_b and in all other cases it has symmetry E_a. The multiplicity g^r and g^n of ψ^r and ψ^n respectively can be defined as follows:

$$g^r(m) = \begin{cases} 1 & m = 0 \\ 2 & \forall m \geq 1 \end{cases} \qquad \text{and} \qquad g^n = \begin{cases} 4 & \psi^n \sim A \\ 2 & \psi^n \sim E_a \quad \text{or} \quad E_b \end{cases}$$

The ratio between population transforming as A and E can be therefore expressed as:

$$\frac{P(A)}{P(E)}(T) = \frac{\sum_{m \in m_A} g^r(m) g^s e^{-\frac{Bm^2}{T}}}{\sum_{m \in m_{E_a}} g^r(m) g^s e^{-\frac{Bm^2}{T}} + \sum_{m \in m_{E_b}} g^r(m) g^s e^{-\frac{Bm^2}{T}}} \qquad (5.51)$$

The population imbalance $\Delta_{A,E}$, as well as the ratio in equation 5.51, are functions of the temperature. The population imbalance $\Delta_{A,E} = P(A) - P(E)$ for the methyl group in γ-picoline at thermal equilibrium at 4 °K can be estimated to be about 60% (see Fig. 5.16).

5.4 One hour long-lived state in solution at room temperature

5.4.1 Introduction

When discussing the approximations introduced in the formalization of LLS through a permutation symmetry approach, we have pointed out that they are accountable for the finite lifetime of enduring nuclear spin species. Ideally one would like to have a system where the impact of the relaxation mechanisms compromising the nuclear spin lifetime is set to a minimum. In order to design or choose a molecular agent with the most extended lifetime a set of criteria needs to be established. Getting a molecule with long lifetime is not just a mere scientific curiosity. It is important when aiming at storing polarization into singlet order [9, 52] and transporting it to a different location. Some of the recent efforts in our group have been pointing in this direction, tackling the daunting task of extending nuclear lifetime through a systematic cooperation between people with expertise spanning from organic chemistry [118] to computational and quantum chemistry. Some quite remarkable lifetimes have been reported so far: $^{15}N_2O$, investigated by Pileio and others [22], has a singlet order lifetime between ^{15}N estimated of the order of 26 minutes at room temperature. Similarly pairs of ^{13}C may display a lifetime of roughly 1/4 of hour in some acetylene derivatives [7]. In either examples experiments were conducted at low magnetic field down to 2 mT.
A number of molecules have been proposed as possible LLS-candidate species. Several times the experimental evidence is disappointing in terms of extended lifetime though, suggesting the necessity of better formalize the dynamics on a microscopic level. Naphthalene has soon been proposed as a possible LLS-candidate being an example of system with two adjacent carbon nuclei without directly bonded hydrogen nuclei [18].
Here we report the investigation of the following naphthalene derivative: 1,2,3,4,5,6,8-heptakis(methoxy-d3)-7-((propan-2-yl-d7)oxy)-naphthalene (compound **I**). ^{13}C labelling of **I** at both positions 4a and 8a (Fig. 5.17-a) generates a $^{13}C_2$ spin pair near the centre of the molecule. The synthetic route to $^{13}C_2$-**I** is reported in Ref. [118]. The accessibility of the nuclear singlet order in the $^{13}C_2$ pair is provided in this case by the asymmetry of the deuterated chains. They generate a small chemical shift difference between the ^{13}C sites of $\Delta\delta \sim 0.06 \pm 0.02$ ppm, as shown by the natural abundance ^{13}C spectrum of unlabelled **I** shown in Fig. 5.17-b. In Fig. 5.17-c the ^{13}C spectrum of $^{13}C_2$-**I** shows a single narrow peak. The system can be modelled as a AB $^{13}C_2$ spin pair and the theoretical splitting $\Delta\delta^2\nu_0^2/2J_{CC} \sim 0.3$ Hz is not resolved at this magnetic field. The 0.05 ppm difference between the mean chemical shift of the natural abundance material and the $^{13}C_2$-labelled compound is attributed to an isotope shift [125].

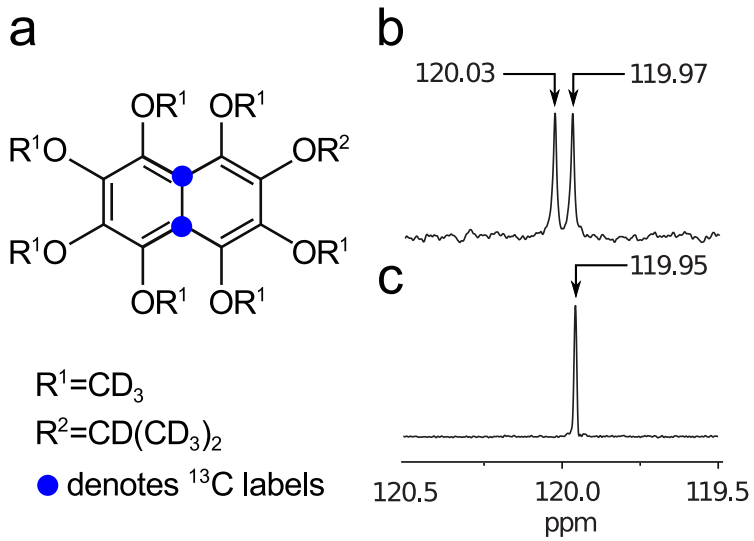

Figure 5.17: (a) Molecular structure of the naphthalene derivative $^{13}C_2$-**I**. Blue filled circles indicate the ^{13}C labelling sites. (b) ^{13}C spectrum of **I** in acetone-d_6 solution, acquired at 9.4 T with 512 transients. The two peaks separated by 0.06 ppm indicate the resonances of the inequivalent ^{13}C nuclei. (c) The ^{13}C spectrum of $^{13}C_2$-**I** acquired at 9.4 T with a single transient shows a single peak with a full-width-at-half-height of 1.5 Hz.

5.4.2 Experiment

$^{13}C_2$-**I** was dissolved in acetone-d_6 at a concentration of 0.1 M. The initial O_2 concentration has been estimated about 2mM considering a Henry coefficient of oxygen in acetone of about 9400 Pa $\cdot$ m^3/mol, and a partial pressure of 19 kPa at 293.2 °K [126]. For the degassed sample used in Fig.5.18 and Table 5.5, molecular oxygen was removed by 10 pump-thaw cycles.

The singlet relaxation time constants (T_S) for $^{13}C_2$-**I** were measured by using the pulse sequence shown in Fig. 5.19 [6, 9]. The following procedure (see Fig. 5.19) was used:

- For each transient, the sample was first equilibrated for almost one hour in the high magnetic field (9.4 T) and then a magnetization-to-singlet (M2S) pulse sequence was run to convert longitudinal magnetization into long-lived singlet order.
- The sample was transported, at a constant speed in a time τ_{tr}, into a region of lower magnetic field, here indicated as the evolution field B_{evol}.
- The sample was left for a variable interval τ_{evol} at this field.
- The sample is returned at 9.4 T where S2M is applied to convert singlet order into readable magnetization.

The M2S and S2M pulse sequences are described in detail in Ref. [6, 9] and represented in Fig. 5.19-b. Sample transport was performed using the simple apparatus described

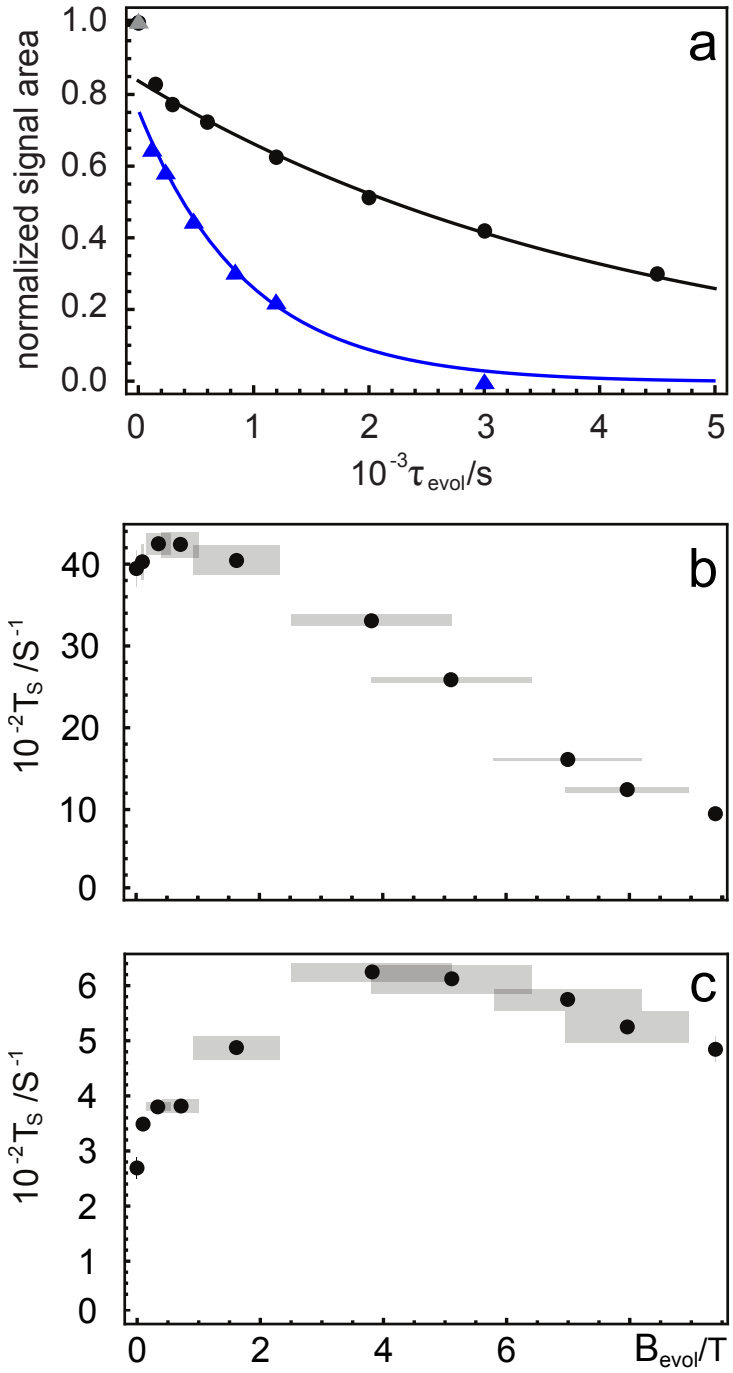

Figure 5.18: (a) Experimental decay curves $^{13}C_2$-**I** dissolved in degassed acetone-d_6 obtained using the pulse sequence in Figure 5.19 for B_{evol} = 9.39 T. (blue triangles) and B_{evol} = 0.4 T (black circles). Experimental points have been normalized to the value of the first point. Solid lines are fits to exponential decays ignoring the first point at τ_{evol} = 1 s. Experimental field dependence of T_S for $^{13}C_2$-**I** in acetone-d_6 for a degassed sample (b), and for a non-degassed sample with $[O_2]\sim$ 2 mM (c). Gray rectangles represent the confidence intervals.

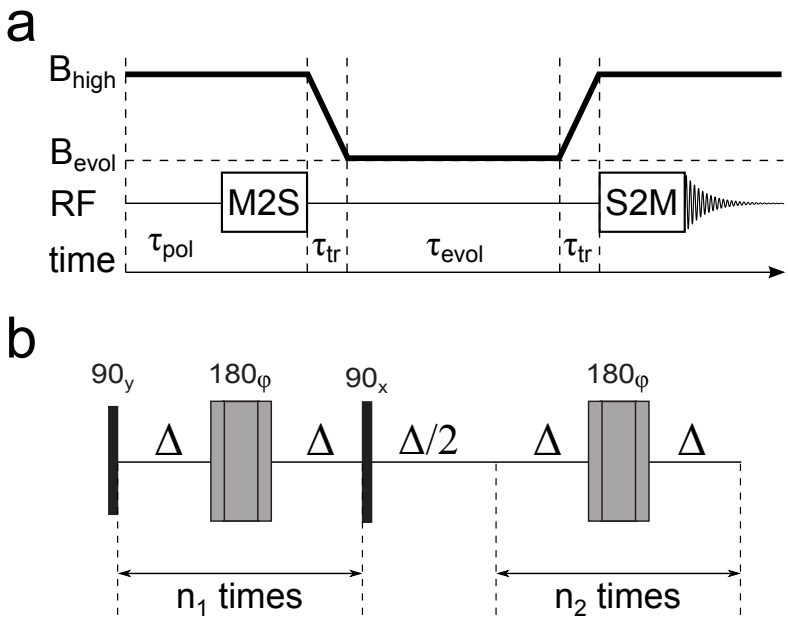

Figure 5.19: (a): Sequence of events used to estimate T_S at different magnetic fields B_{evol}. (b): M2S block described in Ref. [6, 9]. The S2M pulse sequence is identical but time-reversed. The parameters used in the experiments are $\Delta = 4.62$ ms, $n_1 = 14$ and $n_2 = 7$. The polarization time between consecutive acquisitions is $\tau_{pol} = 3000$ s. The transport time at constant speed τ_{tr} varied between 0 and 8 s, depending on the evolution field B_{evol}. The time spent at low magnetic field varied between 1 and 4500 s in 8 steps.

in Ref. [9], which consists of a computer-controlled stepper motor that winds a string attached to the sample holder thus moving the sample along the main field axis.

Fig. 5.18-a shows experimental singlet decay curves measured at 9.4 T (blue triangles)

B_{evol}/T	T_S^a/s	T_1^a/s	T_S^b/s	T_1^b/s
0.002 ± 10^{-4}	3959 ± 220	78 ± 3	270 ± 20	33 ± 1
0.10 ± 0.02	4030 ± 220	72 ± 2	348 ± 8	37 ± 2
0.4 ± 0.2	4250 ± 130	73 ± 2	380 ± 8	40 ± 1
0.7 ± 0.3	4240 ± 150	76 ± 2	381 ± 12	46 ± 1
1.6 ± 0.7	4050 ± 180	73 ± 2	487 ± 22	48 ± 2
3.8 ± 1.3	3310 ± 70	55 ± 2	624 ± 17	37 ± 1
5.1 ± 1.3	2590 ± 30	43 ± 1	611 ± 26	29 ± 1
7.0 ± 1.2	1610 ± 20	29 ± 1	574 ± 19	22 ± 1
8.0 ± 1.0	1240 ± 40	24 ± 1	524 ± 28	19 ± 1
9.39	950 ± 60	19 ± 1	485 ± 23	18 ± 1

Table 5.5: Singlet (T_S) and magnetization (T_1) decay times for $^{13}C_2$-**I** as a function of magnetic field B. Data refer to: (a) Degassed sample; (b) Non-degassed sample with $[O_2] \sim$ 2mM. The solvent used is Acetone-d_6.

and 0.4 T (black circles) with the method described above. As in previous measurements [22] these data exhibit a rapid initial drop due to equilibration of triplet states, followed by a much slower decay attributed to singlet order relaxation. The estimated value for T_S has been obtained by a mono-exponential fitting of the experimental data

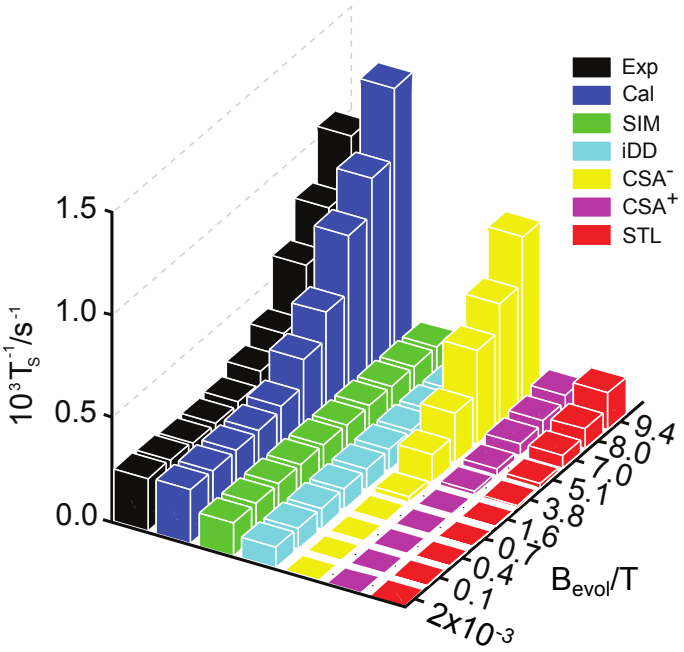

Figure 5.20: Experimental (Exp) and calculated (Cal) singlet state decay rates (T_S^{-1}) for $^{13}C_2$-**I**. The individual simulated contributions of spin internal-motion (SIM), intramolecular dipolar (iDD), symmetric (CSA^+) and antisymmetric (CSA^-) chemical shift anisotropy, singlet-triplet leakage (STL) relaxation are shown for comparison. QM/MM simulations have been performed by Dr. Håkansson and are briefly described in Ref. [10]

.

neglecting the first point. As reported in Table 5.5 singlet lifetime exceeds one hour at the lowest measured magnetic field (2 mT), becoming even longer lived as the magnetic field is increased. The maximum lifetime happens to be at about 0.4 T for the singlet order. A similar field dependence exists for T_1 as reported in Table 5.5 and the maximum T_1 is at about 1.6 T. The ratio $T_S/T_1 \sim 50$ over a wide range of magnetic fields.

5.4.3 Analysis

The relevant thermalization processes that can be identified for a pair of homo-nuclear spins include:

1. *Intramolecular dipole-dipole* (iDD): Dipolar interaction with extras spins outside the pair can be estimated as follows [58]:

$$R_S^{DD} = \frac{4}{3}\sum_j I_j(I_j+1)[c_{C_{1j}}^2 + c_{C_{2j}}^2 - 2c_{C_{1j}}c_{C_{2j}}P_2(\cos(\theta_{C_1jC_2}))]\tau_2 \qquad (5.52)$$

where j is the spin outside the pair, $\theta_{C_1jC_2}$ is the angle $\widehat{C_1jC_2}$, $c_{C_{1j}} = -\mu_0\gamma_{C_1}\gamma_j\hbar/(4\pi r_{C_{1j}}{}^3)$, I_j is the angular momentum quantum number of j, and $P_2(x) = (3x^2-1)/2$ is a

Legendre polynomial. In the case of $^{13}C_2$-**I**, deuteration of the methoxy groups leads to a reduction of this field independent relaxation mechanism.

2. *Chemical shift anisotropy* (CSA): Any 3×3 matrix can be decomposed into a scalar term, a symmetric and an antisymmetric component. Similarly the tensor difference between the Cartesian shielding tensors at the two ^{13}C sites $\Delta\sigma = \sigma_1 - \sigma_2$, can be decomposed in a traceless symmetric part $\Delta\sigma^+$ and an antisymmetric part $\Delta\sigma^-$. Both components contribute to singlet relaxation [7] according to:

$$R_S^{CSA^+} = \frac{2}{9}\gamma_C^2 B_0^2 \tau_2 \|\Delta\sigma^+\|^2 \qquad R_S^{CSA^-} = \frac{2}{9}\gamma_C^2 B_0^2 \tau_1 \|\Delta\sigma^-\|^2 \tag{5.53}$$

assuming rigid isotropic molecular motion and in the extreme narrowing limit. γ_C is the ^{13}C gyromagnetic ratio and τ_j is the rank-j correlation time. The two values of τ_j in equation 5.53, are characterized by following relation [127]:

$$\tau_1 = 3\tau_2 \tag{5.54}$$

The longer correlation time of $R_S^{CSA^-}$ in equation 5.53 renders this term dominant, as can be seen in Fig. 5.20, particularly for magnetic fields higher than 1 T. The mechanism producing relaxation is the rotational modulation of the difference of the instantaneous CSA tensors at the ^{13}C positions. However if the two shielding tensors are identical the CSA contribution to relaxation vanishes, as the singlet is sensitive only to differences in the local magnetic field. This can be accomplished when the local geometry of the spin network is, as in this case, centrosymmetric [95].

3. *Singlet-Triplet leakage* (STL) [7, 9]: This effect is due to symmetry-breaking coherent spin interactions mixing states spanning different irreducible representations. In this case singlet and triplet. In the limit $|\Delta\delta\gamma_C B_0/(2\pi J_{CC})| \ll 1$ (that we consider always valid under the current experimental conditions), this yields an exponential decay of the singlet order. If the traceless symmetric parts of the two shielding tensors at ^{13}C positions, σ_1^+ and σ_2^+, are approximately uniaxial with the same value $\sigma_{CSA} = \sigma_{ZZ} - \sigma_{iso}$ for the largest eigenvalue, the leakage rate constant for singlet decay is predicted to be [7]:

$$R_S^{leak} \sim \frac{\Delta\delta^2 \gamma_C^2 B_0^2 (5c_{DD,CC}^2 + 3\gamma_C^2 B_0^2 \sigma_{CSA}^2)\tau_2}{60\pi^2 J_{CC}^2} \tag{5.55}$$

where $c_{DD,CC} = -\mu_0\gamma_C^2\hbar/(4\pi {r_{CC}}^3)$ is the dipolar coupling constant, $J_{CC} \sim 54$ Hz is the J coupling between the pair $^{13}C_2$. The dipolar component in eq. 5.55 scales as the square of B_0^2, whereas the CSA component goes with B_0^4. Therefore this

contribution to relaxation, as per Fig. 5.20, is minimal except at magnetic fields higher than 7 T.

4. *Spin internal motion* (SIM): Modulation of local dynamics within the molecule that we define as spin internal motion (SIM) also contribute to relaxation as per Fig. 5.20. This term accounts for all internal motions that can induce local magnetic fields. The derivation considers the classical angular velocity as a summation of the over-all and internal angular velocity as per:

$$H^{\mathrm{SIM}} = \sum_k I_k \cdot C_{(k)}(t) \cdot (\Theta(t) + \tilde{\omega}(t)) \tag{5.56}$$

where the interaction tensor $C_{(k)}$ is per unit angular velocity and $\Theta(t)$ and $\tilde{\omega}(t)$ are the overall and internal angular velocity respectively. The corresponding spectral density is computed according to the general expression:

$$J^{\lambda,\lambda'}_{rsuv} = 2\int_0^\infty |r\rangle\langle s|\,\overline{H^{\lambda}(t)\cdot H^{\lambda'}(t+\tau)}\,|u\rangle\langle v|\,e^{-i\omega\tau}d\tau \tag{5.57}$$

where λ is the SIM interaction.

Finally T_S and T_1 field profiles for a 0.1 M concentration of $^{13}C_2$-**I** in acetone-h_6 has been also acquired. Experimental values are reported in Table 5.6. The intermolecular

B_{evol}/T	T_S^a/s	T_1^a/s	T_S^b/s	T_1^b/s
0.002 ± 10^{-4}	2283 ± 51.7	66 ± 1	290 ± 10	31 ± 3
0.10 ± 0.02	1990 ± 85	75 ± 2	300 ± 5	33 ± 2
0.4 ± 0.2	1860 ± 25	74 ± 2	315 ± 20	38 ± 2
0.7 ± 0.3	1920 ± 30	74 ± 2	300 ± 8	38 ± 2
1.6 ± 0.7	1800 ± 130	69 ± 1	340 ± 30	45 ± 2
3.8 ± 1.3	1780 ± 30	50 ± 1	500 ± 20	41 ± 1
5.1 ± 1.3	1600 ± 40	38 ± 1	400 ± 75	34 ± 1
7.0 ± 1.2	1240 ± 40	27 ± 1	490 ± 30	26 ± 1
8.0 ± 1.0	1060 ± 70	23 ± 1	495 ± 40	21 ± 1
9.39	860 ± 15	19 ± 1	415 ± 12	17 ± 2

Table 5.6: (a) Degassed sample; (b) Non-degassed sample with $[O_2]\sim$ 2mM. Solvent used: Acetone-h_6.

relaxation rate due to the dipolar interaction between $^{13}C_2$-**I** and acetone-d_6 molecules can be approximately estimated by comparing the experimental rate constants in the experiments using deuterated and protonated acetone as a solvent. In both experiments the total relaxation is the sum of three terms:

$$\begin{aligned} R_S(d_6) &= R_S(\mathbf{I}) + R_S(\mathbf{II}) + R_S(\mathbf{I}d_6) \\ R_S(h_6) &= R_S(\mathbf{I}) + R_S(\mathbf{II}) + R_S(\mathbf{I}h_6) \end{aligned} \tag{5.58}$$

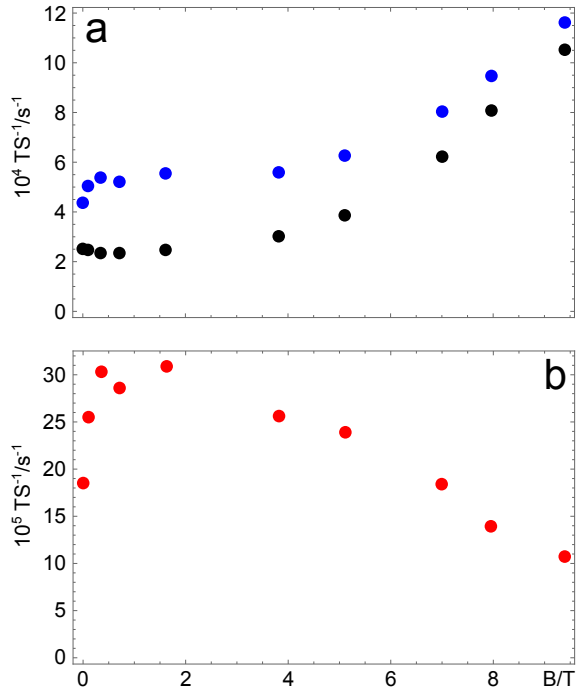

Figure 5.21: (a): Rate constants (T_S^{-1}) field profile for a 0.1 M degassed sample of $^{13}C_2$-**I** in acetone-d_6 (black) and in acetone-h_6 (blue). (b): Magnetic field profile of the difference in rate constants for a 0.1 M degassed sample of $^{13}C_2$-**I** in acetone-d_6 and in acetone-h_6.

where $R_S(d_6)$ and $R_S(h_6)$ indicate the total rate constants for $^{13}C_2$-**I** in deuterated and protonated acetone respectively. $R_S(\mathbf{I})$ is the intra-molecular contribution to the total rate. $R_S(\mathbf{II})$ is represented by the dipole-dipole interaction between different $^{13}C_2$-**I** molecules in the sample. $R_S(\mathbf{I}d_6)$ and $R_S(\mathbf{I}h_6)$ are the dipolar rate constants between $^{13}C_2$-**I** molecule and the deuterated and protonated acetone. Both field profiles have been acquired at approximately 20 °C. Assuming the viscosities in the two experiments equal and a total absence of molecular oxygen, we can estimate the two terms $R_S(\mathbf{I})$ and $R_S(\mathbf{II})$ in equation 5.58 to be also equal. Therefore:

$$R_S(h_6) - R_S(d_6) = R_S(\mathbf{I}h_6) - R_S(\mathbf{I}d_6) \tag{5.59}$$

Equation 5.52 can now be used to estimate the ratio between the two rate constants:

$$\begin{aligned} \frac{R_S(\mathbf{I}h_6)}{R_S(\mathbf{I}d_6)} &= \frac{I(I+1)}{S(S+1)}\left(\frac{\gamma_{^1\mathrm{H}}}{\gamma_{^2\mathrm{H}}}\right)^2 \\ &= \frac{3}{8}\cdot 42.4374 \simeq 16 \end{aligned} \tag{5.60}$$

where $I = 1/2$ is the ^{1}H and $S = 1$ is ^{2}H spin. Therefore in a first approximation $R_S(h_6) - R_S(d_6) = R_S(\mathbf{I}h_6) - R_S(\mathbf{I}d_6) \simeq 15R_S(\mathbf{I}d_6)$. The contribution $R_S(\mathbf{I}d_6)$ was not included in the molecular dynamics simulation in Fig. 5.20. However in the limit of

above approximations and according to the experimental values reported in Table 5.6 and presented in Fig. 5.21, $R_S(\mathbf{I}d_6)$ for $^{13}C_2$-**I** ranges between $7 - 20 \times 10^{-6}s^{-1}$ and is one order of magnitude smaller than the intra-molecular dipolar contribution with other out-of-the-pair spin nuclei.

5.4.4 Water-soluble derivative

$^{13}C_2$-**I** molecular prototype shows a singlet lifetime of more than one hour at moderate magnetic fields. The body of simulations of the reported relaxation mechanisms, performed in our group by Dr. Håkansson, describes the experimental results with a good accuracy as per Fig. 5.20. However paramagnetic relaxation induced by molecular O_2 , according to data in Table 5.5, still remains a major concern to be further investigated. The applicability of $^{13}C_2$-**I** is limited by its insolubility in water.
A further step that was considered, in the wake of the promising $^{13}C_2$-**I** data, was the synthesis of a water-soluble derivative. The variant synthesized and experimentally tested is 2,2'-((1,2,3,4,6-Pentakis(methoxy-d_3)-7-(propan-2-yl-d_7) naphthalene-5,8-diyl(bis(oxy))diacetic acid-4a,8a-$^{13}C_2$ that we will indicate as $^{13}C_2$-**II** and whose molecular structure is reported in Fig. 5.22. The synthesis of both $^{13}C_2$-**I** and $^{13}C_2$-**II** was performed by our organic chemistry collaborators Dr. Pop and Dr. Hill-Cousins [118]. A schematic synthetic route is briefly reported in Appendix.
After dissolving a quantity of 23.5 mg of compound $^{13}C_2$-**II** in 0.5 ml of D_2O, corre-

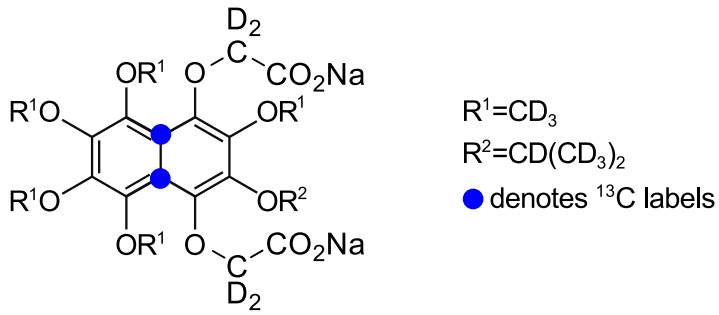

Figure 5.22: Molecular structure of the naphthalene derivative $^{13}C_2$-**II**. Blue filled circles indicate the ^{13}C labelling sites. A schematic synthetic route is provided in Appendix.

sponding to a 0.08 M concentration, carbon T_1 has been estimated at 9.4 T: $T_1(^{13}C)$=3.2 sec. The T_S field profiles were subsequently measured starting from the oxygenated $^{13}C_2$-**II** first and after removal of O_2. The freeze-pump-thaw technique was not used for the current molecule to remove molecular oxygen, given that the increase in volume of D_2O at liquid nitrogen temperatures could easily crack the NMR tube. The first procedure used to de-oxygenate the sample was by bubbling Ar gas for about 10 minutes. The second way was to add 4mg of L-Ascorbic Acid.
The field profiles are reported in Table 5.7. Preliminary tests carried out for $^{13}C_2$-**I** showed a direct proportionality between the solvent viscosity and T_S at high field

(9.4 T). The ratio between the viscosities of the two solvents at 25 °C is:

$$\frac{\eta^{CD_3OD}}{\eta^{Acetone-d_6}} = \frac{0.545\ m \cdot Pa \cdot s}{0.295\ m \cdot Pa \cdot s} \sim 1.8 \tag{5.61}$$

Therefore given that $\eta^{D_2O} = 1.25\ m \cdot Pa \cdot s$ using a viscosity-type of argument one would expect for a molecule like $^{13}C_2$-**I**, if it was water soluble, a value close to 4 minutes at 9.4 T. According to the values in Table 5.7 we have found T_S=1.5 min at 9.4 T. The $^{13}C_2$-**II** derivative has a different molecular structure compared to $^{13}C_2$-**I** and the carboxyl chains, instrumental to make it water-soluble, have probably a non-trivial contribution in the local dynamics of the spin system. So far we have not investigated further the reasons behind a shorter-than-expected lifetime for $^{13}C_2$-**II**.

B_{evol}/T	T_S^a/s	T_S^b/s	T_S^c/s
0.002 ± 10^{-4}	355 ± 20	545 ± 100	520 ± 40
0.10 ± 0.02	320 ± 10	630 ± 130	680 ± 90
0.4 ± 0.2	340 ± 20	540 ± 50	570 ± 30
0.7 ± 0.3	340 ± 30	550 ± 40	600 ± 70
1.6 ± 0.7	300 ± 10	440 ± 40	730 ± 50
3.8 ± 1.3	180 ± 10	310 ± 10	390 ± 20
5.1 ± 1.3	180 ± 10	300 ± 40	280 ± 30
7.0 ± 1.2	100 ± 20	150 ± 10	180 ± 20
8.0 ± 1.0	100 ± 10	150 ± 10	150 ± 10
9.39	80 ± 10	90 ± 10	90 ± 10

Table 5.7: (a) Non-degassed sample; (b) Ar-bubbled sample; (c) Sample added with LAscorbic Acid.

5.5 Hyperpolarized LLS

5.5.1 Introduction

An exceptionally long LLS lifetime at room temperature opens up the possibility to conceive further experiments aiming at enhancing nuclear spin polarization while maintaining spin order for a considerable duration.
Several techniques are currently used by NMR spectroscopists worldwide to create hyperpolarized signals. A methodological exhaustive review can be found for example in a paper from Cavagnero and co-workers [128]. Among the others techniques dissolution dynamic nuclear polarization (dDNP) has contributed in the last decade to foster research investigations not only in NMR but also in MRI applied in a clinical context [129]. The seminal work from Ardenkjaer-Larsen and co-workers [30], that has received so far about 1200 citations, applied the method on aqueous solutions of ^{13}C-Urea. Polarizations of 37% for ^{13}C and 7.8% for ^{15}N, respectively, were obtained in

liquid state at room temperature. These polarizations corresponded to an enhancement of 44,400 for ^{13}C and 23,500 for ^{15}N, respectively, compared with thermal equilibrium polarization at 9.4 T and room temperature. Dissolution DNP equipments are also commercially available under the brand HyperSense.
The method works in brief as follows: a frozen solution of the molecule of interest is kept at low temperature (at about 1.5 °K) in a magnetic field of few Tesla (HyperSense uses 3.35 T) in presence of a radical. The frozen solution is microwave irradiated (power 100 mW) for a time usually up to 1-2 hours in order to transfer polarization from electrons to the nuclei of the target molecule. A hot solvent is then injected to liquefy the sample and the melted solution is rapidly (in less than 10 s) transferred to a high field spectrometer where the signal is read out. Combination between singlet order with dDNP and MRI has been already demonstrated in Ref. [52, 130, 131].
Recently a magnet with two isocenters avoiding the transfer to a different spectrometer has been also developed [132].

5.5.2 Experiment

In collaboration with Ardenkjaer-Larsen's research group at DTU our group performed experiments on hyperpolarization of singlet orders [52], where a recycling protocol in which enhanced nuclear polarization, achieved by dissolution-DNP, is observed with full intensity and then returned to singlet order has been developed. Using this methodology the same batch of highly polarized nuclei is observed with full intensity and its polarization reconverted to long-lived singlet order. A schematic of the pulse sequence used is in Fig. 5.23.

- **Pulse sequence**: The initial M2S block converts the longitudinal magnetization into singlet order [6, 9]. We schematically re-outline the density operator transformations involved in the M2S:
  - The initial equilibrium magnetization is:
    $I_z = |T^1\rangle\langle T^1| - |T^{-1}\rangle\langle T^{-1}|$
  - A 90_y excites single quantum coherences between triplet states:
    $I_x = |T^1\rangle\langle T^0| + |T^0\rangle\langle T^1| + |T^0\rangle\langle T^{-1}| + |T^{-1}\rangle\langle T^0|$
  - A train of n_1 (the number n_1 can be experimentally optimized [6]) echo composite pulses $\tau - 90_x 180_y 90_0 - \tau$ converts the triplet coherences into the following singlet-triplet coherences:
    $I_{1y} - I_{2y} = i(|T^1\rangle\langle S^0| + |S^0\rangle\langle T^1| - |S^0\rangle\langle T^{-1}| - |T^{-1}\rangle\langle S^0|)$
  - A following 90_x rotates the single-quantum coherences into zero-quantum coherences:
    $I_{1z} - I_{2z} = i(|T^0\rangle\langle S^0| + |S^0\rangle\langle T^0|)$

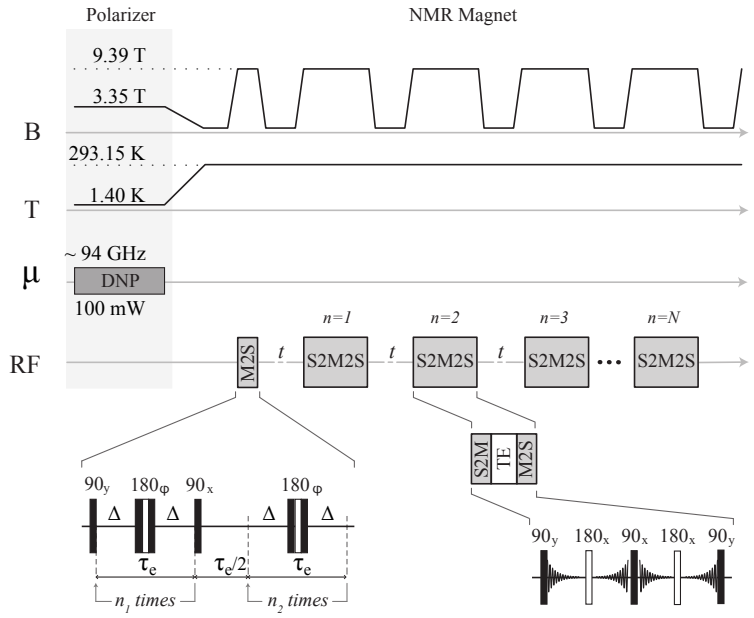

Figure 5.23: S2M2S pulse sequence. Trace B shows the trajectory of magnetic field as the sample is transported from the polarizer (3.35 T) to the high-field (9.4 T) magnet and through a region of low field; trace T shows the temperature changes from about 1.5 °K to room temperature across the experiment; trace μ shows the microwave irradiation (100 mW) applied during dissolution-DNP; trace RF shows the radio-frequency pulses applied at the nuclear resonance frequency in high magnetic field. Expansions of M2S and TE blocks are shown. The S2M pulse sequence is equal to the M2S sequence applied in reverse chronological order. The time axis is not to scale.

- Free evolution for a time indicated as $\Delta = 1/4J_{CC}$ (where J_{CC} is the homonuclear J coulpling expressed in Hz units) in Fig. 5.19 phase shifts these coherences into:
  $(|T^0\rangle\langle S^0| - |S^0\rangle\langle T^0|)$
- A second echo train of $n_2 = n_1/2$ creates a singlet-triplet population difference: $(|S^0\rangle\langle S^0| - |T^0\rangle\langle T^0|)$

The successive parts of the S2M2S pulse sequence repeatedly convert singlet order into detectable magnetization and the left magnetization into singlet order.

As per description in Fig. 5.23 the block denoted by triplet-echo (TE) is formed by a sequence of 5 pulses: $90_y - \tau/4 - 180_x - \tau/4 - 90_x - \tau/4 - 180_x - \tau/4 - 90_y$. The total duration of TE is τ. The first outer 90_y converts longitudinal magnetization generated by S2M into transverse magnetization, whereas the last 90_y reconverts transverse into longitudinal magnetization that is subsequently converted into singlet order by the adjacent M2S block. The role of the 180_x is to refocus chemical shifts and magnetic field inhomogeneities. It is noted in Ref. [52] that the same refocusing is commonly applied in deuterium nuclei spectroscopy in solid state NMR. The triplet manifold in the current case is effectively a spin-1 species. However here the degeneracy between the triplet-triplet transitions is broken by the small chemical shift difference between like-nuclei rather than the

quadrupolar interaction. The central 90_x induces coherence transfer between the two triplet-triplet coherences, refocusing interactions that break the degeneracy of these two transitions. The degeneracy of the triplet transitions is broken in the case of $^{13}C_2$-**I** by the small (0.06 ppm) chemical shift difference between ^{13}C nuclei. The S2M-TE-M2S or S2M2S allows nuclear singlet order to be converted temporarily into transverse readable magnetization. The NMR signal can be observed during all four inter-pulse τ-intervals before being reconverted back into singlet order. With this modality the same batch of long-lived singlet order can be retrieved and reconverted back multiple times in a single experiment and the relaxation decay curve measured by interpolation.

- $\mathbf{T_S^*}$: The measured value of T_S^* is an underestimation of the real T_S. During TE transverse magnetization is excited and decays with a time $T_2 < T_S$. The experimental efficiency of the M2S pulse sequence can also be far from ideal. For clarity, we write again the boundary condition we found in section 4.19 for conversion between longitudinal magnetization and singlet order:

$$b_{\max}(I_z \rightarrow \mathrm{SO} \rightarrow I_z) = b_{\max}(I_z \rightarrow \mathrm{SO}) b_{\max}(\mathrm{SO} \rightarrow I_z) = \frac{2}{3}. \tag{5.62}$$

The above limit has been experimentally investigated by comparing the signal intensity ratio between two experiments:

$$\frac{90_y - \mathrm{M2S} - \mathrm{T_{00}Filter} - \mathrm{S2M} - \mathrm{acquisition}}{90_y - \mathrm{acquisition}} \tag{5.63}$$

In the present case eq. 5.63 returned an experimental value of 0.46 rather than 0.67. Therefore the fraction of initial magnetization that is converted into singlet order and reconverted for read-out is 30% less than the theoretical value. In addition there are other variables that may affect in the present experiment the measured T_S:

  - The presence in the final solution of the radical used in the hyperpolarization procedure (This point is addressed in section 5.5.3).
  - The possible presence of molecular O_2 acting as a relaxation agent.
  - The possible presence of other paramagnetic impurities leaking from the dissolution metal chamber into the dissolved sample during the dDNP procedure (This point will require further investigations).

The advantage of S2M2S is that it gives the chance to reconstruct T_S^* in a single observation fully exploiting the enhanced polarization granted by dDNP.

- **Experimental procedure**: A 1 μL volume containing about 1 mg of $^{13}C_2$-**I** in a 34 mM solution of BDPA radical in 2Me-THF was cooled at about 1.5 °K and

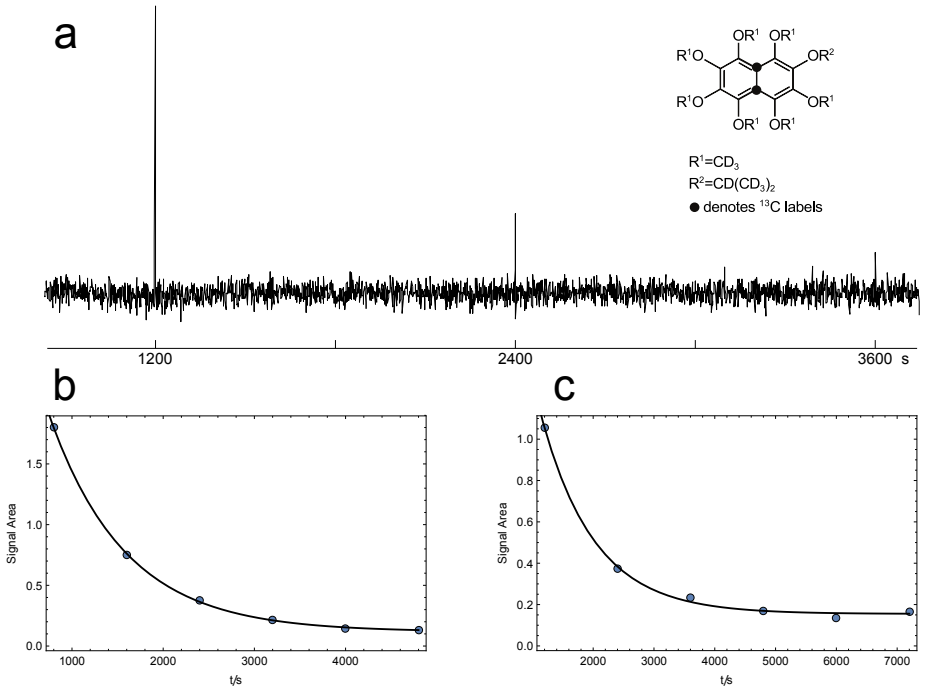

Figure 5.24: (a): First points for T_S^* decay at 0.03 T using the S2M2S pulse sequence described in Fig. 5.23 with $t = 1200$ s for a hyperpolarized sample of $^{13}C_2$-**I** in acetonitrile-d_3. Experimental points and exponential decay fitting curves in (b) for $t = 800$ s gives a $T_S^* = 830 \pm 15$ s and in (c) for $t = 1200$ s a $T_S^* = 875 \pm 60$ s.

irradiated with a 100 mW microwave source at ~ 94 GHz for about 1 hr according to the standard procedure used in dDNP. A volume of ~ 4.5 mL of acetonitrile-d_3, after being extensively degassed by bubbling He gas, has been warmed at 150 °C, injected at high pressure (~ 10 bar) and the resulting solution transferred into the NMR spectrometer in less than 10 seconds. A S2M2S pulse sequence is used to convert hyperpolarized magnetization into singlet order. The singlet order after an evolution time at a magnetic field of about 30 mT, dictated by the parameter t in Fig. 5.23, is temporarily converted into readable magnetization, at 9.4 T, and four FIDs are acquired with an acquisition time reduced to 40 ms. Subsequently, magnetization is converted back into singlet order and the procedure is repeated.

Using a value of $t = 800$ s and $t = 1200$ s the T_S^* measured value are $T_S^* = 830 \pm 15$ s and $T_S^* = 875 \pm 60$ s respectively (see Fig. 5.24). These values represent the T_S^* decay rate at about 30 mT.

5.5.3 Analysis

The above measured values seem not too depend much on the value of t suggesting that $T_S^* \rightarrow T_S$ at that magnetic field. However there is a considerable difference with the measurements performed on the thermal sample (see table 5.5).
It has been argued that the possible lower value on the measured T_S^* could be related

to the presence of BDPA molecules in the sample collected after dissolution. This is certainly a possibility although the final radical concentration is quite low: depending on the sample size it is usually less than 1 mM and most likely between 200 μM and 800 μM (values not measured).
In order to address this issue a thermal sample containing 10 mg of $^{13}C_2$-**I** was dissolved in 0.45 mL of CD_3OD. An amount of BDPA 0.68 mM was added to the sample to investigate the contribution to relaxation due to the radical. We therefore compared the T_S values of the thermal sample dissolved in CD_3OD previously measured in Southampton, with the one containing BDPA radical prepared in Copenhagen. Experimental observations are summarized in Table 5.8.
The sample containing the radical was degassed using the freeze-pump-thaw technique

	Southampton	Copenhagen
B_{evol}/T	T_S^{DEG}/s	$T_S^{DEG+BDPA}$/s
0.002 ± 10^{-4}	2495 ± 80	
0.03 ± 0.02		2900 ± 470
0.5 ± 0.2	3000 ± 130	
1.0 ± 0.7	3400 ± 50	
1.9 ± 0.7	2900 ± 30	
9.39	470 ± 10	490 ± 80

Table 5.8: The table reports in the central column the T_S field profile measured in Southampton on a thermal degassed sample of $^{13}C_2$-**I** in CD_3OD at $\sim$ 0.1 M concentration, and on the right column the T_S measured for the same compound in CD_3OD at $\sim$ 30 mM concentration with a preparation including 0.68 mM of BDPA.

for 10 cycles and sealed. We assume the $[O_2]$ concentration in the two samples to be the same and very low. If we consider the oxygen concentration in the two samples comparable and $[O_2] \to 0$, apparently the radical at micro-molar concentration is not effecting the singlet lifetime. It can be postulated that the difference between the T_S of the order of $\sim$ 3000 s measured on the thermal degassed sample containing BDPA and the $\sim$ 900 s measured on the hyperpolarized sample can be due either to the oxygen present in the dissolution line (or possibly introduced during the dissolution procedure) or to a leaching of paramagnetic metals from the pressure chamber into the dissolution medium. A quantitative analysis, due to time shortage, has not been attempted yet. In particular the exact concentration of the radical after dissolution has not been experimentally measured, nor the presence of other paramagnetic materials eventually leaching from the pressure chamber.
The polarization transfer between electrons and nuclei in a dDNP experiment not only allows to create enhanced magnetization that can then be transferred into singlet order via SLIC [11] or M2S [6, 105], but it also grants direct singlet order enhancement proportional to the square of the achieved level of polarization [64]. If we denote by p the ^{13}C initial polarization after dissolution, hyperpolarized singlet order amounting to $p_{HPSO} = -p^2/3$ is already available without further excitation scheme [64].

A simple argument can be used to derive the singlet order polarization p_{HPSO}.

If we consider an ensemble of non-interacting spin-1/2 particles the polarization p can be defined as $p = (n_\alpha - n_\beta)$, where n_α and n_β are the populations of spin states $|\alpha\rangle$ and $|\beta\rangle$ with the extra constraint that $n_\alpha + n_\beta = 1$. The populations of the two states can therefore be expressed in terms of p as:

$$\begin{aligned} n_\alpha &= \frac{1+p}{2} \\ n_\beta &= \frac{1-p}{2} \end{aligned} \tag{5.64}$$

For an hyperpolarized sample $p \gg p_{\mathrm{thermal}} = \tanh(\hbar\gamma B^0/2kT)$ (see Ref. [128] for derivation) by orders of magnitudes. A complete polarization along the quantization axis would correspond to $p = 1$.

For two inequivalent spins in a strong magnetic field (3.35 T in the polarizer) the eigenstates for the coherent Hamiltonian are $|\alpha\alpha\rangle, |\alpha\beta\rangle, |\beta\alpha\rangle, |\beta\beta\rangle$ and the corresponding population can be expressed resorting to equation 5.64 as:

$$\begin{aligned} n_{\alpha\alpha} &= \frac{(1+p)^2}{4} \\ n_{\alpha\beta} &= \frac{(1+p)(1-p)}{4} \\ n_{\beta\alpha} &= \frac{(1-p)(1+p)}{4} \\ n_{\beta\beta} &= \frac{(1-p)^2}{4} \end{aligned} \tag{5.65}$$

During the dDNP experiment the frozen sample is dissolved by injecting a hot solvent and collected as a room-temperature solution outside the polarizer in a region of magnetic field orders of magnitude smaller than 3.35 T. This dissolution occurs typically in few seconds and the Zeeman eigenstates, for a weakly coupled spin pair with positive J coupling and gyromagnetic ratio, are adiabatically converted into:

$$|\alpha\alpha\rangle \rightarrow |T^1\rangle \quad |\beta\beta\rangle \rightarrow |T^{-1}\rangle \quad |\alpha\beta\rangle \rightarrow |S\rangle \quad |\beta\alpha\rangle \rightarrow |T^0\rangle \tag{5.66}$$

As nuclear singlet order corresponds to the population imbalance between singlet and the mean triplets' population, the corresponding p_{HPSO} polarization is:

$$p_{\mathrm{HPSO}} = n_{\alpha\beta} - \frac{1}{3}(n_{\alpha\alpha} + n_{\beta\alpha} + n_{\beta\beta}) = -\frac{p^2}{3} \tag{5.67}$$

In the case of strong polarization, as for a dDNP experiment, there is an excess in population in the triplet manifold leading to the negative sign in equation 5.67. Although p_{HPSO} is expected to be modest, the detection of HPSO without prior conversion of hyperpolarized magnetization into singlet order was attempted either at high (9.4 T) and

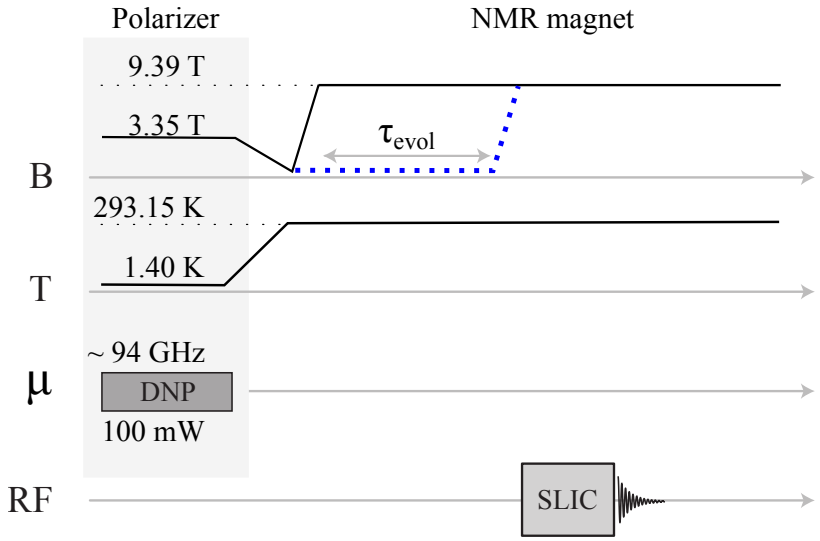

Figure 5.25: Pulse sequence describing direct observation, by a read-out SLIC [11] at 9.4 T, of hyperpolarized singlet order after dissolution and an evolution interval τ_{evol} spent either at 9.4 T or 30 mT.

low (30 mT) magnetic field.

For this experiment, 1 μL volume containing ~ 1 mg of $^{13}C_2$-**I** in a 34 mM solution of BDPA radical in 2 Me-THF has been prepared according to the standard procedure described before. A volume of ~ 4.5 mL of CD_3OD has been degassed thoroughly, warmed at ~ 150 °C and subsequently injected as a dissolution medium. According to the schematic presented in Fig. 5.25 the hyperpolarized solution has been transferred into a NMR tube located either at 9.4 T or at 0.03 T where it evolves for a certain time τ_{evol} (see Fig. 5.25) and subsequently, after being transferred in 2 seconds at 9.4 T, read-out by a SLIC pulse.

The three panels in Fig. 5.26 refer to different experiments. Unfortunately we were not able to see any HPSO signal after 30 minutes spent at 30 mT (panel c in Fig. 5.26). As there was only time for a further experiment, we tried to prepare multiple NMR samples from the same batch of hyperpolarized solution, store them at the top of the magnet at about 30 mT where they evolved for different τ_{evol} times. Every NMR sample was subsequently taken, at steps of 5 minutes, at 9.4 T to read out the signal. Only the first NMR sample gave a signal that confirmed that hyperpolarization occurred successfully, whereas the following did not give any signal at all. We do not have a definitive explanation for that. However one possibility, that will require further experiments, is that paramagnetic impurities from the corroded solvent heating chamber may leak into the dissolved solution. In addition the experimental set-up is not totally immune to the presence of O_2, and we have seen that this is an important relaxation mechanism. As anticipated dDNP experiments on $^{13}C_2$-**I** are still progressing in order to find the best experimental conditions to achieve both high polarization and long lifetime.

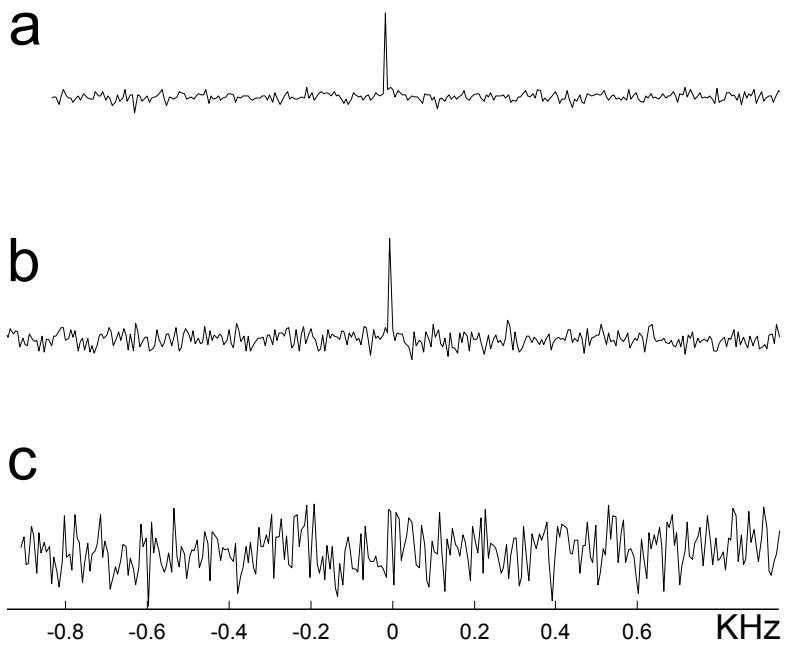

Figure 5.26: (a): HPSO signal after $\tau_{\text{evol}} = 180$ s at 9.4 T. (b): HPSO after $\tau_{\text{evol}} = 900$ s at 30 mT. (c): HPSO after $\tau_{\text{evol}} = 1800$ s at 30 mT. The three experiments we performed according to the pulse sequence described in Fig. 5.25

5.6 Summary

In this chapter LLS on some systems have been investigated. The main results can be summarized in few points:

- Experiments on $^{13}C_2$-AFD have shown that strong inequivalence is not a fundamental bound on LLS existence and detectability. The role of the local geometry of the spin system has been made clear by comparison of $^{13}C_2$-AFD and $^{13}C_2$-AMD.

- The class of rigid molecules displaying long-lived character can be widened to include non rigid systems as methyl group in γ-picoline. The essential ingredient is played by the intermediate dynamics condensed by a rotational correlation time τ_R lower than the tumbling correlation time τ_C.

- The experiment on γ-picoline is important in elucidating the role of fluctuating terms of the complete Hamiltonian to access a long-lived order through incoherent mechanisms.

- The project to find a molecular system displaying long lifetimes in solution and at room temperature led to the design of a derivative of naphthalene that can survive for more than 1 hour at moderate magnetic fields. In addition a set of well-known

criteria can be identified as important when designing or looking for long-lived species:

- The singlet pair should comprise two identical spin-1/2 nuclei with relatively low gyromagnetic ratio. Typically ^{13}C and ^{15}N. The small value of γ minimizes most relaxation mechanisms.
- The spin pair must be physically remote from other magnetic nuclei, especially isotopes with strong magnetism such as ^{1}H and ^{19}F. This minimizes intramolecular relaxation contributions from out-of-pair dipolar couplings.
- The local molecular environment of the singlet pair should display approximate local inversion symmetry and rigidity, in order to minimize relaxation contributions as internal dipole-dipole and CSA.
- In general, quadrupolar nuclei such as ^{2}H should also be remote. This minimizes relaxation contributions due to scalar coupling of the second kind.

As semantic is essential in conveying meaning, it is worth reminding here that long-lived states are not univocally defined. The experimental identification of LLS as spin order surviving longitudinal magnetization may be broader than the theoretical definition as population imbalances insensitive to thermalization processes. There are some parts that need further investigation:

- The T_S lifetimes for the water soluble naphthalene derivative are lower than expected and a complete explanation is still to come.
- The magnetic field profile for $^{13}C_2$-**I** in protonated acetone highlights the role of intermolecular relaxation mechanisms. This contribution has not been implemented in molecular dynamics simulations yet.
- dDNP experiments have shown that $^{13}C_2$-**I** can be successfully hyperpolarized, although the qualitative measurements performed in Copenhagen are inconclusive in order to explain the reduction in lifetime compared to the thermal signal.

Part IV

Final remarks

Chapter 6

Conclusions

The present work fits in the line of research on long-lived nuclear spin states currently being conducted in Prof. Levitt group in Southampton (UK). The focus is dedicated to nuclear long-lived orders particularly in multi-spin systems, trying to generalize the applicability of LLS analysis to larger spin environments. The work has been divided into two main categories: a theoretical and an experimental part. A large use of the theoretical introduced concepts has been made in the discussion of experimental data.

6.1 Theory

The symmetry-related nature of LLS in pairs of homo-nuclei has been the starting point encouraging a theoretical generalization of the subject to multiple spin systems. In this context the natural mathematical language to convey symmetry is represented by the group theory. Indeed the identification of the singlet order as a scalar spin operator has been already formulated as an invariance symmetry property with respect to rotation [6, 57, 59, 133].

In this work we have rather considered the invariance of nuclear spin Hamiltonian operators, characterizing the dynamics of the nuclear spin ensemble, with respect to a finite set of permutations exchanging the labels of nuclear spins. These permutations are identified as symmetry operations for the different components of the internal complete Hamiltonian. This approach, applied to the coherent part of the complete Hamiltonian, allows a clear identification of the two main classes of LLS that can be coherently accessed:

- LLS between spins nearly chemically equivalent [7, 59]
- LLS between spins chemically equivalent by nearly magnetic inequivalent. These states are also named "disconnected eigenstates" as no dipole moment connects singlet to triplet manifolds [3, 18, 134]

However the classification of nuclear wave functions according to the symmetry invariance of the coherent part of the nuclear spin Hamiltonian grants the definition of a

suitable symmetrized basis that can be in turn used to classify incoherent interactions as well. This treatment permits the representation of long-lived orders as population imbalances between states spanning across different irreducible representations giving an immediate and intuitive picture of LLS in multi-spin environments. Although this approach does not replace the analysis in the N^2-dimensional Liouville space to determine the value of the rate constants, it offers the possibility to work in the more comfortable N-dimensional Hilbert space to accomplish an analytic expression for LLS. In addition this formalism well adapts to the generalization of the Sørensen bound, recently discussed by Levitt [17], in presence of symmetry. We presume a deeper connection between rotational and permutation symmetries is probably present and would require a further effort to be properly examined and established.

6.2 Experiments

The standard quantum mechanical analysis of long-lived orders in multi-spin systems requires to set up the Liouvillian superoperator starting from the coherent and fluctuating terms[59, 133]. A numerical and analytical treatment of LLS in a variety of systems has been provided by Vinogradov and co-workers [93, 94]. As they correctly suggested together with Hogben [115] the presence of a local inversion geometry is instrumental to populate the null space of the Liouvillian superoperator and therefore to have LLS.

The experimental part encompasses investigations on strongly inequivalent (AFD-$^{13}C_2$ and AMD-$^{13}C_2$), equivalent ($^{13}CH_3$ in γ-picoline) and near magnetic equivalent spin environments (naphthalene derivatives). We review separately all of them, summarizing the principal outcomes.

- **Experiments on AFD-$^{13}C_2$ and AMD-$^{13}C_2$**: We took the conclusion of Vinogradov and Hogben on centrosymmetry as the starting point to prove that long-lived order can be *geometrically* imposed even if the system itself lives outside the regime of near magnetic equivalence. To accomplish that we compared at the beginning of Chapter 5 two isomers that are asymmetric derivatives of fumarate and maleate: AFD-$^{13}C_2$ and AMD-$^{13}C_2$ [55]. A long-lived order of 1 min ($T_1(^1H) \leq T_1(^{13}C) \sim$ 6 s.) has been detected, running four different multi-channel experiments, only for AFD-$^{13}C_2$. This lifetime pertains to a state that has been formalized as the population imbalance between states transforming according to different irreducible representations A_g and B_u. The same state has been accessed with an identical procedure for AMD-$^{13}C_2$. However the lifetime in this case is considerably shorter than proton and carbon T_1: $\sim$ 2.5 s.

  Fumarate-related systems are interesting not just to prove the symmetry of dipolar (or rank-2 in general) terms upon geometrical inversion but, from an application point of view, to monitor cell necrosis and cancer response to treatment [135, 136]. Indeed [1,4-$^{13}C_2$] Fumarate is an example of a substrate whose intracellular

metabolism is rapid but cellular uptake is slow. This property has been exploited in hyperpolarized studies to detect cellular necrosis.

Many of the long-lived molecules analysed, including AFD-$^{13}C_2$ and AMD-$^{13}C_2$, can be formally treated as rigid spin systems. In these molecules the presence of deuterated mobile groups as CD_2 and CD_3 is responsible for the sub-ppm chemical shift difference between homo-nuclei but, except for the molecular dynamics simulations, has not been considered when formalizing the nuclear spin system. Nonetheless long-lived orders exist in systems that cannot be approximated as rigid. This has been demonstrated, for example, in Ref. [100–102] for methyl rotors in γ-picoline and Toluene.

- **Experiments on γ-picoline**: The second set of experiments in chapter 5 concerns the characterization of methyl rotor in γ-picoline. This is a non-rigid system without an inversion geometry and, as a result, the dipolar Hamiltonian is expected to induce transitions between states of different symmetry: in this case C_3 symmetry with irreducible representations A, E_a, E_b (the character table has been derived in chapter 3). The conundrum of an experimental evidence, showing the existence of a LLS, contradicting the theoretical model can be resolved resorting to the dynamics of the methyl group. The intra-molecular dipolar interaction is in fact modulated not only by the molecular tumbling of the molecule in solution but also by the internal rotation in the methyl group. This additional motion imposes an extra symmetry on the dipolar term and, as a result, the dipolar Hamiltonian is (approximately) total-symmetric with respect to C_3. Therefore states transforming according to different irreducible representations are not mixed in the limit of an infinite fast rotation ($\tau_R \rightarrow 0$). The non-zero value of the rotational correlation time τ_R is eventually responsible for the finite value of the long-lived order lifetime in γ-picoline.

  The population imbalance $\Delta_{A,E}$ can be created in the case of γ-picoline by cooling the sample at liquid Helium temperature. The tunneling frequency of the methyl group in γ-picoline is about 126 GHz corresponding to a temperature of about 6 °K. The same efficiency, using identical methodology, cannot be obtained for methyl rotors in different systems. For example the tunneling splitting in Toluene is about 7 GHz corresponding to a tunneling splitting temperature of about 0.3 °K. Indeed the enhancement with respect to thermal polarization observed by Icker and Berger in Toluene is only 3% of the one observed in γ-picoline [101]. The enhancement, in this class of experiments, is related to the amount of polarization achieved at liquid He temperature. It depends on the tunnelling separation between A and E states: a phenomenon named as quantum rotor induced polarization (QRIP) [102, 137].

- **Experiments on naphthalene derivatives**: In the last part of chapter 5 some studies on two different derivatives of naphthalene are presented. Naphthalene

itself has been proposed as an example of system comprising carbon nuclei with no attached protons, and as such a possible recipient of long-lived disconnected eigenstates [18]. However the research line historically pursued by our group has been to look for and test molecules with pairs of chemically inequivalent nuclei. The degree of asymmetry is typically introduced by means of asymmetric ester groups, as in AFD-$^{13}C_2$ and AMD-$^{13}C_2$, and being field dependent, can be modulated shuttling the NMR sample in and out of the magnet. Over the last ten years a set of mechanisms have been recognized and studied [57, 58, 104, 138] as responsible for the singlet order relaxation. The local inversion geometry of the spin system together with a certain degree of local rigidity can be effective to minimize several thermalization processes on LLS [55, 95]. These consideration together with deuteration of ester groups in order to minimize intramolecular dipolar interactions and the presence of a intra-pair J coupling stronger than the asymmetric contribution may lead to suitable LLS candidates.

Figure Fig. 5.20 presents the results of a set of molecular dynamics simulations for the naphthalene derivative indicated as $^{13}C_2$-**I** (performed by Dr. Håkansson) where the impact of the relaxation mechanisms is plotted at different magnetic fields. Whereas chemical shift anisotropy and singlet-triplet leakage quickly decay to small values lowering the static magnetic field, a considerable low field relaxation mechanism is represented by the internal mobility of different regions of the molecule (SIM). This mechanism is not modulated by the tumbling correlation time of $^{13}C_2$-**I** in solution, but its characteristic correlation time is in the sub-picoseconds region, two orders of magnitude smaller than τ_C.

The effect of intermolecular relaxation has been investigated by reproducing in table 5.6 the T_1 and T_S field profiles for $^{13}C_2$-**I** by using acetone-h_6 rather than acetone-d_6. By assuming that the viscosity, the amount of O_2 in solution and the intermolecular $^{13}C_2$-**I**-$^{13}C_2$-**I** interactions in the two samples are the same, a coarse estimation of intermolecular contribution to the overall relaxation rate due to dipolar interactions with the solvent has been estimated.

The magnetic field profile for a water-soluble derivative of naphthalene denoted as $^{13}C_2$-**II** has also been presented. For this particular derivative there is a discrepancy with the expected results that cannot be explained solely in terms of solvent's viscosity effect. A complete analysis for this system has not been done yet, and the dynamic effect induced by the presence of carboxyl groups is currently under scrutiny.

The final part of chapter 5 presents some very preliminary attempts to obtaining a hyperpolarized and long-lived singlet order in $^{13}C_2$-**I**. The methodology chosen is dDNP [30]. Following standard dDNP procedures a level of ^{13}C polarization of about 10% is obtained. The lifetime of the hyperpolarized signal at low magnetic field (with the sample sitting at the top of the 400 MHz magnet $\sim$ 30 mT) has been measured using the pulse sequence S2M2S [52]. This lifetime is consider-

ably smaller than that of the thermal signal. A set of possibilities were considered to account for this difference: (i) radical-induced relaxation, (ii) presence of O_2 and/or (iii) presence of paramagnetic impurities leaking from the pressurized metal chamber containing the solvent used during the dissolution process. At this stage we only addressed (i) by preparing a thermal sample with a radical content comparable to that present in a dDNP experiment that is typically in the sub-mM range. The solvent used was CD_3OD. The O_2 contribution to relaxation has been singled out by extensive degassing using the freeze-pump-thaw procedure. Data are reported in table 5.8. Apparently the radical used at 680 μM concentration is not an effective mechanism of relaxation.

Finally we focused on the direct detection of singlet order present upon strong polarization regimes without the prior conversion of magnetization into singlet order by a preparatory M2S or SLIC. The direct detection using the experimental procedure illustrated in Fig. 5.25 is presented in Fig. 5.26. We could not see any signal after an evolution at $\sim$ 30 mT for 30 minutes. As previously indicated further investigation is required to address the shorter lifetime of the hyperpolarized signal.

6.3 Future Outlook

The theoretical part has been described and successfully applied in some multi-spin systems, but still requires further investigation as clarified below. The experimental part clearly accounts for the large variety of long-lived orders. A future interesting line of research will be the possibility to improve dDNP performance in systems exceptionally long-lived as $^{13}C_2$-**I**, but also the possibility to transfer spin order and polarization between different molecules using other methodologies. The following points need additional analysis:

- As pointed out during the exposition, the long-lived order accessibility through incoherent mechanisms has not been formalized although probably relevant in explaining experiments on methyl rotors [53, 102], and more recently on fumarate [121] and para-ethanol [56]. This may be an important aspect to further explore as it may concern a wide range of experiments where strong polarization can be converted into readable magnetization in magnetic equivalent systems.

- Strictly related to this topic is the estimation of the maximum conversion from a long-lived order into detectable magnetization in presence of different sources of thermalization. Essentially the operator responsible to break the magnetic-equivalence-symmetry perturbs the long-lived order introducing terms leaking into observable magnetization. However the spin system's evolution under relaxation does not preserve the observable vectors' norms and, therefore, is not

unitary. The topic is presently under investigation following the approach used by Khaneja [139, 140].

- In the experimental part, a further step on $^{13}C_2$-AFD investigation is the deuteration of the trans-^{1}H. Deuteration pulls the system back into the near equivalence regime and a long-lived order can be possibly investigated.

- The long-lived order and the QRIP phenomenon have been shown for γ-picoline, a system with a relatively large rotational splitting [53]. Similar experiments performed on other systems like toluene [100] have still shown the presence of a long-lived order but a reduced QRIP . The ratio between enhancements in γ-picoline and toluene has been correlated to the ratio between rotational splitting [100]. Other systems like for example 4-Methyltoluene do not show any increased polarization. Even deuteration of methyl group in γ-picoline is counterproductive in terms of observed enhancement [102]. The lack of signal enhancements in such systems is usually attributed to small tunnelling splitting caused by a rotational-hindrance of methyl group.

  We notice that $\Delta_{A,E}$ population imbalance can be created also by other means: for example by dDNP. The clear advantage is in this case that the methodology of dDNP can be applied irrespective of the characteristic tunnelling frequency. Systems of biochemical importance containing methyl rotors as [1,2-$^{13}C_2$]pyruvate have been hyperpolarized by dDNP but focusing on the singlet order between ^{13}C in position 1 and 2 [131]. In those experiments the singlet order was long-lived in blood but only at low magnetic field ($\sim$ 1 mT): $T_S \sim 19$ s and $T_1 \leq 5$ s. We anticipate, for example, that [1-^{13}C]pyruvate, [2-^{13}C]pyruvate, or [3-^{13}C]pyruvate can be hyperpolarized in this way and possibly a long-lived order detected.

  Although only partially related to the approach described in this work, it is worth noting that carboxylate carbons in pyruvate have been recently hyperpolarized through PHIP from 2-propynyl-2-oxopropanoate [141]. The method requires precursors containing a side harm capable of hydrogenation that is subsequently hydrolysed to yield hyperpolarized target signals by magnetic field cycling the sample from earth to (almost) zero magnetic field [141].

- The last part of the experimental session involves experiments on naphthalene derivatives. We are currently working on testing the possibility to store LLS by (i) freezing the sample once the singlet order has been populated (ii) letting the system evolve in presence/absence of an external magnetic field (iii) melting the system back to room temperature (iv) observing the signal. This set of experiments is a first step in order to create a hyperpolarized singlet order imbalance, store enhanced polarization into singlet order, transport it to a different location and retrieve it at will.

Appendix

Dipolar relaxation superoperator in CH_3 groups

Here we describe the derivation of equation 5.38 in a regime of isotropic diffusion. We consider the dipolar interaction mechanism so that λ = DD. A similar derivation is possible when λ represents some other interaction.

Within the main frame of Redfield relaxation theory [73, 120] we will start by writing the dipolar Hamiltonian for a pair of spins i, j in the laboratory system. This expression involves a number of Wigner rotation matrices to translate the information from the PAS (Principal Axes System) where the tensor representing the interaction is diagonal to the RS (Rotational System) in solid with rotating protons, to the MS (molecular System) rigid with the molecule, to the LS (Laboratory System) where experiment is performed. The stochastic motion of the molecule with respect to the laboratory frame is accounted for by the tumbling correlation time τ_C . The proton rotational motion in the methyl group will be described by the rotational correlation time τ_R . We would then expect to find out a dependence on both τ_C and τ_R in the final expression of the Liouvillian Super-operator. Transformations among different frames can be schematically represented as follow:

$$\text{PAS} \rightarrow \text{RS} \rightarrow \text{MS} \rightarrow \text{LS}$$

A generic time-dependent dipolar interaction between particles i, j is modulated as follows:

$$H_{ij}^{\text{DD}}(t) = \sum_{m_1,m_2,m_3,m_4} [A_2^{ij}]_{m_1}^P D_{m_1 m_2}^2(\Omega_{PR}^{ij}) D_{m_2 m_3}^2(\Omega_{RM}^{ij}(t)) D_{m_3 m_4}^2(\Omega_{ML}^{ij}(t))(-1)^{m_4} T_{2,m_4}(I_i, I_j) \tag{6.1}$$

where $[A_2^{ij}]_m^P$ is the m component of the rank 2 spherical tensor for DD interaction, D^2 is a second rank Wigner rotation matrix and $\Omega_{ML}^{ij}(t)$ is a time-dependent set of Euler-angles describing the orientation of the M-frame with respect to the L-frame. Equation 6.1 can be used to derive the correlation function $\langle H_{ij}^{\text{DD}}(0) H_{i'j'}^{\text{DD}}(\tau)\rangle$, where $\langle \dots \rangle$ denotes ensemble average.

First we calculate the term $H_{ij}^{\mathrm{DD}}(0)H_{i'j'}^{\mathrm{DD}}(\tau)$:

$$\begin{aligned} H_{ij}^{\mathrm{DD}}(0)H_{ij}^{\mathrm{DD}}(\tau) = \sum_{m_1,m_1'}\sum_{m_2,m_2'}\sum_{m_3,m_3'}\sum_{m_4,m_4'} & [A_2^{ij}]_{m_1}^{P}[A_2^{i'j'}]_{m_1'}^{P*} \times \\ & \times D^2_{m_1m_2}(\Omega_{PR}^{ij})D^{2*}_{m_1'm_2'}(\Omega_{PR}^{i'j'}) \times \\ & \times D^2_{m_2m_3}(\Omega_{RM}^{ij}(0))D^{2*}_{m_2'm_3'}(\Omega_{RM}^{i'j'}(\tau)) \times \\ & \times D^2_{m_3m_4}(\Omega_{ML}^{ij}(0))D^{2*}_{m_3'm_4'}(\Omega_{ML}^{i'j'}(\tau)) \times \\ & \times (-1)^{m_4+m_4'}T_{2,m_4}(I_i,I_j)T^{\dagger}_{2,m_4'}(I_{i'},I_{j'}) \end{aligned} \tag{6.2}$$

For dipolar interactions only the components with $m_1 = m_1' = 0$ ($[A_2^{ij}]_0^P \neq 0$) survive. In order to simplify equation 6.2 we need to define a dynamic model for the molecule. As already stated we have two kinds of motion: the tumbling motion undergoing an isotropic molecular diffusion and the protons' rotation, which cannot be modelled in the same way. In the latter case there is a preferential axis of rotation passing through the carbon's position. For the isotropic molecular diffusion it can be shown [120] that:

$$\langle D^2_{m_3m_4}(\Omega_{ML}^{ij}(0))D^{2*}_{m_3'm_4'}(\Omega_{ML}^{i'j'}(\tau))\rangle = \frac{1}{5}e^{-\tau/\tau_C}\delta_{m_3,m_3'}\delta_{m_4,m_4'} \tag{6.3}$$

In general the following expression needs to be calculated:

$$D^2_{m_2m_3}(\Omega_{RM}^{ij}(0))D^{2*}_{m_2'm_3'}(\Omega_{RM}^{i'j'}(\tau)) = \int D^2(\Omega_0)D^{2*}(\Omega_\tau)P(\Omega_0)P(\Omega,\tau|\Omega_0,0)d\Omega_0 d\Omega \tag{6.4}$$

Where $P(\Omega_0)$ is the probability density function for the values of Ω_0, and $P(\Omega,\tau|\Omega_0,0)$ is the probability density function for Ω at time τ assuming it was Ω_0 at initial time [41]. For the present case then we will assume that P obeys to the equation:

$$\frac{\partial}{\partial\tau}P(\Omega,\tau|\Omega_0,0) = -DL_z^2P(\Omega,\tau|\Omega_0,0), \tag{6.5}$$

where D is the rotational diffusion constant and L_z is the angular momentum operator. We seek a solution for equation 6.5 in term of eigenfunctions of L_z^2. We indicate $f_m(\alpha)$ the set of functions satisfying the following:

$$\begin{aligned} f_m(\alpha) &= \frac{e^{im\alpha}}{\sqrt{2\pi}} \\ L_z^2 f_m(\alpha) &= m^2 f_m(\alpha) \\ f_m(2\pi) &= f_m(0) \end{aligned} \tag{6.6}$$

As $f_m(\alpha)$ form a complete basis set we expand the probability P as:

$$P(\alpha, \tau|\alpha_0, 0) = \sum_{m=-\infty}^{+\infty} A_m(\tau|\alpha_0, 0)\frac{e^{im\alpha}}{\sqrt{2\pi}} \tag{6.7}$$

The above equation is the starting point to represent equation 6.5.

$$\begin{aligned} \frac{\partial}{\partial\tau}A_m(\tau|\alpha_0, 0) &= -Dm^2 A_m(\tau|\alpha_0, 0) \\ A_m(\tau|\alpha_0, 0) &= A_m(0|\alpha_0, 0)e^{-Dm^2\tau} \end{aligned} \tag{6.8}$$

The initial condition:

$$P(\alpha, 0|\alpha_0, 0) = \delta(\alpha - \alpha_0) \tag{6.9}$$

implies that:

$$A_m(0|\alpha_0, 0) = \frac{e^{-im\alpha_0}}{\sqrt{2\pi}} \tag{6.10}$$

Finally we have that:

$$P(\alpha, \tau|\alpha_0, 0) = \sum_{m=-\infty}^{+\infty} \frac{e^{im(\alpha-\alpha_0)}}{2\pi} \cdot e^{-Dm^2\tau} \tag{6.11}$$

The last equation can then be used to calculate:

$$D^2_{m_2m_3}(\Omega^{ij}_{RM}(0))D^{2*}_{m'_2m'_3}(\Omega^{i'j'}_{RM}(\tau)) = e^{-im_2\alpha(0)}e^{+im'_2\alpha(\tau)}d^2_{m_2m_3}(\beta(0))d^2_{m'_2m'_3}(\beta(\tau))e^{-im_3\gamma(0)}e^{+im'_3\gamma(\tau)} \tag{6.12}$$

with $\beta(0) = \beta(\tau) = 0$ and $\gamma(0) = \gamma(\tau) = 0$. The previous expression needs to be averaged over the ensemble:

$$\begin{aligned} \langle D^2_{m_2m_3}(\alpha(0), 0, 0)D^{2*}_{m'_2m'_3}(\alpha(\tau), 0, 0)\rangle &= \\ \langle e^{im_2\alpha(0)}d^2_{m_2m_3}(0)e^{-im'_2\alpha(\tau)}d^2_{m'_2m'_3}(0)\rangle &= \\ \langle e^{im_2\alpha(0)}e^{-im'_2\alpha(\tau)}\rangle d^2_{m_2m_3}(0)d^2_{m'_2m'_3}(0) & \end{aligned} \tag{6.13}$$

and the ensemble average can be expressed:

$$\begin{aligned}\langle e^{im_2\alpha(0)}e^{-im_2'\alpha(\tau)}\rangle &= \\ \frac{1}{2\pi}\int_0^{2\pi}\int_0^{2\pi} e^{im_2\alpha(0)}e^{-im_2'\alpha(\tau)}P(\alpha(\tau),\tau|\alpha(0),0)d\alpha(\tau)d\alpha(0) &= \\ \frac{1}{2\pi}\sum_{-\infty}^{+\infty}\int_0^{2\pi} e^{i(m_2-m)\alpha(0)}d\alpha(0)\cdot e^{i(m_2'-m)\alpha(\tau)}d\alpha(\tau)\frac{e^{-Dm^2\tau}}{2\pi} &= \\ \sum_{m=-\infty}^{+\infty}\delta(m_2-m)\delta(m_2'-m)e^{-Dm^2\tau} &\end{aligned} \tag{6.14}$$

where $\delta(l,l')$ is the Dirac's delta that is zero when $l \neq l'$ and is one when $l = l'$. Therefore we have that equation 6.13 becomes:

$$e^{-Dm^2\tau}d^2_{m_2m_3}(0)d^2_{m_2'm_3'}(0)\delta_{m_2m_2'} \tag{6.15}$$

As a result:

$$\begin{aligned}\langle H^{\mathrm{DD}}_{ij}(0)H^{\mathrm{DD}}_{ij}(\tau)\rangle = \frac{1}{5}\sum_{m_2,m_4}[A_2^{ij}]_0^P[A_2^{i'j'}]_0^{P*} \quad\times \\ D^2_{0m_2}(\Omega^{ij}_{PR})D^{2*}_{0m_2'}(\Omega^{i'j'}_{PR})e^{-Dm_2^2\tau}e^{-\tau/\tau_C} \quad\times \\ T_{2m_4}(I_i,I_j)T^{\dagger}_{2m_4'}(I_{i'},I_{j'})\end{aligned} \tag{6.16}$$

Transforming from the interaction frame to the laboratory frame we get to the final expression:

$$\begin{aligned}\hat{\Gamma}_{DD} = \sum_{i<j,i'<j'}\sum_{m_2,m_4}\Big(\int_0^{\infty} e^{-Dm_2^2\tau}e^{-\tau/\tau_C}e^{-im_4\omega_0\tau}d\tau\Big)\times \\ [A_2^{ij}]_0^P[A_2^{i'j'}]_0^{P*}D^2_{0m_2}(\Omega^{ij}_{PR})D^{2*}_{0m_2'}(\Omega^{i'j'}_{PR})\times \\ \hat{T}_{2m_4}(I_i,I_j)\hat{T}^{\dagger}_{2m_4'}(I_{i'},I_{j'})\end{aligned} \tag{6.17}$$

where the hat symbol has been used to indicate a superoperator. By defining $\tau_R = \frac{1}{D}$ and $[A_2^{ij}]_0^P = c_{ij}^{DD}$ we finally have:

$$\hat{\Gamma}_{DD} = -\sum_{i<j,i'<j'} c_{ij}^{DD}c_{i'j'}^{DD}J_0^{ij,i'j'}\sum_m(-1)^m\hat{T}_{2m}(I_i,I_j)\hat{T}^{\dagger}_{2-m'}(I_{i'},I_{j'}) \tag{6.18}$$

where

$$J_0^{ij,i'j'} = \frac{1}{5}\sum_{m=-2}^{+2}\frac{\tau_R\tau_C}{\tau_R+m^2\tau_C}D^2_{0m}(\Omega^{ij}_{PR})D^{2*}_{0m}(\Omega^{i'j'}_{PR}) \tag{6.19}$$

Synthesis of the water-soluble naphthalene derivative

We include for completeness a schematic route to the synthesis of compound $^{13}C_2$-**II** performed and provided by Dr. Pop. A more detailed paper about the synthesis is currently under preparation.
A mixture of regioisomers **2.1a** and **2.1b** was obtained as described in Ref. [118]. Thermal rearrangement under microwave irradiation of a mixture of **2.1a**/**b** (1:1) converged upon a common, naphthalene-1,4-diol intermediate which was immediately treated with KOH and methyl bromoacetate-2,2-d_2 in THF to afford naphthalene **2.2** in 60% yield over the two steps. Diester **2.2** was hydrolysed in refluxing methanol affording diacid **2.3** in 91% yield. Treatment of naphthalene **2.3** with 1M NaOH in H_2O afforded the water soluble naphthalene derivative **2.4**

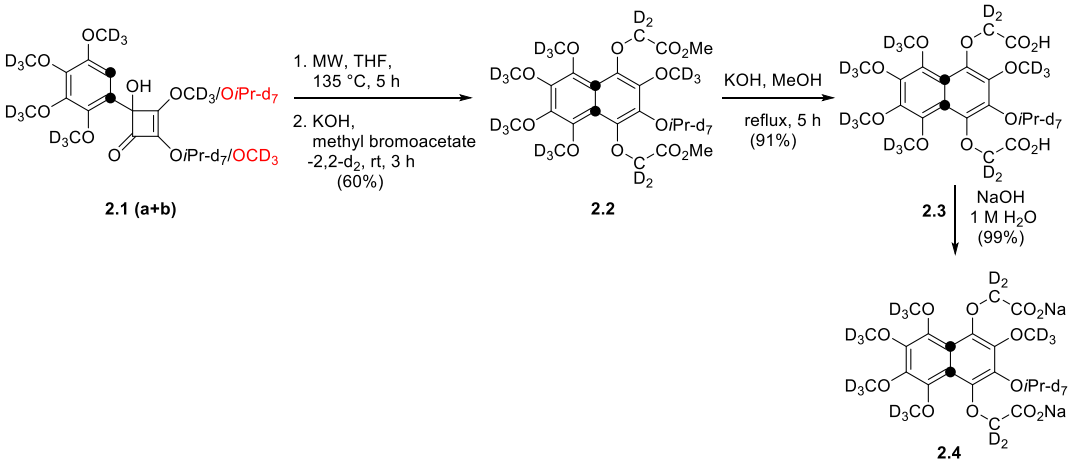

Figure 6.1: Synthesis of labeled naphthalene system **2.4** analysed in section 5.4.4 and indicated there as $^{13}C_2$-**II**.

Dimethyl 2,2'((1,2,3,4,6-Pentakis(methoxy-d_3)-7-(propan-2-yl-d_7) naphthalene-5,8-diyl)bis(oxy))diacetate-4a,8a-$^{13}C_2$ (2.2)

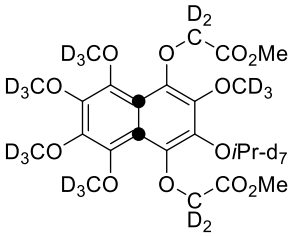

Figure 6.2: Step **2.2**.

A solution of cyclobutenones **2.1a** and **2.1b** (300 mg, 0.39 mmol) in THF (3 mL) was purged with N_2 while sonicated in an US bath for 30 min before being heated un-

der microwave irradiation in a sealed tube at 135 °C for 5 h. The reaction mixture was diluted with THF (15 mL), treated with KOH (94 mg, 1.68 mmol) and methyl bromoacetate (0.18 mL, 1.91 mmol) and stirred at rt for 1 h. The mixture was filtered and the solvent removed *in vacuo*. Purification by column chromatography eluting with Et_2O/petroleum ether (20:80) afforded the *title compound* **2.2** (250 mg, 0.46 mmol, 60%) as a white solid.

2,2'((1,2,3,4,6-Pentakis(methoxy-d_3)-7-(propan-2-yl-d_7) naphthalene-5,8-diyl)bis(oxy))diacetic acid-4a,8a-$^{13}C_2$ (2.3)

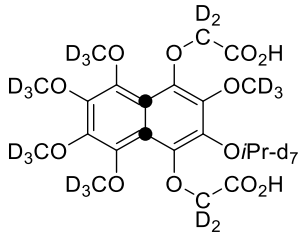

Figure 6.3: Step **2.3**.

To a suspension of diester **2.2** (220 mg, 0.41 mmol) in MeOH (5 mL) was added KOH (114 mg, 2.04 mmol) and the reaction mixture heated at reflux for 16 h. After cooling to rt, the mixture was filtered and the solvent removed *in vacuo*. The white residue was dissolved with H_2O (5 mL) and was washed with EtOAc (3 × 5 mL). The combined organic phases were dried (Na_2SO_4) and concentrated *in vacuo* to afford the *title compound* **2.3** (190 mg, 0.37 mmol, 91%) as white solid.

Sodium 2,2'((1,2,3,4,6-Pentakis(methoxy-d_3)-7-(propan-2-yl-d_7) naphthalene-5,8-diyl)bis(oxy))diacetate-4a,8a-$^{13}C_2$ (2.4)

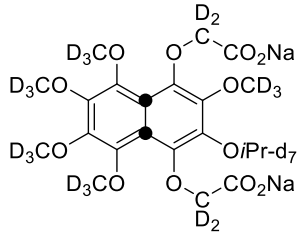

Figure 6.4: Step **2.4**.

To neat acid **2.3** (230 mg, 0.45 mmol) was added 1M NaOH (0.92 mL, 0.95 mmol) turning the white suspension to a pale pink suspension. The mixture was concentrated *in vacuo* to afford the *title compound* **2.4** (250 mg, 0.45 mmol, 100%) as a pink solid.

Bibliography

[1] P. J. Hore, *Nuclear Magnetic Resonance*, Oxford University Press, Inc., 1995.

[2] K. Claytor, T. Theis, Y. Feng, and W. Warren, *J. Magn. Reson.* **239**, 81 (2014).

[3] Y. Feng, R. M. Davis, and W. S. Warren, *Nat. Phys.* **8**, 831 (2012).

[4] Y. Feng, T. Theis, T.-L. Wu, K. Claytor, and W. S. Warren, *J. Chem. Phys.* **141**, 134307 (2014).

[5] K. Claytor, T. Theis, Y. Feng, J. Yu, D. Gooden, and W. S. Warren, *J. Am. Chem. Soc.* **136**, 15118 (2014).

[6] M. C. D. Tayler and M. H. Levitt, *Phys. Chem. Chem. Phys.* **13**, 5556 (2011).

[7] G. Pileio, J. T. Hill-Cousins, S. Mitchell, I. Kuprov, L. J. Brown, R. C. D. Brown, and M. H. Levitt, *J. Am. Chem. Soc.* **134**, 17494 (2012).

[8] A. Shaka, J. Keeler, and R. Freeman, *J. Magn. Reson.* **53**, 313 (1983).

[9] G. Pileio, M. Carravetta, and M. H. Levitt, *PNAS* **107**, 17135 (2010).

[10] G. Stevanato, J. T. Hill-Cousins, P. Håkansson, S. S. Roy, L. J. Brown, R. C. D. Brown, G. Pileio, and M. H. Levitt, *Angew. Chemie Int. Ed.* **54**, 3740 (2015).

[11] S. J. DeVience, R. L. Walsworth, and M. S. Rosen, *Phys. Rev. Lett.* **111**, 173002 (2013).

[12] H. J. Hogben, M. Krzystyniak, G. T. P. Charnock, P. J. Hore, and I. Kuprov, *J. Magn. Reson.* **208**, 179 (2011).

[13] I. Kuprov, *J. Magn. Reson.* **209**, 31 (2011).

[14] O. W. Sørensen, *Prog. Nucl. Magn. Reson. Spectrosc.* **21**, 503 (1989).

[15] N. Nielsen and O. Sorensen, *J. Magn. Reson. Ser. A* **114**, 24 (1995).

[16] N. Nielsen, T. Schulte-Herbrüggen, and O. Sørensen, *Mol. Phys.* **85**, 1205 (1995).

[17] M. H. Levitt, *J. Magn. Reson.* **in press** (2015).

[18] W. S. Warren, E. Jenista, R. T. Branca, and X. Chen, *Science* **323**, 1711 (2009).

[19] A. Bettini, *Introduction to Elementary Particle Physics*, Cambridge University Press, ii edition, 2014.

[20] J. Akitt and B. Mann, *NMR and Chemistry*, 2000.

[21] M. H. Levitt, *spin dynamics. Basics of Nuclear Magnetic Resonance*, 2006.

[22] G. Pileio, M. Carravetta, E. Hughes, and M. H. Levitt, *J. Am. Chem. Soc.* **130**, 12582 (2008).

[23] W. S. Warren, *The physical basis of chemistry*, Harcourt Academy Press, ii edition, 2000.

[24] S. Glöggler, J. Colell, and S. Appelt, *J. Magn. Reson.* **235**, 130 (2013).

[25] K. F. Bonhoeffer and P. Harteck, *Naturwissenschaften* **17**, 182 (1929).

[26] R. Eisenberg, *Acc. Chem. Res.* **24**, 110 (1991).

[27] M. Carravetta, O. Johannessen, and M. Levitt, *Phys. Rev. Lett.* **92**, 153003 (2004).

[28] M. Carravetta and M. H. Levitt, *J. Am. Chem. Soc.* **126**, 6228 (2004).

[29] J. Bargon, *Helv. Chim. Acta* **89**, 2082 (2006).

[30] J. H. Ardenkjaer-Larsen, B. Fridlund, A. Gram, G. Hansson, L. Hansson, M. H. Lerche, R. Servin, M. Thaning, and K. Golman, *Proc. Natl. Acad. Sci. U. S. A.* **100**, 10158 (2003).

[31] C. R. Bowers and D. P. Weitekamp, *Phys. Rev. Lett.* **57**, 2645 (1986).

[32] S. B. Duckett and R. E. Mewis, *Acc. Chem. Res.* **45**, 1247 (2012).

[33] P. Hamill, *Lagrangians and Hamiltonians*, Cambridge University Press, 2014.

[34] O. Stern and W. Gerlach, *Zeitschrift fur Phys.* **9**, 353 (1922).

[35] I. Duck and E. C. G. Sudarshan, *Pauli and the spin-statistics theorem*, World Scientific Publishing Co. Pte. Ltd., 1997.

[36] D. E. Neuenschwander, *Emmy Noether's Wonderful Theorem*, The Johns Hopkins University Press, 2011.

[37] E. Noether, *Nachrichten von der Gesellschaft der Wissenschaften zu Göttingen, Mathematisch-Physikalische Klasse* **1918**, 235 (1918).

[38] J. Sakurai, *Modern Quantum Mechanics*, Addison-Wesley Publishing Company, Inc., (r.e.) edition, 1985.

[39] G. M. Barrow, *The Structure of Molecules*, W.A. Benjamin, INC, 1964.

[40] P. R. Bunker and P. Jensen, *Molecular Symmetry and Spectroscopy*, Academic Press, London, ii edition, 2006.

[41] A. Abragam, *Principles of Nuclear Magnetism*, Oxford University Press, 1961.

[42] G. Wilkinson and J. Gribbin, *80* , 588 (1978).

[43] C. L. Dumoulin and H. R. Hart, *Radiology* **161**, 717 (1986).

[44] D. Le Bihan, *Neuroimage* **62**, 1131 (2012).

[45] S. Ogawa and T. Lee, *Proc. NatI. Acad. Sci. USA* **87**, 9868 (1990).

[46] E. Terreno, D. D. Castelli, E. Violante, H. M. H. F. Sanders, N. A. J. M. Sommerdijk, and S. Aime, *Chem. - A Eur. J.* **15**, 1440 (2009).

[47] G. Ferrauto, E. Di Gregorio, S. Baroni, and A. Silvio, *Nano Lett.* **14**, 6857 (2014).

[48] T. Theis, M. Truong, A. M. Coffey, E. Y. Chekmenev, and W. S. Warren, *J. Magn. Reson.* **248C**, 23 (2014).

[49] M. Emondts, M. P. Ledbetter, S. Pustelny, T. Theis, B. Patton, J. W. Blanchard, M. C. Butler, D. Budker, and A. Pines, *Phys. Rev. Lett.* **112**, 077601 (2014).

[50] T. Theis, M. L. Truong, A. M. Coffey, R. V. Shchepin, K. W. Waddell, F. Shi, B. M. Goodson, W. S. Warren, and E. Y. Chekmenev, *J. Am. Chem. Soc.* **137**, 1404 (2015).

[51] M. B. Franzoni, L. Buljubasich, H. W. Spiess, and K. Münnemann, *J. Am. Chem. Soc.* **134**, 10393 (2012).

[52] G. Pileio, S. Bowen, C. Laustsen, M. C. D. Tayler, J. T. Hill-Cousins, L. J. Brown, R. C. D. Brown, J. H. Ardenkjaer-Larsen, and M. H. Levitt, *J. Am. Chem. Soc.* **135**, 5084 (2013).

[53] B. Meier, J.-N. Dumez, G. Stevanato, J. T. Hill-Cousins, S. S. Roy, P. Håkansson, S. Mamone, R. C. D. Brown, G. Pileio, and M. H. Levitt, *J. Am. Chem. Soc.* **135**, 18746 (2013).

[54] Y. Zhang, P. C. Soon, A. Jerschow, and J. W. Canary, *Angew. Chemie - Int. Ed.* **53**, 3396 (2014).

[55] G. Stevanato, S. Singha Roy, J. Hill-Cousins, I. Kuprov, L. J. Brown, R. C. D. Brown, G. Pileio, and M. H. Levitt, *Phys. Chem. Chem. Phys.* **17**, 5913 (2015).

[56] D. Mammoli, B. Vuichoud, A. Bornet, J. Milani, J.-N. Dumez, S. Jannin, and G. Bodenhausen, *J. Phys. Chem. B* **119**, 4048 (2015).

[57] G. Pileio and M. H. Levitt, *J. Chem. Phys.* **130**, 214501 (2009).

[58] G. Pileio, *Prog. Nucl. Magn. Reson. Spect.* **56**, 217 (2010).

[59] M. H. Levitt, *Annu. Rev. Phys. Chem.* **63**, 89 (2012).

[60] J.-N. Dumez, P. Håkansson, S. Mamone, B. Meier, G. Stevanato, J. T. Hill-Cousins, S. S. Roy, R. C. D. Brown, G. Pileio, and M. H. Levitt, *J. Chem. Phys.* **142**, 044506 (2015).

[61] R. Sarkar, P. R. Vasos, and G. Bodenhausen, *J. Am. Chem. Soc.* **129**, 328 (2007).

[62] N. Salvi, R. Buratto, A. Bornet, S. Ulzega, I. Rentero Rebollo, A. Angelini, C. Heinis, and G. Bodenhausen, *J. Am. Chem. Soc.* **134**, 11076 (2012).

[63] R. Buratto, D. Mammoli, E. Chiarparin, G. Williams, and G. Bodenhausen, *Angew. Chem. Int. Ed. Engl.* **53**, 11376 (2014).

[64] M. C. D. Tayler, I. Marco-Rius, M. I. Kettunen, K. M. Brindle, M. H. Levitt, and G. Pileio, *J. Am. Chem. Soc.* **134**, 7668 (2012).

[65] T. Theis, P. Ganssle, G. Kervern, S. Knappe, J. Kitching, M. P. Ledbetter, D. Budker, and A. Pines, *Nat. Phys.* **7**, 571 (2011).

[66] R. Sato and R. V. Ramachandran, *Symmetry and Economic Invariance*, Springer, 2014.

[67] P. R. Bunker and P. Jensen, *Fundamentals of molecular symmetry*, Institute of Physics, 2005.

[68] D. M. Bishop, *Group Theory and Chemistry*, The Clarendon Press, Oxford, 1973.

[69] P. Atkins and J. de Paula, *Physical Chemistry*, Oxford University Press, 2006.

[70] A. Cayley, *Philos. Mag.* **7**, 40 (1854).

[71] N. Jacobson, *Basic Algebra*, 1989.

[72] J. D. van Beek, M. Carravetta, G. C. Antonioli, and M. H. Levitt, *J. Chem. Phys.* **122**, 244510 (2005).

[73] J. Kowalewski and L. Mäler, *Nuclear spin relaxation in liquids: Theory, Experiments, and Applications*, CRC press Taylor & Francis Group, 2006.

[74] R. S. Mulliken, *Phys. Rev.* **43**, 279 (1933).

[75] H. Longuet-Higgins, *Mol. Phys.* **6**, 445 (1963).

[76] R. G. Jones, The Use of Symmetry in Nuclear Magnetic Resonance, in *NMR Basic Princ. Prog. / Grundlagen und Fortschritte*, pp. 97–174, Springer Berlin Heidelberg, Berlin, Heidelberg, 1969.

[77] J. Pople, W. Schneider, and H. Bernstein, *High-Resolution Nuclear Magnetic Resonance*, McGraw-Hill Co., 1959.

[78] P. Diehl, R. Harris, and R. Jones, *Prog. Nucl. Magn. Reson. Spectrosc.* **3**, 1 (1967).

[79] C. Woodman, *Mol. Phys.* **11**, 109 (1966).

[80] N. Pyper, *Mol. Phys.* **21**, 1 (1971).

[81] N. Pyper, *Mol. Phys.* **22**, 433 (1971).

[82] Y. Hovav, A. Feintuch, and S. Vega, *J. Chem. Phys.* **134**, 074509 (2011).

[83] Y. Hovav, I. Kaminker, D. Shimon, A. Feintuch, D. Goldfarb, and S. Vega, *Phys. Chem. Chem. Phys.* **17**, 226 (2015).

[84] D. Shimon, Y. Hovav, I. Kaminker, A. Feintuch, D. Goldfarb, and S. Vega, *Phys. Chem. Chem. Phys.* **17**, 11868 (2015).

[85] J. W. Hennel and J. Klinowski, Magic-Angle Spinning: a Historical Perspective, pp. 1–14, 2005.

[86] D. Kruk, *Theory of Evolution and Relaxation of Multi-spin Systems*, Abramis, 2007.

[87] I. Bertini, O. Galas, C. Luchinat, L. Messori, and G. Parigi, *J. Phys. Chem.* **99**, 14217 (1995).

[88] D. Kruk, A. Kubica, W. Masierak, A. F. Privalov, M. Wojciechowski, and W. Medycki, *Solid State Nucl. Magn. Reson.* **40**, 114 (2011).

[89] L. M. Broche, G. P. Ashcroft, and D. J. Lurie, *Magn. Reson. Med.* **68**, 358 (2012).

[90] A. W. Overhauser, *Phys. Rev.* **89**, 689 (1953).

[91] I. Solomon, *Phys. Rev.* **99**, 559 (1955).

[92] J. Kowalewski, Paramagnetic relaxation in solution, in *Encycl. Nucl. Magn. Reson.*, pp. 3456–3462, 1996.

[93] E. Vinogradov and A. K. Grant, *J. Magn. Reson.* **188**, 176 (2007).

[94] A. K. Grant and E. Vinogradov, *J. Magn. Reson.* **193**, 177 (2008).

[95] A. Buckingham and S. Malm, *Mol. Phys.* **22**, 1127 (1971).

[96] L. G. Werbelow and A. G. Marshall, *J. Am. Chem. Soc.* **95**, 5132 (1973).

[97] A. Horsewill, *Prog. Nucl. Magn. Reson. Spectrosc.* **35**, 359 (1999).

[98] A. J. Horsewill and C. Sun, *J. Magn. Reson.* **199**, 10 (2009).

[99] A. J. Horsewill and S. M. M. Abu-Khumra, *Phys. Rev. Lett.* **107**, 127602 (2011).

[100] M. Icker, P. Fricke, and S. Berger, *J. Magn. Reson.* **223**, 148 (2012).

[101] M. Icker and S. Berger, *J. Magn. Reson.* **219**, 1 (2012).

[102] M. Icker, P. Fricke, T. Grell, J. Hollenbach, H. Auer, and S. Berger, *Magn. Reson. Chem.* **51**, 815 (2013).

[103] G. Pileio, M. Concistre', M. Carravetta, and M. H. Levitt, *J. Magn. Reson.* **182**, 353 (2006).

[104] G. Pileio and M. H. Levitt, *J. Magn. Reson.* **187**, 141 (2007).

[105] G. Pileio, M. Carravetta, and M. H. Levitt, *Proc. Natl. Acad. Sci. U. S. A.* **107**, 17135 (2010).

[106] M. C. D. Tayler and M. H. Levitt, *J. Am. Chem. Soc.* **135**, 2120 (2013).

[107] M. C. Butler, G. Kervern, T. Theis, M. P. Ledbetter, P. J. Ganssle, J. W. Blanchard, D. Budker, and A. Pines, *J. Chem. Phys.* **138**, 234201 (2013).

[108] S. S. Roy, J.-N. Dumez, G. Stevanato, B. Meier, J. T. Hill-Cousins, R. C. D. Brown, G. Pileio, and M. H. Levitt, *J. Magn. Reson.* **250C**, 25 (2014).

[109] J. Stoustrup, O. Schedletzky, S. J. Glaser, C. Griesinger, N. C. Nielsen, and O. W. Sørensen, *Phys. Rev. Lett.* **74**, 2921 (1995).

[110] M. Carravetta and M. H. Levitt, *J. Chem. Phys.* **122**, 214505 (2005).

[111] M. C. D. Tayler and M. H. Levitt, *Phys. Chem. Chem. Phys.* **13**, 9128 (2011).

[112] R. Sarkar, P. Ahuja, P. R. Vasos, and G. Bodenhausen, *Phys. Rev. Lett.* **104**, 053001 (2010).

[113] A. Bornet, R. Sarkar, and G. Bodenhausen, *J. Magn. Reson.* **206**, 154 (2010).

[114] M. Prager and A. Heidemann, *Chem. Rev.* **97**, 2933 (1997).

[115] H. J. Hogben, P. J. Hore, and I. Kuprov, *J. Magn. Reson.* **211**, 217 (2011).

[116] L. Buljubasich, M. B. Franzoni, H. W. Spiess, and K. Münnemann, *J. Magn. Reson.* **219**, 33 (2012).

[117] T. Theis, Y. Feng, T.-l. Wu, and W. S. Warren, *J. Chem. Phys.* **140**, 014201 (2014).

[118] J. T. Hill-Cousins, I.-A. Pop, G. Pileio, G. Stevanato, P. Håkansson, S. S. Roy, M. H. Levitt, L. J. Brown, and R. C. D. Brown, *Org. Lett.* **17**, 2150 (2015).

[119] M. H. Levitt, SpinDynamica, 2013.

[120] A. G. Redfield, *Adv. Magn. Res.* **1**, 1 (1965).

[121] A. Bornet, X. Ji, D. Mammoli, B. Vuichoud, J. Milani, G. Bodenhausen, and S. Jannin, *Chemistry* (2014).

[122] D. Mammoli, N. Salvi, J. Milani, R. Buratto, A. Bornet, A. A. Sehgal, E. Canet, P. Pelupessy, D. Carnevale, S. Jannin, and G. Bodenhausen, *Phys. Chem. Chem. Phys.* (2015).

[123] J. Granwehr, J. Leggett, and W. Köckenberger, *J. Magn. Reson.* **187**, 266 (2007).

[124] P. S. Allen, *Faraday Symp. Chem. Soc.* **13**, 133 (1978).

[125] P. E. Hansen, *Prog. Nucl. Magn. Reson. Spectrosc.* **20**, 207 (1988).

[126] P. Luehring and A. Schumpe, *J. Chem. Eng. Data* **34**, 250 (1989).

[127] J. Kowalewski and L. Werbelow, *J. Magn. Reson.* **128**, 144 (1997).

[128] J. H. Lee, Y. Okuno, and S. Cavagnero, *J. Magn. Reson.* **241**, 18 (2014).

[129] I. Park, P. E. Z. Larson, M. L. Zierhut, S. Hu, R. Bok, T. Ozawa, J. Kurhanewicz, D. B. Vigneron, S. R. VandenBerg, C. D. James, and S. J. Nelson, *Neuro. Oncol.* **12**, 133 (2010).

[130] C. Laustsen, G. Pileio, M. C. D. Tayler, L. J. Brown, R. C. D. Brown, M. H. Levitt, and J. H. Ardenkjaer-Larsen, *Magn. Reson. Med.* **68**, 1262 (2012).

[131] I. Marco-Rius, M. C. D. Tayler, M. I. Kettunen, T. J. Larkin, K. N. Timm, E. M. Serrao, T. B. Rodrigues, G. Pileio, J. H. Ardenkjaer-Larsen, M. H. Levitt, and K. M. Brindle, *NMR Biomed.* **26**, 1696 (2013).

[132] J. Leggett, R. Hunter, J. Granwehr, R. Panek, A. J. Perez-Linde, A. J. Horsewill, J. McMaster, G. Smith, and W. Köckenberger, *Phys. Chem. Chem. Phys.* **12**, 5883 (2010).

[133] M. Carravetta and M. H. Levitt, *J. Chem. Phys.* **122**, 214505 (2005).

[134] Y. Feng, T. Theis, X. Liang, Q. Wang, P. Zhou, and W. S. Warren, *J. Am. Chem. Soc.* **135**, 9632 (2013).

[135] F. A. Gallagher, M. I. Kettunen, D.-E. Hu, P. R. Jensen, R. i. t. Zandt, M. Karlsson, A. Gisselsson, S. K. Nelson, T. H. Witney, S. E. Bohndiek, G. Hansson, T. Peitersen, M. H. Lerche, and K. M. Brindle, *Proc. Natl. Acad. Sci.* **106**, 19801 (2009).

[136] K. M. Brindle, S. E. Bohndiek, F. a. Gallagher, and M. I. Kettunen, *Magn. Reson. Med.* **66**, 505 (2011).

[137] C. Ludwig, M. Saunders, I. Marin-Montesinos, and U. L. Günther, *Proc. Natl. Acad. Sci. U. S. A.* **107**, 10799 (2010).

[138] G. Pileio, *J. Chem. Phys.* **135**, 174502 (2011).

[139] N. Khaneja, B. Luy, and S. J. Glaser, *Proc. Natl. Acad. Sci.* **100**, 13162 (2003).

[140] N. Khaneja, T. Reiss, B. Luy, and S. J. Glaser, *J. Magn. Reson.* **162**, 311 (2003).

[141] F. Reineri, T. Boi, and S. Aime, *Nat. Commun.* (2015).